CARBON MONOXIDE GENERATION AND TRANSPORT FROM COMPARTMENT FIRES

by

Christopher John Wieczorek

Dissertation submitted to the Faculty of the
Virginia Polytechnic Institute and State University
in partial fulfillment of the requirements for the degree of

DOCTOR OF PHILOSOPHY
in
Mining and Minerals Engineering

Committee:
Uri Vandsburger, Chairman
Erik Westman, Co-Chairman
Thomas Novak
Brian Lattimer
Jason Floyd

June 2003
Blacksburg, Virginia

Keywords: carbon monoxide, building fires, mining fires, species generation, species transport

Carbon Monoxide Generation and Transport from Compartment Fires with Prototypical Building Features

by

Christopher John Wieczorek

Dr. Uri Vandsburger, Chairman

Mechanical Engineering

(ABSTRACT)

The aim of the present research was to gain a better understanding of the species generation and transport from enclosure fires. The species generation experiments were conducted with a half-scale ISO 9705 enclosure with three different ventilation conditions and heat release rates ranging from 50 kW to 500 kW. The transport study was conducted with a 6.1 m long hallway connected to the compartment in a head-on configuration. All measurements were performed at the compartment or hallway exit plane during the steady-state period of the fire. Measurements included species mole fractions of oxygen, carbon dioxide, carbon monoxide, and unburned hydrocarbons, along with gas pressure (used to determine gas velocities) and gas temperatures.

Species mappings performed at the exit plane of the compartment indicated that the exiting species are not spatially uniform. Horizontal and vertical gradients in the species mole fractions were observed for all ventilation conditions and heat release rates examined.

Predictive techniques developed previously were applied to the data obtained in the present study and were determined to be inappropriate for situations were the plume equivalence ratio was not equal to the global equivalence ratio. A new methodology for predicting species levels at the exit plane of an enclosure was developed. The proposed methodology correlates the species yields based on the combustion within the compartment as a function of a non-dimensional heat release rate, $\widetilde{Q}$. The non-

dimensional heat release rate is based on the fuel load and geometrical parameters of the enclosure. The present methodology in applicable to situations where a well-mixed uniform layer is not present and the overall global conditions are of interest.

Species transport to remote locations was also examined. Experiments were conducted with the baseline ventilation at x = 0 m (the compartment/hallway interface) and three different ventilation conditions at x = 6.1 m (end of hallway). The three ventilation conditions consisted of the narrow, baseline, and wide doorways. Experiments were conducted for heat release rates of 85 kW, 127 kW, and 150 kW. The results from the tests indicated that, for over-ventilated compartment fires, the hallway and hallway ventilation had no impact on the species generation within the compartment. This allows the correlations developed from the compartment study to be applied to more complex scenarios.

Differences in species mole fractions between x = 0 m and x = 6.1 m were shown to be a result of air entrainment into the upper layer within the hallway, which acted as a dilutent or as a source of oxygen for further oxidation reactions. For $\widetilde{Q} < 1.0$, the reduction in carbon monoxide levels along the hallway was a result of dilution, while for $\widetilde{Q} \geq 1.0$ the reduction in carbon monoxide levels along the hallway was a combination of dilution and further oxidation reactions.

DEDICATION

This work is dedicated to the two most important people in my life, mom and dad. Thank you dad for working so hard so that you could give me everything I ever wanted. Thank you mom for all your love and especially all of your prayers. When I was child and hated school you prayed that I would do well… see what all those prayers got you.

"*Yes, I will sail my vessel, 'Til the river runs dry*." Garth Brooks

ACKNOWLEDGMENTS

I would first like to thank Dr. Uri Vandsburger for being my major advisor and more importantly my friend. He was patient with me when times got rough and never gave up on me. He motivated me to overcome the barriers and become a better researcher and grow as a person.

I want to give a special thank you to the Mining and Minerals Department, especially Dr. Erik Westman and Dr. Thomas Novak for their support. First I want to thank them for accepting me into the Mining and Minerals program, and second for being part of my committee. Thank you for helping me achieve this goal.

A very special thanks goes out to Dr. Jason Floyd who while performing his post-doctoral work went above and beyond what was expected and spent many hours and days getting dirty with me out at the firelab. In addition, his contributes to the analysis of the data were innumerable.

I would also like to thank Dr. Brian Lattimer for assisting me and helping me through this project. His ideas and advice greatly contributed to the successful outcome of the project.

A successful research project can not be completed without financial support; much appreciation is extended to the people at NIST/BFRL for providing the majority of the funding for this research. Conversations with Dr. W. M. Pitts were always insightful. Partial funding was also provided by the Society of Fire Protection Engineers, Educational Foundation, directed by Kathleen Almond.

A thank you and a passing of the torch (igniter stick if you may) to Mr. Laurent Mounaud. Good luck in carrying the project on into the future. Also, I want to extended my appreciation to the people I have worked with in the Reacting Flows Laboratory over the years: Christopher McKay, Steve LePera, Vivek Khanna, Denzil John, Adam Hendricks, Wajid Christy, and Prateep Chatterjee. In addition, all of the undergraduate

students who have assisted with me over the years, in particular Patrick Early and Nicholas Hanak.

The largest thank you goes to my family. Thank you mom, dad, and Steven, without your love and support I would not have survived the trials and tribulations that went along with getting this far. I love you all. A special note of thanks also needs to be given to the Szikorski brothers; I will always be there for you, as you have for me.

Special thanks goes to my roommate Dave Moorcroft who helped me stay sane. Without David I may have quit a long time ago, but his constant advice of "Wait it out one more day, one more month, one more semester" kept me here long enough for the powers-to-be to finally give me a degree.

I would like to thank, three of my good friends, Nicholas Dembsey, Phil Gunning, and Olga Phactor who were always available for consultation when I needed advice in any aspect of this project and more importantly my life.

To all my dancing friends. You got me out of the house and away from the lab when I needed a break. You helped me dance my fears, problems, and worries away one song at a time. Thank you for the dance.

Finally, I would like to thank God for without him watching over me I would not have achieved this goal, for he knew which prayers to answer and which ones to modify. (Thanks again mom for reminding me to call on him when I needed it most.)

TABLE OF CONTENTS

LIST OF FIGURES

LIST OF TABLES

NOMENCLATURE

SYMBOL	DESCRIPTION	UNITS
A	constant or area of the ventilation opening	m^2
a	constant or coefficient	
A_s	surface area	m^2
B	constant	
c	stoichiometric ratio of CO_2 and water or flow coefficient	
c_p	heat capacity	kJ/(kg K)
D	diameter	m
dA	differential area	m^2
db	differential length	m
dH	differential height	m
f_i	normalized yields	
H	height of the ventilation opening	m
h_c	convective heat transfer coefficient	kW/(m^2 K)
k	thermal conductivity	W/(m K)
L_f	horizontal length of flame along ceiling	m
$\dot{m}$	mass flow rate	kg/s
$\dot{m}_{fuel}$	mass flow rate of fuel	kg/s
$\dot{m}_{fuel,\ compartment}$	mass flow rate of fuel consumed within the compartment	kg/s
$\dot{m}_{total}$	total mass flow rate	kg/s
MW_i	molecular weight of species i	kg/kmol
$MW_{mixture}$	molecular weight of mixture	kg/kmol
$\left(\frac{\dot{m}_{fuel}}{\dot{m}_{air}}\right)_{st}$	stoichiometric fuel to air ratio	
n	constant	
Nu	Nusselt number = $\frac{h_c D}{k}$	
$\tilde{Q}$	non-dimensional heat release rate	
$\dot{Q}_{compartment}$	heat release rate within the compartment	kW
$\dot{Q}_{Flame\ Extensions}$	heat release rate required for flame tip to reach the opening	kW
$\dot{Q}_{ideal}$	ideal heat release rate	kW
$\dot{Q}_{Stoichiometric}$	stoichiometric heat release rate	
r	stoichiometric fuel to air ratio	

R	Universal gas constant	J/(mol K)
Re	Reynolds number	
T_m	film temperature = $\frac{(T_g - T_j)}{2}$	K
T_g	gas temperature	K
T_j	junction temperature	K
U	velocity	m/s
V	velocity or volume	m/s or m^3
$\dot{V}$	volumetric flow rate out of the compartment	m^3/s
x	distance	m
$\overline{X}_i$	area averaged mole fraction of species i	
$X_{i,dry}$	mole fraction of species i on a dry basis	
$X_{i,wet}$	mole fraction of species i on a wet basis	
y	elevation	m
Y_i	yield of species i	kg_i/kg_{fuel}
$\overline{Y_i}$	area averaged yield of species i	
y_i	mass fraction of species i	
$\overline{y}_i$	area averaged mass fraction of species i	
z	height	m

Greek

ΔH_c	heat of combustion	kJ/kg
$\Delta H_{c,ox}$	heat of combustion per gram of oxygen consumed	kJ/kg_{o2}
ΔP	pressure difference	kPa
ξ	correlation constant	
κ	confinement coefficient	
ρ	density	kg/m^3
ρ_i	density of species i	kg/m^3
ϕ	global equivalence ratio	
τ_t	thermal response time	sec
ν	dynamic viscosity	m^2/s
χ	combustion efficiency	

Subscripts

air	ambient air
amb	ambient
avg	average
compartment	compartment

CO	carbon monoxide
CO_2	carbon dioxide
d	doorway
f	compartment gases
hall	hallway
in	into control volume, compartment, or hallway
o	ambient
O_2	oxygen
out	out of control volume, compartment, or hallway
max	maximum
n	neutral plane
UHC	unburned hydrocarbons
UL	upper layer

CHAPTER 1

INTRODUCTION

1.1 INTRODUCTION

This chapter is dedicated to providing an overview for this project along with justification for its execution. Statistics have shown that carbon monoxide is the primary species generated in fires responsible for fatalities occurring in both the mining and building industries. In this chapter a discussion of previous research related to toxic species generation is presented and discussed along with the currently used methodologies for predicting species generation stemming from these studies. Based on this discussion the objectives for the present study are presented.

1.2 MOTIVATION

1.2.1 Carbon Monoxide

Fires can generate products of incomplete combustion. When fires occur in buildings or in underground mines, these products pose a serious hazard to the occupants. Products of incomplete combustion include but are not limited to carbon monoxide (CO), nitrogen oxides (NO_x), hydrogen cyanide (HCN), unburned hydrocarbons (UHC), and soot. Research has shown that CO is the primary toxicant formed in compartment fires, and therefore is the primary focus of this research study. [Gann *et al.* 1994]

Carbon monoxide is a colorless, odorless, and tasteless gas that is toxic to humans. Carbon monoxide is toxic since it reduces the blood's capacity to carry oxygen. This is a result of hemoglobin in the blood that has a preference for carbon monoxide that is 3000 times greater than that for oxygen. [Hartman *et al.* 1997] The effects of increased carbon monoxide levels in the body include loss of consciousness, asphyxiation, and

death. [Pon *et al.* 2001] The potential effects of carbon monoxide levels with exposure time on humans are listed in Table 1-1. [NFPA 2000]

Table 1-1: Carbon Monoxide Effects on Humans [NFPA 2000]

Level	Physiological Effect
50 ppm	Threshold limit value for no adverse effects
200 ppm	Possible mild headache after 2-3 hours
400 ppm	Headache and nausea after 1-2 hours
800 ppm	Headache, nausea, and dizziness after 45 minutes; collapse and possible unconsciousness after 2 hours
1000 ppm	Loss of consciousness after 1 hour
1600 ppm (0.16 %)	Headache, nausea, and dizziness after 20 minutes
3200 ppm (0.32 %)	Headache and dizziness after 5-10 minutes; unconsciousness after 30 minutes
6400 ppm (0.64 %)	Headache and dizziness after 1-2 minutes, unconsciousness and danger of death after 10-15 minutes
12,800 ppm (1.28 %)	Immediate physiological effects; unconsciousness and danger of death after 1-3 minutes

1.2.2 Building Industry

Lifestyle developments, on a global scale, which manifest themselves in increased travel, increased elderly populations in assisted care facilities, and urbanization require increased attention to fire safety in dense occupation environments. Statistics spanning decades have shown that the key factor in fire fatalities is carbon monoxide inhalation, not only in the fire enclosure but also in areas remote from the flames. The cause of death in building fires continues to be dominated by smoke inhalation.

Hall [1997] reported that 75% of all deaths in building fires are caused by toxic gases, and that approximately 66% of all deaths can be attributed to the presence of carbon monoxide. Trends in fatality statistics indicate that the percentage of deaths due

to toxic gas inhalation rises 1% every year. The transport of toxic gases from the fire origin to locations remote from the source can generate environments that are hazardous to occupants at these locations. In 1999 there were a total of 3,040 deaths in structure fires due to toxic gases, of these two-thirds of victims were found at locations remote from the fire source. [Hall 1997, Karter 2000]

The following description of two such instances is taken from Lattimer [1996].

> On October 5, 1989 at the Hillhaven Nursing Home in Norfolk,Virginia, a fire in a patient's room resulted in the death of 13 people. Each victim died of carbon monoxide poisoning with 12 of the victims found in a room or position down the hallway from the room containing the fire. Twenty-three patients resided along the wing containing the burning room, 9 of the victims were found in rooms on the opposite side of the hallway from the burning room while only one victim was found on the burning room side of the hallway. This was attributed to a wind from the south causing a draft, which drove the toxic gases across the hallway into the victims' rooms. A similar type fire in a Southern Michigan hospice on December 15, 1985 claimed the lives of 8 people, 6 of which were at locations down the hallway from the room containing the fire and were all caused by carbon monoxide poisoning.

1.2.3 Mining Industry

Although statistics indicate that the occurrence of mine fires is decreasing in recent years due to stricter regulations, mine fires are still considered the number one cause of mine disasters in the United States. [Loomis 2001, Launhardt 2001] The National Institute for Occupational Safety and Health (NIOSH) reported a total of 717 mine disasters, where a disaster is defined as 5 or more fatalities, between the years of 1839 and 2001. [NIOSH 2001] Of these, 74 are attributed directly to fire and account for 1,532 fatalities; an additional 11 incidents causing 106 fatalities are attributed to

suffocation and asphyxiation due to gases and fumes. It is not known if the latter were generated due to fires, blasting, equipment use/malfunction, or other sources. The reported fires occurred in copper, gold, iron, lead, zinc, salt, silver, and coal mines. No differentiation between the causes of the fire fatalities, i.e. carbon monoxide poisoning versus burns, is made in the statistics; however McPherson [1993] reports that "a majority of deaths arising from mine fires and explosions are caused not by burning or blast effects, but the inhalation of toxic gases, in particular, carbon monoxide."

Not all mine fires are 'disasters', as defined by the mining industry. The Mine Safety and Health Administration (MSHA) reported that between 1991 and 2000, 137 fires occurred in underground mines in the United States, resulting in 2 fatalities and 34 injuries; it is also believed that a significantly large number of fires go unreported each year. [Conti 2001]

Fires occurring in underground mines have an additional degree of complexity that is normally not seen in structural fires… distance. In structural fires, regulations require that the travel distance to an exit be no greater than 15 m, in underground mines the travel distance to an exit may be several kilometers and take more than an hour to reach. [McPherson 1993, NFPA 1994]

One recent incident occurred at the Emery Mining Company Wilberg operation on December 19, 1984. A fire occurred due to a faulty compressor near the intake of the fifth right longwall panel. Twenty-eight people were present at the time. Most of the miners attempted to escape down the intake or belt entry and were quickly overcome by smoke and carbon monoxide. Three of the miners tried to escape through the tailgate return entry, the entry had been allowed to collapse several weeks prior and the miners' bodies were found at the blockage. The last miner "wiggled through a 'squeeze' in the bleeders where the roof had caved in and the floor had heaved up. He made it into the clear and walked several hundred feet before being overcome by carbon monoxide poisoning and dying, with an unopened self-contained self-rescuer around his neck." [NIOSH 2000]

1.3 PREVIOUS WORK

1.3.1 Species Production in Compartment Fires

Toxic species generation is a complex function of air supply, nature of mixing, and fuel and oxidant properties. [Beyler 1983, Karlsson 2001] Species generation from free burning diffusion flames positioned under an exhaust hood has been the subject of numerous experimental investigations, including work by Beyler [1983, 1986a], Cetegen, Lim, Toner [1987], and Morehart [1990].

The most widely referenced work, and the basis for current predictive engineering tools for species generation, is the work of Beyler [1983, 1986b]. Beyler proposed that it might be possible to correlate the species yields and species production rates to an overall fuel-to-air ratio. Two key assumptions for a valid correlation, according to Beyler, are:

1. The species production rate (and species yield) of major species is insensitive to the detailed structure of the flame.
2. A meaningful fuel-to-air ratio can be defined.

The parameter proposed by Beyler was the global equivalence ratio (GER), which in his experiments was equivalent to the plume equivalence ratio (PER) during the steady-state period. The equivalence ratio, defined in the classical way, Equation 1-1, determines whether a fire is fuel or oxygen limited.

$$\phi = \frac{\left(\frac{\dot{m}_{fuel}}{\dot{m}_{air}}\right)}{\left(\frac{\dot{m}_{fuel}}{\dot{m}_{air}}\right)_{st}} \qquad (1\text{-}1)$$

Beyler's experiments were conducted with a burner located underneath a 1 m diameter exhaust hood with gas sampling taken within the exhaust stream. The experiment was designed to simulate the upper layer of a compartment fire. Pitts [1994] summarized the following major conclusions of Beyler's work.

1. Major combustion species can be correlated in terms of the PER.
2. Relatively constant concentrations of CO are generated at low and high PERs.
3. The generation of CO under fuel-rich conditions is considerably greater than for fuel-lean conditions.
4. The concentrations of CO generated for rich conditions are fuel dependent, but can be correlated with fuel structure.

In addition it is reported that:

5. A reasonably well mixed uniform upper layer both in temperature and composition existed for steady-state conditions. [Gottuk *et al.* 2002]

Although these conclusions are based on small-scale open fires under an exhaust hood, over the years these conclusions have been extended to reduced and full-scale compartment fires.

Beyler's results presented as carbon monoxide yields as a function of the plume equivalence ratio are shown in Figure 1-1. [Gottuk *et al.* 2002] Data for gaseous, liquid, and solid fuels are included in Figure 1-1. Beyler concluded that CO production was constant under fuel-lean ($\phi < 0.7$) and fuel-rich ($\phi > 1.2$) conditions, with a transition stage from the lower level to a higher level occurring in the range $0.7 < \phi < 1.2$. When presented as unnormalized yields the data indicates a minor dependence on fuel type; however, Beyler [1983] reported that if presented as a normalized yield, a carbon monoxide dependence on fuel is seen and can be correlated with the fuel structure.

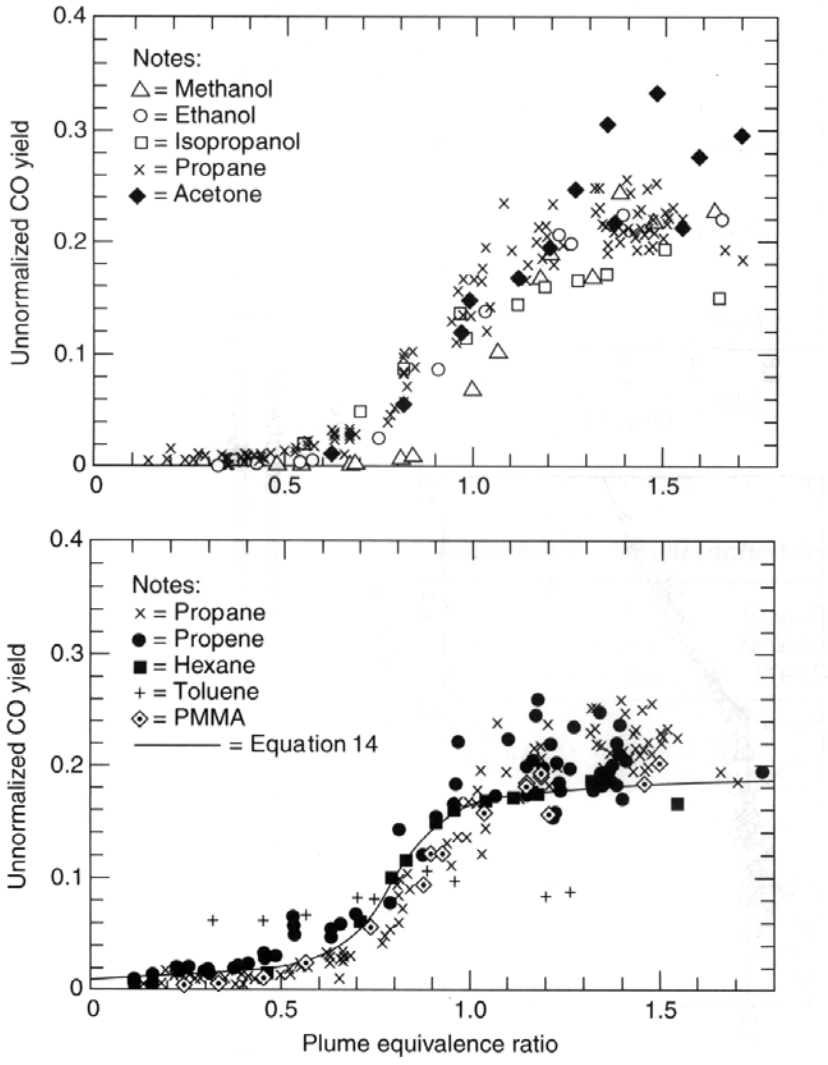

Figure 1-1: Unnormalized carbon monoxide yields as a function of the plume equivalence ratio for gaseous, liquid, and solid fuels studied by Beyler [1983] under a hood. (Taken from Gottuk *et al.* 2002)

Tewarson [2002] performed a series of tests in the ASTM E2058 fire propagation apparatus and in the Fire Research Institute's enclosure. The Fire Research Institute enclosure was a 0.022 m^3 enclosure measuring 0.25 m by 0.25 m and 0.35 m high. Tewarson [2002] presented the data as a ratio of species yields for ventilation-controlled

(vc) to well-ventilated (wv) fires. Tewarson [2002] concluded, from the study, that the ratios of oxygen and carbon dioxide were independent of the chemical composition of the materials, while the ratios of carbon monoxide and hydrocarbons did exhibit a dependence on the chemical structure of the materials. This agrees with the findings of Beyler [1983] who reported that normalized carbon monoxide yields had a fuel dependency. Tewarson [2002] proposed the following relationship for calculating the carbon monoxide yields.

$$\frac{\left(Y_{co}\right)_{vc}}{\left(Y_{co}\right)_{wv}} = 1 + \frac{a}{\exp\left(2.5\,\phi^{-\xi}\right)} \qquad (1\text{-}2)$$

where a and ξ are coefficients which are material dependent, see Tewarson [2002]. No values for the coefficients for propane were reported by Tewarson. Similar correlations were proposed for the other species.

In another publication, Tewarson [1984] reported the results for wood crib fires conducted in a special small-scale test apparatus at Factory Mutual Research Corporation (FM) along with results from three other studies. The results from the three studies consisted of wood crib fires in seven different enclosures, ranging in volume from 0.21 to 21.8 m^3. The enclosures had single and dual horizontal and vertical openings. Based on the results, Tewarson concluded that the global equivalence ratio was a useful parameter for the correlation of species yields for ventilation controlled fires; although the reported data ranged for equivalence ratios between $0 < \Phi < 5.0$, i.e. ventilation and fuel controlled fires.

Gottuk [1992] performed scaled experiments using a special test apparatus that separated the incoming and exiting flows and generated upper layer gas temperatures similar to those obtained in actual post flashover fires. The test apparatus consisted of a 1.2 m by 1.5 m cross-section by 1.2 m high fire chamber, with a 1.2 m by 1.5 m by 0.3 m high air distribution plenum below the fire chamber. The test apparatus was designed so

air was entrained into the compartment through a fixed diameter inlet duct located at the base of the compartment and exhaust gases were vented through a variable opening in the upper frontal portion of the compartment. This allowed air to be entrained into the base of the fire over the entire circumference. The area of the exhaust vent ranged between 404 cm^2 and 1615 cm^2. The experiments were performed using liquid *n*-hexane in circular pans ranging in diameter from 15 to 28 cm located in the center of the compartment. With this test setup, Gottuk simulated an ideal two-layer system, in which the actual air mass flow rate into and combustion species out of the compartment could be determined directly.

Gottuk [1992] reported that based on a series of measurements within the upper layer, a well-mixed, uniform layer existed; and therefore all measurements were performed by positioning a sampling probe horizontally 0.13 m into the compartment through the center of the exhaust vent. The test apparatus represented more of an idealized two-layer system, a scaled-up hood experiment, than a typical compartment scenario. Similar to free burning open fires, air entrainment into the fire occurred via the full perimeter of the fire. In addition, the well-mixed upper layer that developed prior to being vented, was similar to the exhaust hood experiments performed by Beyler. Therefore, good correlation between the species levels and the global equivalence ratio was expected and indeed seen, Figure 1-2.

Bryner *et al.* [1994] performed tests within a $^2/_5$-scaled ISO 9705 standard compartment, measuring 0.98 m by 1.46 m by 0.98 m high. A single doorway was located in the center of the short wall measuring 0.48 m wide by 0.81 m high. The experiments were performed using a 15 cm diameter natural gas burner, located 15 cm above the floor in the center of the compartment. The heat release rates for the fires ranged between 10 and 670 kW, corresponding to global equivalence ratios between 0.1 and 1.5.

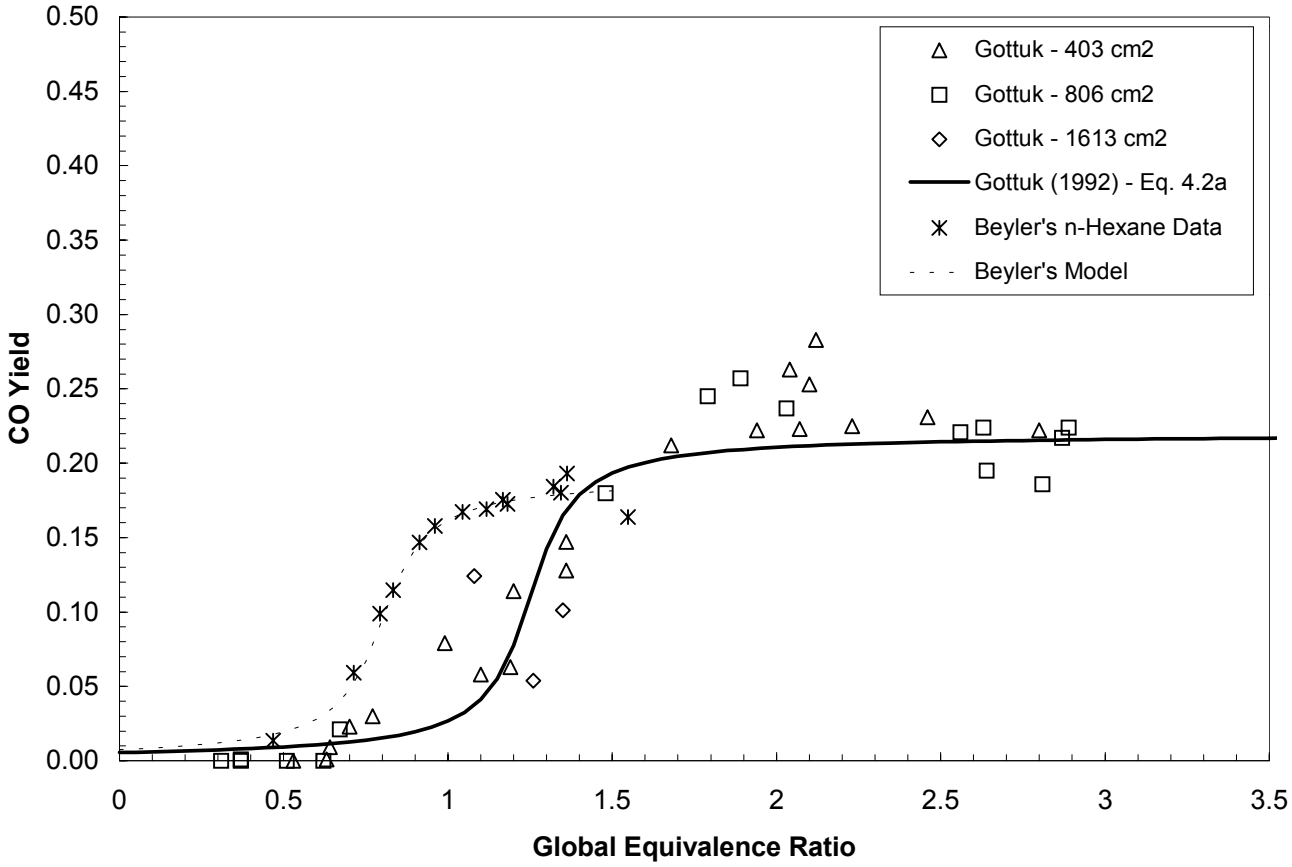

Figure 1-2: Unnormalized carbon monoxide yields as a function of the global equivalence ratio based on the work by Gottuk [1992] compared with *n*-hexane data from Beyler [1983].

A portion of Bryner's study consisted of performing horizontal and vertical scans of species measurements within the compartment. Horizontal measurements were taken 0.2 m below the ceiling for two different heat release rates, 400 kW and 600 kW. A fixed probe continuously monitored the species levels, in the front of the compartment (0.29 m from the left wall, 0.1 m in from the front, and 0.1 m below the ceiling). The data, presented as species concentrations versus time, are shown in Figure 1-3 and Figure 1-4 for the 400 kW and 600 kW fires respectively.

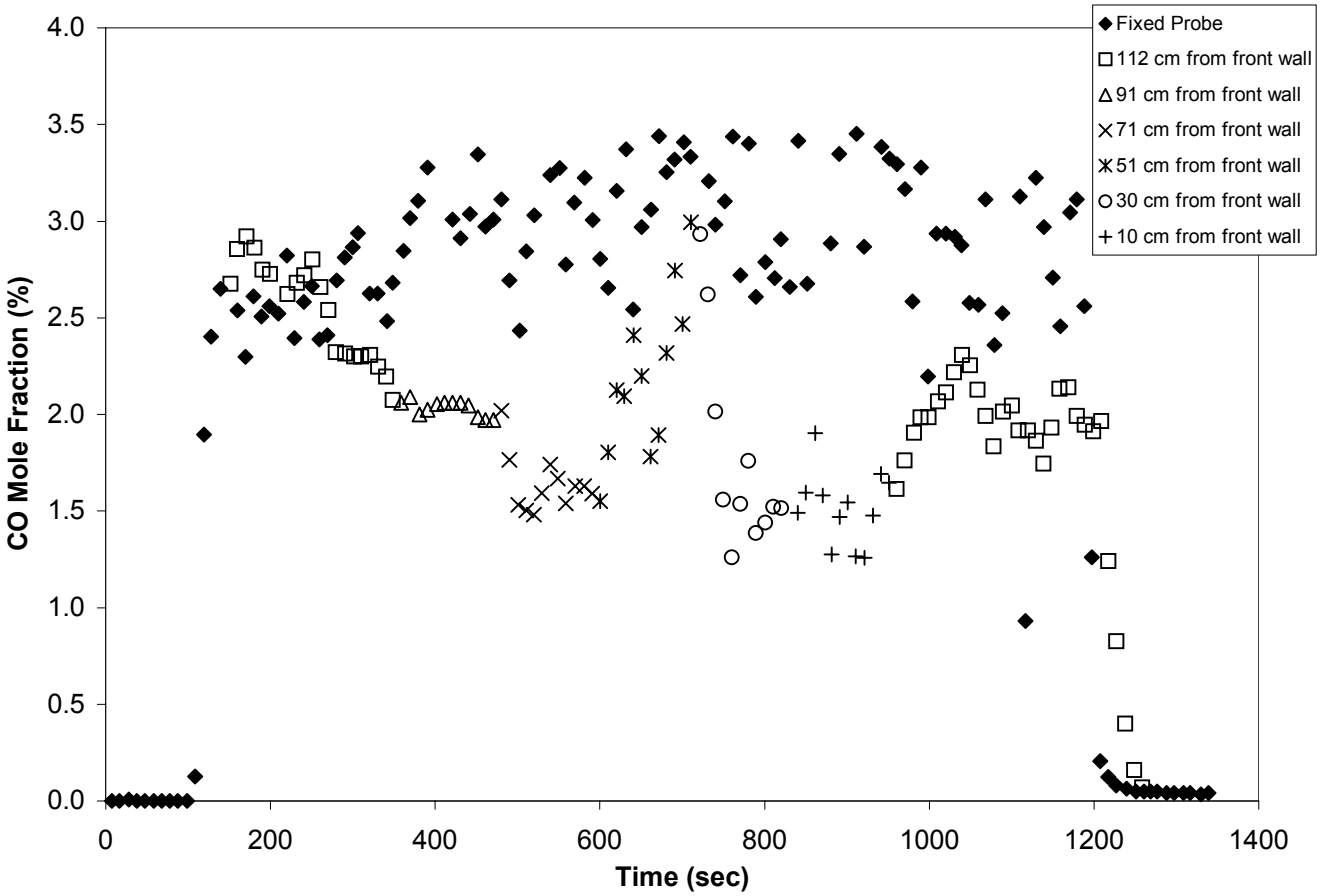

Figure 1-3: Horizontal mapping of carbon monoxide concentration data for a 400 kW fire, $\phi = 0.8$. (Bryner *et al.* [1994])

As can be seen, horizontal variations exist within the compartment for both heat release rates. High concentrations of carbon monoxide, between 3.0 % and 4.0 %, are reported for both heat release rates. For the 400 kW fire the measured CO concentrations vary between 1.0 % and 3.0 % depending on the horizontal distance from the front wall. Data for the 600 kW fire indicate fairly uniform CO concentrations within the compartment at this elevation. Both data sets show a region of high CO at a horizontal distance of 0.51 m from the front of the compartment, this is attributed to the location of the natural gas burner, which was positioned 0.71 m from the front wall.

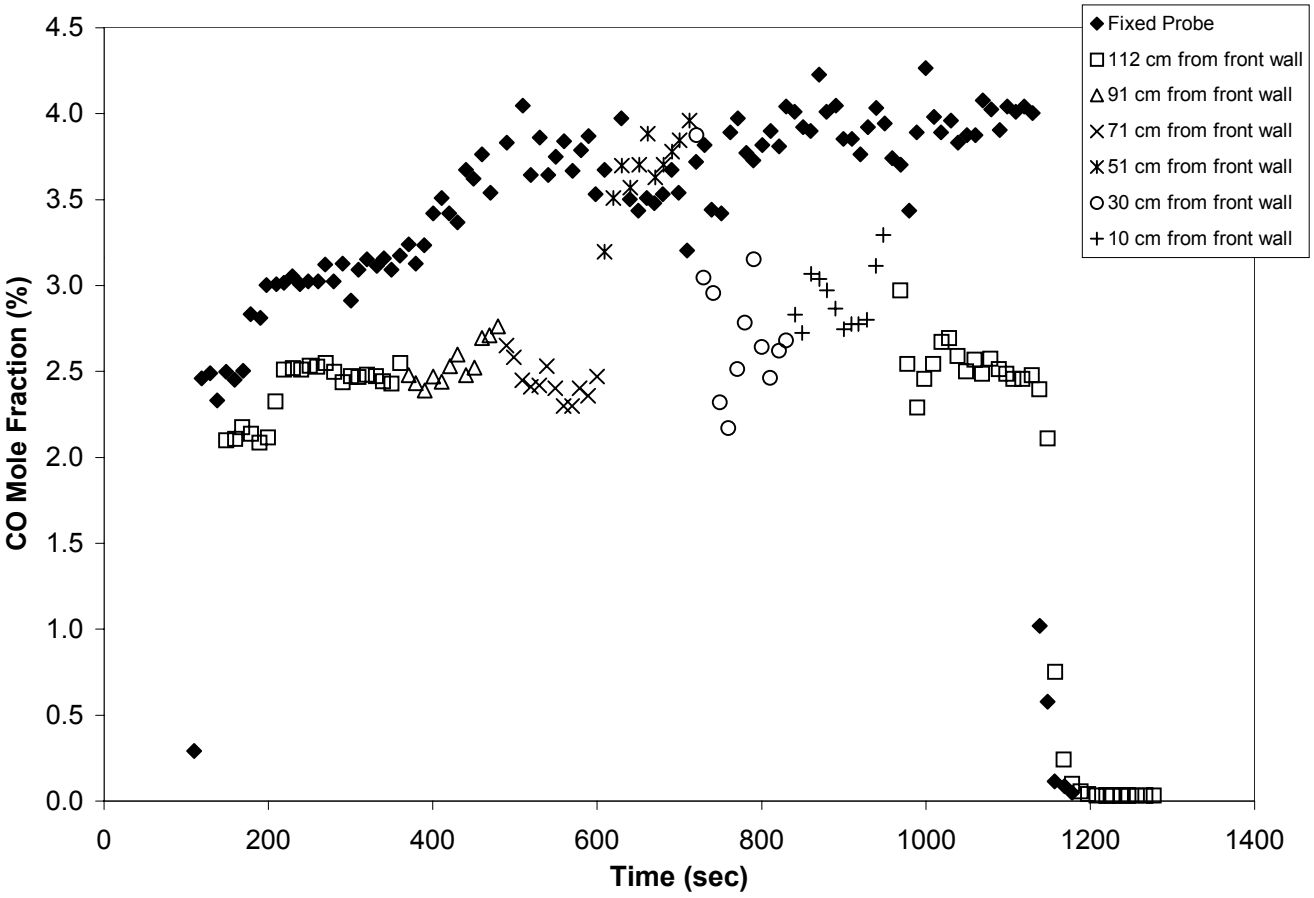

Figure 1-4: Horizontal mapping of carbon monoxide concentration data for a 600 kW fire, $\phi = 1.3$. (Bryner *et al.* [1994])

Data for vertical variations in the species levels were presented by Bryner *et al.* [1994], for 250 kW and 600 kW fires. The probe was positioned inside the doorway and moved vertically from top to bottom. The data are shown in Figure 1-5 and Figure 1-6 for the 250 kW and 600 kW fires respectively.

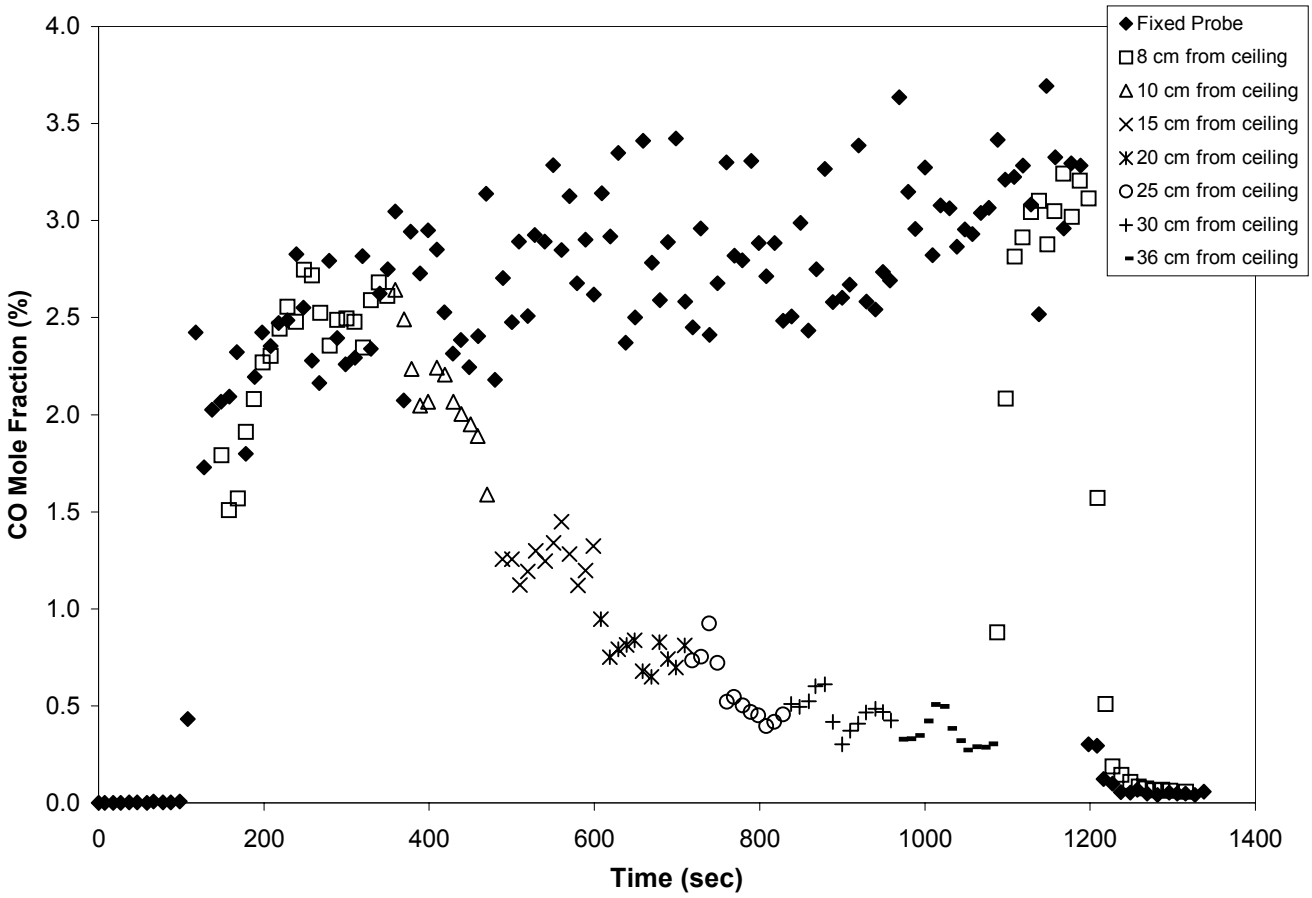

Figure 1-5: Vertical mapping of carbon monoxide concentration data for a 250 kW fire, $\phi = 0.5$. (Bryner *et al.* [1994])

The data indicate vertical variations in the species levels, as opposed to the typically assumed uniform composition of the upper layer. For the 250 kW fire, at distances greater than 0.15 m below the ceiling the CO levels decrease rapidly from approximately 2.5 % - 3.0 % to less than 1.0 %. For the 600 kW fire the CO levels appear to be uniform but lower, for distances between 0.15 m and 0.41 m below the ceiling, than those measured by the fixed probe.

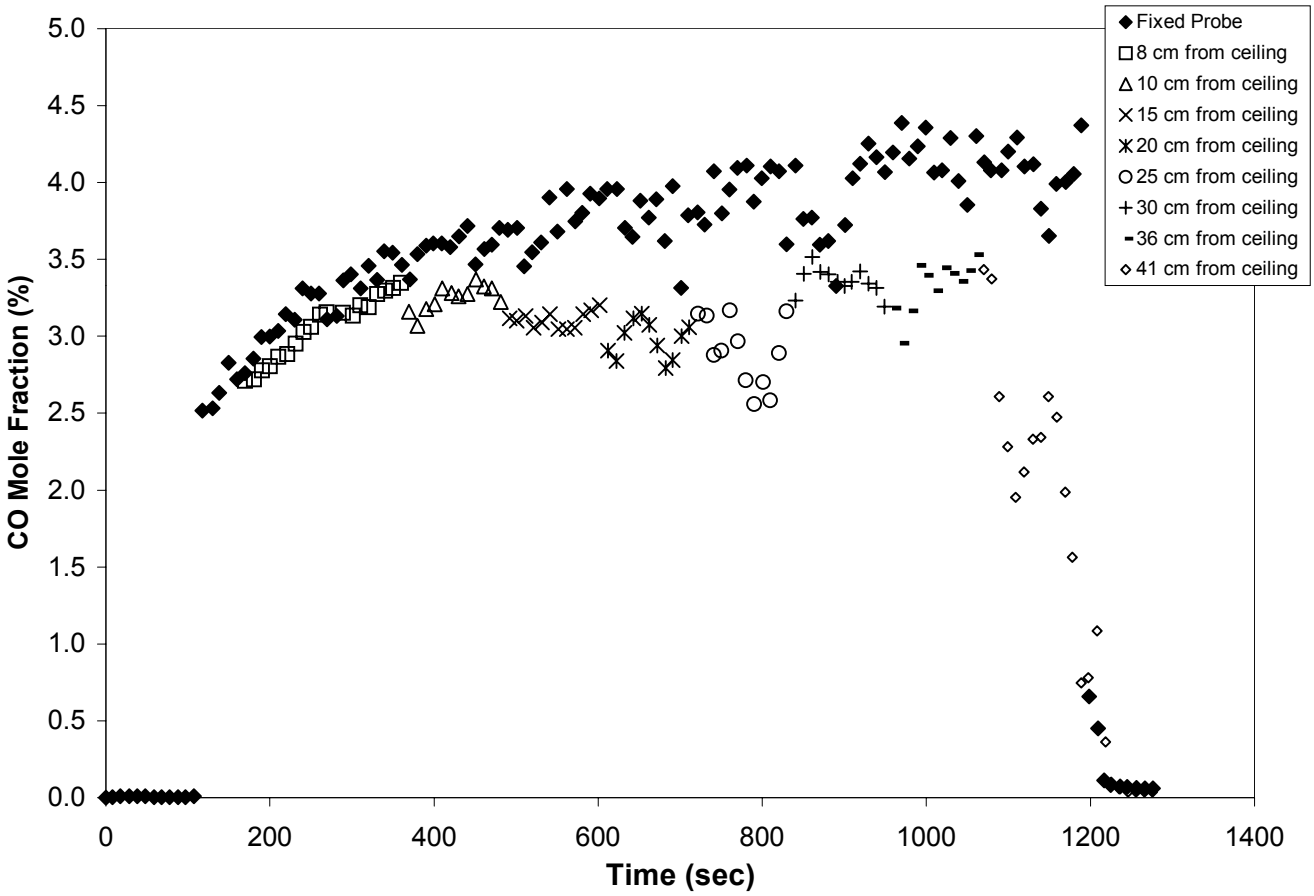

Figure 1-6: Vertical mapping of carbon monoxide concentration data for a 600 kW fire, $\phi = 1.3$. (Bryner *et al.* [1994])

Based on the species mapping, Bryner *et al.* [1994] concluded that in the upper layer gas species concentrations can vary significantly over small vertical and horizontal distances. Therefore, Bryner *et al.* [1994] stipulated that the concentrations within the compartment could not be correlated to a single global equivalence ratio for the compartment, instead local equivalence ratio would be required. The non-uniformity of the species concentrations within the compartment were attributed to the presence of a door in their compartment, which was not present in the previous compartment studies. Also, the compartment clearly presented a different reactor geometry than in the hood experiments of Beyler [1983, 1986a], Morehart [1990], and Toner [1987].

Bryner *et al.* [1994] made no attempt to correlate the species yields versus the global equivalence ratio. Therefore, species yields based on the reported mole fractions and global equivalence ratio, were calculated using Equation 1-2,

$$Y_i = \overline{X}_i \left(\frac{MW_i}{MW_{UL}} \right) \left(1 + \frac{1}{\phi \left(\dot{m}_{fuel} / \dot{m}_{air} \right)_{st}} \right) \qquad (1\text{-}3)$$

The calculated carbon monoxide yield as a function of the global equivalence ratio from Bryner *et al.* [1994] are presented in Figure 1-7, together with a data set based on measurements conducted using the phi meter reported by Pitts [1994] and the correlations from Beyler [1983] and Gottuk [1992].

The data from Bryner *et al.* [1994] was calculated using two different values of the equivalence ratio. A mistake in the code used to calculate the air entrainment into the compartment was found after the data from Bryner *et al.* was published. The error resulted in the need to apply a correction factor of $\sqrt{8}$ to the reported global equivalence ratios. [Pitts 1999] A phi-meter, developed by NIST to measure the local equivalence ratio, was used during a small number of tests. Pitts [1994] reported that good agreement was found between the local equivalence ratio and the global equivalence ratio (uncorrected). Therefore, since the reported species mole fractions are based on single point measurements, at the same location where the local equivalence ratio was measured, it is appropriate to calculate the species yields, using Equation 1-2, and the uncorrected global equivalence ratio, which should be considered the local equivalence ratio. For comparison sake only the yields were calculated using both the corrected and uncorrected equivalence ratios.

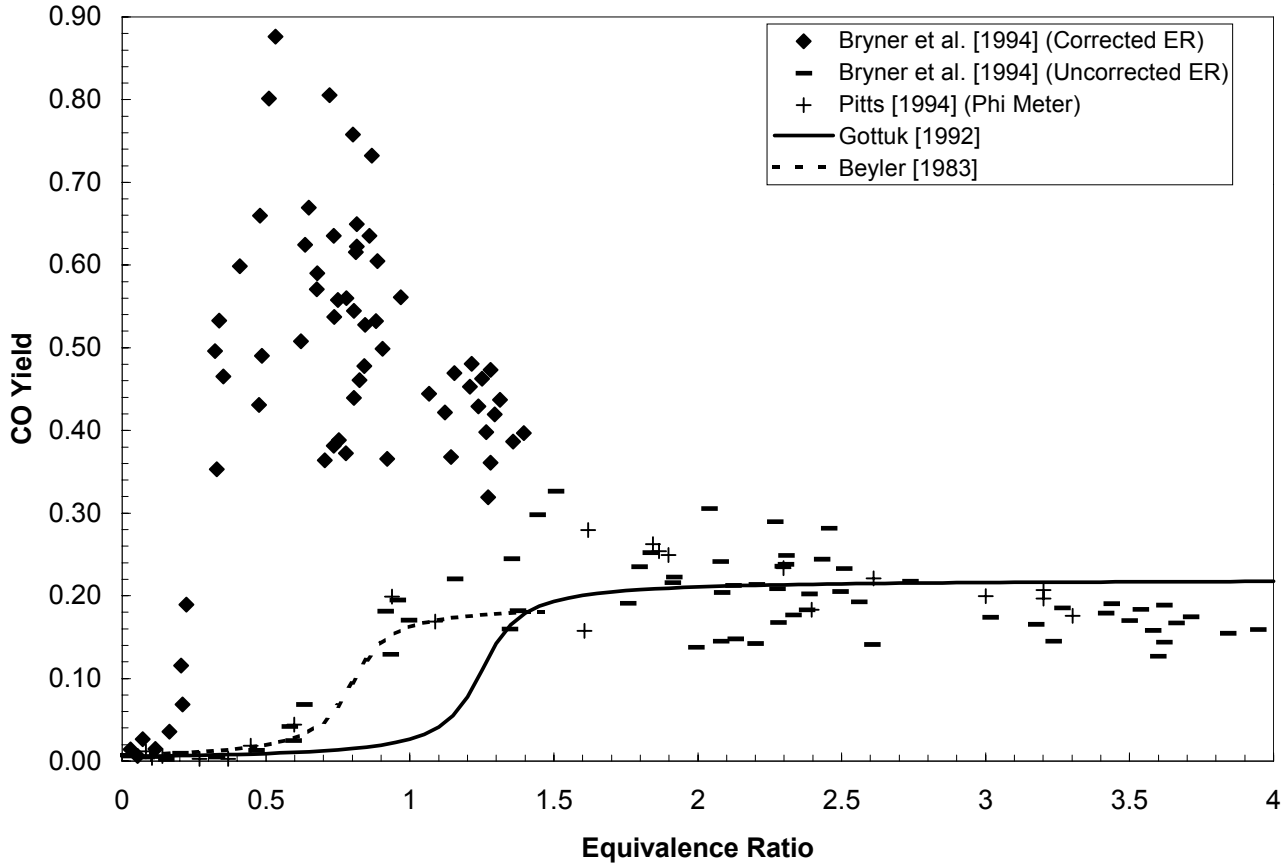

Figure 1-7: Calculated carbon monoxide yield based on reported mole fractions and global equivalence ratios from Bryner *et al.* [1994] Data presented as unnormalized carbon monoxide yields.

The data, based on the corrected equivalence ratio, do not agree with either correlation and are significantly higher for all equivalence ratios. However, the species yields based on the uncorrected, local equivalence ratio, indicate a significantly better agreement with the studies of Beyler [1983] and Gottuk [1992]. Also, good agreement is seen with the data based on the local equivalence ratio, determined via the phi-meter. Based on these observations, the species yields of oxygen, carbon dioxide, and carbon monoxide presented in Chapter 3 for comparison with the results from the present study

will be based on the species yields determined using the local equivalence ratio (uncorrected global equivalence ratio).

Recently, full-scale tests were performed at the Swedish National Testing and Research Institute, SP, [Blomqvist 2001, Lönnermark 1997] using an ISO 9705 room with solid and liquid fuel sources. The compartment ventilation was varied by maintaining the same door width and changing the sill height. Five fuel sources were used in the study, polypropene (PP), Nylon 66 (Ny), Tetramethylthiuram monosulfide (TMTM), chlorobenzene (CB), and chloronitrobenzoic acid (CNBA). Measurements within the exit plane were performed using a probe with seven equally spaced holes; the probe was positioned diagonally across the exiting flow of the opening, thereby spatially averaging any potential spatial distributions. Species measurements included O_2, CO_2, CO, NO_x, THC, HCl, HCN, NH_3, and soot. Data was reported as species yields versus the global equivalence ratio; however, based on the discussion by Blomqvist [2001] in the paper, it is believed that only single point measurements using the phi-meter were made; therefore, it would have been more appropriate to report the data as local species levels and a local equivalence ratio. The data covers a range of equivalence ratios up to 1.4. No quantitative conclusions based on the research have been published. A qualitative discussion indicated that the CO and THC yield data for polypropene and nylon had a dependence on the equivalence ratio, door geometry, fuel source, and scale. No data for O_2 or CO_2 is presented.

There is no doubt that the reacting flow field inside the compartment is different in the presence of a door compared with the, purposeful yet artificial, hood experiments or separated vent system of Gottuk [1992]. The present study was developed to determine if for realistic compartment configurations, such as that in the NIST/BFRL study and the SP study the global equivalence ratio concept could be used to develop correlations for the species levels generated during a fire.

1.3.2 Species Production and Transport from Compartment Fires

In addition to collecting data within the compartment, Gottuk [1992] and Lönnermark *et al.* [1997] collected data downstream of the compartment exit plane in the exhaust hood. This data provides a means of examining species transported from the compartment.

Data for three exhaust ventilation conditions, one for measurements within the hood (625 cm^2), referred to as hood data, and two for layer measurements (403 cm^2 and 806 cm^2), referred to as layer data, from Gottuk [1992] are presented in Figure 1-8. Data at both locations for the same ventilation conditions was not available; therefore, a direct comparison between the two measurement locations cannot be made. One would anticipate that results for the 625 cm^2 vent would lie between the other two vents, however, this is not the case. Data for the 403 cm^2 and 806 cm^2 vents show the CO mole fraction rising starting at an equivalence ratio, near 0.6 and peaking near $\phi = 2.0$ with a mole fraction of 3.5 %. The exhaust hood data peaks near $\phi = 1.5$ at 3.0 % and drops rapidly thereafter.

Agreement between the layer data and the hood data is seen for $\phi < 1.5$. The differences seen between the layer and hood data, beyond $\phi = 1.5$, can be attributed to external burning. Gottuk [1992] reported that initial flashes of external burning were first observed at an equivalence ratio of 1.4 ± 0.4 and sustained external burning occurred at an average equivalence ratio of 1.9 ± 0.3. The constant CO levels, for the layer data beyond $\phi = 1.5$, are attributed to the condition where maximum burning with available oxygen has occurred in the compartment; additional reactions will only occur externally where more oxygen is available. This is seen in the hood data where at higher equivalence ratios, lower carbon monoxide levels were measured as a result of additional reactions occurring between the exit of the compartment and the measuring location. These carbon monoxide levels do not represent the species production within the compartment.

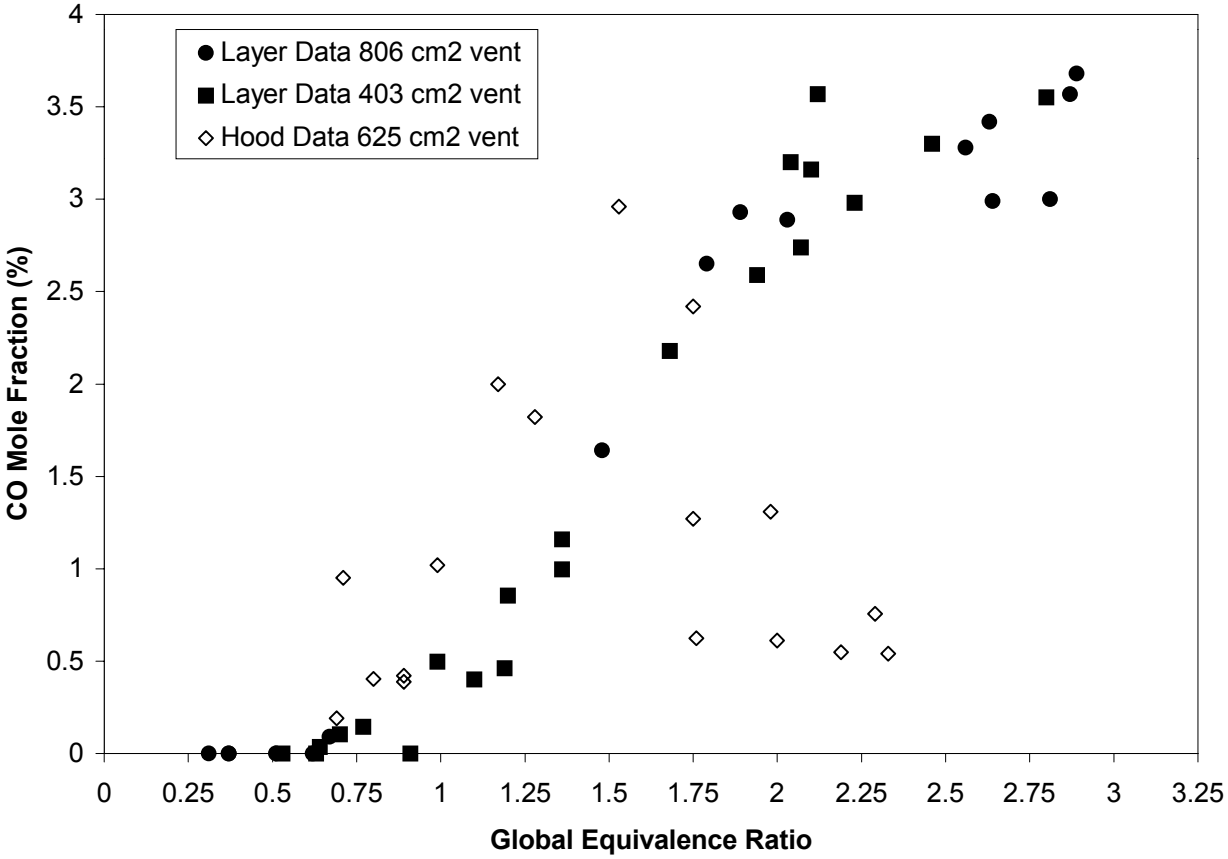

Figure 1-8: Comparison between carbon monoxide levels measured in the compartment upper layer and the exhaust hood by Gottuk [1992].

Although, Lönnermark *et al.* [1997] attempted to take measurements at both the exit plane and in the exhaust hood for each test condition, it is reported that, later examination of the data indicated possible errors in the measurements/evaluations that prohibited the comparison of the data beyond that for the chlorobenzene test series (CB6). Data for chlorobenzene at three equivalence ratios (1.51, 1.88, and 2.51) measured at the exit plane of the compartment and in the hood are presented in Figure 1-9.

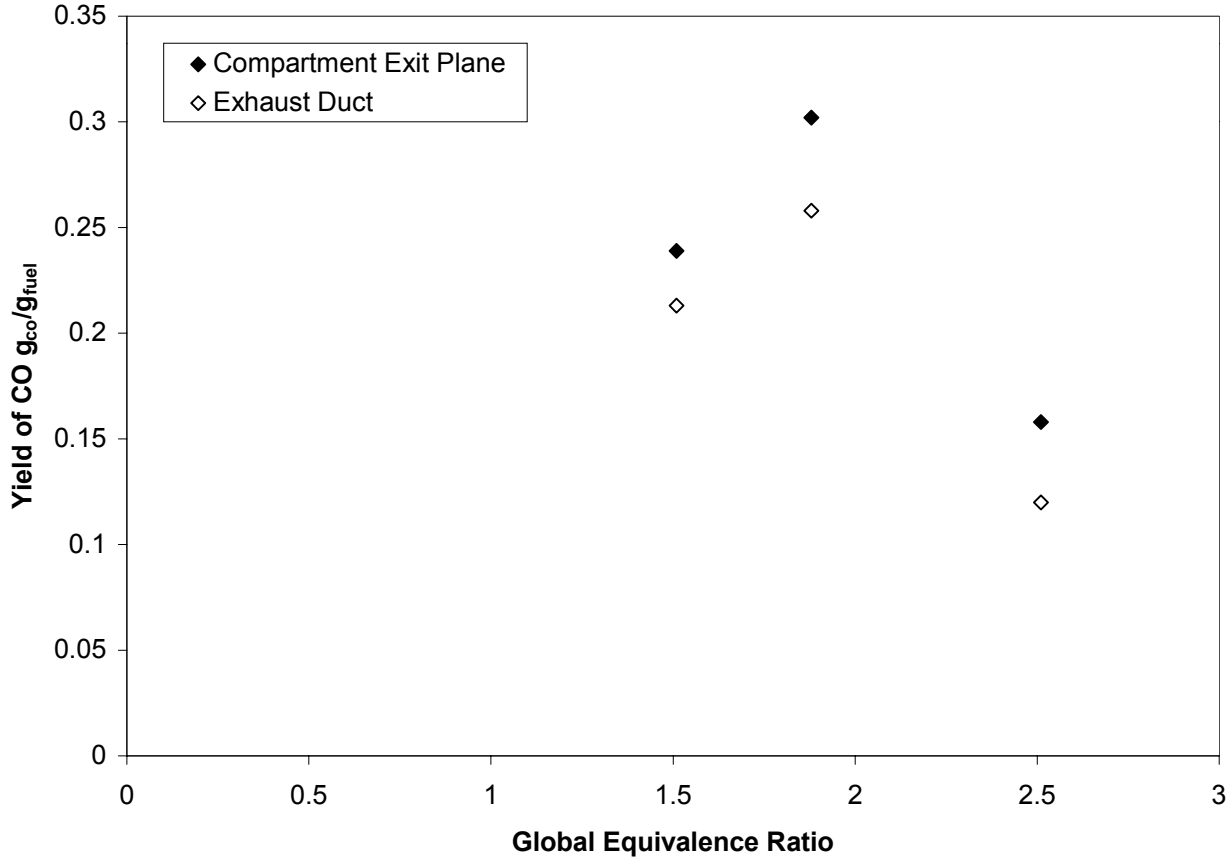

Figure 1-9: Carbon monoxide yield data measured at the compartment exit plane and in the exhaust duct for test series CB6 (adopted from Lönnermark *et al.* [1997])

The data indicates that the yields of carbon monoxide measured in the exhaust hood are lower than those measured at the exit plane. This is expected since the high temperatures and the presence of additional oxygen in the hood provided favorable conditions for the conversion of CO to CO_2. This is also seen in the measured CO_2 yields, Figure 1-10, which show higher CO_2 yields in the exhaust duct, an indication of the conversion of CO to CO_2.

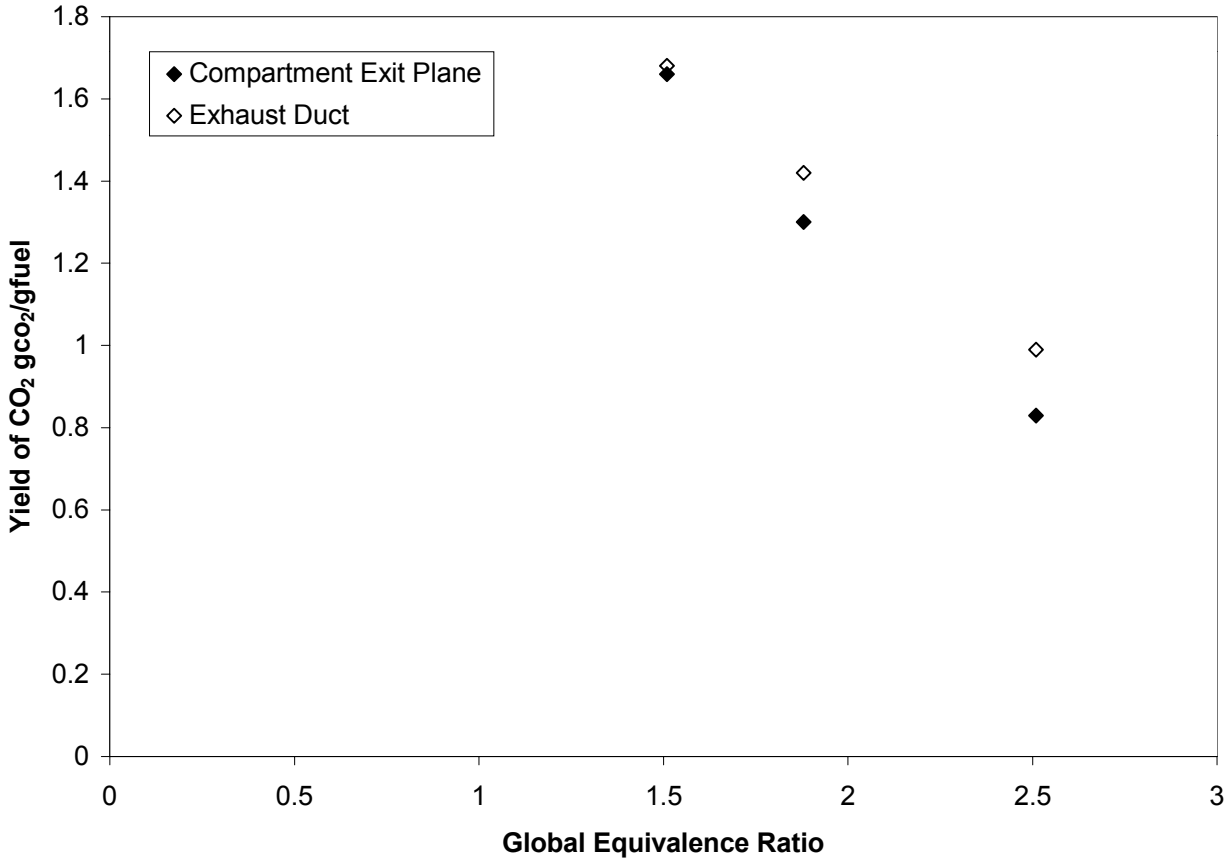

Figure 1-10: Carbon dioxide yield data measured at the compartment exit plane and in the exhaust duct for test series CB6 (adopted from Lönnermark *et al.* [1997])

Lönnermark *et al.* [1997] did not report at what equivalence ratio, if any, external burning occurred. It is expected, based on the definition of the global equivalence ratio and prior experience with compartment fire dynamics that at equivalence ratios greater than 1.0 external burning will have occurred, typically external burning occurs at even lower equivalence ratio. This data, therefore, qualitatively agrees with the data from Gottuk [1992].

In the studies of Gottuk [1992] and Lönnermark *et al.* [1997] the exiting smoke and fire plumes from the experimental compartments were unconfined. In the

experiments of Ewens [1994] and Lattimer [1996] the exiting smoke and fire plumes were confined by walls and a ceiling in the adjacent space prior to the combustion products being vented to an exhaust hood. Species measurements were taken in the adjacent space as opposed to the exhaust duct. Although, researchers in both the building [Purser 2000, Nelson, Hinkley 1984] and mining [Litton 1989, Egan 1991] industries have conducted experiments in multiple enclosure facilities, typically, the focus of the research efforts have been on the toxicological and behavioral effects of different fuel sources on the occupants downstream of the fire. Only Ewens [1994] and Lattimer [1996] examined the geometrical parameters that impacted the oxidation of combustion products in the adjacent space.

Ewens [1994] conducted experiments to investigate the evolution of compartment fire exhaust gases during transport through an adjacent space for underventilated compartment fires. The experiments were conducted with a 3.66 m long hallway connected to the compartment used by Gottuk [1992] in a head-on configuration, Figure 1-11. Ewens [1994] examined the effect of hallway fluid dynamics on the oxidation process by varying the hallway inlet and exit soffit depths.

Ewens [1994] concluded that the oxidation of exhaust gases in the adjacent space was a function of the hallway fluid mechanics, the stoichiometry of the gases entering the hallway, gas temperatures in the hallway, and the fuel vaporization rate in the compartment. Ewens noted that unburned hydrocarbons were oxidized more completely then carbon monoxide or soot, and attributed this to the low hallway gas temperatures.

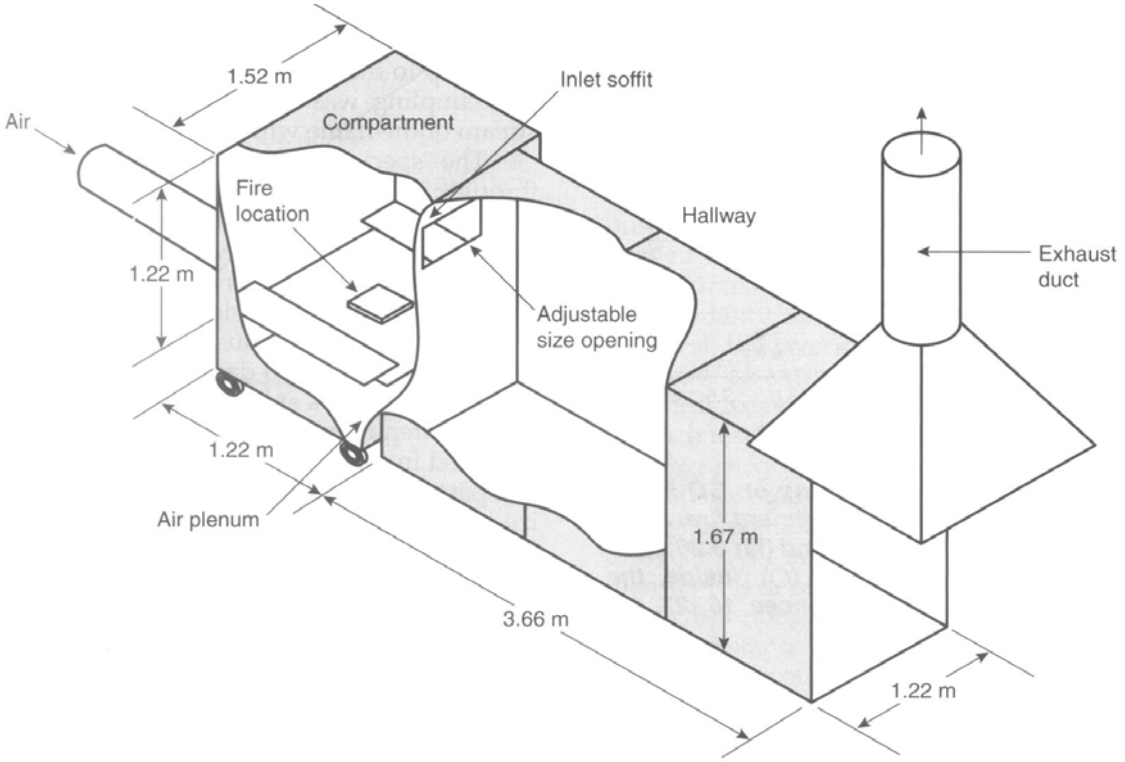

Figure 1-11: Compartment/hallway orientation for species transport study conducted by Ewens [1994]. (Image taken from Gottuk and Lattimer [2002])

Lattimer [1996] extended the work of Ewens [1994] by performing experiments with the compartment in a side-on configuration to the hallway, Figure 1-12. Lattimer varied the opening size, air inlet duct diameter, fire size, and the inlet and exit soffit heights to conclude that the existence of a deep oxygen deficient upper-layer in the adjacent space contributed significantly to the transport of fatally high levels of carbon monoxide. Lattimer also noted that, in the side-on configuration, a spatially non-uniform distribution of carbon monoxide existed in the adjacent space, higher carbon monoxide levels were measured along the wall opposite the compartment. Also, corner vortices were seen to impact the oxidation of carbon monoxide in the adjacent space.

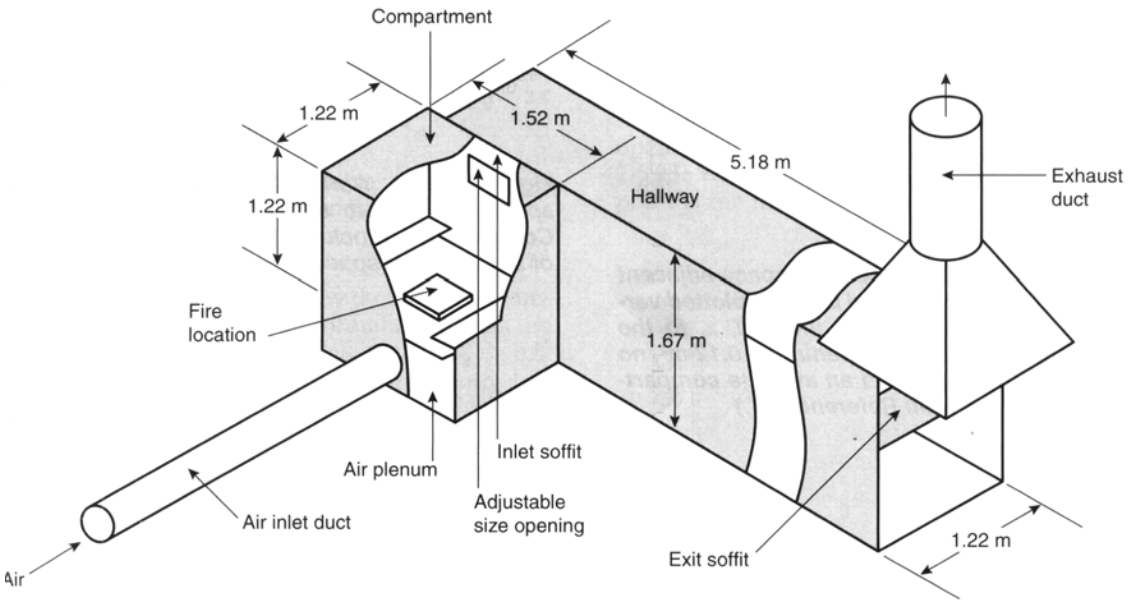

Figure 1-12: Compartment/hallway orientation for species transport study conducted by Lattimer [1996]. (Image taken from Gottuk and Lattimer [2002])

1.4 CURRENT ENGINEERING PRACTICE

The current engineering practice for predicting species levels generated in a compartment fire is best outlined by Karlsson *et al.* [2000]. Two methodologies are presented. One is based on the data from Tewarson [1995, 2002] for tests conducted in the bench-scale Factory Mutual flammability apparatus; the second methodology is based on the data from Beyler [1983]. Both methodologies require the knowledge of the equivalence ratio. The methodology based on Tewarson's data also requires the knowledge of the fuel source, while the methodology based on Beyler's data is independent of the fuel source.

Karlsson *et al.* [2000] states "Using Tewarson's data requires that his value for well-ventilated yield, $Y_{i,Wv}$, be taken from the extensive tables in the SFPE Handbook. Figure 1-13 then provides the quotient between the well-ventilated and the ventilation-

controlled case, $Y_{i,Wv}/Y_{i,Vc}$. The yield value (at a certain equivalence ratio) for ventilation control, $Y_{i,Vc}$, can then be arrived at."

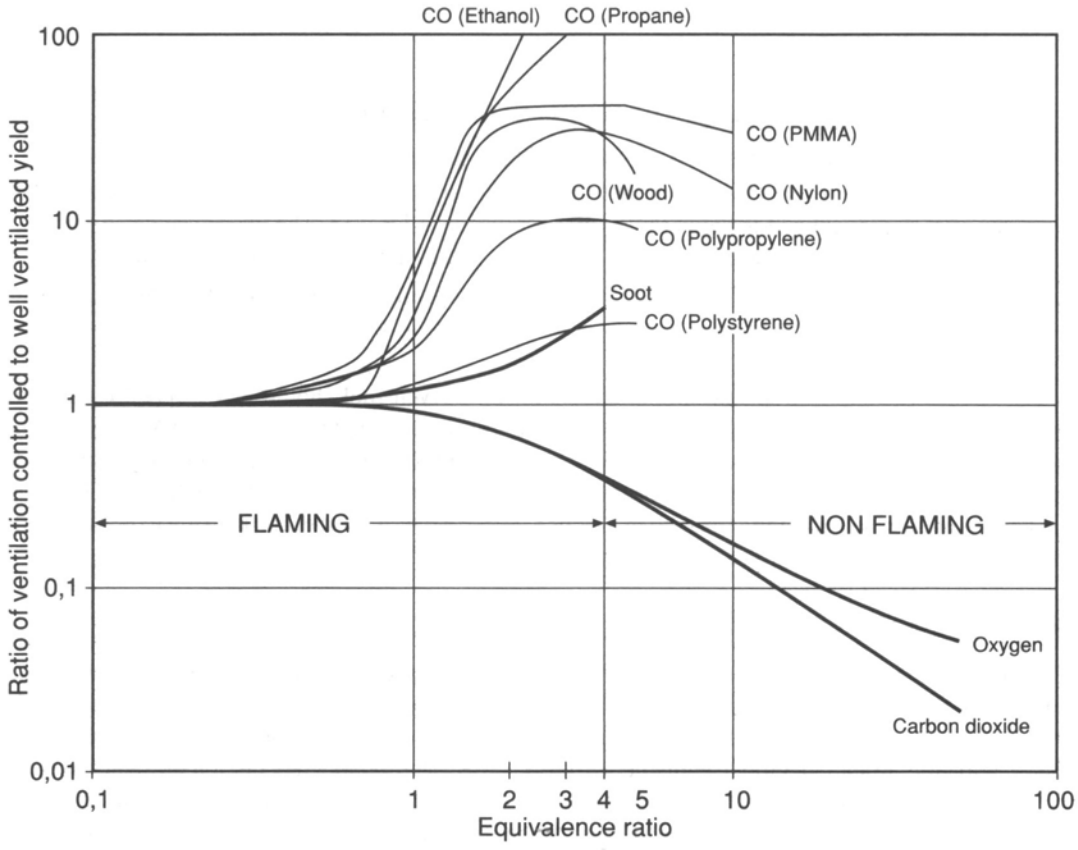

Figure 1-13: Ratio of ventilation controlled to well-ventilated species yields for oxygen, carbon dioxide, and carbon monoxide for various fuels. (Taken from Karlsson *et al.* [2000])

The second methodology is described by Karlsson *et al.* as "Beyler's data can be used by first calculating the ultimate air yield, $Y_{i,\infty}$, and using Equations 1-4 and Equations 1-5 to calculate the yields of species i." The ultimate air yield is defined by Karlsson *et al.* [2000] as being equal to well-ventilated yield and being dependent on the fuel and burning configuration.

For $\phi < 1.0$

$$\frac{Y_{CO_2}}{Y_{CO_2,\infty}} = \frac{Y_{H_2O}}{Y_{H_2O,\infty}} = \frac{Y_{O_2}}{Y_{O_2,\infty}} = 1 \qquad (1\text{-}4a)$$

and

$$Y_{CO} = Y_{H_2} = Y_{UHC} = 0 \qquad (1\text{-}4b)$$

for $\phi > 1.0$

$$\frac{Y_{CO_2}}{Y_{CO_2,\infty}} = \frac{Y_{H_2O}}{Y_{H_2O,\infty}} = \frac{Y_{O_2}}{Y_{O_2,\infty}} = \frac{1}{\phi} \qquad (1\text{-}4c)$$

$$Y_{UHC} = 1 - \frac{1}{\phi} \qquad (1\text{-}4d)$$

For carbon monoxide yields the equations are:

$$\begin{aligned} Y_{CO} &= 0 && \text{for } \phi < 0.5 \\ Y_{CO} &= 0.3\,\phi - 0.15 && \text{for } 0.5 < \phi < 1.2 \\ Y_{CO} &= 0.21 && \text{for } \phi > 1.2 \end{aligned} \qquad (1\text{-}5)$$

It is important to note that Karlsson *et al.* [2000] have a disclaimer which states "Although the generality of the experimentally derived yield data are not well established, they offer the best way to estimate species concentrations" prior to

presenting either methodology for predicting species levels generated in compartment fires.

An alternative method to those presented by Karlsson *et al.* [2000] is given by the British Standard on Fire Safety Engineering, DD240: Part 1: 1997, a performance based fire protection code prepared by Technical Committee FSH/24. A method for determining carbon monoxide generation rates is presented in Section 11.6.12. The standard provides the following equation for determining the carbon monoxide production rate from a fully ventilated fire.

$$\dot{m}_{co} = 0.013\, \dot{m}_{fuel} \qquad (1\text{-}6)$$

In the companion publication, British Standard DD240: Part 2:1997, which discusses the limitations of the equations presented in Part 1, it is written, in regards to the applicability of Equation 1-6, that "It is important to establish whether the fire is well ventilated or not. Without this qualification, CO generation may vary within a factor of 100." No methodology or guidance for determining carbon monoxide generation from under-ventilated compartment fires is provided.

1.5 OBJECTIVES OF RESEARCH

Understanding the phenomena controlling the levels of carbon monoxide produced and transported to adjacent spaces during enclosure fires would significantly increase occupant safety in both the building and mining industries. Furthermore, it is desirable to be able to predict these levels based on physical parameters like fuel mass loss rate and air entrainment rate through various vents based on geometric and thermophysical properties. These physical parameters can then be cast as non-dimensional groups like the global equivalence ratio (GER), which serves as the prime experimental parameter in the present study.

The objectives for the research were:

- Evaluate the species generated, oxidized, and transported from compartment fires with prototypical features.
- Determined the effects of geometrical parameters of the compartment and hallway on species generation, oxidation, and transport.
- Develop useful predictive tools for species formation in and transport from a compartment into an adjacent space.

CHAPTER 2

EXPERIMENTAL APPARATUS AND PROCEDURE

2.1 INTRODUCTION

This chapter describes the experimental apparatus, setup, test procedure, and data reduction principles used in the study reported. The chapter is divided into three sections: 1) experimental apparatus, 2) data reduction calculations and procedure, 3) experimental procedure.

2.2 EXPERIMENTAL APPARATUS

2.2.1 Scaled Test Compartment and Concrete Enclosure

The experiments were performed in a compartment whose outside dimensions were scaled to be geometrically equal to a half-scale ISO 9705 standard compartment, Figure 2-1. The compartment was constructed of a steel skeleton with a steel sheet skin to insure that the compartment walls were airtight. The compartment frame dimensions were 1.22 m wide by 1.83 m deep by 1.22 m high, the actual interior compartment dimensions were 1.17 m wide by 1.78 m deep by 1.17 m high. The compartment was lined with 25.4 mm (1 inch) thick Thermal Ceramics M-board. The baseline doorway dimensions were scaled based on dynamic flow similarity (ventilation and residence time parameters) to insure that the velocities and residence times of the gases within the compartment were scaled appropriately as well. [McKay 2002]

Four ventilation conditions were examined; the area of the openings were 0.06 m^2, 0.15 m^2, 0.27 m^2, and 0.54 m^2. Maintaining a fixed doorway height of 0.82 m, while changing the doorway width generated the four ventilation conditions. The width of the four ventilation conditions were 0.076 m, 0.165 m, 0.33 m, and 0.66 m and are presented as sliver, narrow, baseline, and wide doorways respectively. The four ventilation

conditions influenced the flow and mixing patterns in the compartment. In order to allow the formation of an upper layer, a 0.4 m deep soffit was used above the door.

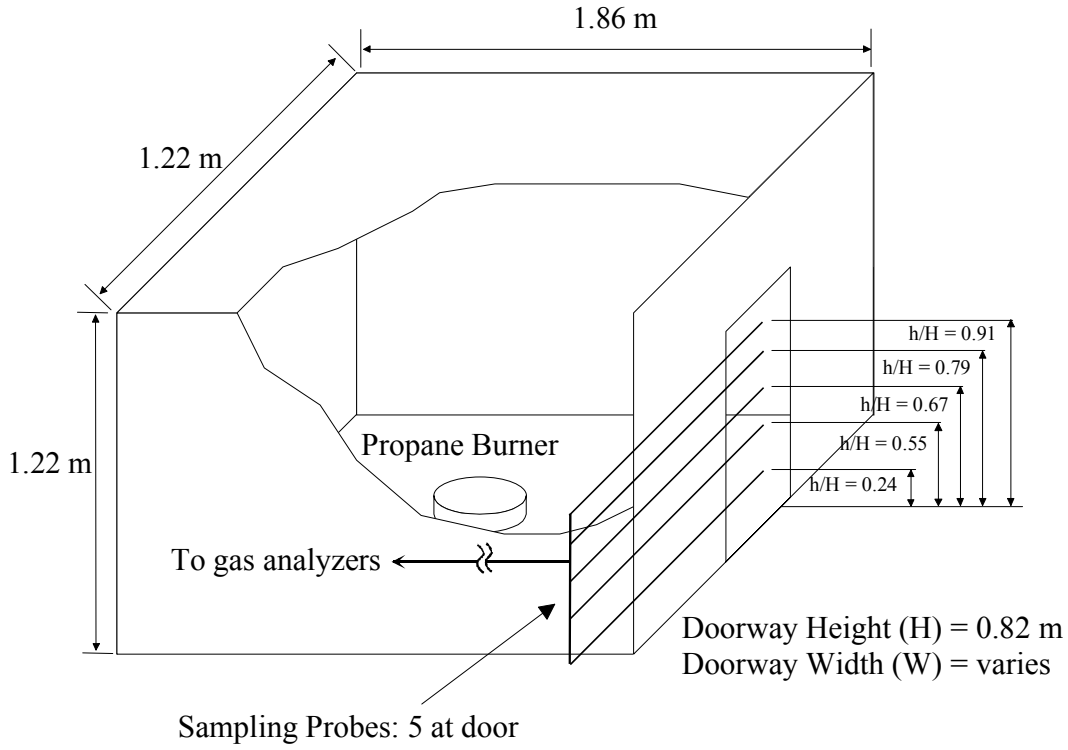

Figure 2-1: Scaled ISO Compartment

The test compartment was located in a concrete enclosure with a partial ceiling. The concrete enclosure measured 3.1 m wide by 3.05 m deep, by 2.84 m high. A steel ceiling covered the front part of the enclosure, while the back 0.81 m was open. The enclosure consists of a large roll-up door, measuring 2.44 m wide by 2.03 m high and a standard door on the opposite wall. During all tests the standard door remained closed in an effort to eliminate any cross wind effects or forced ventilation effects due to the wind. The test compartment sits slightly off-center in the concrete enclosure, a plan and side view of the facility is shown in Figure 2-2.

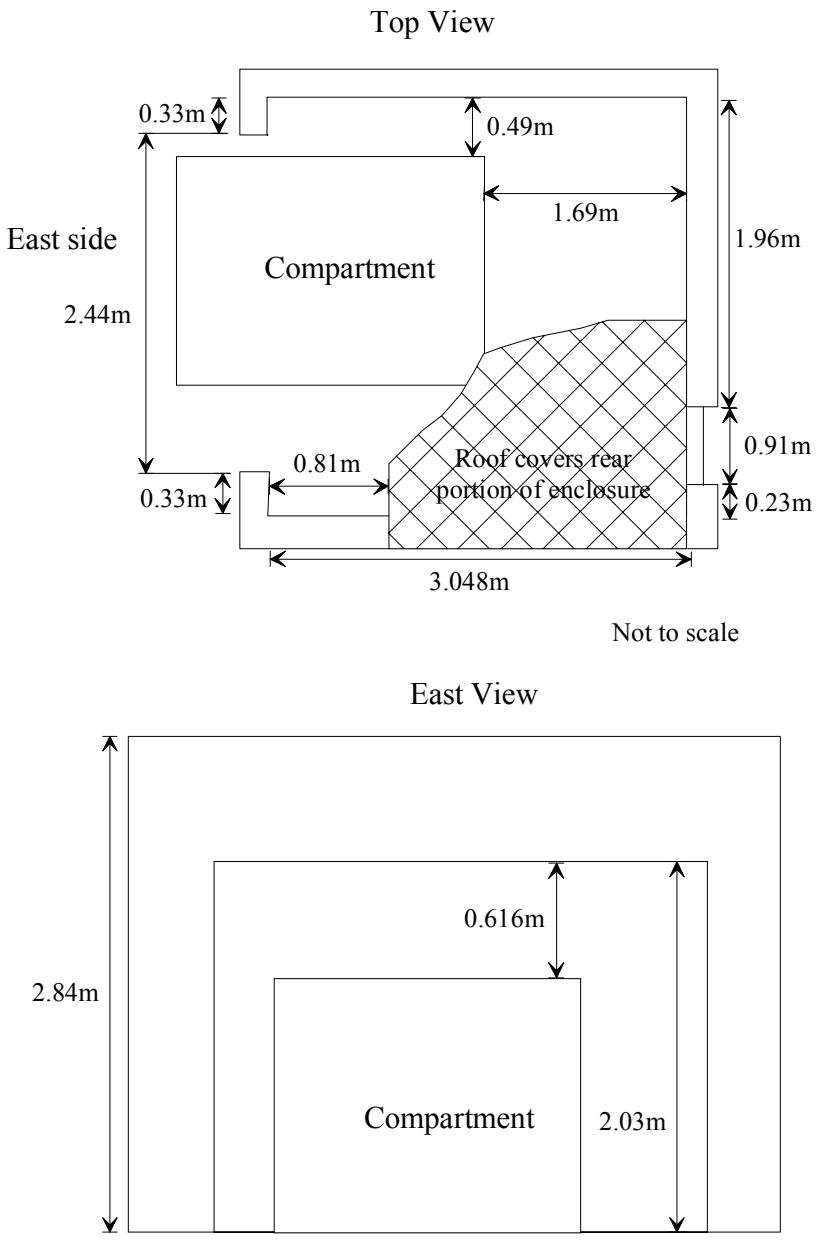

Figure 2-2: Plan view of test compartment and concrete enclosure.

2.2.2 Hallway

The species transport phase was performed with a hallway connected to the compartment in the head-on configuration, Figure 2-3. The hallway was designed to have a cross-sectional area equal to that of the compartment, 1.2 m wide by 1.2 m high and a length of 6.1 m. The hallway walls were constructed of a steel frame used to support the wall panels, which were 25.4 mm thick Thermal Ceramics M-board fiberboard.

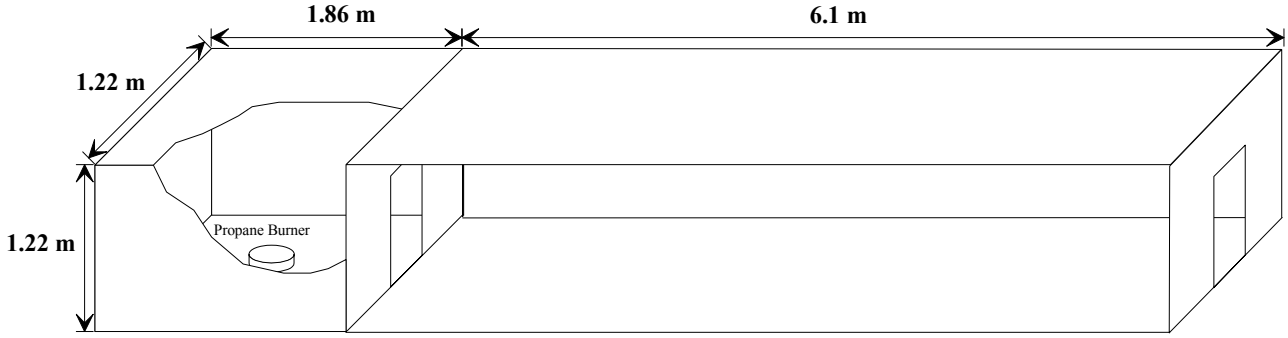

Figure 2-3: Compartment/hallway design

The ceiling was constructed of panels measuring, 1.2 m by 0.91 m. Each panel was constructed of one layer of fiberboard and a layer of dry wall. Three angle irons evenly spaced, on each panel, provide support and rigidity and provide a means for connecting one ceiling panel to another.

The floor of the hallway consisted of fiberboard panels laid over the concrete foundation of the laboratory facility.

The end of the hallway was designed in a manner allowing various ventilation conditions to be examined. The degree of air entrainment into the hallway could be controlled by leaving the end of the hallway fully open, installing different soffits, and/or different doorways.

2.2.3 Fume Hood

A 1.5 m by 1.5 m fume hood was situated directly over the exit of the compartment to collect escaping combustion gases. The hood is connected to a 0.46 m diameter duct, termed the exhaust duct, Figure 2-4. A 142 m^3/min (5000 cfm) blower connected to the exhaust duct draws the combustion gases into the hood. Louvers located just prior to the blower allow for the exhaust rate to be adjusted between 5 different settings. The settings were defined as 1 being completely closed and 5 being completely open. Quantitative values for the different flow rates at each setting were not available. The majority of the tests were performed with the louvers setting at 5. This setting provided a safe environment around the test apparatus.

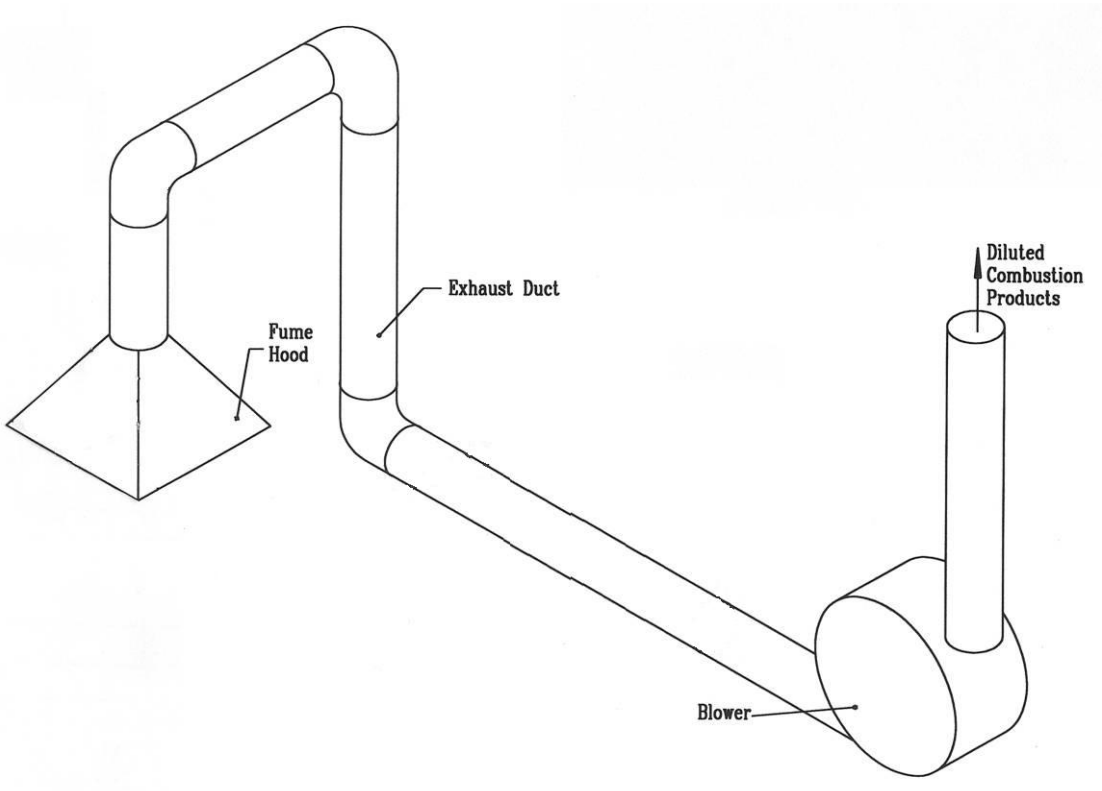

Figure 2-4: Exhaust hood schematic (Image adopted from Lattimer [1996])

2.2.4 Continuous Gaseous Fuel Supply System

The gaseous burner is a buoyancy driven, diffusion flame burner capable of the same range of fire powers as were obtained with the liquid *n*-hexane pool fires used in the past at Virginia Tech. [Gottuk 1992, Ewens 1994, Lattimer 1996, McKay 2002] The burner was 0.305 m in diameter and 0.102 m high and capable of providing fires ranging between 50 kW and 1.2 MW, although the heat release rates used during the experiments were limited to a maximum of 500 kW to prevent damage to the structural integrity of the facility. To insure that buoyancy dominated and not momentum dominated jet flames were produced, a large pressure drop between the gas inlet port and the top of the burner was required. This was achieved with the burner construction as shown in Figure 2-5.

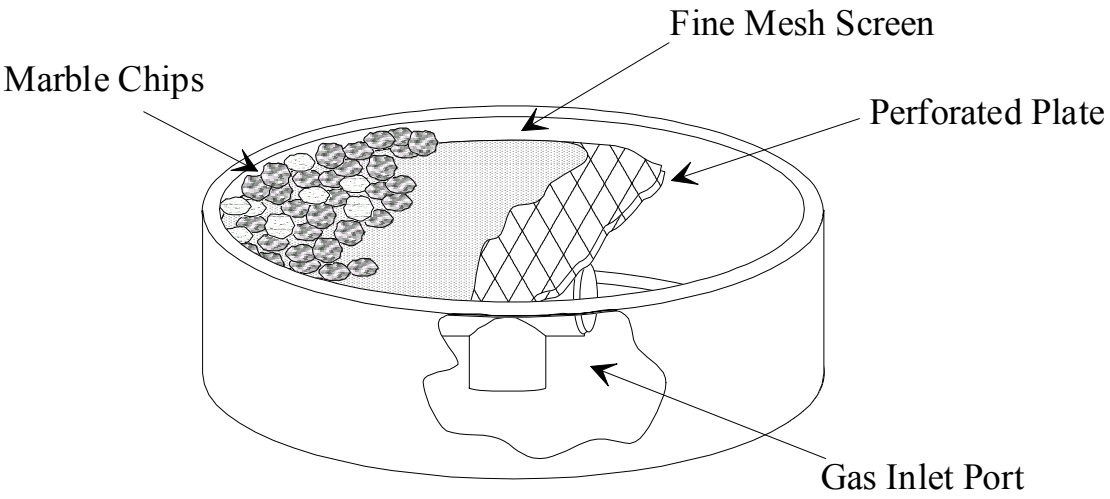

Figure 2-5: Schematic of burner

The gas flowed into a two-inch plenum in the lower portion of the burner. A perforated plate covered in a fine wire mesh was placed above the plenum and the wire mesh was covered with a 1.5-inch layer of fine marble chips. A schematic of the fuel supply and metering system, consisting of a fuel tank, control panel, and the burner, is shown in Figure 2-6.

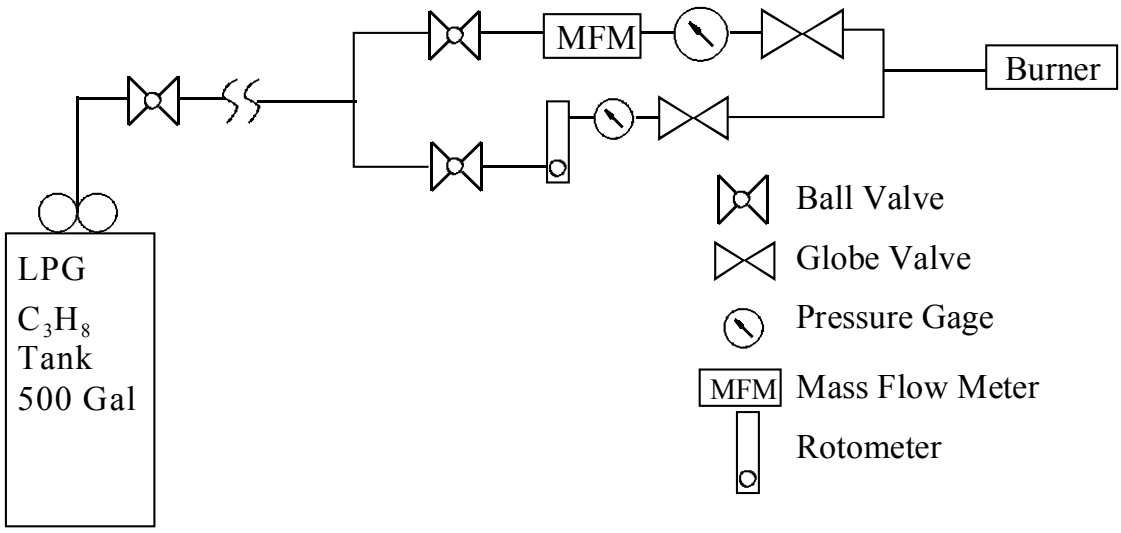

Figure 2-6: Continuous gaseous fuel system.

The required flow rates of propane were in the range of 36 slpm to 360 slpm for fire sizes between 50 kW and 500 kW respectively. The large flow rates require the use of a large propane tank to prevent the tank and the lines from freezing (Joule-Thomson effect); therefore a 500-gallon LPG tank was installed. The gas pressure was regulated at the outlet to a maximum of 10 psig. A one-inch fuel line supplied gas to the control panel at which point the gas was divided into two lines a pilot line and the main fuel line. The pilot line provided the minimum amount of fuel necessary to ignite the burner.

The burner was located at the center of the compartment with the base of the burner flush with the floor.

Conducting experiments using gaseous fuels is conducive to research in order to obtain long duration tests and repeatable results, however, the experimental conditions must also represent actual burning scenarios. In the present study the experiments were conducted using a fixed diameter burner and varying the mass flow rate of fuel to generate heat release rates between 50 kW and 500 kW. To understand if these values are representative of actual full-scale fires, a comparison with published heat release rate

data for various commodities is needed. Typically heat release rate data are reported as peak heat release rates divided by the floor area occupied by the commodity. Values for a variety of commodities reported by Nelson [1990] are listed in Table 2-1. In the present study the range of heat release rates per unit area of burner were between 685 kW/m^2 and 6849 kW/m^2 (based on the surface area of the burner, 0.073 m^2, and the heat release rates examined). Comparing these values to those listed in Table 2-1, it is seen that these values fall into the range of values reported by Nelson [1990] for typical commodities.

Table 2-1: Peak heat release rate data per floor area occupied by the commodity for various commodities. [Nelson 1990]

Description	Heat Release Rate (kW/m^2)
Fire retarded treated mattress (including bedding)	17
Mail bags (full) stored 5 ft high	400
Cotton/polyester innerspring mattress (including bedding)	565
Wooden pallets 1 ½ ft high	1420
Empty cartons 15 ft high	1700
Particle board wardrobe/chest of drawers	2550
Thin plywood wardrobe (50 in. by 24 in. by 72 in high)	6800
Wooden pallets 16 ft high	10200

2.2.5 Gas Sampling Rakes

2.2.5.1 Compartment Gas Rake

Gas sampling was performed via a five point sampling probe assembly located at the doorway of the compartment. The five sampling points were located at heights of approximately h/H equal to 0.91, 0.79, 0.67, 0.55, and 0.24, where H is the height of the doorway, 0.82 m. The height for each sampling probe was chosen to provide four sampling locations in the outflow and one sampling location in the inflow, a discussion

on the impact of the grid resolution on the calculations is presented in Appendix C. During some tests thermal expansion resulted in the probes deflection from the original heights listed above. When this occurred the probe locations were measured after the completion of the test and those values used in the data analysis. The five sampling locations provided a detailed profile of the gases exiting the compartment. Ball valves located on each sampling line were used to switch between the sampled locations.

For the baseline and wide doorway configurations, measurements were taken at three horizontal locations of w/W = 0.25, 0.5, and 0.75, where W is the width of the doorway. Due to the small width of the sliver (0.076 m) and narrow doorways (0.165 m) only measurements along the doorway centerline were performed.

2.2.5.2 Hallway Gas Rake

Determination of measurement locations along the hallway, was assisted by the Fire Dynamics Simulator [McGrattan 2000a, 2000b], executed by Floyd [2001]. Based on the modeling results accommodations for gas sampling were made at five axial locations along the hallway, y = 0.0 m, 0.61 m, 1.2 m, 3.7 m, and 6.1 m.

A specially designed seven point sampling rake was used for the data collection, including gas sampling, gas velocities, and gas temperatures, Figure 2-7. The rake consists of seven sampling points at heights of h/H equal to 0.17, 0.42, 0.5, 0.71, 0.76, 0.85, and 0.93, where H is the ceiling height, 1.2 m.

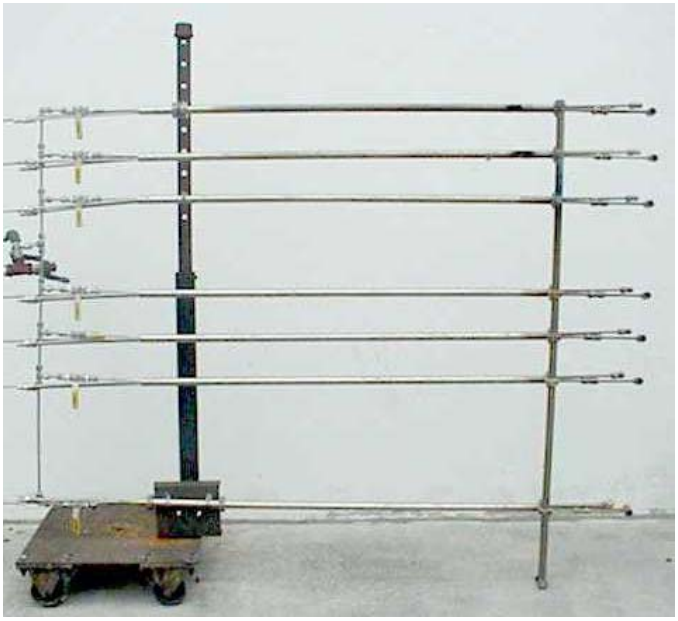

Figure 2-7: Gas sampling rake

2.2.6 Aspirated Thermocouple Rakes

The aspirated thermocouple rakes were designed and constructed based on the recommended suction velocities of Blevins et al. [1999] The thermocouple rake tubing and pump were sized based on a minimum suction velocity of 20 m/s at each inlet. The pumps used for this application were Gast model #2567 rotary vane pumps. The manufacturers pump specifications were 21.0 cfm open flow at a maximum pressure of 15 psi. The body of the rake was made of $^{3}/_{8}$-inch stainless steel pipe. The inlet ports, housing the thermocouples, were ¼-inch stainless steel tubes. For the purpose of removing moisture and soot particles in order to protect the pumps, the hot gases were cooled in a cold trap and then passed through a series of filters. Each thermocouple rake consisted of only 4 thermocouples in order to limit the size of the pump required to provide the desired velocities.

Four thermocouple rakes were used to obtain the temperature profiles in the corner of the compartment and the doorway. The body of the thermocouple rake was insulated with 37.2 mm thick Durablanket Strip from Fiberfrax, and the inlet ports were

insulted using Fiberfrax 970 Paper insulation. The insulation was used to reduce the thermal radiation loading on the inlet port tubes and the rake body.

A hot wire anemometer (AA Labs model #AN-1003) was used to determine the suction velocities at the inlet of each probe. The measured velocities, under ambient conditions, P = 690 mmHg, T = 20 °C, exceeded 30 m/s. Exact values could not be obtained since the anemometer was only calibrated between 0 m/s and 30 m/s. An estimate of the maximum velocity can be made from the pump specification data and the number of inlet ports for each rake. The Gast model #2567 rotary vane pump has a maximum flow rate of 14.5 cfm, therefore, for four sampling ports the maximum velocity is 77 m/s.

It should be noted that the hot wire anemometer values were obtained under ideal conditions in which all of the plumbing was clean and free of soot, under actual operating conditions soot accumulates in the lines and therefore reduces the suction flow rates, actual operating suction rates are not known. To maintain the best possible performance of the aspirated thermocouples, the lines were blown out with compressed air between tests.

Blevins et al. [1999] reported that with suction velocities of 20 m/s the errors between the actual and the measured temperatures in the upper layer were approximately 5 %, while in the lower layer errors as high as 20 % could be expected. It was also reported that as suction velocities increased the errors decreased. Therefore, during the fully developed phase of the fire, which is the period of most significance in this study, the measured temperatures are expected to deviate by 5 % or less from the actual gas temperatures.

ocedure

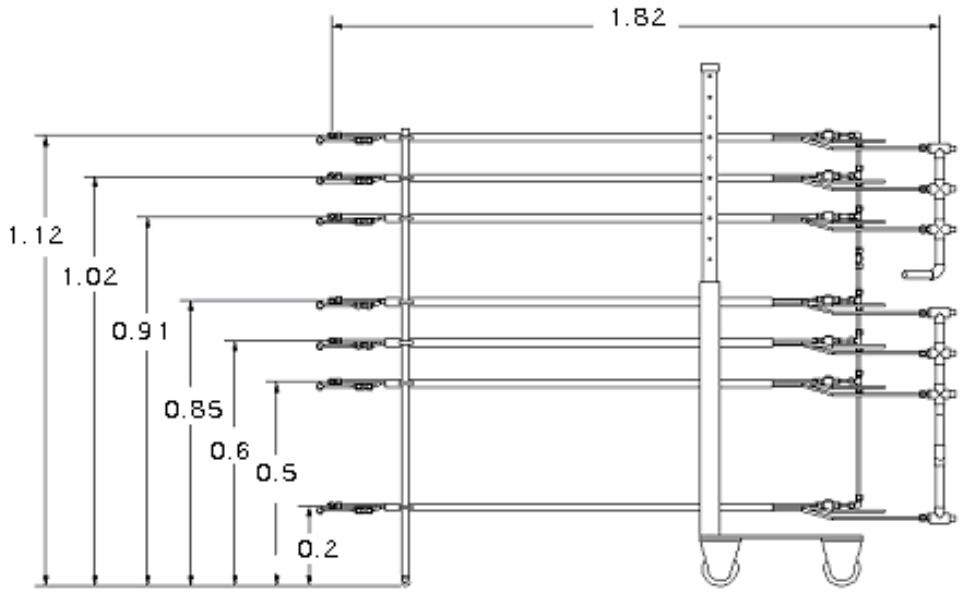

Figure 2-8: Schematic of the sampling rake with thermocouple rakes integrated into the system.

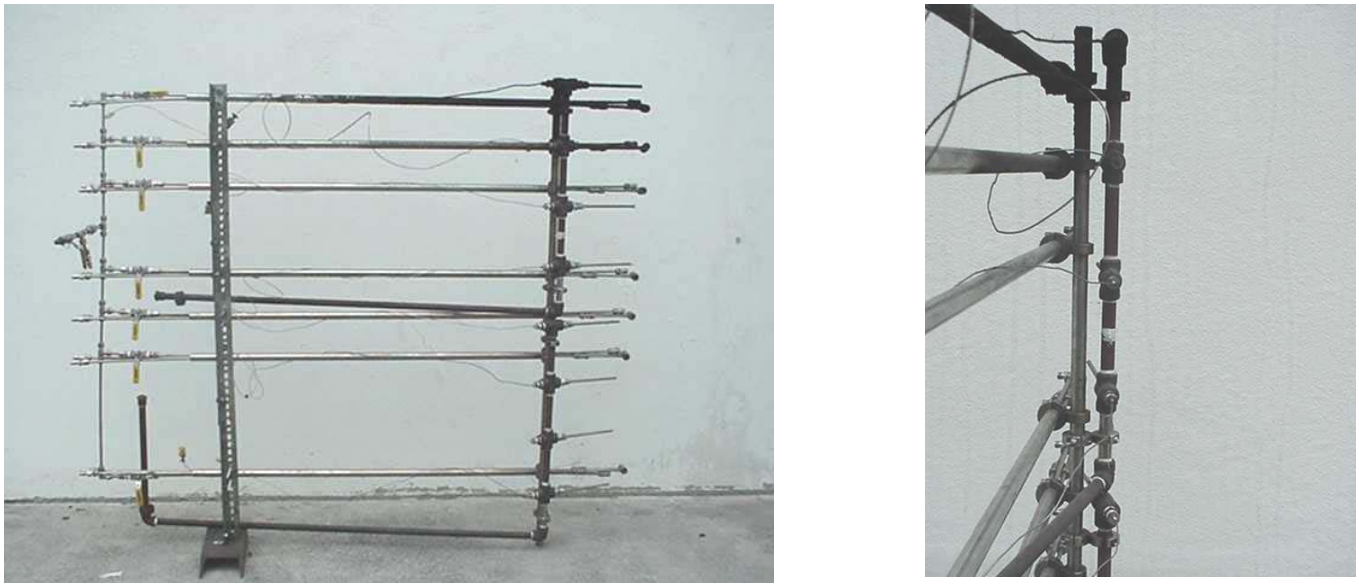

(a) (b)

Figure 2-9: Sampling rake along with thermocouple rakes connected, (a) head-on view (b) side-on view

Along the hallway, the aspirated thermocouples were designed such that both horizontal and vertical temperature measurements could be performed at each cross sectional area. Two gas sampling rakes were constructed, one for measurements within the hallway and one for measurements at the end of the hallway. For the sampling rake used in the hallway, the aspirated thermocouple rakes were integrated into the design, Figure 2-8. By combining all of the tubing, i.e. sampling probe, bi-directional pressure probe, and aspirated thermocouple probe, into one bundle, smaller openings in the hallway wall were required for the sampling rake.

For the sampling rake located at the end of the hallway, the aspirated thermocouple rakes were simply connected to the side of the sampling rake, Figure 2-9.

2.2.6.1 Thermocouple Time Constant

The time constant for a thermocouple can be determined by using a lumped capacitance heat transfer analysis,

$$\tau_t = \frac{V \rho c_p}{h_c A_s} \qquad (2\text{-}1)$$

assuming a cylindrical geometry for the thermocouple Equation 2-1 reduces to,

$$\tau_t = \frac{\rho c_p D}{4 h_c} \qquad (2\text{-}2)$$

The convective heat transfer coefficient is determined by calculating the appropriate Nusselt number (Nu), $\frac{h_c D}{k}$. Pitts *et al.* [1998] recommended the following form of the Nusselt number for flow over small diameter wires,

$$Nu\left(\frac{T_m}{T_j}\right)^a = A + B\,Re^n = A + B\left(\frac{UD}{\nu}\right)^n \qquad (2\text{-}3)$$

where T_m is the film temperature defined as $\frac{(T_g - T_j)}{2}$ and a, A, B, n are constants equal to 0.17, 0.24, 0.56, and 0.45 respectively.

The gas velocity was assumed to be 30 m/s, based on the discussion in Section 2.2.6. The thermocouple wire diameter was 0.0003 m. A Type-K thermocouple consists of nickel-chromium and nickel-aluminum wires. Properties for nickel-chromium are given as, c_p = 0.444 kJ/kg K and ρ = 8,666 kg/m^3. [SFPE Handbook, 1995] The thermophysical properties of air at three different gas temperatures are given in Table 2-2.

Table 2-2: Thermophysical properties of air [SFPE Handbook, 1995]

Air Temperature (K)	Thermal Conductivity (kW/m K)	Viscosity (m^2/s)	Nu
300	0.0000263	0.0000159	10.01
700	0.0000524	0.0000681	5.32
1200	0.0000763	0.0001629	3.67

Neglecting the temperature dependence in Equation 2-3, since the actual gas and junction temperatures are not known, the Nusselt number and time constant were determined to be 0.331 s, 0.313 s, and 0.311 s for air temperatures of 300 K, 700 K, and 1200 K respectively. Examination of Equation 2-3 indicates that the temperature effect is small. Substituting for h_c into Equation 2-2,

$$\tau_t = \frac{\rho\, c_p\, D^2}{4\, Nu\, k} \qquad (2\text{-}4)$$

it is seen that including the temperature dependence would decrease the calculated Nusselt number and therefore increase the calculated time constant. In addition, the diameter of the thermocouple wire was used for the calculations, instead of the junction diameter, which was at a minimum a factor of two larger. Repeating the calculations for the average measured bead diameter of 0.00093 m, the calculated time constants for gas temperatures of 300 K, 700 K, and 1200 K were 1.93 s, 1.84 s, and 1.85 s respectively.

2.2.7 Velocity Measurements

Velocity measurements were obtained using bi-directional probes located at each sampling location. The bi-directional probes were designed based on the probe description discussed by Emmons [1995] and McCaffrey and Heskestad [1976]. Each of the probes was connected to a Setra Inc. model 264 low differential pressure transducer. Higher velocities were expected with increased height above the neutral plane, therefore two different range transducers were used to measure the pressure difference. Three pressure transducers had a range of ± 0.1 inches of water column and two transducers had a range of ± 0.25 inches of water column, all pressure transducers had an accuracy of 1.0 % full scale. The response time of the pressure transducers was given by the manufacturer as approximately 50 msec.

Measurements of the local temperature and differential pressure allow the local velocities to be determined using the following equation, based on simple Bernoulli analysis,

$$V = C\sqrt{\frac{2\Delta P}{\rho}} \qquad (2\text{-}5)$$

where C is the flow coefficient equal to 0.93 as recommended by Emmons [1995].

The maximum corresponding velocities for each of these transducers at ambient conditions is ± 5.9 m/s for the ± 0.1 in-H_2O pressure transducer and ± 9.5 m/s for the ± 0.25 in-H_2O pressure transducer.

2.2.8 Gas Flow Train

The sample rake was connected to a series of three filters. The first filter was stainless steel wool, used to remove the coarse particulates, followed by a Balston Model 30/25 with a 100-25-DH filter element, the final filter was a Gelman Sciences Inc. glass fiber filter type A/E (47 mm).

The gas then traveled through heated Teflon tubing for 3 meters and heated stainless steel tubing for another 3 meters. The Teflon tubing section was used to allow the position of the sample probe to be adjusted as needed and for ease of routing through the lab. Just prior to dividing the gas sample into two, a second Gelman Sciences Inc. glass fiber filter was installed to trap any remaining particulates. The gas sample was then split with one half flowing through heated stainless steel tubing directly to the FID total hydrocarbon analyzer and the balance flowing through a water trap and finally to the non-dispersive infrared CO/CO_2 and paramagnetic O_2 analyzers. A series of valves and bypasses were used to maintain required flow rates and pressures for each analyzer. A schematic of the set is shown in Figure 2-10. The “downstream sampling” location was not used in these studies, but is included for completeness.

To avoid diluting the gas stream with fresh air and to protect the personnel working in the control room, the gas flow train was leak tested prior to every test and whenever the filters were cleaned. The leak test was performed by pressurizing the sample line to 20 psig with an air compressor and a series of valves at both ends of the sampling line. The pressure in the line was monitored using a pressure gage.

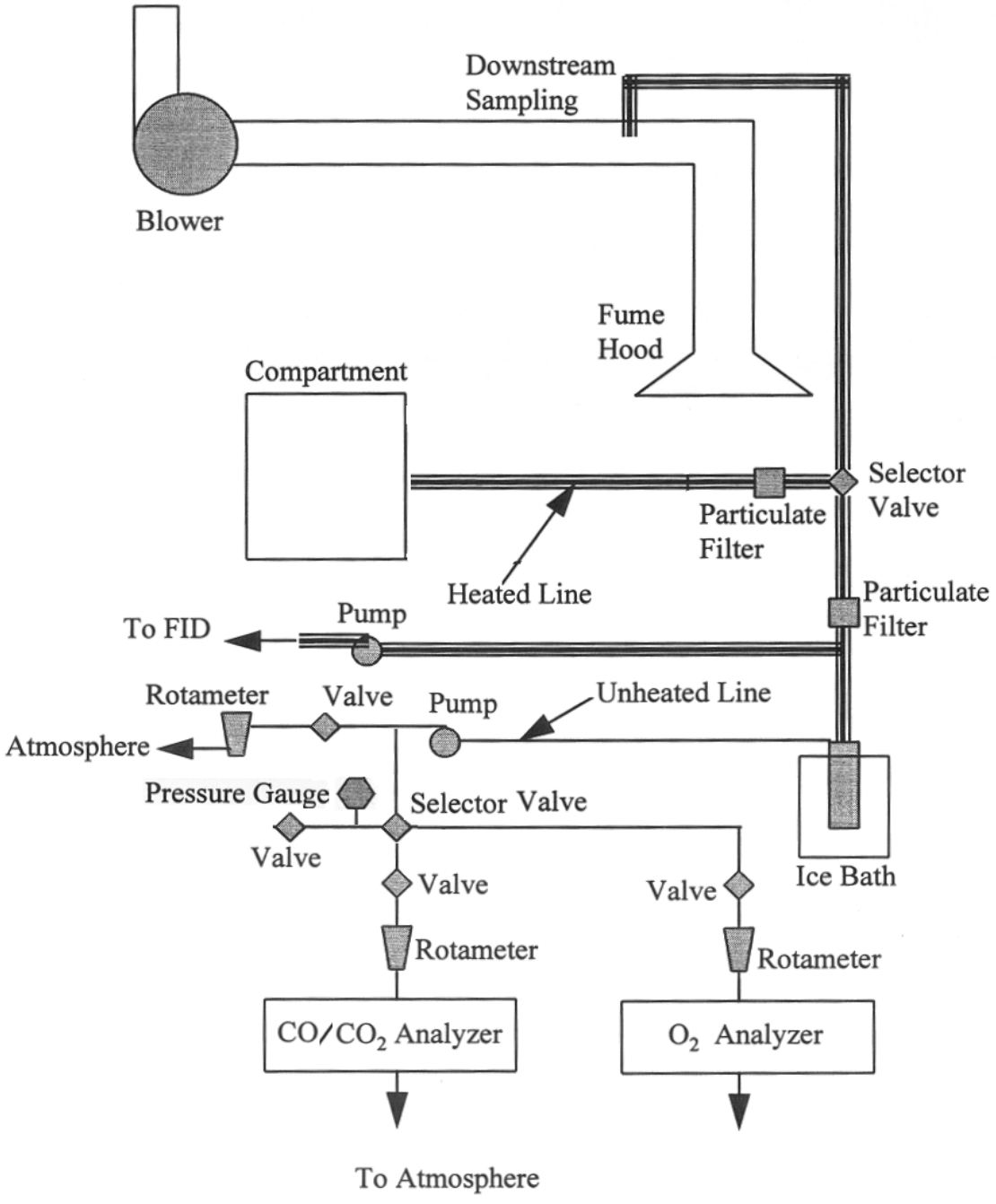

Figure 2-10: Gas flow train (Image adopted from Lattimer [1996])

2.2.9 Gas Analysis

2.2.9.1 CO and CO_2 Measurements

The CO and CO_2 mole fraction was measured using a Siemens Ultramat 6 dual channel gas analyzer. The output of the instrument is 4 mA to 20 mA, which was converted to 0 V to 5 V signal via 250 ohm resistors across the output leads. The signal was linearized with respect to the mole fraction. This linearization was performed internally using software calibration and a zero gas. An appropriate CO and CO_2 containing span gas was used to verify the calibration. Three ranges were available for each channel, two factory set and one user defined. The factory set CO ranges were 0 % to 1 % and 0 % to 5 %, and the CO_2 ranges were 0 % to 5 % and 0 % to 25 %, the user-defined option was not used. For all tests the maximum ranges were used for both species.

2.2.9.2 O_2 Measurements

The O_2 mole fractions were measured using a Siemens paramagnetic Oxymat 5E analyzer. This analyzer produced a 4 mA to 20 mA output, which was converted to a 0 V to 5 V signal. The analyzer was operated in the range of 0 % to 22 %, however a low calibration span point, 4.71 %, was used to ensure that the low levels of oxygen, expected in the measurements, were measured accurately.

2.2.9.3 Unburned Hydrocarbon Measurements

The unburned hydrocarbon wet mole fractions were measured using a Gow-Mac model #12-800 flame ionization detector (FID) attached to a Gow-Mac model #40-900 electrometer for signal processing. The FID was contained inside an oven maintained at 105 °C and used a hydrogen flame produced by a mixture of 40 % hydrogen and 60 % helium as the fuel and purified air as the oxidant.

The hydrogen flame products were vented from the oven into a cooling chamber. The cooling chamber was kept cool using a cooling coil at –10 °C that ran from the

refrigerated circulating bath. For safety reasons, a hydrogen detector was located within the cooling chamber; the hydrogen detector monitored the levels of hydrogen being vented. If high levels of hydrogen were detected, a warning light was activated. A diagram of the system is shown in Figure 2-11.

The flame ionization detector electrometer had four possible sensitivity ranges for signal amplification, although only one range was used for the experiments reported. Before each test the FID was calibrated using a zero and span gas to determine the zero and span points. The span gas was 4.71 % ethylene (C_2H_4) with a nitrogen balance. To verify the calibration, two additional gases 5456 ppm ethylene and 20 % ethylene were used.

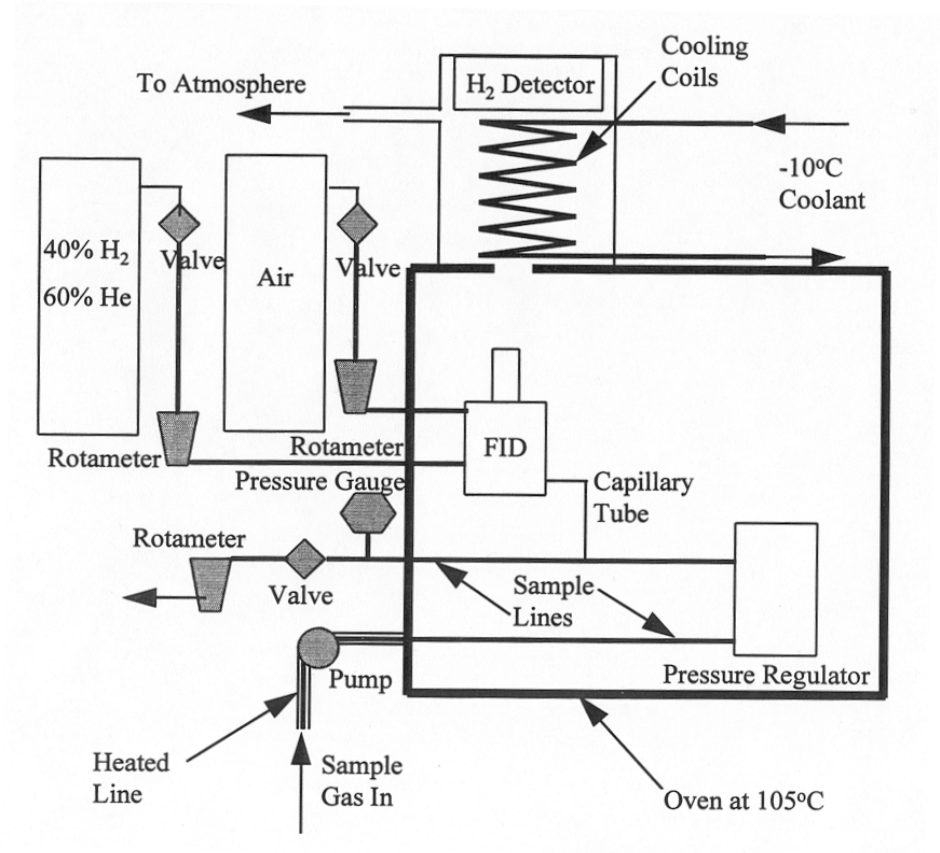

Figure 2-11: Schematic of flame ionization detector (Taken from Lattimer [1996])

2.2.10 Data Acquisition System

The data from the gas analyzers, thermocouples, pressure transducers, and heat flux gages were collected using four Data Translation, Inc. DT2801-A data acquisition computer cards. Each card was connected to an external screw terminal. Two of the screw terminal boards were DT756-Y thermocouple amplifier boards, to which all the thermocouples used in the facility were attached. These boards provided cold junction compensation for the thermocouples and multiplexing, which allowed 16 thermocouples to be attached per board. The other two terminal boards were DT707 direct input boards. Each board accepted eight differential voltage inputs. Due to Data Translation, Inc. hardware specifications, only three boards could be installed per computer; therefore, two computers were required.

LabTech Notebook Pro data acquisition software was used to monitor, acquire, and store the measurement data. The software allowed a visual interface to monitor conditions and outputs of all the sensors and analyzers. After the competition of each test, the data from both computers was merged together using Microsoft EXCEL.

2.3 DATA REDUCTION CALCULATIONS AND PROCEDURES

2.3.1 Wet Species Concentrations

The oxygen and carbon dioxide/carbon monoxide analyzers operate on a dry gas basis, this requires that water be removed from the gas sample and a corrected mole fraction calculated using Equation 2-6. Therefore, the measured species mole fractions are higher than the actual wet mole fractions.

$$X_{i,wet} = (1 - X_{H_2O})\, X_{i,dry} \qquad (2\text{-}6)$$

Reliable water concentration measurements are difficult to obtain, and depending on the conditions the contribution from water vapor can be between 10 and 20 percent by volume. [Gottuk et al. 2002] To account for the water vapor removed from the sample, previous investigators [Gottuk 1992, Ewens 1994, Lattimer 1996, McKay 2002] have

calculated wet species mole fractions using the assumption that the molar ratio, c, of H_2O to CO_2 at any equivalence ratio is equal to the calculated molar ratio at stoichiometric conditions. Therefore, Equation 2-7 can be used to calculate the wet species concentrations.

$$X_{i,wet} = \frac{X_{i,dry}}{1 + c\left(X_{CO_{2dry}}\right)} \qquad (2\text{-}7)$$

The stoichiometric ratio of water vapor to carbon dioxide for propane is determined from the balanced equation:

$$C_3H_8 + 5(O_2 + 3.76N_2) \rightarrow 3CO_2 + 4H_2O + 18.8N_2$$

Therefore,

$$c = \frac{X_{H_2O}}{X_{CO_2}} = \frac{4}{3}$$

Lattimer [1996] reported that Equation 2-7 becomes less accurate in the very fuel rich environments, global equivalence ratios greater than 3.0. In the present study, a global equivalence ratio near 3.0 was only achieved with the sliver doorway in one test; all of the other data corresponded to global equivalence ratios below 2.25. However, as a further improvement, taking into account that all of the hydrogen in the fuel will be associated with either the unburned hydrocarbons or with water vapor present in the carbon dioxide and carbon monoxide species, the measured dry carbon monoxide mole fractions can be added to Equation 2-7. [Floyd 2003]

$$X_{i,wet} = \frac{X_{i,dry}}{1 + c\left(X_{CO_{dry}} + X_{CO_{2dry}}\right)} \tag{2-8}$$

At low equivalence ratios, where carbon monoxide levels are negligible, Equation 2-8 reduces to Equation 2-7.

2.3.2 Heat Release Rate

The ideal heat release rate (fire size) is determined by,

$$\dot{Q}_{ideal} = \dot{m}_{fuel}\, \Delta H_c \tag{2-9}$$

2.3.3 Global Equivalence Ratio

Toxic species generation is a complex function of air supply, nature of mixing, and fuel and oxidant properties. [Beyler 1983, Karlsson et al. 2001] Beyler [1983] proposed that it might be possible to correlate the species yields and species production rates to an overall fuel-to-air ratio.

The equivalence ratio, defined in the classical way, Equation 2-10, determines whether a fire is fuel or oxygen limited.

$$\phi = \frac{\left(\frac{\dot{m}_{fuel}}{\dot{m}_{air}}\right)}{\left(\frac{\dot{m}_{fuel}}{\dot{m}_{air}}\right)_{st}} \tag{2-10}$$

Although typically used to define premixed combustion conditions, several different pseudo equivalence ratios have been defined for non-premixed (diffusion) flames.

Plume Equivalence Ratio (PER) – the ratio of the gaseous fuel generation rate at the fuel surface to the air entrainment rate into the flame between the fuel surface and the hot layer/cold layer interface normalized by the stoichiometric ratio for the fuel. [Beyler 1983, Pitts 1994]

Upper Layer Equivalence Ratio – the ratio of the mass of gas in the upper layer derived from the fuel divided by that introduced from air normalized by the stoichiometric ratio for the fuel. [Morehart et al. 1990, Pitts 1994, Gottuk et al. 2002]

Global Equivalence Ratio – The ratio of the fuel mass loss rate within the compartment to the air flow rate into the compartment, normalized by the stoichiometric ratio for the fuel. [Pitts 1994, Gottuk et al. 2002]

Under steady-state conditions, provided no air or fuel enters the upper layer except via the fire plume, all three are equivalent. [Pitts 1994] The inherent assumption that all of the air flow into the compartment is entrained into the fire plume and drawn into the upper layer may not be valid. However, typically, steady-state, well mixed, conditions are assumed and the term global equivalence ratio (GER) is used. A fire is considered over ventilated, under ventilated, or stoichiometric for $\phi < 1$, $\phi > 1$, and $\phi = 1$ respectively.

2.3.4 Species Yields

The generation of species in a fire has typically been defined in terms of a species yield, which is the mass of species produced per mass of fuel consumed. The species yields for the products of combustion, based on measurements of mass fuel flow rates and air flow rates, are determined by using,

$$Y_i = \frac{m_i}{m_{fuel}} = \frac{\dot{m}_i}{\dot{m}_{fuel}}$$

where

$$\dot{m}_i = y_{i,avg}\ \dot{m}_{total} = y_{i,avg}\left(\dot{m}_{air} + \dot{m}_{fuel}\right)$$

and

$$y_{i,avg} = \frac{MW_i}{MW_{UL}} X_{i,avg}$$

which together lead to the species yield expression, Equation 2-11, of:

$$Y_i = \frac{X_{i,avg} MW_i (\dot{m}_{fuel} + \dot{m}_{air})}{\dot{m}_{fuel} MW_{UL}} \qquad (2\text{-}11)$$

Since oxygen is consumed and not produced, based on a similar derivation O_2 depletion is calculated as the amount of O_2 depleted per unit mass of fuel burned,

$$Y_{O_2} = \frac{m_{O_2,amb} - m_{O_2}}{m_{fuel}} = \frac{\dot{m}_{O_2,amb} - \dot{m}_{O_2}}{\dot{m}_{fuel}}$$

where

$$\dot{m}_{O_2,amb} = y_{O_2,amb}\ \dot{m}_{air}$$

and

$$\dot{m}_{O_2} = y_{O_2,avg}\ \dot{m}_{total}$$

which leads to:

$$Y_{O_2} = \frac{MW_{O_2}\left(X_{O_2,amb}\dot{m}_{air} - X_{O_2,avg}\dot{m}_{total}\right)}{\dot{m}_{fuel}MW_{UL}} \qquad (2\text{-}12)$$

It is helpful to consider the normalized yields of carbon dioxide and oxygen, which are species whose reference levels are those for complete combustion. Normalized yields are determined by dividing the unnormalized yields by the theoretical maximum species yields, the maximum mass of a species produced or consumed by complete combustion of one mole of fuel, Equation 2-13.

$$f_i = \frac{Y_i}{Y_{i,max}} \qquad (2\text{-}13)$$

For example, propane (C_3H_8) has maximum theoretical yields of CO_2 and O_2 of 3.0 and 3.64 respectively. The normalized CO_2 and O_2 yields range between 0 and 1.0 and can be used as indicators of the completeness of combustion; where a value of 1.0 represents complete combustion.

Beyler [1983] and Gottuk [1992] showed that the normalized CO_2 and O_2 yields could be correlated to the global equivalence ratio for a wide variety of fuels. The CO and UHC yields on the other hand were shown not to correlate with their equilibrium levels of complete combustion of the fuel, and therefore the normalized yields do not enhance the data reduction. Beyler [1983] reported that if carbon monoxide yields are presented as a normalized yield, a fuel dependence is seen and can be correlated with the fuel structure.

2.3.5 Integrated Mass Flow Rates Based on Individual Species

Several techniques are currently available for determining the air entrainment rates into the compartment. [Vandsburger 2001] The most common technique is the methodology proposed by Janssens and Tran [1992] based on temperature data obtained from thermocouple rakes mounted within the compartment and at the compartment doorway. This methodology has a major limitation due to the slow response time of the thermocouples, see Section 2.2.6.1. Also, the methodology can not be applied to measurements along the hallway. Another, methodology that is available is based on the velocities, temperatures, and species mole fractions measured at any cross sectional area.

The mass flow rate of the exhausted gases is given by:

$$\dot{m}_{out} = \sum \dot{m}_i = \sum \int_{Z_n}^{Z_d} y_i \, \rho \, V \, dA \qquad (2\text{-}14)$$

The density of each species is calculated using,

$$\rho_i = \frac{P \, MW_i}{R \, T} = \frac{12.19 \, \frac{kg \, K}{m^3} \, MW_i}{T} \qquad (2\text{-}15)$$

which assumes that the pressure is equal to ambient, 101,325 Pa and is only a function of the temperature at that point.

The neutral plane was determined using the pressure data collected during the test and interpolating between the data points to determine the height at which the velocity in the door was zero. No measurements are taken directly at the edge of the doorway; therefore, the velocities, temperatures, and species mole fractions, at the door edge are assumed to be equal to those adjacent to them.

The amount of air entering the compartment is based on a mass balance at the door,

$$\dot{m}_{out} = \dot{m}_{air,in} + \dot{m}_{fuel} \tag{2-16}$$

2.3.6 Species Measurements – Integrated Average Doorway Species Mole Fractions

Since the species concentrations vary with elevation within the doorway, an integrated average over the mass flows out of the doorway was performed. The mass flow rate of species i, out of the doorway is,

$$\dot{m}_{out,i} = \int \rho\, y_i\, V\, dA = \overline{y_i} \int \rho\, V\, dA \tag{2-17}$$

where

$$y_i = \frac{X_i MW_i}{MW_{mixture}} \tag{2-18}$$

and

$$\overline{y_i} = \frac{\int \rho\, y_i\, V\, dA}{\int \rho\, V\, dA} = \frac{\int \rho(x,y)\, y_i(x,y)\, V(x,y)\, db\, dH}{\int \rho(x,y)\, V(x,y)\, db\, dH} \tag{2-19}$$

Finally converting back from mass fractions to mole fractions,

$$\overline{X}_i = \frac{y_i\, MW_{mixture}}{MW_i} \tag{2-20}$$

the integrated average mole fractions are obtained. Equation 2-19 was solved using numerical integration techniques, i.e. trapezoidal rule.

2.4 EXPERIMENTAL PROCEDURE

2.4.1 Compartment Study

The experimental procedure consisted of first performing a full calibration of all the gas analyzers. Zero and span gases were used to calibrate each analyzer and the calibration data was collected using the data acquisition software. Upon completion of the calibration procedure, the filters located on the gas sampling line and the aspirated thermocouples were cleaned and assembled. A leak test on the gas sampling line was performed to insure that the filters were properly connected and tightened. The leak test was performed by pressurizing the sampling line to 20 psig and monitoring the pressure. If leaks were found, all the connections were checked and tightened and the leak test was repeated.

Following the calibration procedure, the sampling pumps and thermocouple pumps were turned on. The data acquisition software was started and baseline data was collected for two minutes. The baseline data was used during the data processing to provide the appropriate zero offsets for the pressure transducer data. Once the baseline data was collected the hood was turned on.

The gas burner was ignited using a small pilot flame, generated by a handheld ignition torch, positioned over the burner. Once the pilot flame was properly positioned the main propane gas was slowly turned on, upon ignition, the pilot flame was removed. For most tests, just prior to igniting the gas burner, a video camera was activated to provide a permanent record of each test.

At the start of a test series, the mass flow rate of fuel was gradually increased in an effort to eliminate damage to the compartment due to rapid temperature changes. Data was not collected until the temperatures within the compartment were steady, determined by observation of the change in compartment temperatures $\Delta T/t \approx 10$ K/min, typically

this constituted a warm-up period of approximately 1000 s to 2000 s, during the first test of the day. The first test of each series constituted as a sufficient warm up period for all remaining tests and all successive tests were performed immediately after the pervious test without any cool down period.

The data was collected during the steady-state period of the fire, at a sampling rate of 1 hz. Data was collected from each of the five species sampling probes for approximately 180 s to 240 s depending on the test. Data averaging was performed over the middle 60 s of each sampling period. The sampling rake was manually moved to each subsequent axial location after all the data was collected at each of the five sampling points. While moving the sampling rake, all efforts not to disturb the flow were taken, in situations where the flow patterns may have been disturbed, time was allotted for steady-state conditions to return prior to collecting further data. To verify repeatability of the results, sampling at some locations was repeated at the end of the test. In addition several tests were repeated in their entirety.

Between successive tests or if the gas sampling flow rate was impaired by soot during a test, the gas sampling system was purged of any soot deposits by blowing out the lines using pressurized air and replacing the filters. Typically the aspirated thermocouple rakes and filters were cleaned after two or three successive tests. All sampling lines, filters, and rakes were cleaned at the end of each test day.

2.4.2 Hallway Study

Experiments conducted during the hallway study consisted of the same initial procedures, from calibration to ignition, as those used for the compartment study described above. The experimental procedure, however, varied depending on the parameter(s) being examined; therefore, descriptions regarding the testing procedures are presented along with the corresponding results.

CHAPTER 3

RESULTS AND DISCUSSION: COMPARTMENT STUDY – CUSTOMARY ANALYSIS

3.1 INTRODUCTION

Experiments were conducted with four different doorway widths, 0.083 m, 0.165 m, 0.33 m, and 0.66 m, termed sliver, narrow, baseline, and wide doorways respectively. The primary basis for all analysis, in Chapters 3 and 4, stems from a total of 28 tests, of which 11 were performed with the narrow doorway, 13 with the baseline doorway, and 4 with the wide doorway. In hindsight, it was noticed that the area of the sliver doorway, was smaller then the surface area of the gas burner, in the compartment. Therefore, the compartment became, in effect, the burner and all measurements performed at the exit plane of the compartment were taken at the base of the flame and are similar to that of a jet diffusion flame. Since the sliver doorway is a special case, the results from the 10 tests conducted are presented and discussed separately in Appendix B.

In this chapter, the results are presented and discussed systematically, first species mappings at the compartment exit plane are presented. The data are then presented as species mole fractions versus the ideal heat release rate and finally, the data are cast into standard fire protection engineering variables and presented as the species yields versus the global equivalence ratio.

3.2 SPECIES MOLE FRACTIONS AT EXIT PLANE

The results from three tests for different doorway widths but the same global equivalence ratio are presented to examine the species distributions at the compartment exit plane. Mole fraction maps for each of the measured species, for each doorway width are shown in Figure 3-1 through Figure 3-3. Each figure consists of four spatially non-

dimensional plots of (a) oxygen, (b) carbon dioxide, (c) carbon monoxide, and (d) unburned hydrocarbon mole fractions at the doorway. The heat release rates for the narrow, baseline, and wide doorways were approximately 153 kW, 270 kW and 470 kW respectively, resulting in the same global equivalence ratio for all three doorways of approximately 0.6. The solid black line in each of the figures indicates the calculated neutral plane elevations.

Although the global equivalence ratio was approximately 0.6, it should be noted that for all three doorways external burning due to flame extensions had occurred. Based on the calculations in Appendix A, the heat release rate and global equivalence ratios at which external burning begins to occur for each doorway are listed in Table 3-1. Visual observations during testing agree with the theoretical calculations.

Table 3-1: Minimum Heat Release Rate and Equivalence Ratio for Flame Extension

Test Configuration	Ideal Heat Release Rate (kW)	Equivalence Ratio Theoretical
Narrow	95	0.51
Baseline	127	0.34
Wide	190	0.26

Therefore, in Figure 3-1 through Figure 3-3, the data include measurements in the exiting stream, i.e. above the neutral plane, which consists of both the fire plume and hot combustion product gases.

The data shown in Figure 3-1 through Figure 3-3 indicate that as the doorway width increases the uniformity of the upper layer diminishes. Spatial variations in the vertical direction appear with the narrow doorway, Figure 3-1. Oxygen mole fractions in the upper layer range between 2.0 % and 16 %, with carbon dioxide levels ranging between 2.8 % and 8.5 %. It is interesting to note that although the most substantial

external burning occurred with the narrow doorway, carbon monoxide levels were below 0.2 % and unburned hydrocarbon levels were below the range of the gas analyzer.

Spatial variations in both the vertical and horizontal directions are seen with the baseline and wide doorways, Figure 3-2 and Figure 3-3. The highest levels of combustion products, carbon dioxide, carbon monoxide, and unburned hydrocarbons and lowest levels of oxygen are seen in the upper corners of the doorways, which correspond to measurements taken directly in the flame. Although the exact contour of the flame was not documented during any of the tests, one would expect, based on the commonly accepted assumption that a uniform upper layer exists within the compartment, that below the fire plume a well mixed uniform environment would exist. This well-mixed, well-defined layer does not exist. Instead, for the baseline doorway, above the calculated neutral plane $h/H \approx 0.42$, oxygen levels vary between 0.0 % and 18.7 % and carbon dioxide levels vary between 1.0 % and 9.0 %.

The wide doorway data, Figure 3-3, exhibit a similar trend to that of the baseline doorway; however, the levels of carbon monoxide and unburned hydrocarbons are significantly higher than seen with either the narrow or baseline doorways. Carbon monoxide levels as high as 3.0 % along with unburned hydrocarbon levels of 0.5 % are seen in the upper corners of the doorway. The high levels of carbon monoxide and unburned hydrocarbons indicate that although the global equivalence ratio is the same for all three doorways, the species levels at the doorway are primarily dependent on the heat release rate. In the upper region of the doorway, measurements for both the narrow and wide doorways were taken directly in the fire plume; however, the heat release rate for the wide doorway was more then three times greater then the heat release rate for the narrow doorway, and resulted in carbon monoxide levels that are 15 times higher. Although the global equivalence ratio indicates that the same fuel and air ratio exists for all three doorways, the combustion occurring in the compartment is not the same. This can be considered the first indication that the global equivalence ratio does not provide an accurate means of comparing compartment fires.

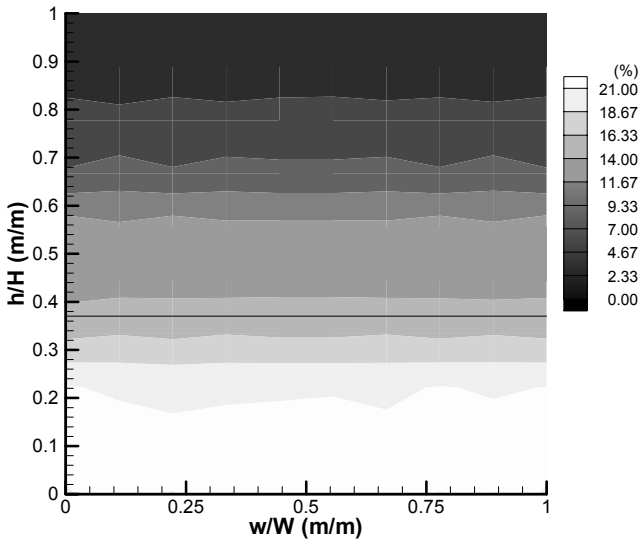

a

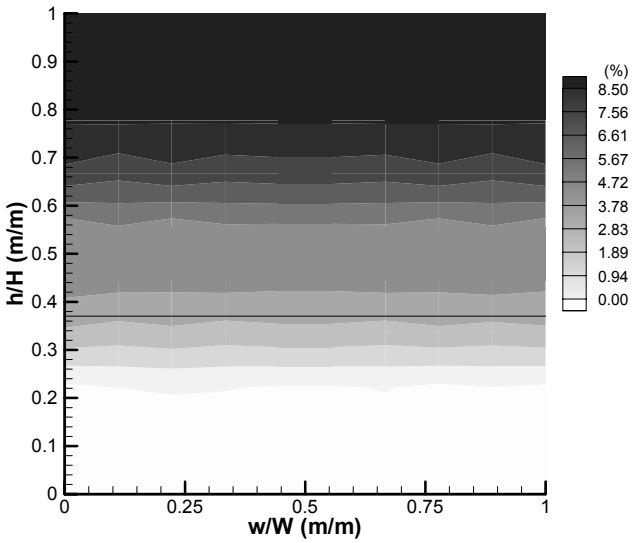

b

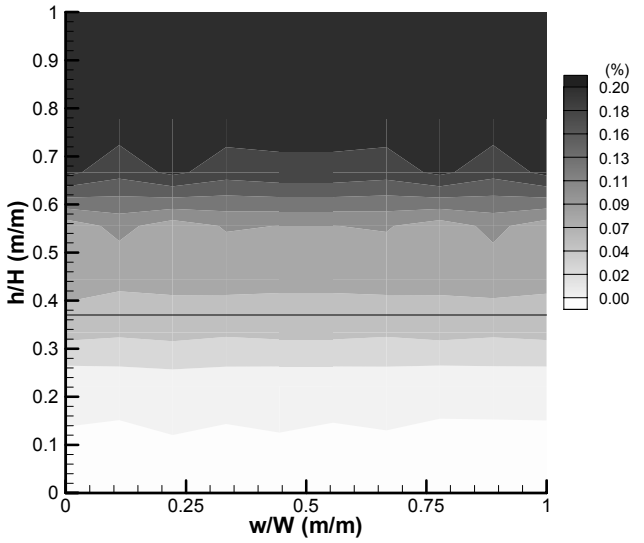

c

Unburned hydrocarbon levels below the limit of the analyzer.

d

Figure 3-1: Narrow doorway species mapping of (a) O_2, (b) CO_2, (c) CO, and (d) UHC mole fractions (%), 153 kW (GER of 0.58), neutral plane determined from velocity probe data.

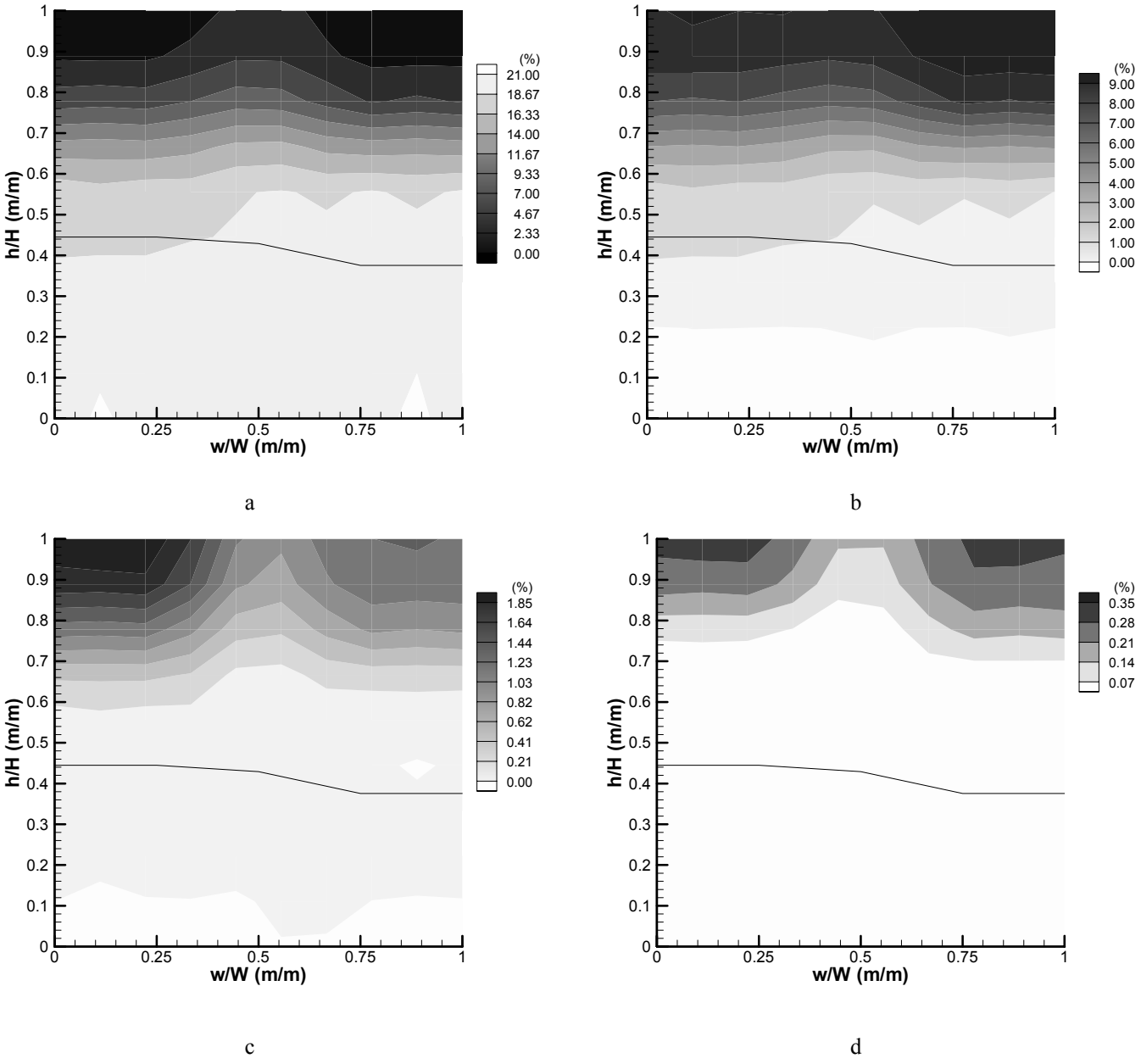

Figure 3-2: Baseline doorway species mapping of (a) O_2, (b) CO_2, (c) CO, and (d) UHC mole fractions (%), 270 kW (GER of 0.56), neutral plane determined from velocity probe data.

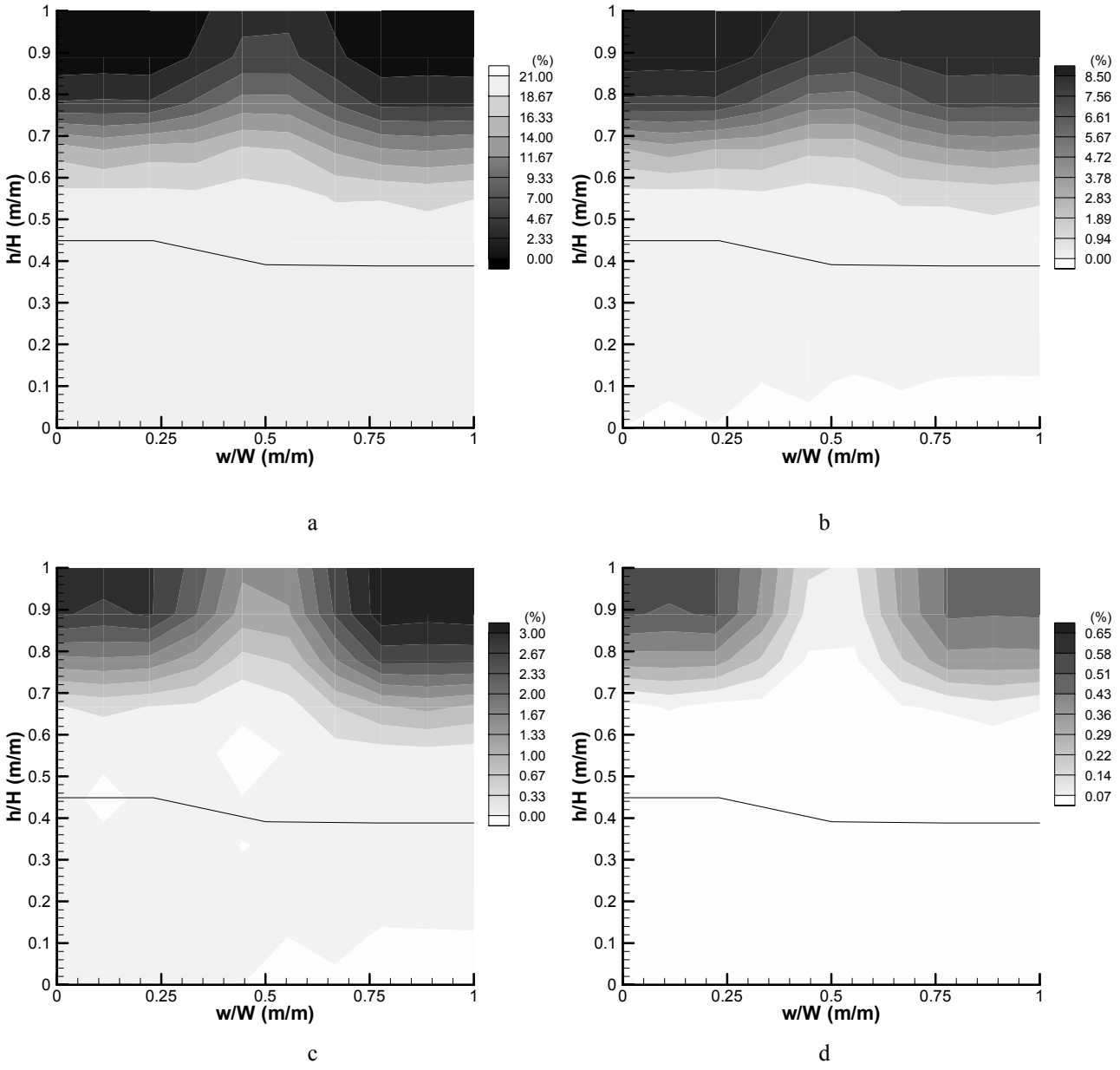

Figure 3-3: Wide doorway species mapping of (a) O_2, (b) CO_2, (c) CO, and (d) UHC mole fractions (%), 470 kW (GER of 0.64), neutral plane determined from velocity probe data.

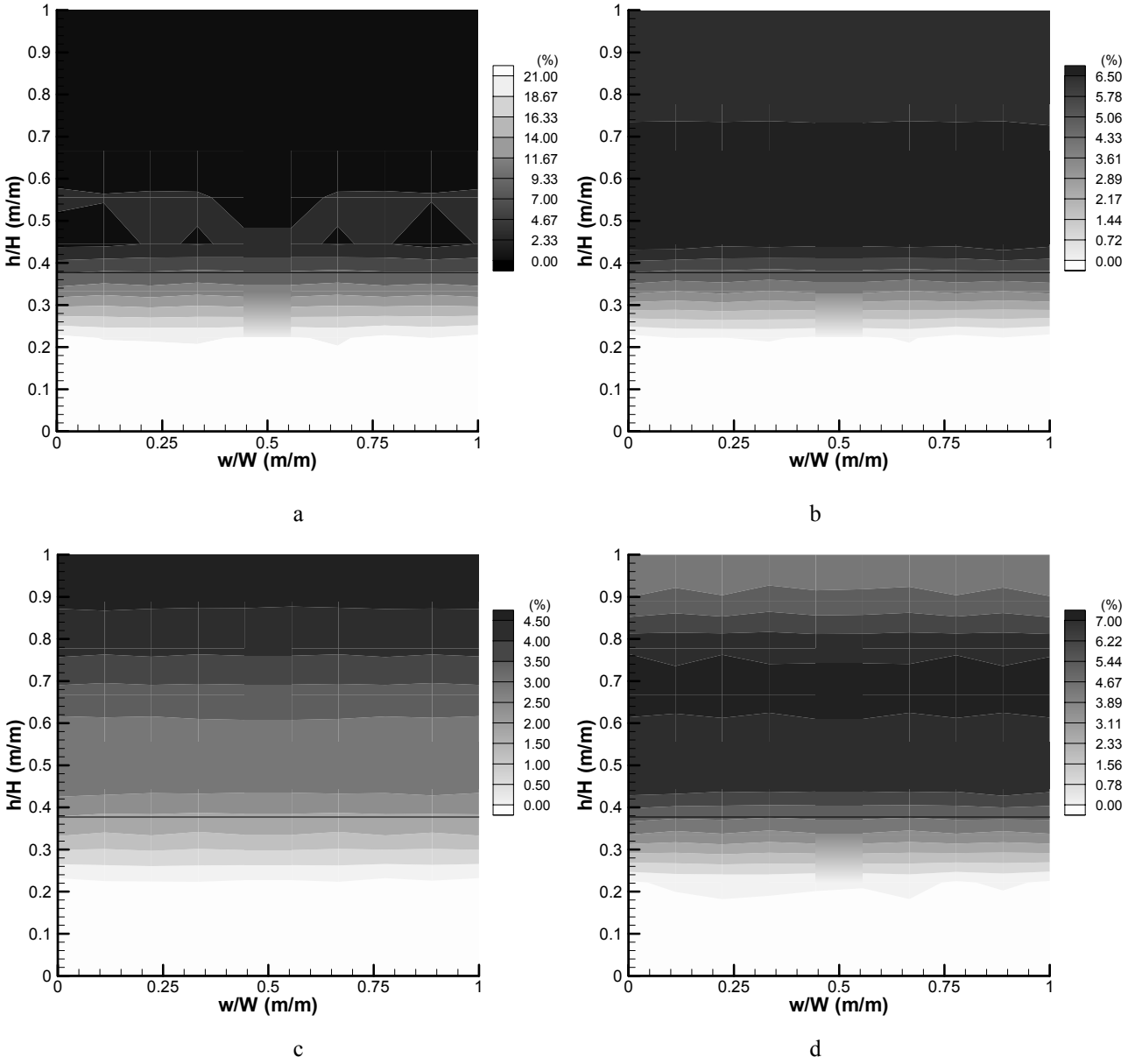

Figure 3-4: Narrow doorway species mapping of (a) O_2, (b) CO_2, (c) CO, and (d) UHC mole fractions (%), 470 kW (GER of 2.05), neutral plane determined from velocity probe data.

Species levels at the narrow doorway for a heat release rate of 470 kW (the corresponding global equivalence ratio is 2.05) are shown in Figure 3-4. This is the same heat release rate as for the wide doorway data shown in Figure 3-3. Under the present conditions the compartment with the narrow doorway is completely ventilation limited. Therefore, all of the measurements were taken in the fire plume. The data shown in Figure 3-4 represents a cross-sectional slice of the fire plume. Very little variation in each species is seen above the neutral plane, with some mixing due to shear forces between the in-flowing and out-flowing gases occurring at the neutral plane.

Although the data presented in Figure 3-3 and Figure 3-4 are for the same heat release rate, the upper layer carbon monoxide levels are significantly higher with the narrow doorway then those seen with the wide doorway. High carbon monoxide levels, greater than 2.0 % are seen throughout the upper layer, the maximum measured carbon monoxide mole fraction was 4.4 %; while with the wide doorway the maximum carbon monoxide mole fraction was 3.0 %. The most important observation is the extremely high levels of unburned hydrocarbons with the narrow doorway, 4.5 % to 7.0 %, Figure 3-4, compared to the highest levels reported previously of 0.7 %, Figure 3-3, for the wide doorway. This is attributed to the fact that although the unburned hydrocarbons are measured in the fire plume, with the wide doorway only “small wisps” of flames are exiting the compartment and the measurements are being taken in the flame tip; for the narrow doorway substantial external burning is occurring and the measurements are taken deep in the fire plume.

3.3 SPECIES YIELDS VERSUS GLOBAL EQUIVALENCE RATIO

The calculated species yields for oxygen, carbon dioxide, carbon monoxide, and unburned hydrocarbons are presented in Figure 3-5 through Figure 3-8, numerical values corresponding to the data presented in the figures are listed in Table 3-2. The oxygen and carbon dioxide data are presented as normalized yields, while the carbon monoxide and unburned hydrocarbon yields are presented as unnormalized yields. Reported data

from previous studies of Gottuk [1992] and Beyler [1983, 1986] are also included for comparison. As mentioned previously, Bryner *et al.* [1994] did not report yield data, therefore the species yields were calculated based on the reported mole fraction and the local equivalence ratio, see Chapter 1, Section 1.3.1.

The normalized oxygen data shown in Figure 3-5 indicate good agreement with the studies of Beyler [1983], Gottuk [1992], and Bryner *et al.* [1994] and correlate well with the model for complete combustion. Similar agreement is seen for the carbon dioxide yields in Figure 3-6. For equivalence ratios greater then 0.5, the carbon dioxide yields are lower than the theoretical levels for complete combustion. This is anticipated since the model for complete combustion assumes that at all equivalence ratios only carbon dioxide is generated and no other species are presented. In reality, at higher equivalence ratios, complete conversion of the fuel carbon to carbon dioxide does not happen, and intermediate species, i.e. carbon monoxide and unburned hydrocarbons, are formed.

Data at low equivalence ratios, less then 0.5 in Figure 3-5 and Figure 3-6 indicate values that exceed the theoretical limit by as much as 30 %, the data implies that more oxygen was consumed and more carbon dioxide was generated then physically possible. A carbon balance comparing the amount of carbon available from the fuel to that accounted for in the measurements was performed for each test, the values for the carbon error are listed in Table 3-2. A positive carbon error indicates an excess of carbon while a negative carbon error indicates an omission of carbon. The carbon balance is based on carbon present as carbon dioxide, carbon monoxide, and unburned hydrocarbons; solid carbon in the form of soot was not accounted for and is believed to be responsible for the negative carbon errors obtained at higher equivalence ratios, where soot generation is expected. Similar to the data seen in Figure 3-5 and Figure 3-6 errors as high as 30 % are observed in the carbon balance for equivalence ratios below 0.5. This discrepancy between the measured and theoretical data is attributed to the experimental uncertainty

associated with the grid resolution used for performing the species mapping at the compartment doorway, see Appendix C.

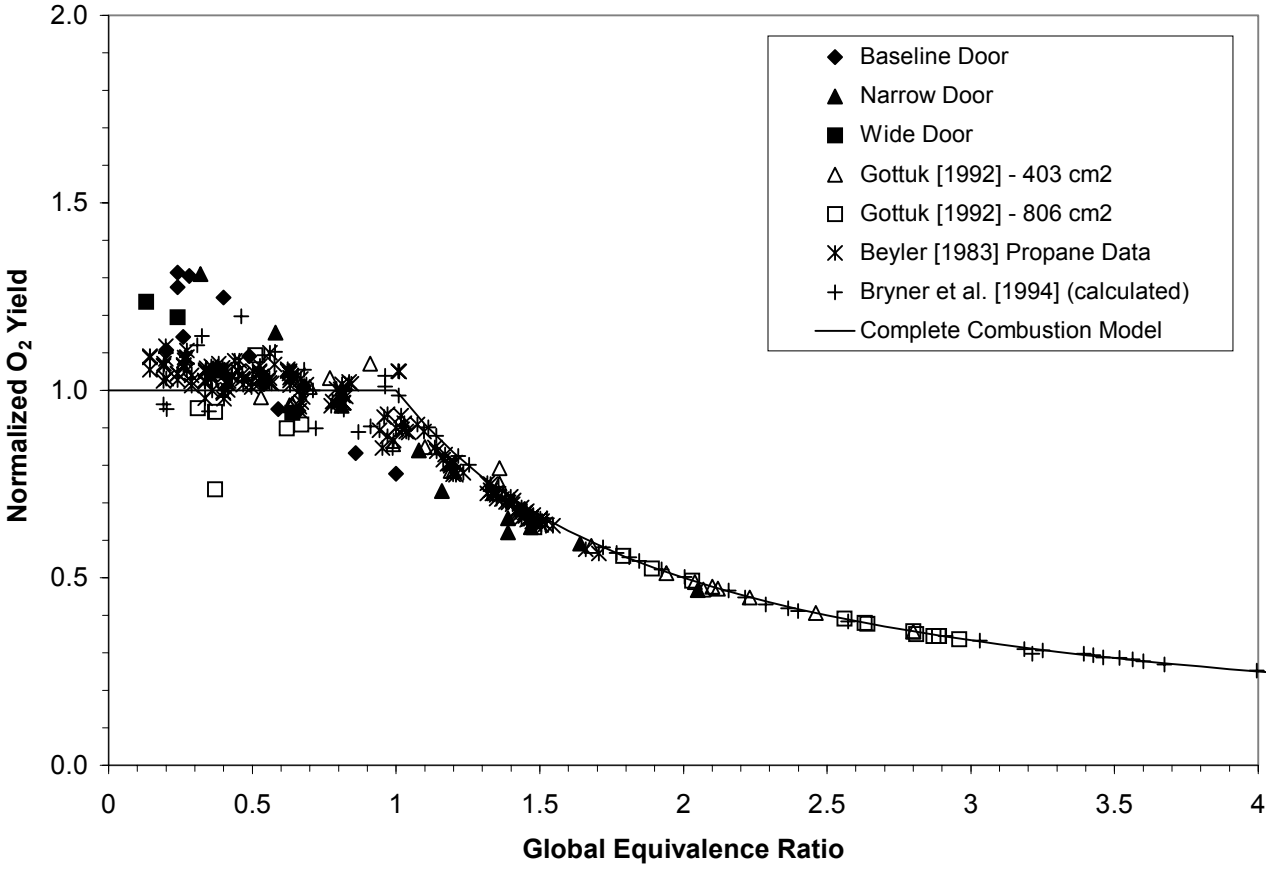

Figure 3-5: Normalized O_2 yields as a function of the equivalence ratio and doorway width compared with data from Gottuk [1992], Beyler [1983], and Bryner *et al.* [1994] in addition to the model for complete combustion.

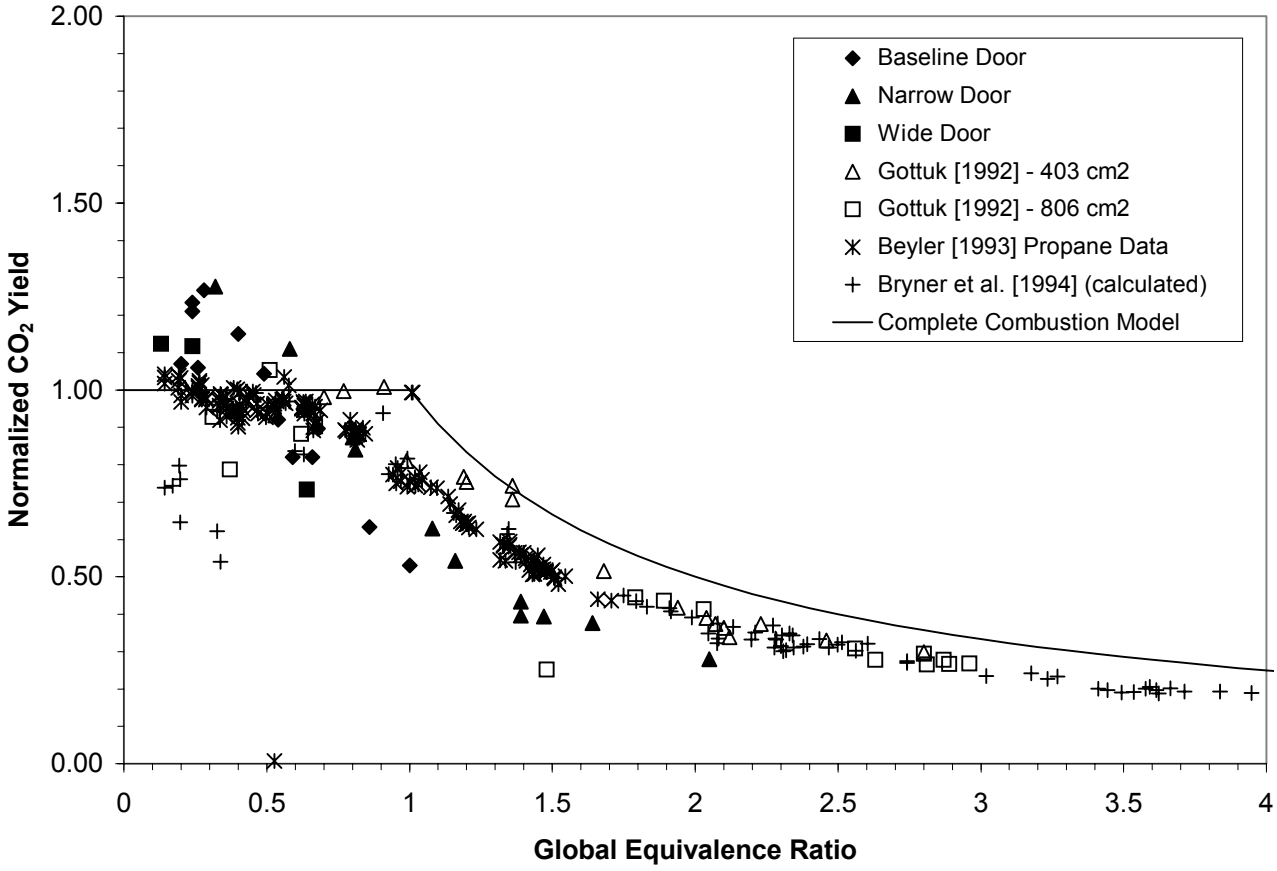

Figure 3-6: Normalized CO_2 yields as a function of the equivalence ratio and doorway width compared with data from Gottuk [1992], Beyler [1983], and Bryner *et al.* [1994] in addition to the model for complete combustion.

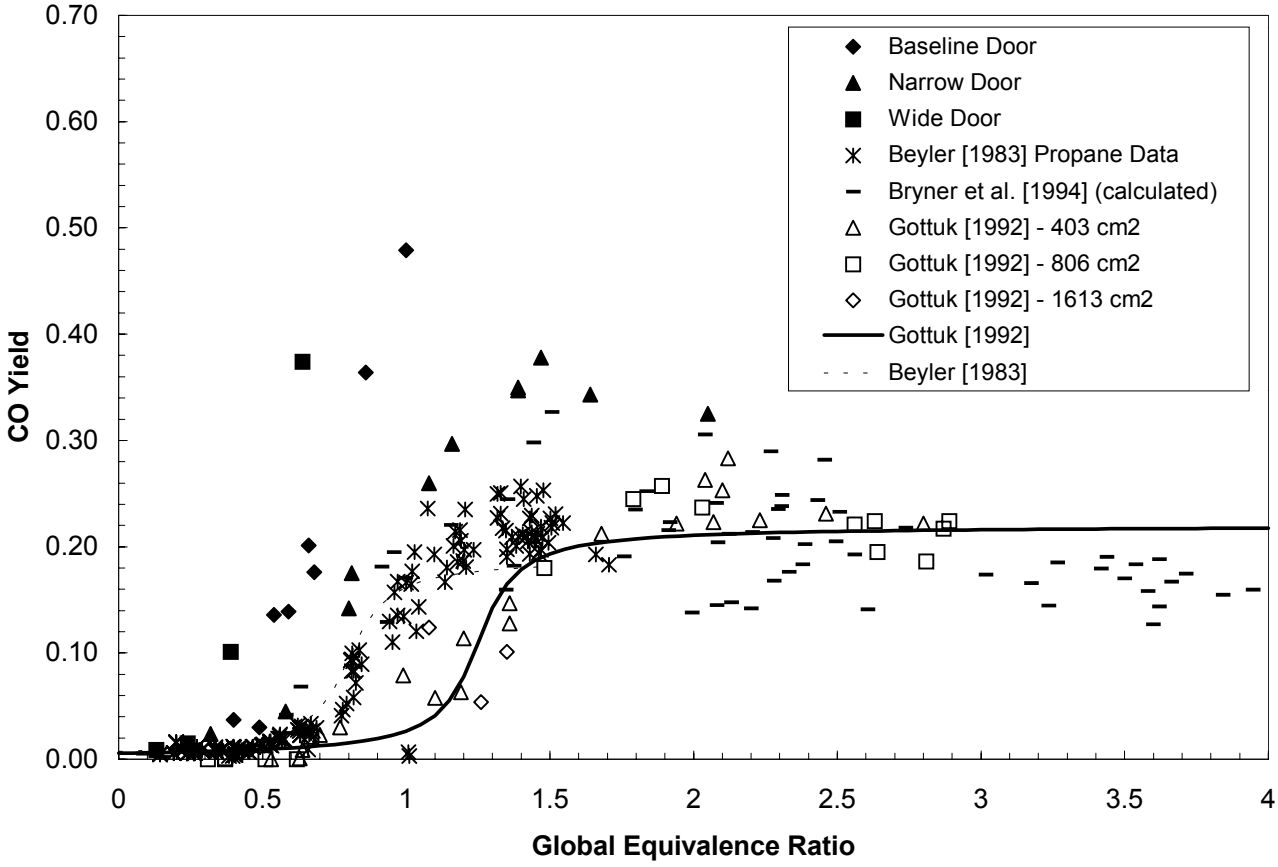

Figure 3-7: Carbon monoxide yields as a function of the equivalence ratio and doorway width compared with data from Gottuk [1992], Beyler [1983], and Bryner *et al.* [1994] in addition to correlations from Gottuk [1992] and Beyler [1983].

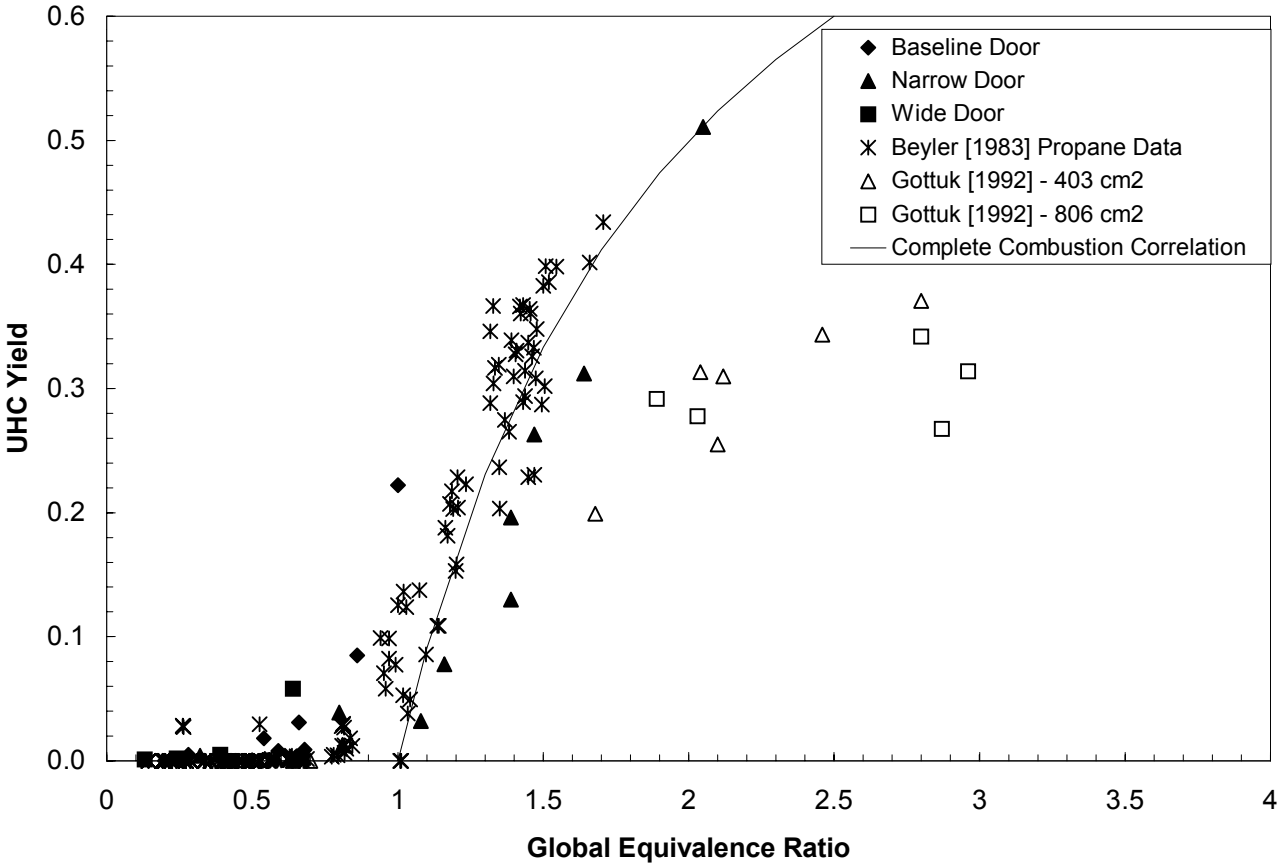

Figure 3-8: Unburned hydrocarbon yields as a function of the equivalence ratio and doorway width compared with data from Gottuk [1992] and Beyler [1983] in addition to the model for complete combustion, $Y_{UHC} = 1 - 1/\phi$**. [Gottuk *et al.* 2002]**

Table 3-2: Numerical values corresponding to data presented in Figure 3-5 through Figure 3-8 along with the calculated carbon balance errors for each test.

Compartment Ventilation	ϕ	Normalized O_2 Yield	Normalized CO_2 Yield	CO Yield	UHC Yield	Carbon Error
Baseline	0.2	1.11	1.07	0.009	0.000	7.4
	0.24	1.27	1.23	0.008	0.001	23.9
	0.24	1.13	1.21	0.011	0.000	21.5
	0.26	1.14	1.06	0.008	0.000	6.4
	0.28	1.30	1.27	0.009	0.005	27.8
	0.40	1.25	1.15	0.037	0.000	17.0
	0.49	1.09	1.04	0.030	0.000	5.8
	0.54	1.02	0.92	0.136	0.018	-0.05
	0.59	0.95	0.82	0.139	0.008	-9.7
	0.66	0.95	0.82	0.201	0.031	-4.1
	0.68	1.01	0.90	0.176	0.009	-0.16
	0.86	0.83	0.63	0.364	0.085	-8.9
	1.00	0.78	0.53	0.479	0.222	1.4
Narrow	0.32	1.31	1.28	0.024	0.004	29.2
	0.58	1.15	1.11	0.045	0.003	13.6
	0.80	0.97	0.87	0.142	0.039	-1.3
	0.81	0.96	0.84	0.175	0.013	-5.4
	1.08	0.84	0.63	0.260	0.032	-20.1
	1.16	0.73	0.54	0.297	0.078	-21.8
	1.39	0.66	0.43	0.347	0.130	-24.7
	1.39	0.62	0.40	0.350	0.196	-21.6
	1.47	0.63	0.39	0.378	0.263	-13.2
	1.64	0.59	0.38	0.343	0.312	-11.8
	2.05	0.47	0.28	0.325	0.511	-1.6
Wide	0.13	1.24	1.12	0.009	0.001	12.9
	0.24	1.20	1.12	0.015	0.002	12.6
	0.39	1.05	0.94	0.101	0.005	0.22
	0.64	0.94	0.73	0.374	0.058	-1.2

The curves for the yields of the products of incomplete combustion, carbon monoxide and unburned hydrocarbons, Figure 3-7 and Figure 3-8, appear to have an additional dependency on the ventilation conditions to that captured by the global equivalence ratio. The carbon monoxide yields as a function of the global equivalence ratio, shown in Figure 3-7, indicate a different curve for each of the three ventilation conditions. The carbon monoxide yields begin to increase at lower global equivalence ratios as the width of the doorway increases. The increase in carbon monoxide yields is attributed to the start of external burning from the compartment, due to flame extensions. The increase in carbon monoxide levels appear at the corresponding global equivalence ratios for the onset of external burning, i.e. 0.54, 0.34, and 0.26 for the narrow, baseline, and wide doorways respectively.

The narrow doorway data appear to increase and peak at about a yield of 0.36 g_{co}/g_{fuel} and an equivalence ratio of 1.5, while both the baseline and wide doorway data have continuously increasing yields. For neither the baseline nor the wide doorway were equivalence ratios greater than 1.0 achieved. Therefore, the peak carbon monoxide yield and corresponding global equivalence ratio are unknown. It should be noted that at the lower global equivalence ratios, where comparison between all three doorways can be made, the carbon monoxide yields appear to double by doubling the doorway width.

Comparing the carbon monoxide yield data to previously published data of Beyler [1983, 1986], Gottuk [1992], and Bryner *et al.* [1994] it is seen that the values for the present study are significantly higher. This is attributed to the differences in the physics of each test apparatus used in the research studies. As previously discussed, both Beyler's and Gottuk's experimental apparatuses allowed air to be entrained into the fire plume via the entire circumference of the flame. Also, the collection hood above the fire in Beyler's setup and the specially build test compartment of Gottuk generated a well-mixed layer in which there was ample time for the gases to mix and for the conversion of carbon monoxide to carbon dioxide to take place. Both Beyler [1983] and Gottuk [1992] reported that the calculated global equivalence ratios and the plume equivalence ratios

were equal. Even the data from Bryner *et al.* [1994], although taken within the compartment and reported as a function of the local equivalence ratio, are based on single point measurements, which based on the reported sampling location, are assumed to be taken within the fire plume. Therefore, the local equivalence ratio is actually a local plume equivalence ratio and, therefore, agrees well with the data from Beyler [1983] and Gottuk [1992].

Returning to the discussed in Section 1.3.1, a very important conclusion that must be drawn from the work of Bryner *et al.* [1994] is that for scaled compartments with prototypical building features the local (plume) and global equivalence ratios are not equal. This is attributed to the non-homogeneity of the upper layer. This has been a key assumption in all of the previous studies. [Beyler 1983, Gottuk 1992]

An increase in the unburned hydrocarbon yields, shown in Figure 3-8, is seen for all three ventilation conditions, and corresponds to the equivalence ratios at which flame extensions begin to occur. Gottuk reported that the unburned hydrocarbon yields begin to plateau at global equivalence ratios greater than 1.8 at a value of 0.3 $g_{C_2H_4}/g_{fuel}$. The present data follow the same trend as that of Beyler [1983] and neither study indicates any tapering of the data. The maximum unburned hydrocarbon yield, for propane fires, when measured as equivalent ethylene, C_2H_4, is 0.96 $g_{C_2H_4}/g_{fuel}$. It is expected that the unburned hydrocarbon yields will follow the trend predicted by the model for complete combustion and will approach this value asymptotically as the equivalence ratio increases. Bryner *et al.* [1994] did not report unburned hydrocarbon data.

At higher equivalence ratios incomplete products of combustion are formed, yet a competition for the available oxygen exists between the oxidation of unburned hydrocarbons and the oxidation of carbon monoxide to carbon dioxide. Since the levels of carbon monoxide and carbon dioxide are related and are a function of the available oxygen and gas temperatures; the dependence of carbon monoxide and unburned hydrocarbons on the equivalence ratio and the size of the ventilation openings should also be seen in the carbon dioxide yields. Reexamination of Figure 3-6 indicates that a

slight dependence on the ventilation size exists, although not as obvious as with the carbon monoxide and unburned hydrocarbon data. As expected, this dependence in the carbon dioxide data is opposite to that of the carbon monoxide and unburned hydrocarbon yields, i.e. lower levels of carbon dioxide are seen for the wide doorway and increase with decreasing doorway width.

3.4 LIMITATIONS OF GLOBAL EQUIVALENCE RATIO CONCEPT

In Section 3.3, the species yields versus the global equivalence ratio were presented. When presented in this fashion, the highest carbon monoxide yields are seen for the wide doorway and the lowest for the narrow doorway. However, when presented as species mole fractions versus the ideal heat release rate, Figure 3-9, the highest **average** species mole fractions are seen for the narrow doorway and the lowest for the wide doorway.

This behavior can be explained by examining Equation 2-10 and Equation 2-11, the global equivalence ratio and species yield equations. Neglecting the constants in both equations, it is seen that,

$$Y_i \propto \overline{X}_i \left(\frac{\dot{m}_{fuel} + \dot{m}_{air}}{\dot{m}_{fuel}} \right)$$

or

$$Y_i \propto \overline{X}_i \left(1 + \frac{1}{\phi} \right) \qquad (3\text{-}1)$$

and,

$$\phi \propto \frac{\dot{m}_{fuel}}{\dot{m}_{air}} \qquad (3\text{-}2)$$

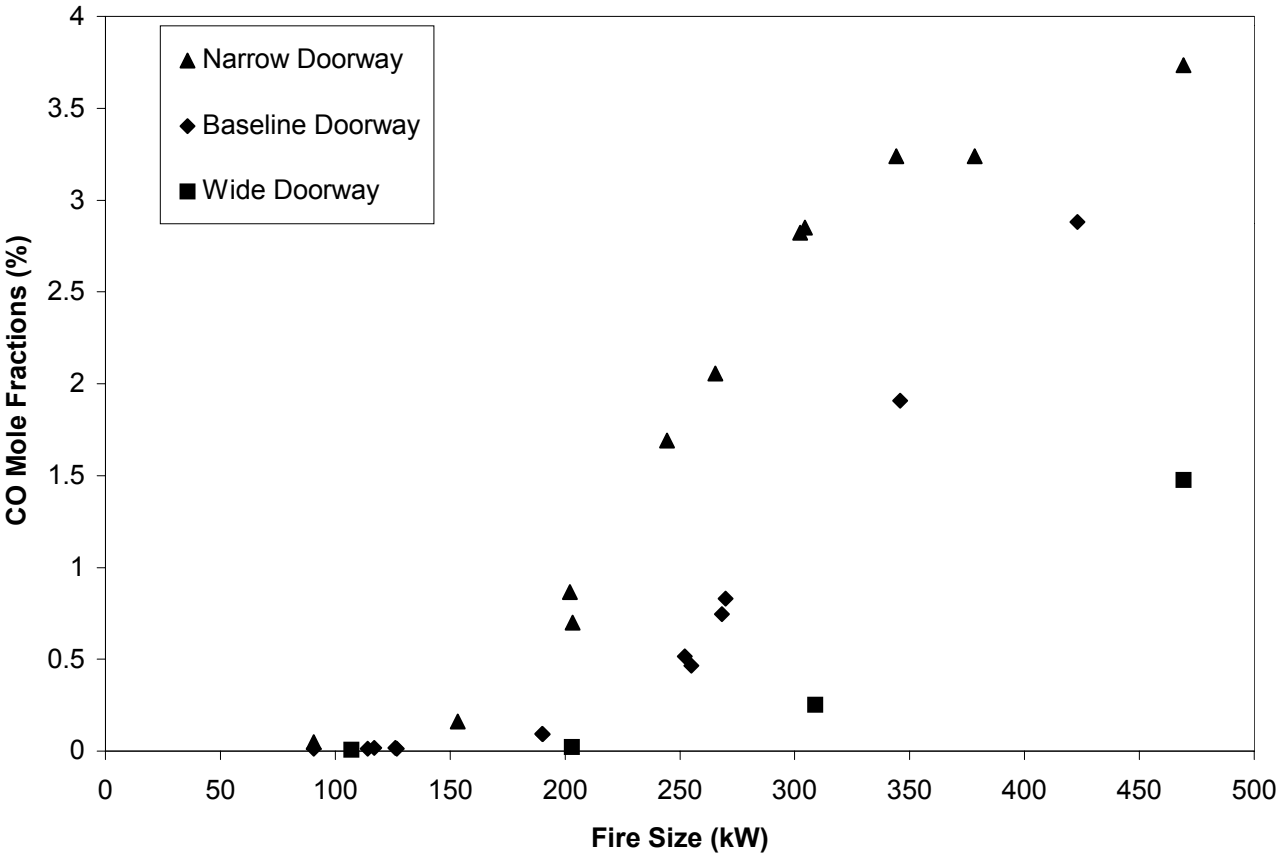

Figure 3-9: Carbon monoxide mole fractions as a function of the ideal heat release rate and doorway width.

Assuming a **fixed ideal heat release rate**, i.e. a fixed $\dot{m}_{fuel}$. The species yield, therefore, is directly proportional to the species mole fraction and $\dot{m}_{air}$, while the global equivalence ratio is inversely proportional to only $\dot{m}_{air}$. Noting that $\dot{m}_{air}$ is directly proportional to the width of the doorway results in $\phi_{wide} < \phi_{baseline} < \phi_{narrow}$ for a fixed heat release rate. Therefore, the shift in the data, seen between Figure 3-7 and Figure 3-9, must be attributed to the independent variable, the global equivalence ratio. This is significant since it illustrates the fact that using the global equivalence ratio as a

correlating parameter skews the data in a counterintuitive manner, since it implies that higher yields, based on average integrated mole fractions, are seen for the wide doorway compared to the narrow doorway.

Based on the present analysis of the global equivalence ratio concept, it has been shown that the methodology fails when extended to scaled-compartment fires. Key weaknesses in the methodology are:

1. The global equivalence ratio concept does not account for flame extensions at the compartment exit plane.
2. Using the global equivalence ratio as the independent variable while correlating the data shifts the data in a counterintuitive manner, indicating the highest levels of carbon monoxide yields for conditions where the lowest average mole fractions were measured.
3. Local species yields do not correlate well with a global condition parameter.
4. The data does not collapse, separate curves are observed for each ventilation condition.

In view of these limitations a new methodology that takes into account these issues was developed.

CHAPTER 4

RESULTS AND DISCUSSION: COMPARTMENT STUDY – NEW ANALYSIS

4.1 INTRODUCTION

The use of the global equivalence ratio to characterize the combustion occurring in a compartment provides no indication of external burning occurring at the compartment exit. Under-ventilated burning conditions occur at an equivalence ratio of 1.0, however, external burning due to flame extensions may occur at equivalence ratios well below 1.0. The exact equivalence ratio, and corresponding heat release rate, for the flame tip to reach the compartment doorway is a function of the compartment dimensions, ventilation dimensions, fuel source location in the compartment, and fuel type. The species mappings shown previously, all for $\phi = 0.6$, had some degree of external flaming at the exit plane. Therefore, although species measurements were taken in the out-flowing gases, some of the measurements were taken both inside and outside of the flaming region. A new parameter that quantifies the degree of external burning occurring at the compartment exit plane is required, and was developed based on fuel load and geometrical parameters of the compartment.

4.2 NEW PARAMETER DEVELOPMENT

4.2.1 Non-Dimensional Heat Release Rate

The proposed parameter is a non-dimensional heat release rate, $\widetilde{Q}$, Equation 4-1, defined as the ideal heat release rate, $\dot{Q}_{ideal}$, divided by the heat release rate required for the flame to reach the compartment doorway, $\dot{Q}_{Flame\ Extensions}$.

$$\widetilde{Q} = \frac{\dot{Q}_{ideal}}{\dot{Q}_{Flame\ Extensions}} \tag{4-1}$$

where

$$\dot{Q}_{ideal} = \dot{m}_{fuel}\ \Delta H_c \tag{4-2}$$

At the present time there is no agreed-on methodology for predicting flame extensions from a compartment based on theoretical calculations, therefore, the values for $\dot{Q}_{Flame\ Extensions}$ used in this analysis are based on experimental observations from the present study. A methodology based on an extension of a correlation from Hasemi *et al.* [1995] is proposed as a potential methodology for theoretical flame extension calculations. This methodology has not been validated for compartment fires but appears to be appropriate for the analysis in the present study, more details can be found in Appendix A.

There are four important regions to consider for $\widetilde{Q}$, illustrated in Figure 4-1:

$$\widetilde{Q} = \begin{cases} < 1.0 \text{ - Combustion within the compartment} \\ = 1.0 \text{ - Flame tip at the compartment doorway} \\ > 1.0 \text{ - External burning due to flame extensions} \\ \geq \widetilde{Q}_{critical} = \dfrac{\dot{Q}_{Ventilation-limit}}{\dot{Q}_{Flame\ Extensions}} = \dfrac{r\ \dot{m}_{air}\ \Delta H_c}{\dot{Q}_{Flame\ Extensions}} \\ \qquad \text{- External burning due to under - ventilated conditions} \end{cases}$$

where, $\dot{Q}_{Ventilation-limit}$, is the heat release rate corresponding to ventilation limit.

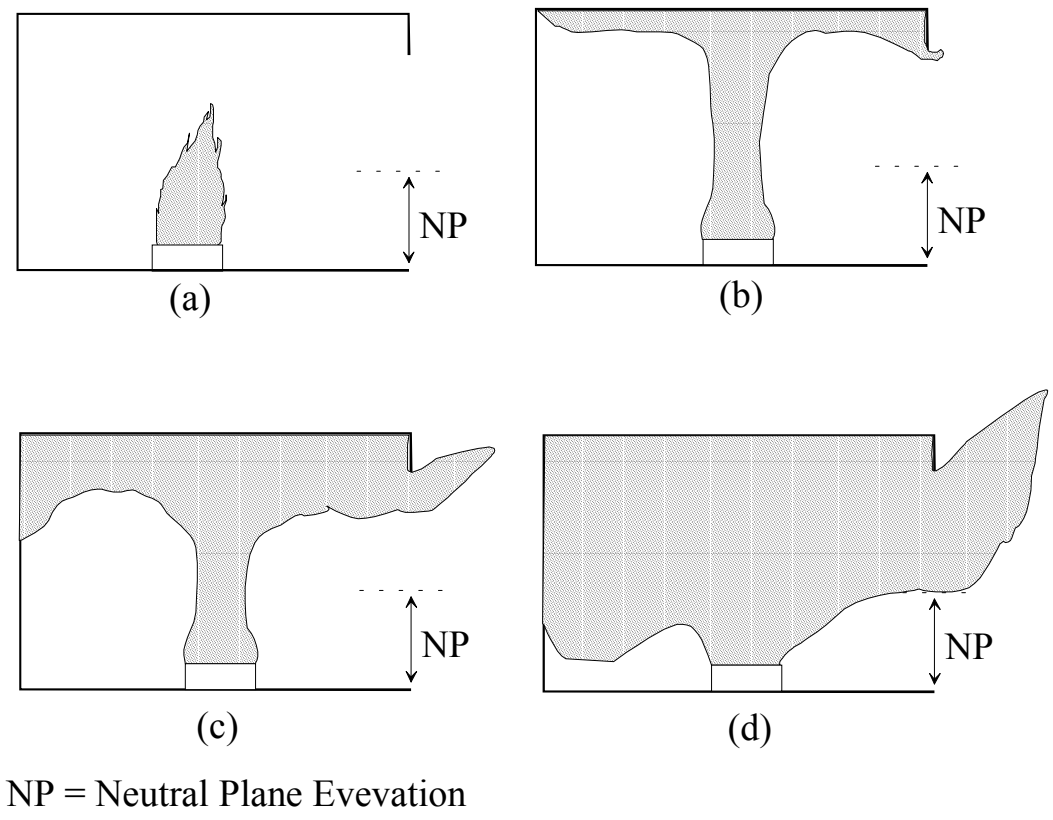

Figure 4-1: Illustration of four $\tilde{Q}$ conditions (a) $\tilde{Q} < 1.0$, (b) $\tilde{Q} = 1.0$, (c) $1.0 < \tilde{Q} < \tilde{Q}_{critical}$, (d) $\tilde{Q} > \tilde{Q}_{critical}$.

For the case of $\tilde{Q} < 1.0$ the fire plume is completely contained within the compartment, and only product gases generated by the fire are exiting the compartment. For $\tilde{Q} = 1.0$ the length of the flame is such that the tip of the flame reaches the compartment opening. When $1.0 < \tilde{Q} < \tilde{Q}_{critical}$ the conditions at the compartment exit plane will comprise of both a flaming region and a hot gas region; therefore, species measurements performed in the out-flowing gases will be taken both inside and outside

of the flaming region. Beyond $\widetilde{Q}_{critical}$ all measurements in the exiting flow will be in the flaming region.

The values for $\dot{Q}_{Flame\ Extensions}$ used in the calculations are based on visual observations. The minimum heat release rates for which flames were experimentally observed to begin to exit the compartment are listed in Table 4-1, the calculated values for $\dot{Q}_{Ventilation-limit}$ and $\widetilde{Q}_{critical}$ are also listed. For the baseline doorway the fire size was gradually increased until the flames just began to exit the compartment. For the narrow doorway at a heat release rate of 91 kW "tiny wisps of flames" were observed to exit the compartment. For the wide doorway only four tests were performed. At the lowest heat release rate, 107 kW, no flames were observed coming from the compartment, while a continuous flame extending from the compartment was observed at a heat release rate of 203 kW. For lack of a more precise value the average of the two values, 155 kW, will be used in the calculations as the heat release rate at which flame extensions first began to occur for the wide doorway.

Table 4-1: $\dot{Q}_{Flame\ Extensions}$, $\dot{Q}_{Ventilation-limit}$, and $\widetilde{Q}_{critical}$ for the present geometries

Doorway Geometry	$\dot{Q}_{Flame\ Extensions}$ **(kW)**	$\dot{Q}_{Ventilation-limit}$ **(kW)**	$\widetilde{Q}_{critical}$
Narrow	91	183	2.01
Baseline	127	365	2.88
Wide	107 – 203 (155)	730	4.71

4.2.2 Species Yields based on Combustion within the Compartment

Since all of the measurements were performed at the exit plane of the compartment, conditions with external burning led to species measurements directly within the fire plume. These species levels are not the final 'frozen' species levels that

would be transported to remote locations, provided all of the combustion occurred in the compartment. Therefore, calculating the species yields based on the total amount of fuel injected into the compartment is not appropriate and the data need to be adjusted for the burning occurring within the compartment alone, i.e. not including external burning. Based on this, a new species yield is defined as $m_i / m_{\text{fuel, compartment}}$.

Since the amount of oxygen consumed by the fire is known, the amount of burning occurring in the compartment is determined using Equation 4-3, taken from Drysdale [2001],

$$\dot{Q}_{\text{compartment}} = \left(0.21 - X_{o_2,\text{scrubbed}}\right) \rho_{O_2} \; \Delta H_{c,ox} \; \dot{V} \qquad (4\text{-}3)$$

where $X_{O_2,\text{scrubbed}}$ is the mole fraction of oxygen in the scrubbed exhaust gases. "The process of scrubbing removes products of combustion from the flow of gas which is supplied continuously to the oxygen analyzer…" [Drysdale 2001] In the present study the products of combustion were not scrubbed, therefore, the correct oxygen mole fraction is determined from the conservation of mass,

$$y_{O_2,\text{scrubbed}} = y_{O_2}\left(\frac{\dot{m}_{air}}{\dot{m}_{air} - \left(\dot{m}_{co} + \dot{m}_{co_2} + \dot{m}_{o_2}\right)}\right) = y_{O_2}\left(\frac{\dot{m}_{air}}{\dot{m}_{air} - \left(y_{co}\dot{m}_{air} + y_{co_2}\dot{m}_{air} + y_{o_2}\dot{m}_{air}\right)}\right)$$

$$y_{O_2,\text{scrubbed}} = y_{O_2}\left(\frac{1}{1 - \left(y_{co} + y_{co_2} + y_{o_2}\right)}\right)$$

and

$$X_{O_2,\text{scrubbed}} = \frac{y_{O_2,\text{scrubbed}}\ MW_{UL}}{MW_{O_2}}$$

Also, volumetric flow rate of air is equal to,

$$\dot{V} = \frac{\dot{m}_{air}}{\rho_{air}}$$

Therefore, Equation 4.3 becomes

$$\dot{Q}_{compartment} = \left(0.21 - X_{o_2,\text{scrubbed}}\right)\dot{m}_{air}\ \frac{\rho_{O_2}}{\rho_{air}}\ \Delta H_{c,ox} \qquad (4\text{-}3b)$$

however, since air and oxygen are at the same conditions, the density ratio in Equation 4-3b can be replaced with a molecular weight ratio.

$$\frac{\rho_{O_2}}{\rho_{air}} = \frac{\left(\frac{P\ MW_{O_2}}{R\ T}\right)}{\left(\frac{P\ MW_{air}}{R\ T}\right)} = \frac{MW_{O_2}}{MW_{air}}$$

hence,

$$\dot{Q}_{compartment} = \left(0.21 - X_{o_2,\text{scrubbed}}\right)\dot{m}_{air}\ \frac{MW_{O_2}}{MW_{air}}\ \Delta H_{c,ox} \qquad (4\text{-}3c)$$

Where $\Delta H_{c,ox}$ is defined as the heat of combustion per gram of oxygen consumed. For propane, $\Delta H_{c,ox}$ has a value of 12,800 kJ/kg. This value is based on complete combustion where the products of combustion are only CO_2 and H_2O. In compartment fires complete combustion is seldom seen and products of incomplete combustion, CO and soot, are also present. Therefore, a combustion efficiency, χ, is included to account for incomplete combustion.

$$\dot{Q}_{compartment} = \left(0.21 - X_{o_2,scrubbed}\right) \dot{m}_{air} \frac{MW_{O_2}}{MW_{air}} \left(\chi \, \Delta H_{c,ox}\right) \qquad (4\text{-}3d)$$

The amount of fuel burned in the compartment is determined using the calculated heat release rate from Equation 4-3d and the effective heat of combustion of propane, $\chi \, \Delta H_c$, again accounting for incomplete combustion,

$$\dot{m}_{fuel,\,compartment} = \frac{\dot{Q}_{compartment}}{\chi \, \Delta H_c} = \frac{\left(0.21 - X_{o_2,scrubbed}\right) \dot{m}_{air} \frac{MW_{O_2}}{MW_{air}} \left(\chi \, \Delta H_{c,ox}\right)}{\Delta H_c} \qquad (4\text{-}4)$$

The calculated $\dot{m}_{fuel,\,compartment}$ can then be used in the denominator of Equation 2-11 and Equation 2-12 to determine the species yields based solely on the combustion in the compartment.

Prior to applying this analysis to the data, verification of the methodology used to determine the amount of combustion occurring in the compartment is needed. The calculated heat release rates in the compartment as a function of the ideal heat release rates for each of the three doorway widths are shown in Figure 4-2. Also included are the calculated ventilation limit heat release rates based on each ventilation condition. If the

data fall on the diagonal line below the corresponding ventilation limit, then the burning conditions are fuel limited.

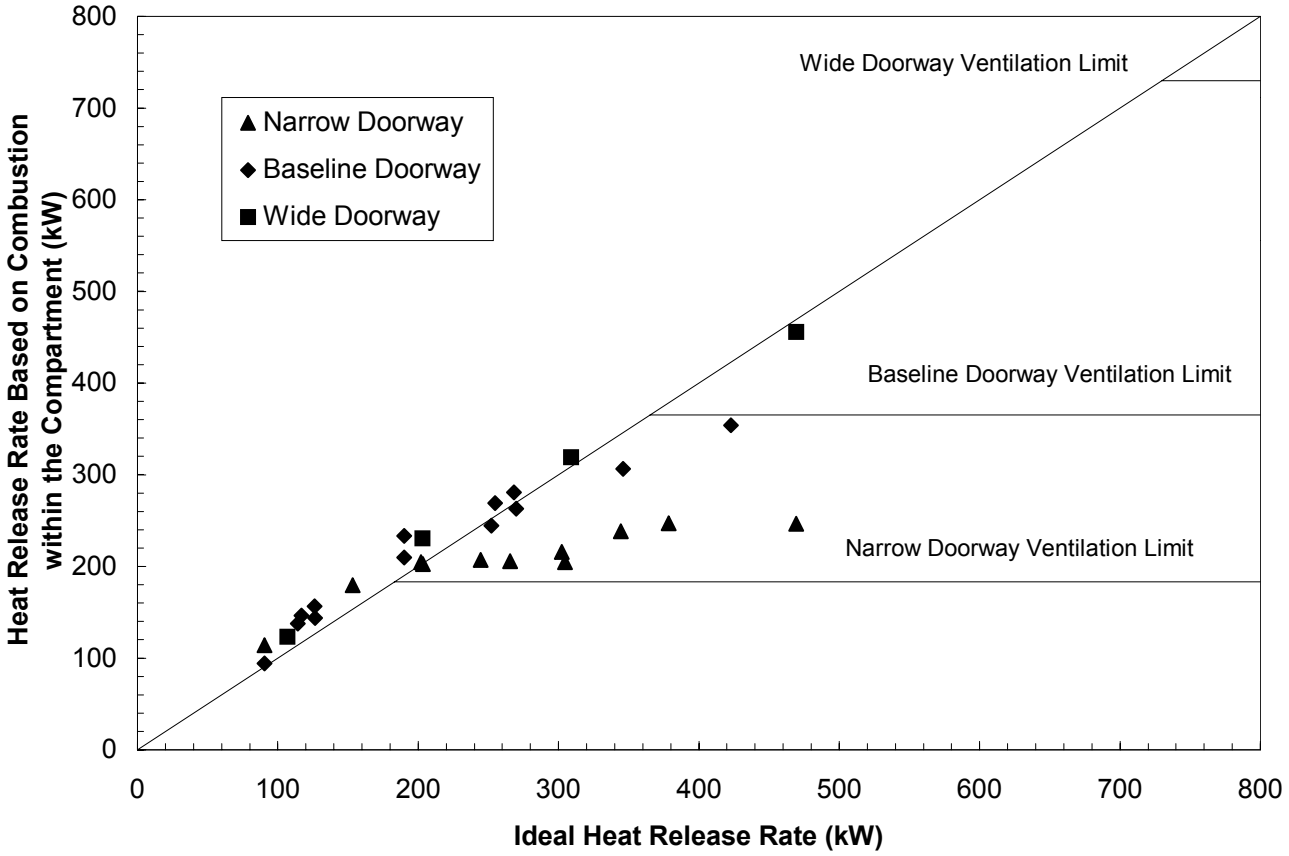

Figure 4-2: Heat Release Rate within Compartment versus Ideal Heat Release Rate

The ideal heat release rate, $\dot{m}_{fuel}\Delta H_c$, is based on the amount of propane injected into the compartment and the heat of combustion of propane. The horizontal lines are the theoretical maximum heat release rate supported in the compartment based on the ventilation limit. The ventilation limit heat release rates are 183 kW, 365 kW, and 730 kW for the narrow, baseline, and wide doorways respectively. Comparison of the fuel limited heat release rates with the ventilation limited heat release rates, Figure 4-2,

indicate that for the test conditions the baseline and wide doorways were always fuel limited. Both burning regimes were observed with the narrow doorway.

The agreement between the calculated heat release rate for combustion occurring within the compartment and the ventilation limit heat release rates indicates that using Equations 4-4 and 4-5 to determine the amount of fuel consumed within the compartment is valid for this analysis.

4.3 SPECIES MOLE FRACTIONS VERSUS NON-DIMENSIONAL HEAT RELEASE RATE

The integrated species mole fractions as a function of $\widetilde{Q}$ are shown in Figure 4-3 through Figure 4-6. It should be noted that the oxygen mole fractions shown are the amount of oxygen depleted in the compartment, i.e. 21% – $\overline{X}_{O_2}$, since it is a consumed species.

Examination of the oxygen and carbon dioxide mole fractions as a function of $\widetilde{Q}$, Figure 4-3 and Figure 4-4, indicates that the data for all three ventilation conditions follow the same trends but form three separate curves, one for each doorway. The wide doorway data indicate the lowest depleted fraction of oxygen and lowest generation of carbon dioxide, while the highest depletion of oxygen and generation of carbon dioxide is seen for the narrow doorway. The baseline doorway data fall in-between.

Using this methodology the carbon monoxide and the unburned hydrocarbon data, Figure 4-5 and Figure 4-6, collapse to a single curve for all three ventilation conditions. The carbon monoxide levels, Figure 4-5, begin to increase at approximately $\widetilde{Q}$ = 1.25, while the unburned hydrocarbons do not increase until $\widetilde{Q}$ = 2.25. The carbon monoxide mole fractions, Figure 4-5, increase linearly and begin to taper off slightly at $\widetilde{Q}$ = 3.6. Similarly, the unburned hydrocarbon mole fractions, Figure 4-6, increase linearly. It is

anticipated that this trend would continue as $\tilde{Q}$ increases, and that the unburned hydrocarbon levels will approach 100 % as $\tilde{Q}$ approaches infinity.

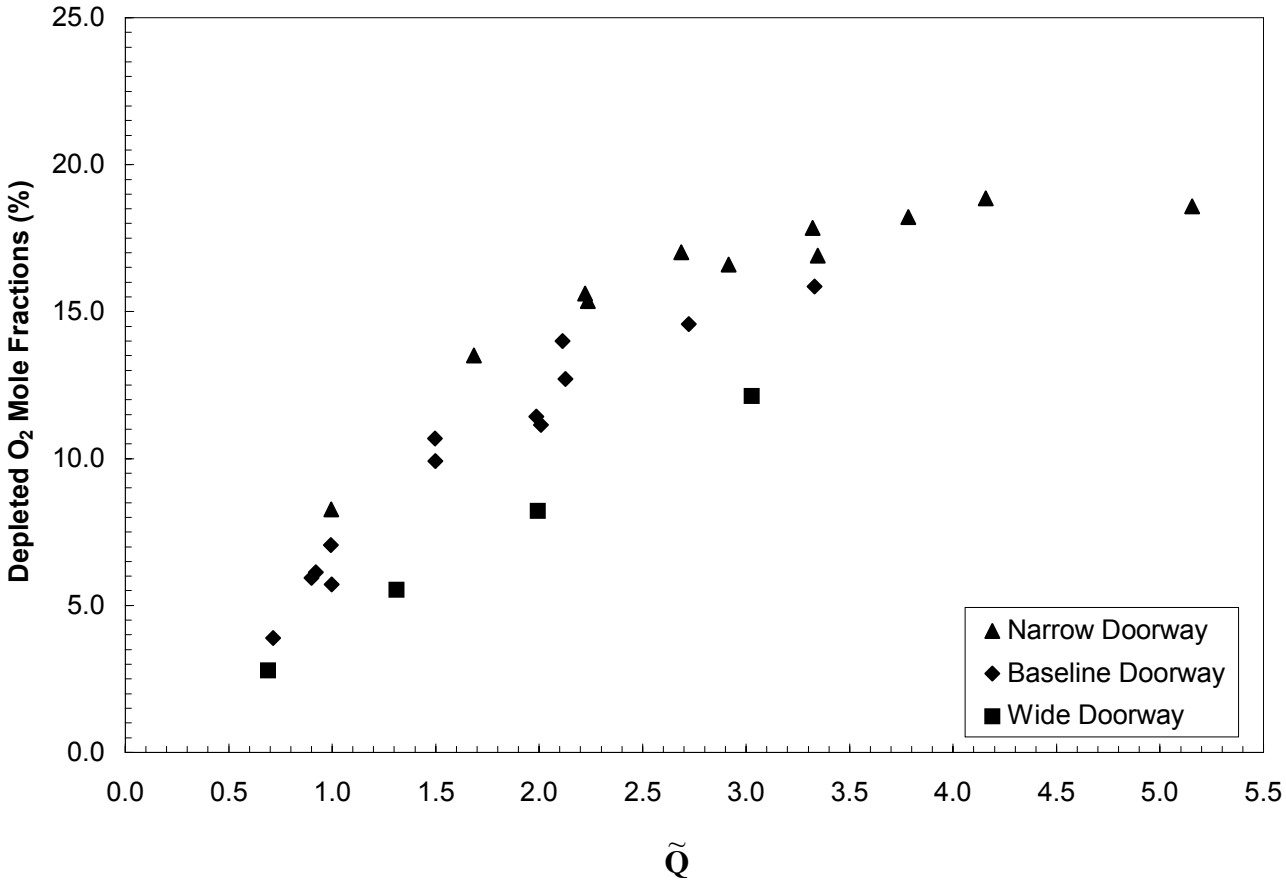

Figure 4-3: Integrated average oxygen mole fractions (depleted) as a function of the non-dimensional heat release rate parameter, $\tilde{Q}$.

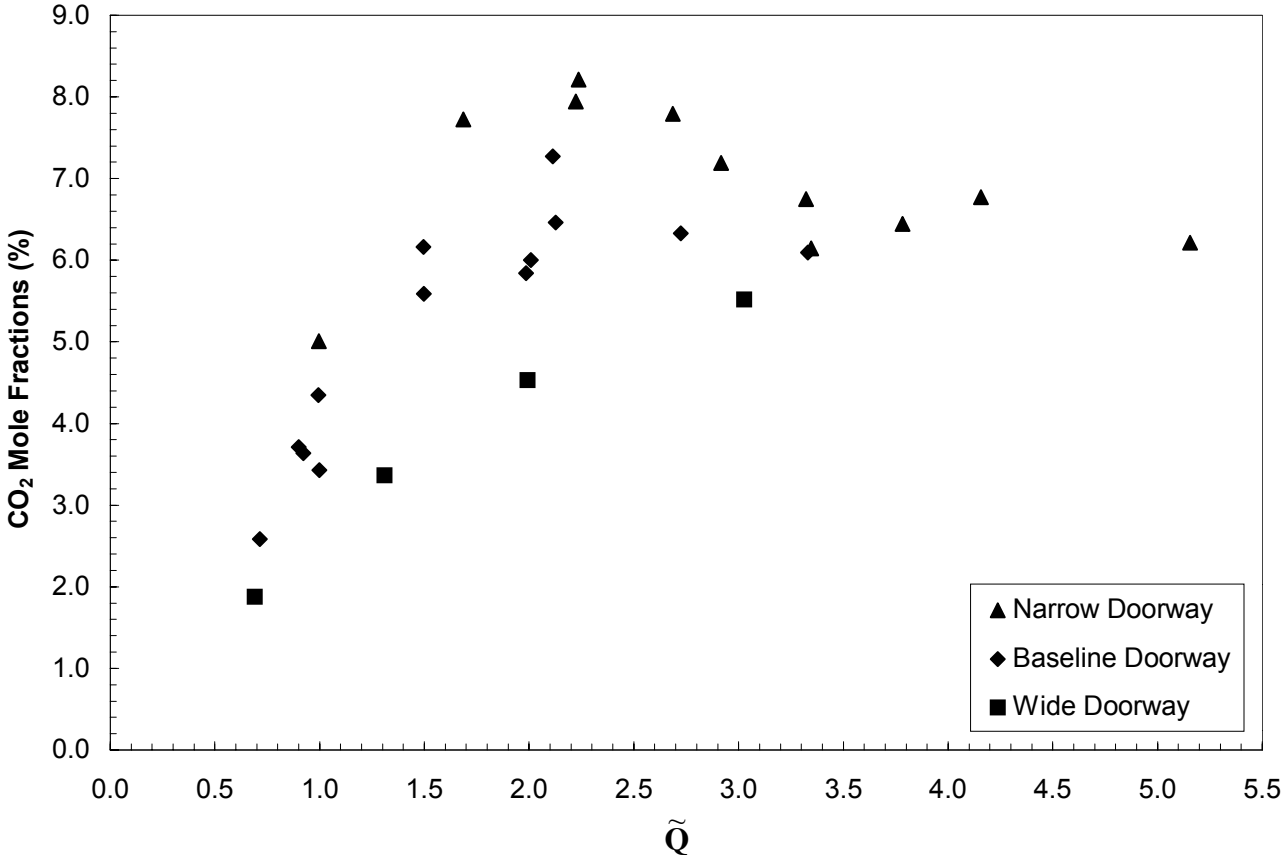

Figure 4-4: Integrated average carbon dioxide mole fractions as a function of the non-dimensional heat release rate parameter, $\tilde{Q}$.

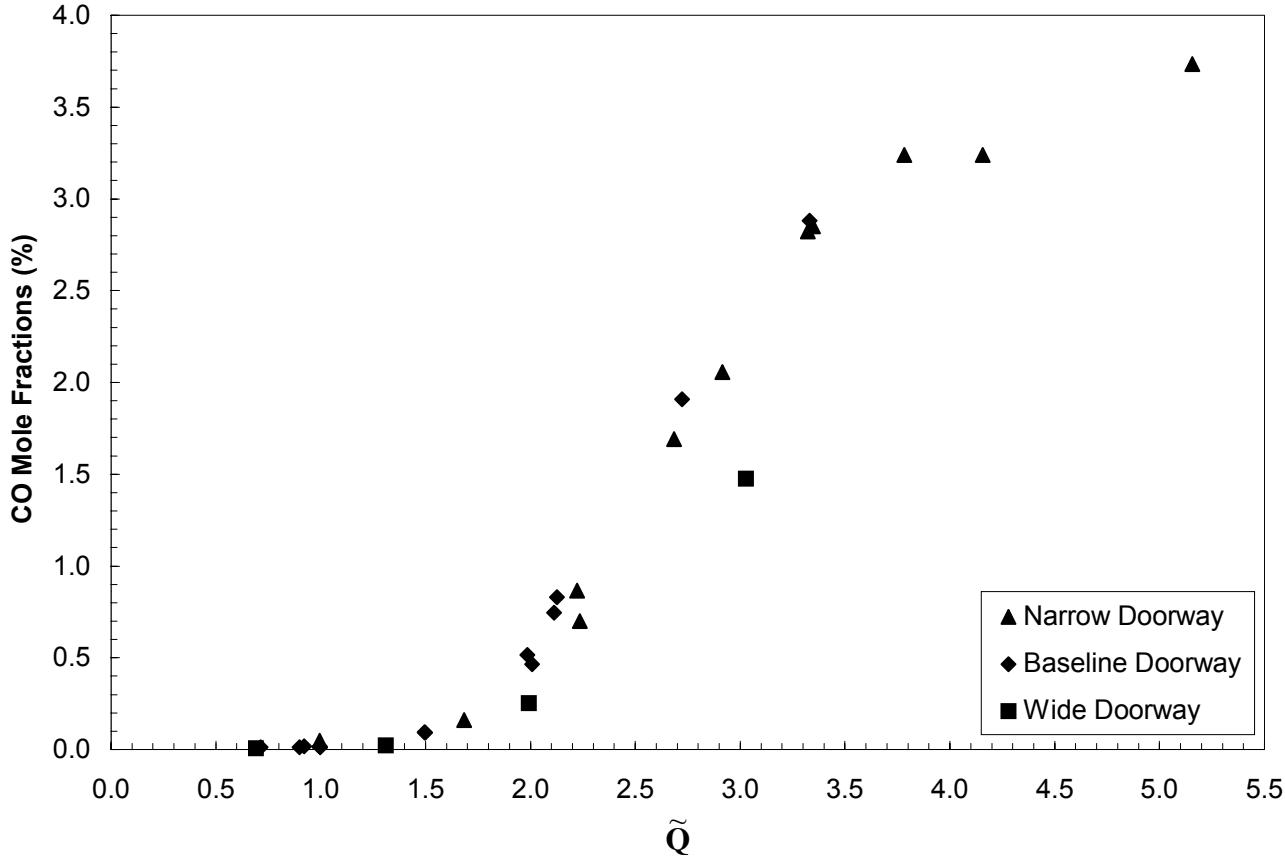

Figure 4-5: Integrated average carbon monoxide mole fractions as a function of the non-dimensional heat release rate parameter, $\tilde{Q}$.

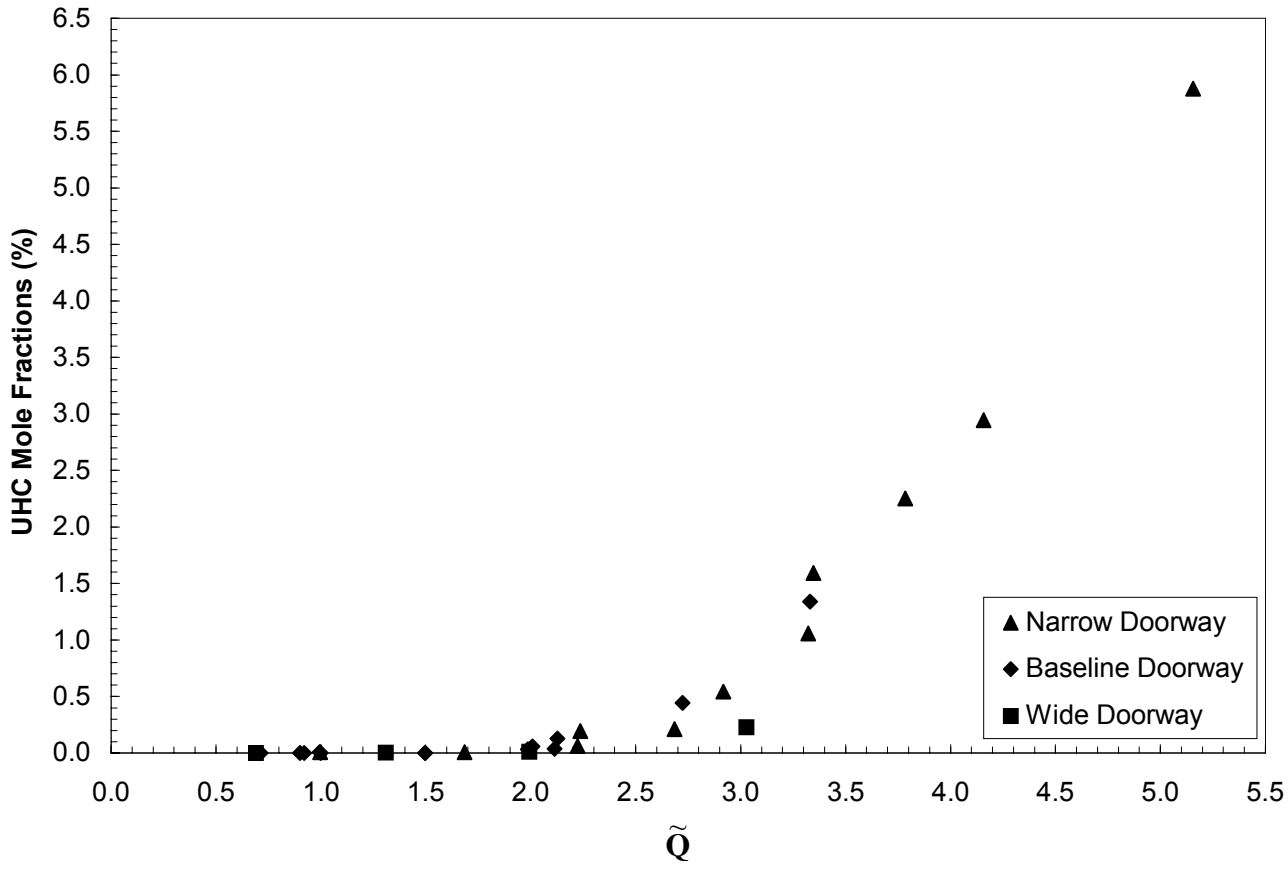

Figure 4-6: Integrated average unburned hydrocarbon mole fractions as a function of the non-dimensional heat release rate parameter, $\tilde{Q}$.

The entire fire plume was contained within the compartment for 5 data points, 1 narrow, 3 baseline, and 1 wide, indicated by $\tilde{Q} < 1.0$. From the data it can be determined that the hot gases exiting the compartment consisted only of oxygen and carbon dioxide, no carbon monoxide or unburned hydrocarbons were present.

In general most tests in the present study fell into $1.0 < \tilde{Q} < \tilde{Q}_{critical}$ range indicating that the exiting hot gases from the compartment consisted of the fire plume and hot combustion gases. It is interesting to note that within this range for the narrow doorway, where $\tilde{Q}_{critical} = 2.01$, the gases exiting from the compartment consisted of

oxygen, carbon dioxide, and carbon monoxide, no unburned hydrocarbons were present. For the baseline and wide doorways all four species were present, once $\widetilde{Q}$ exceeded 2.5, which is lower then $\widetilde{Q}_{critical}$ for each doorway.

For the narrow doorway, conditions that exceeded $\widetilde{Q}_{critical}$ were also achieved. The most interesting observation in the data for this condition is the decrease in carbon dioxide levels beyond $\widetilde{Q}_{critical}$. Examination of Figure 4-4 indicates that at $\widetilde{Q}_{critical}$ for the narrow doorway, the carbon dioxide mole fraction peaks at 8.0 %, beyond $\widetilde{Q}_{critical}$ the carbon dioxide mole fractions decrease. It is assumed that similar results would be observed for the baseline and wide doorways.

It is interesting to note that the carbon monoxide and unburned hydrocarbons mole fractions, Figure 4-5 and Figure 4-6, collapse to a single curve when correlated as a function of $\widetilde{Q}$. The data indicate that the levels of species of incomplete combustion, at the compartment exit plane, are independent of the degree of burning within the compartment. This should be considered fortunate in view of the fact that the burning conditions are different for each doorway. The observation that the data collapse to a single curve requires justification, and an explanation for these trends is presented next.

For a given $\widetilde{Q}$, for example $\widetilde{Q}$ = 2.0, the heat release rate for the narrow, baseline, and wide doorways are 182 kW, 254 kW, and 310 kW respectively. Therefore, the carbon monoxide and unburned hydrocarbon levels measured are attributed only to the respective heat release rates.

Unlike the products of incomplete combustion, depleted oxygen and carbon dioxide, are a function of both $\widetilde{Q}$ and the doorway width. Examining the mole fractions of oxygen depleted in the compartment, Figure 4-3, it is seen that the least amount of oxygen was depleted under the wide doorway conditions and the most under the narrow doorway conditions. Therefore, noting that the carbon monoxide and unburned hydrocarbon mole fractions are the same independent of the doorway width, it can be

reasoned that the lowest levels of carbon dioxide, formed in the compartment, will be seen for the wide doorway and the highest for the narrow doorway. Examining Figure 4-4, these trends are indeed observed.

It is shown in the following section that when the species yields, based only on the combustion occurring within the compartment, are correlated as a function of $\widetilde{Q}$ the data for all four species collapse to four separate curves and are independent of the doorway width.

Due to the external burning that begins to occur once $\widetilde{Q}$ exceeds 1.0 for all three doorway widths, the species levels transported down stream of the compartment exit plane will be different than those observed at the exit plane. The final species observed at a downstream location of the compartment exit plane will be a function of not only the conditions in the compartment but also of additional oxygen and fuel sources available in the adjacent space.

4.4 SPECIES YIELDS VERSUS NON-DIMENSIONAL HEAT RELEASE RATE

The calculated species yields based on the combustion occurring in the compartment as a function of $\widetilde{Q}$ for oxygen, carbon dioxide, carbon monoxide, and unburned hydrocarbons are presented in Figure 4-7 through Figure 4-10 respectively. The oxygen and carbon dioxide data are presented as normalized yields.

Presenting the data in this manner, the data collapse to a single curve for each species, respectively. The normalized oxygen yields (mass of O_2 depleted), Figure 4-7, indicate a value of approximately 0.9 for all $\widetilde{Q}$. This is expected since the current analysis is based only on the amount of oxygen consumed within the compartment. It has been shown in Figure 4-2, that the heat released in the compartment is constant once the ventilation limit is reached.

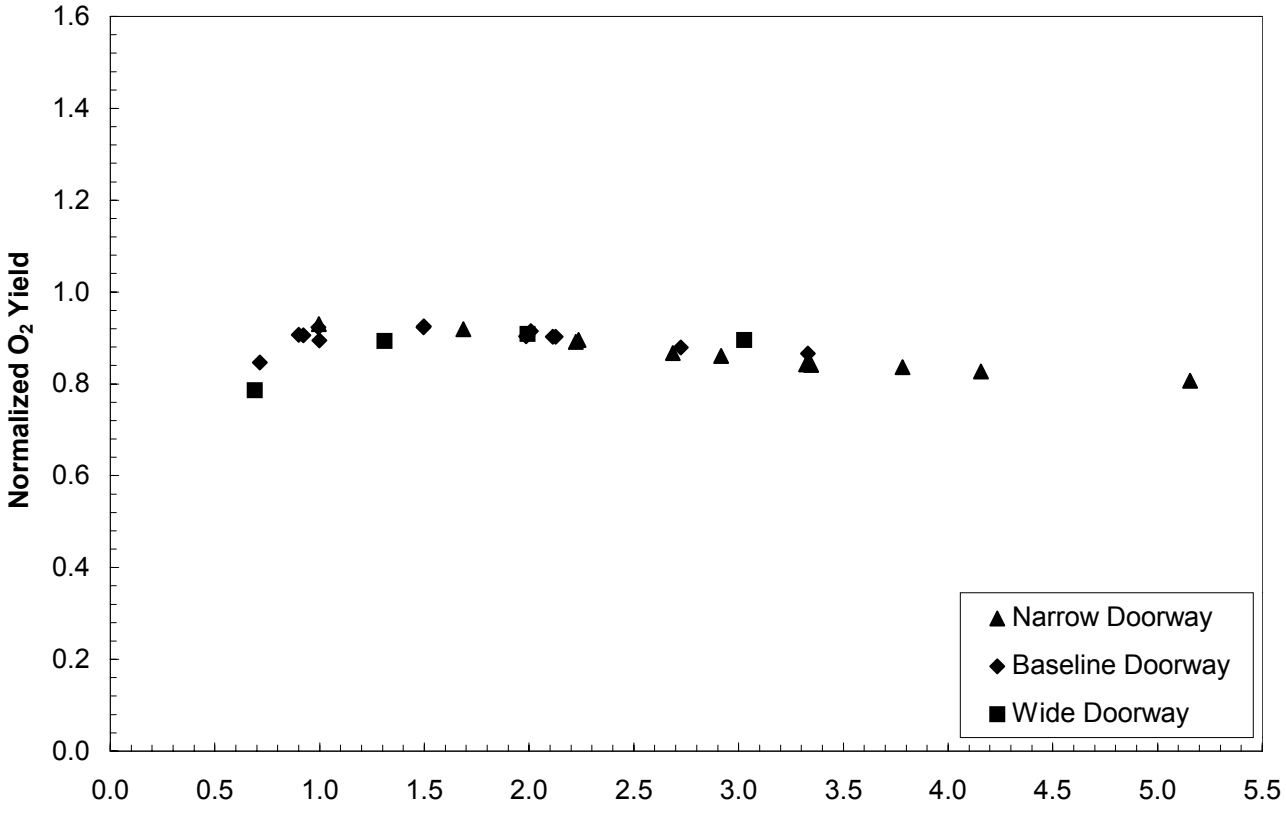

Figure 4-7: Normalized oxygen species yield versus $\tilde{Q}$.

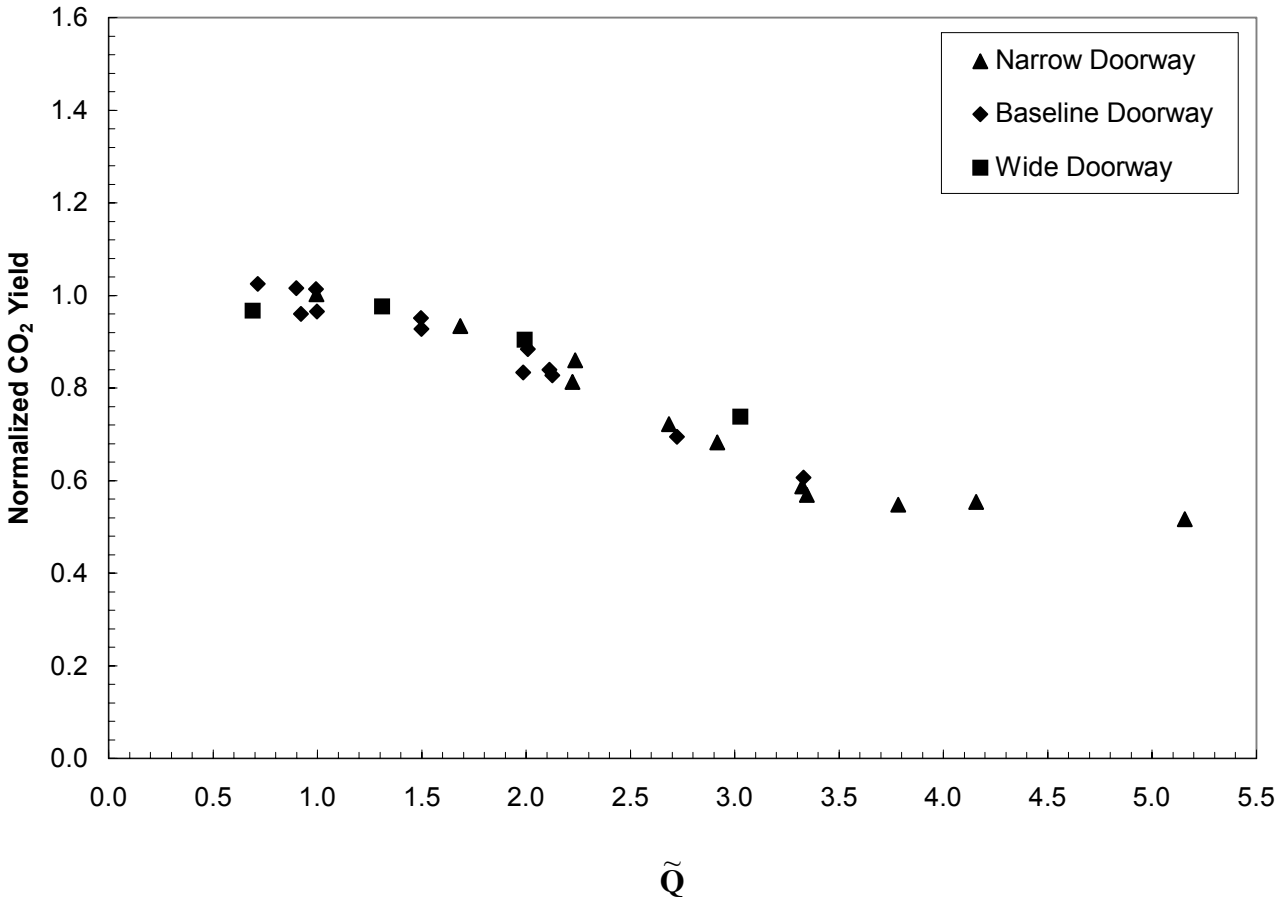

Figure 4-8: Normalized carbon dioxide species yield versus $\tilde{Q}$.

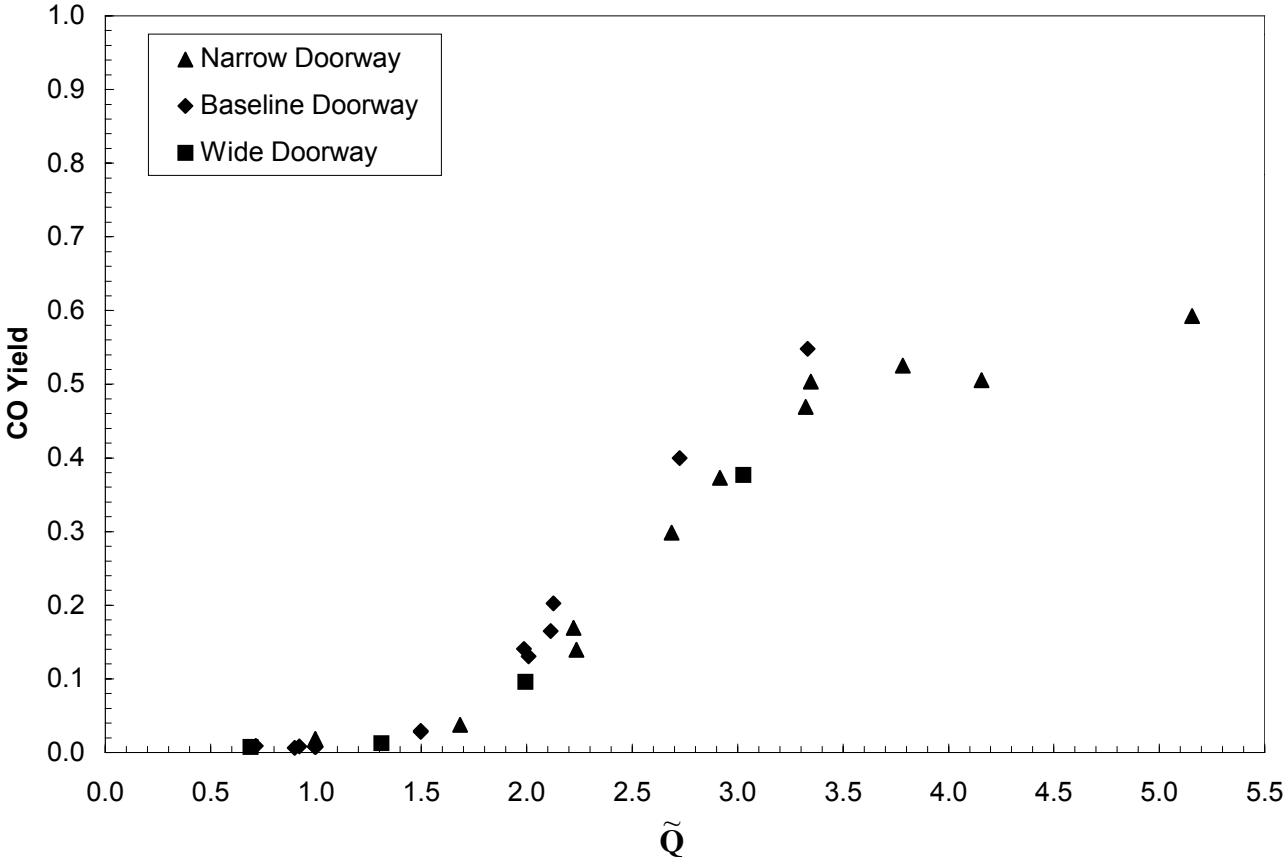

Figure 4-9: Carbon Monoxide species yield versus $\tilde{Q}$.

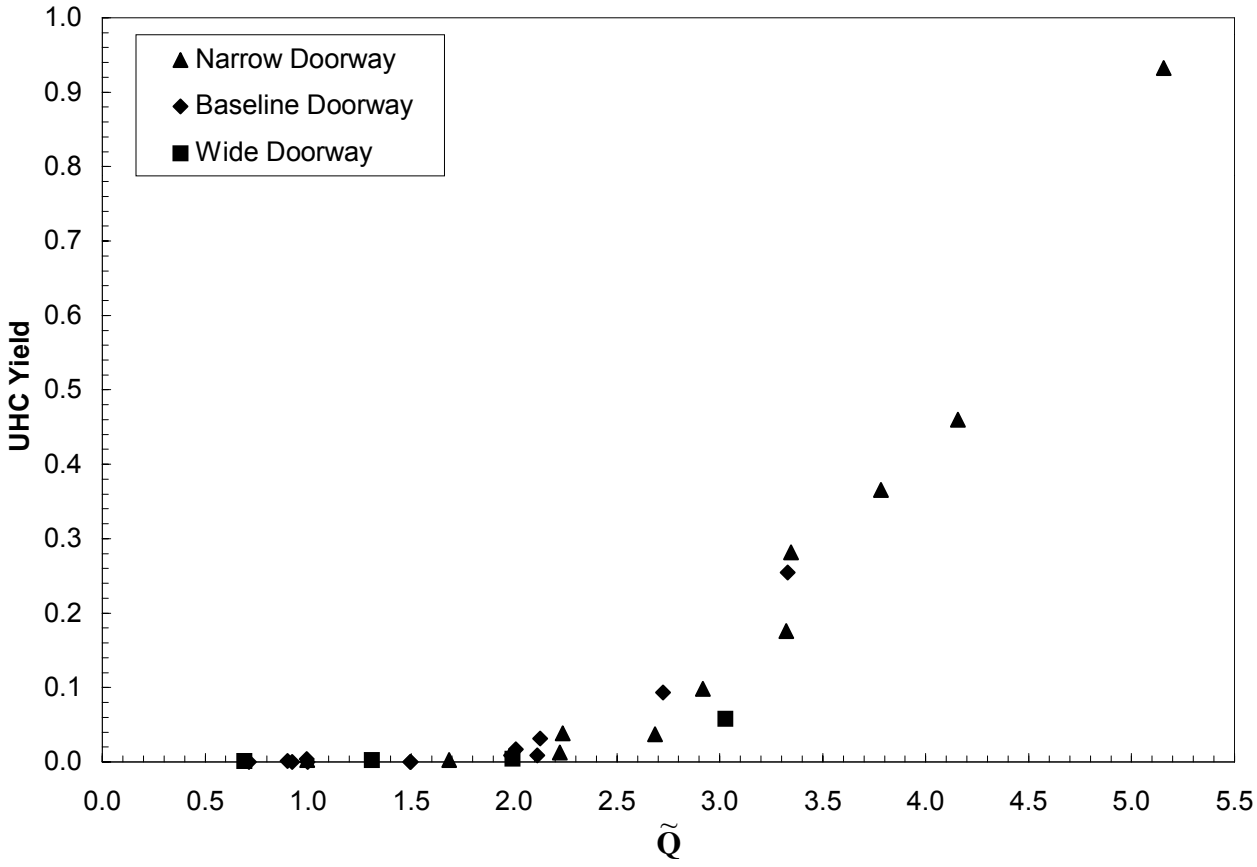

Figure 4-10: Unburned Hydrocarbon species yield versus $\tilde{Q}$.

The normalized carbon dioxide yields, Figure 4-8, appear to correlate well with $\tilde{Q}$. The data indicate a value of 1.0 for $0 < \tilde{Q} < 1.0$, and as $\tilde{Q}$ increases beyond 1.0, the CO_2 generated within the compartment decreases, this coincides with an increase in carbon monoxide and unburned hydrocarbons seen in Figure 4-9 and Figure 4-10. As $\tilde{Q}$ goes to infinity it is anticipated that the carbon dioxide yields will decrease to zero.

The carbon monoxide yields, Figure 4-9, indicate that incomplete combustion within the compartment begins to occur around $\tilde{Q}$ = 1.25, corresponding to a $\tilde{Q}$ just beyond that for which flame extensions begin to occur. The upper bound for the CO yield is the theoretical maximum yield for propane, 1.91 g_{co}/g_{fuel}. The current data, however, appear to begin to plateau at $\tilde{Q}$ > 3.5 approaching a species yield of

approximately 0.50 g_{co}/g_{fuel}. Similar to the carbon dioxide yields, as $\tilde{Q}$ goes to infinity, only fuel will be present; therefore, it is expected that, the carbon monoxide yields will begin to decrease and approach zero at higher values of $\tilde{Q}$.

The unburned hydrocarbon yields, Figure 4-10, begin to increase at $\tilde{Q}$=2.0 and indicate a continuous rise. As opposed to the old analysis where the maximum UHC yield could not exceed 0.96 g_{uhc}/g_{fuel}, under the modified analysis there is no upper bound for the UHC yield.

The species yields at the compartment exit plane should be viewed as the inlet boundary conditions to the hallway and not as the final species transported to remote locations. Once the onset of external burning occurs, $\tilde{Q}$ > 1.0, the species transported downstream can no longer be defined based solely on compartment parameters. The final species levels will be a function of the conditions in the adjacent space, i.e., available oxygen, geometry, and secondary fuel sources.

4.5 CORRELATION DEVELOPMENT

Correlations based on the data presented in Section 4.4 are developed based on a data regression analysis for normalized carbon dioxide, carbon monoxide, and unburned hydrocarbon yields as a function of the non-dimensional heat release rate, $\tilde{Q}$. The correlations developed using the software program CurveExpert (version 1.34) are based on non-linear regression techniques for carbon dioxide and carbon monoxide data. The data for the range of $\tilde{Q}$ examined are best represented as a Sigmoidal or "S-shaped" growth curve. A linear regression analysis was applied to the unburned hydrocarbon data.

The results from the regression analysis are presented along with the data for each of the three species in Figure 4-11 through Figure 4-13. The carbon dioxide yields are represented as a MMF curve, Equation 4-5, and presented along with the data in Figure 4-11.

$$Y_{CO_2} = \frac{a \cdot b + c \cdot \widetilde{Q}^d}{b + \widetilde{Q}^d} \qquad (4\text{-}5)$$

The values for the coefficients a, b, c, and d are

a = 0.487
b = 0.016
c = 1.00
d = -4.40

The data regression analysis indicated that the standard error for the curve was 0.029 and the R^2 value was 0.995.

The carbon monoxide yields were also represented as a MMF curve, Equation 4-5; the curve fit to the data is presented in Figure 4-12. The values for the coefficients in Equation 4-5 for the carbon monoxide data are,

a = 0.0062
b = 219.4
c = 0.58
d = 5.77

and had a reported standard error was 0.030 and the R^2 value was 0.99.

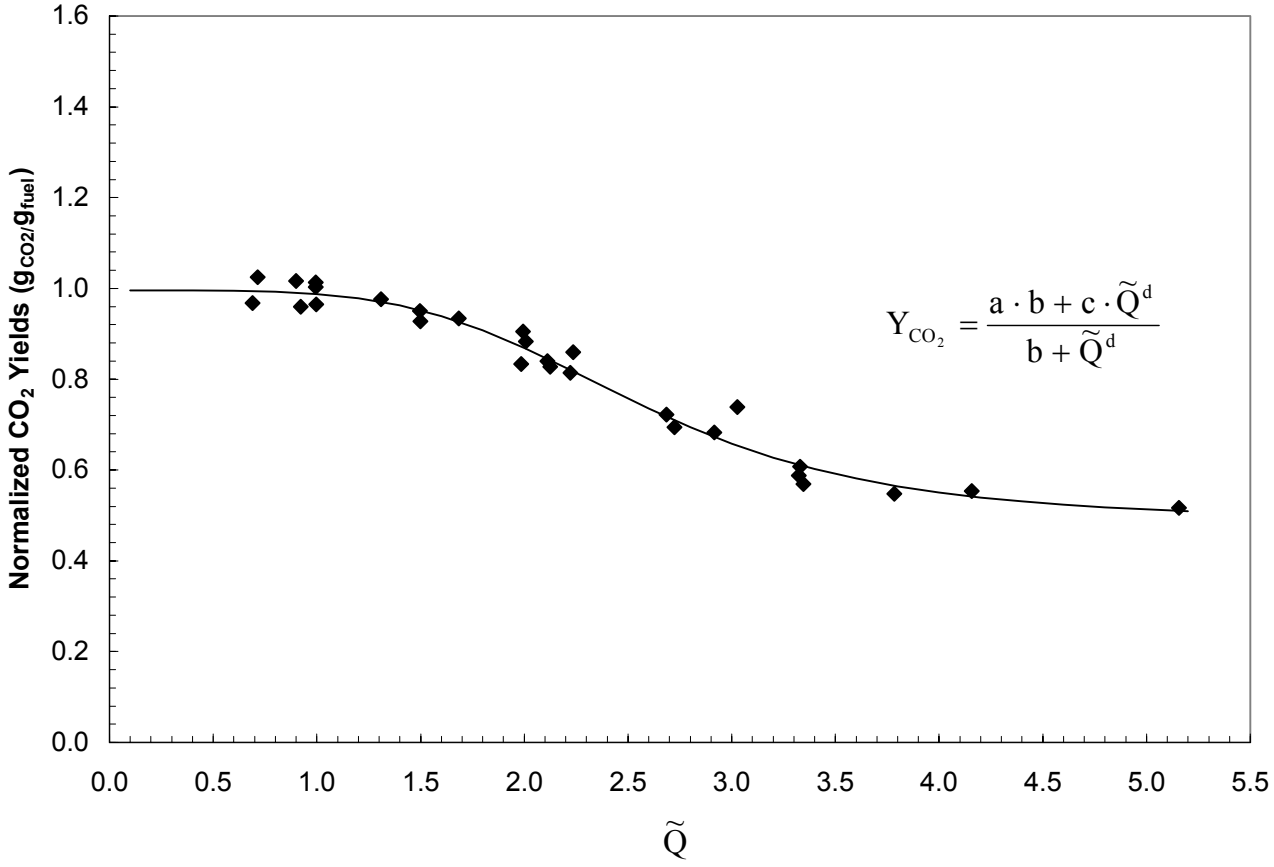

Figure 4-11: Carbon dioxide yields (based on combustion within the compartment) as a function of $\tilde{Q}$ along with a curve fit to the data based on the MMF Sigmoidal growth curve.

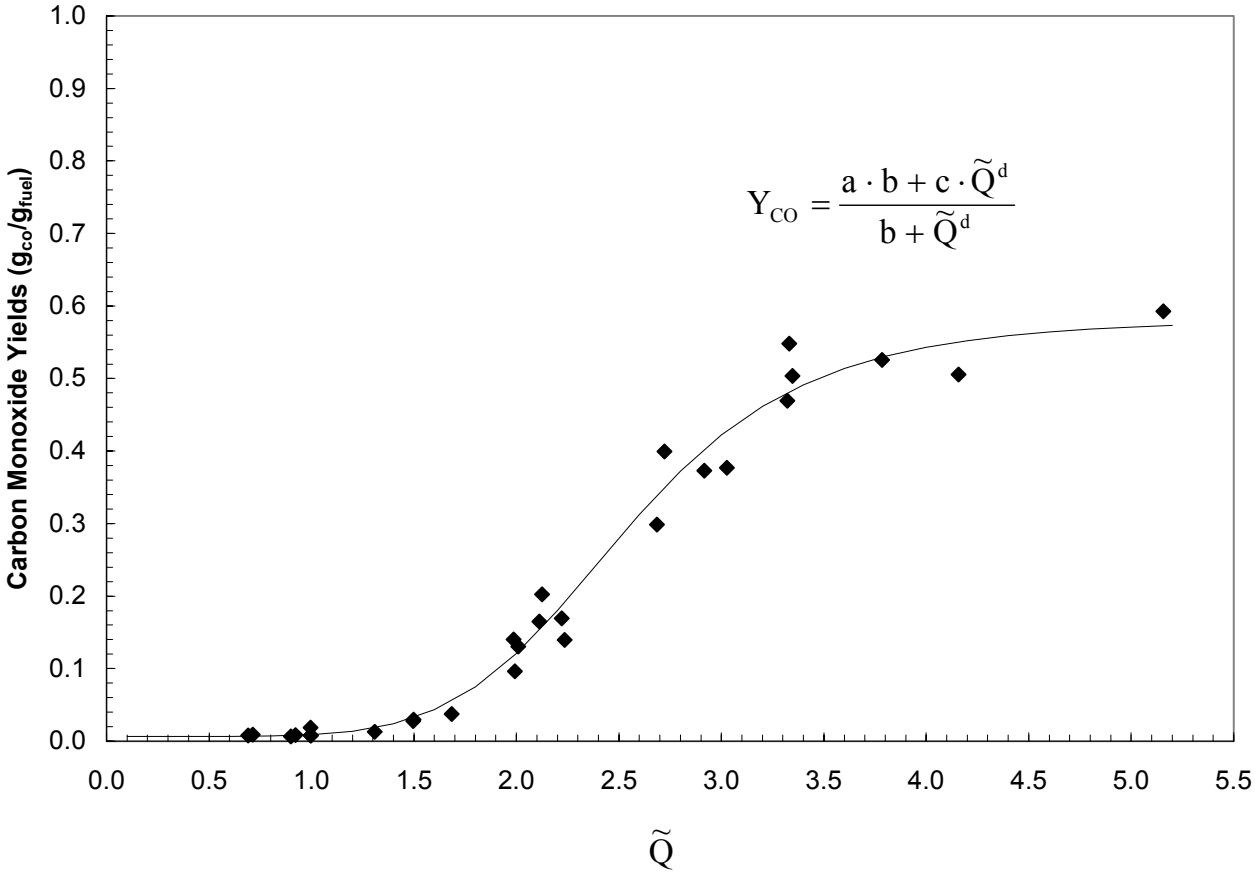

Figure 4-12: Carbon monoxide yields (based on combustion within the compartment) as a function of $\tilde{Q}$ along with a curve fit to the data based on the MMF Sigmoidal growth curve.

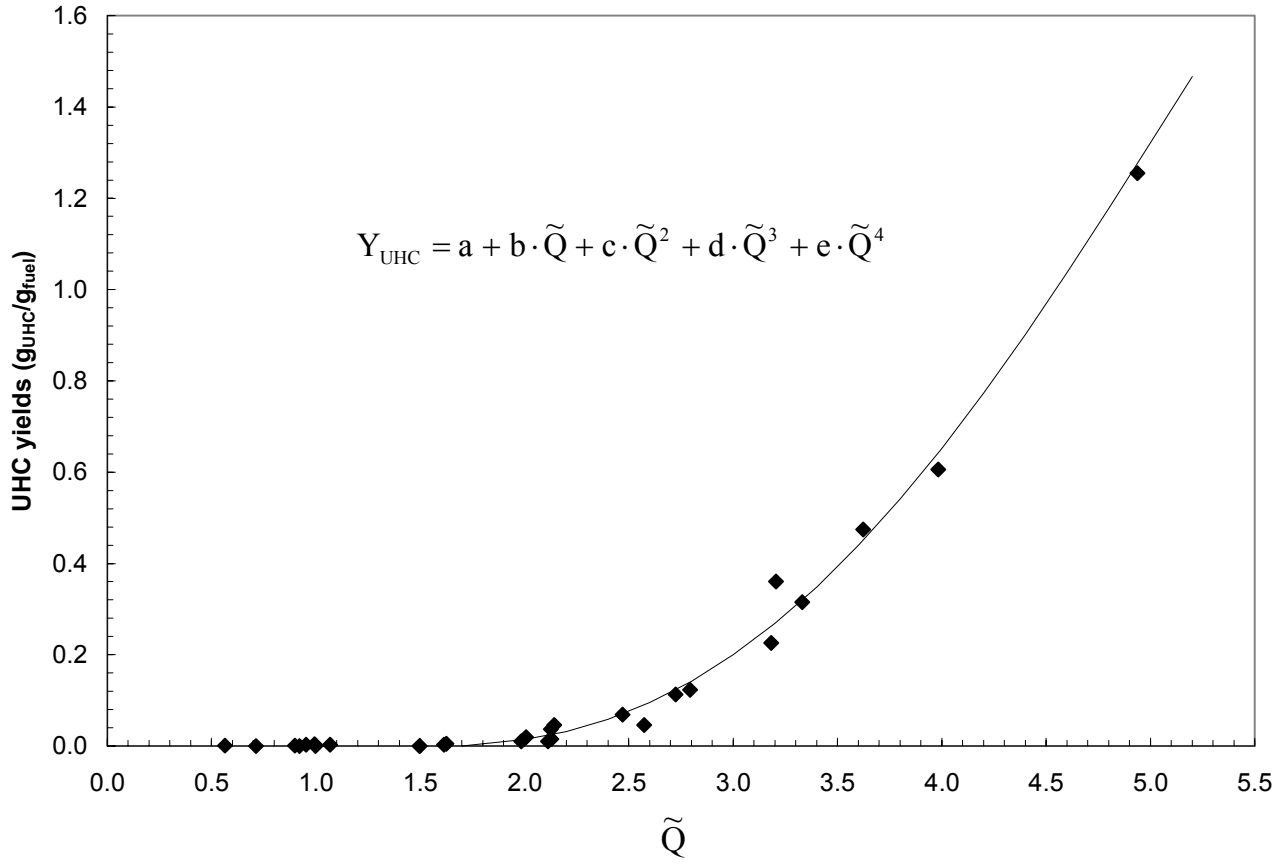

Figure 4-13: Unburned hydrocarbon yields (based on combustion within the compartment) as a function of $\tilde{Q}$ along with a curve fit to the data based on a 4th order polynomial linear regression analysis.

The unburned hydrocarbon data are presented in Figure 4-13. The data for unburned hydrocarbons are divided into two ranges. The first range is for $\tilde{Q} < 2.0$ where the unburned hydrocarbon yield is zero, Equation 4-6a.

$$Y_{UHC} = 0 \qquad \text{for } \tilde{Q} < 2.0 \qquad (4\text{-}6a)$$

For $2.0 \leq \widetilde{Q} \leq 5.2$ the unburned hydrocarbons yields are determined via Equation 4-6b.

$$Y_{UHC} = a + b \cdot \widetilde{Q} + c \cdot \widetilde{Q}^2 + d \cdot \widetilde{Q}^3 + e \cdot \widetilde{Q}^4 \qquad \text{for } 2.0 \leq \widetilde{Q} \leq 5.2 \qquad (4\text{-}6b)$$

where,

a = -0.063
b = 0.208
c = -0.209
d = 0.074
e = -0.006

Equation 4-6b is a 4th order polynomial, with a standard error of 0.031 and a R^2 value of 0.995.

Due to a limited range of values examined in this study and limitations in the correlating functions, the correlations developed in this section should be used only within the range of values for which they were developed. As $\widetilde{Q}$ increases, the Sigmoidal MMF curve, Equation 4-5 reaches a constant value, however, as mentioned previously, it is anticipated that both the carbon dioxide and carbon monoxide yields will decrease to zero as $\widetilde{Q}$ goes to infinity. With regards to the unburned hydrocarbon yield correlation, the regression analysis is based on a 4th order polynomial, and the equation is only valid within the range for which it was defined. Unburned hydrocarbon yields for values exceeding $\widetilde{Q} = 5.2$ should be extrapolated graphically.

CHAPTER 5

RESULTS AND DISCUSSION - TRANSPORT STUDY

5.1 INTRODUCTION

As reported in Sections 1.2.2 and 1.2.3, statistics in both the mining and building industries have shown that the transport of carbon monoxide from a fire is the leading cause of death to occupants located remote from the fire origin. [Hall 1997, Karter 2000, McPherson 1993] The second phase of the project was aimed at evaluating the species levels transported from the fire as a function of the ventilation conditions and the heat release rate of the fire. The focus of the study was for the steady-state portion of the fire; therefore, prior to conducting the study it was necessary to determine if steady-state conditions existed and to evaluate the effects of initial boundary temperatures on the species levels transported. The focus of the transport study was then aimed at examining the species levels present at the exit plane of the baseline compartment doorway as a function of the hallway exit doorway width for three heat release rates.

5.2 HALLWAY STUDY WITH SLIVER COMPARTMENT DOORWAY

5.2.1 Steady-State Issues

Steady-state conditions are required in order to achieve a consistent data set over the course of each experiment. Performing mappings at the compartment doorway, along the hallway, and at the end of the hallway, require that steady-state conditions be maintained for several hours.

Steady-state conditions were evaluated for the system with the sliver doorway at x = 0 m (compartment/hallway interface) and no doorway or soffit at x = 6.1 m (end of hallway). The measurements during the test were taken in the order of x = 6.1 m, 3.7 m, and 1.2 m, after an initial warm-up period of 6,000 seconds. The heat release rate during

the test was 130 kW. A time trace of the carbon monoxide mole fractions is shown in Figure 5-1. It should be noted that at each axial location, x, five samples along the vertical, z, were taken at three horizontal locations, y. The data in Figure 5-1 corresponds to these sampling locations.

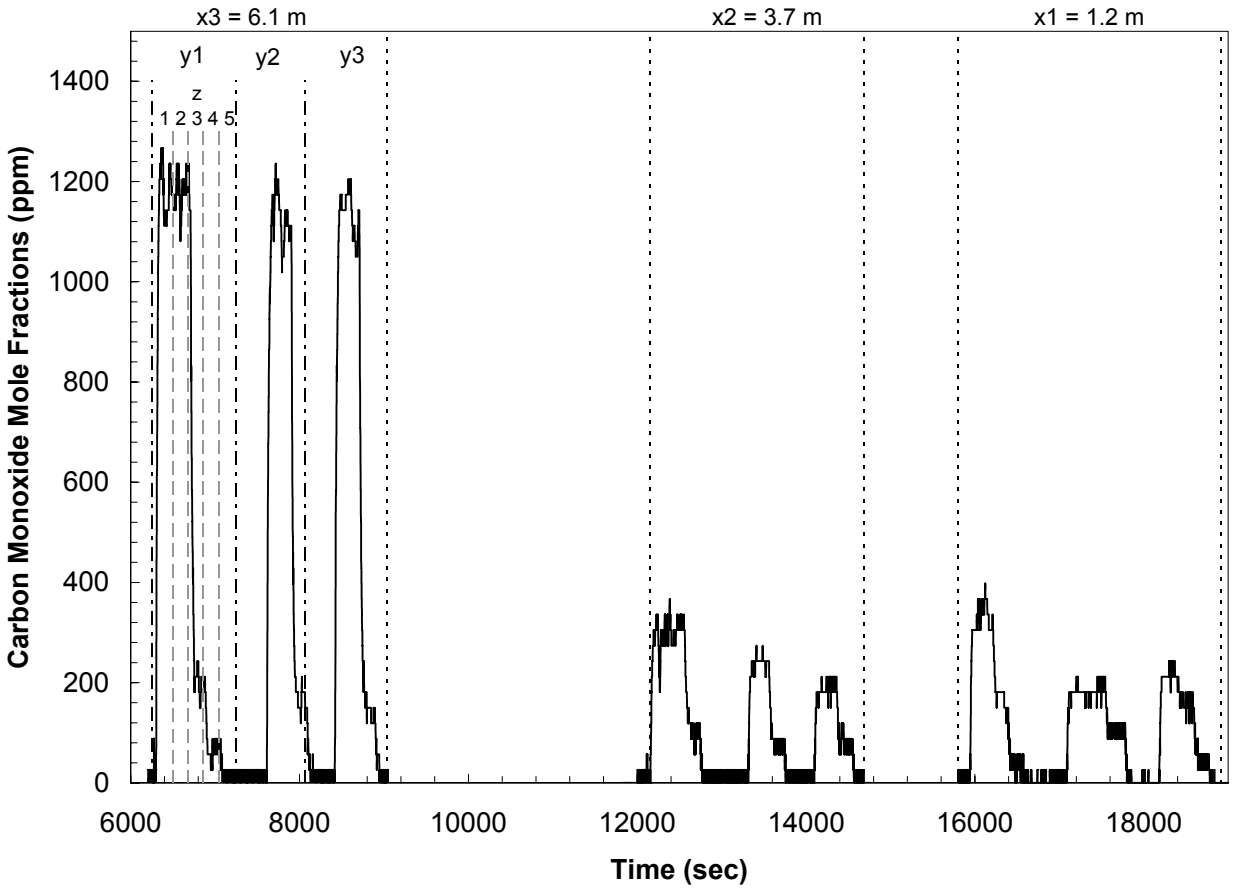

Figure 5-1: Time trace of carbon monoxide mole fractions for three axial locations along the hallway, x = 6.1 m, x = 3.7 m, and x = 1.2 m. At each axial location the time trace consists of data for three horizontal and five vertical locations.

Visual observations indicated that the flame extension out of the compartment was less then 1.0 m, therefore all of the measurements were taken beyond the flame tip. The results from this test indicate that species variations existed in all three coordinates.

Most importantly, the results indicated lower carbon monoxide levels at x = 1.2 m compared to carbon monoxide levels at x = 6.1 m. If steady-state conditions really existed during this test, the data implies that carbon monoxide was being generated along the hallway, instead of being transported, diluted, or oxidized. Since no additional fuel was present within the hallway, the generation of carbon monoxide is physically impossible, indicating that steady-state conditions had not been achieved.

The flame structure at the compartment/hallway interface also changed with time. In the early stages of the fire, the flame structure at the doorway appeared to be similar to that shown in Figure 5-2a, flames extend out of the compartment from approximately 2/3 of the upper portion of the doorway, and air is entrained into the compartment through the lower 1/3 of the doorway.

a b

Figure 5-2: Flame structure at the compartment/hallway interface

After a period of time, approximately 3 to 4 hours after external burning began, the flame structure transitioned from that seen in Figure 5-2a, to that of Figure 5-2b,

where the flame extends out of the compartment over the entire doorway area, and no air was entrained into the compartment. The continuously changing flame dynamics in this situation did not provide a steady-state period over which consistent data could be collected at all the sampling locations.

5.2.2 Effects of Initial Gas Temperatures

Since a steady-state period could not be maintained for the duration of the test, a consistent data set could not be obtained from a single test. A series of experiments were therefore conducted to examine the repeatability of the results. As a consequence, the effect of initial gas temperatures on the species levels was examined. The carbon monoxide mole fractions measured along the hallway centerline, 0.1 m below the ceiling, at x = 1.2 m are shown in Figure 5-3 for varying boundary temperatures. The initial gas temperatures were controlled between tests through varying duration cool down periods. The ideal heat release rate for all tests was held constant at 95 kW. The compartment/hallway arrangement consisted of the sliver doorway at x = 0 m and a 0.34 m deep soffit at x = 6.1 m.

The temperatures that were available for comparison in these tests were from two bare bead thermocouples located within the compartment and three bare bead thermocouples located along the centerline of the hallway at the ceiling. The temperatures indicated in Figure 5-3 are those measured in the compartment using a bare bead type K thermocouple located in the front left corner of the compartment at a height of 0.9 m just prior to igniting the fire.

As can be seen in Figure 5-3 the gas temperatures had a significant impact on the carbon monoxide levels measured along the hallway centerline. It appears that the carbon monoxide mole fractions transported down the hallway were inversely related to the initial gas temperatures. When the tests were conducted with elevated gas temperatures, the carbon monoxide levels along the ceiling were significantly lower then those measured when the gas temperatures were ambient.

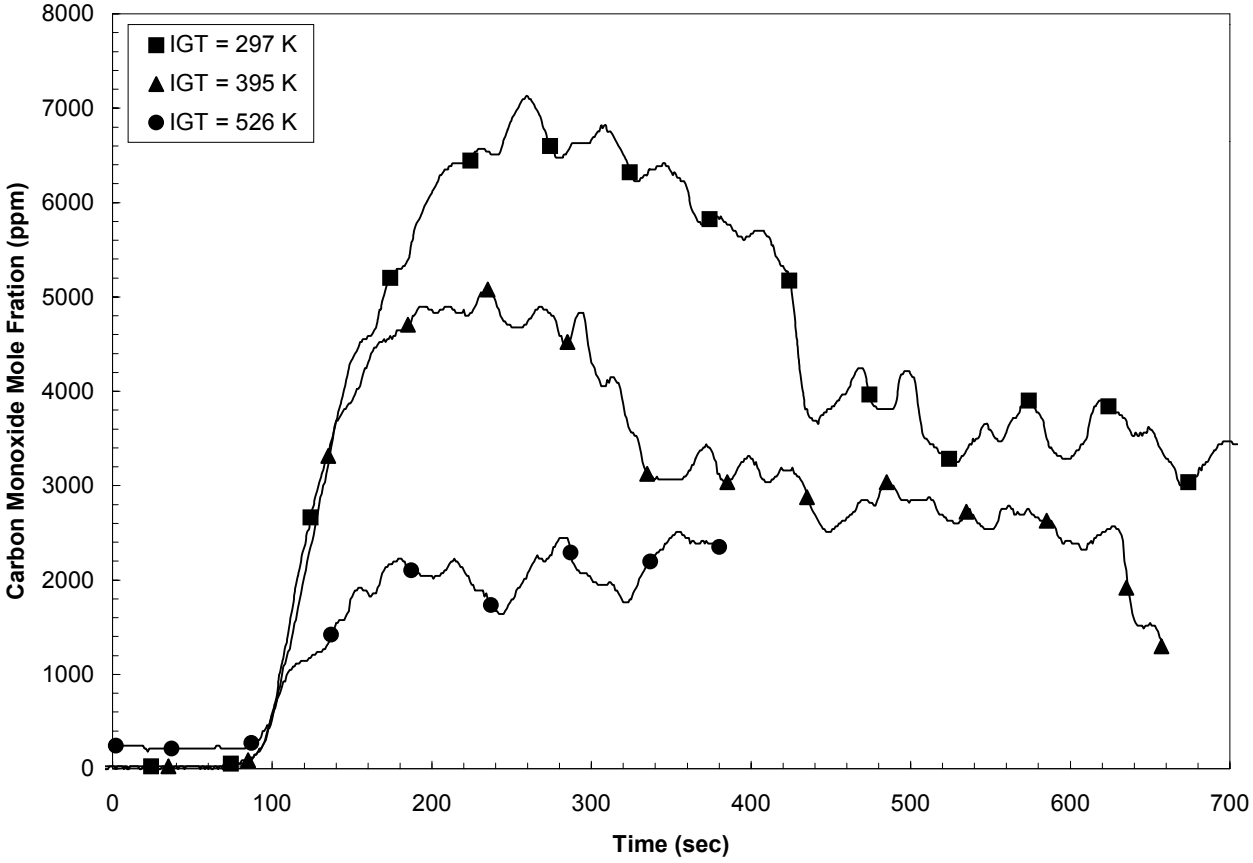

Figure 5-3: Carbon monoxide mole fractions measured at x = 1.2 m, along the hallway centerline, 0.1 m below the ceiling, as a function of time for three different initial gas temperatures.

The data shown in Figure 5-4 are from the first tests of the day, performed on two successive days. Both tests were conducted with an ideal heat release rate of 95 kW and an initial gas temperature of 296 K. The data indicates that when the initial gas temperatures are kept constant very repeatable results can be obtained.

In addition to examining the carbon monoxide mole fractions at x = 1.2 m, measurements were also taken at x = 3.7 m, for the same test configuration and heat release rate. The carbon monoxide mole fractions as a function of time for three different tests are shown in Figure 5-5. Two tests were conducted for the same initial gas

temperature of 311 K, and the third was conducted at an elevated gas temperature of 732 K. As mentioned previously, the temperatures for which comparisons were based, were for those measured in the compartment using a bare bead type K thermocouple located in the front left corner of the compartment at a height of 0.9 m just prior to igniting the fire.

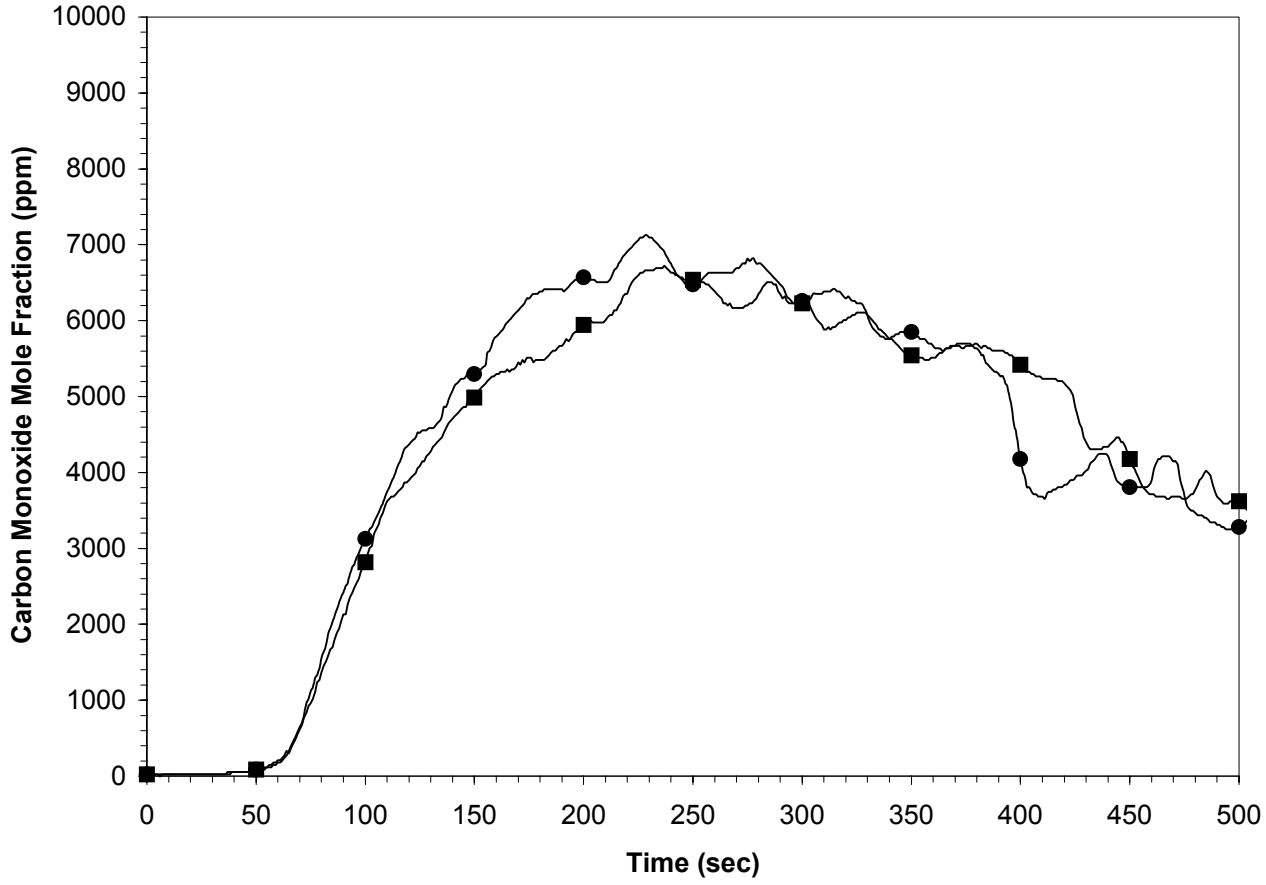

Figure 5-4: Comparison of carbon monoxide mole fractions measured at x = 1.2 m, along the hallway centerline, 0.1 m below the ceiling, for the same ambient conditions, from two different experiments.

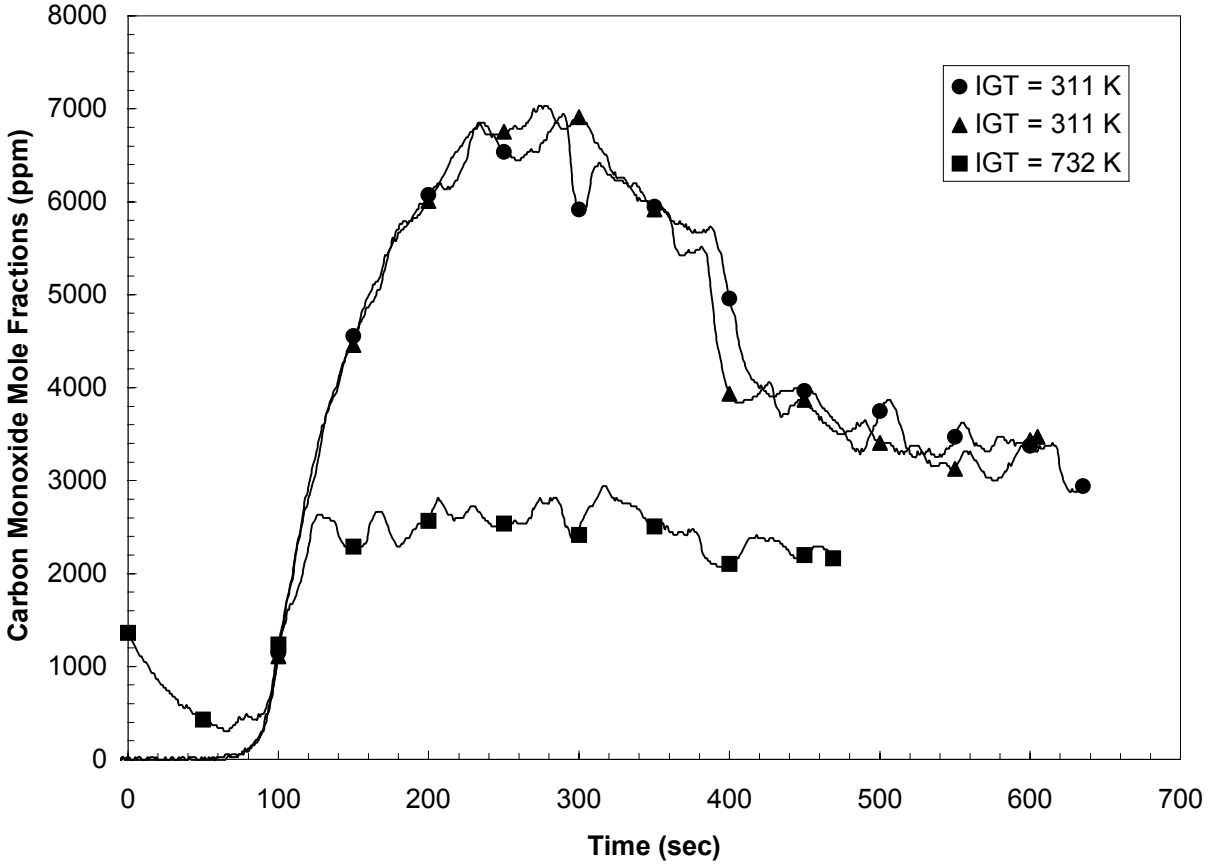

Figure 5-5: Comparison of carbon monoxide mole fractions measured at x = 3.7 m, along the hallway centerline, 0.1 m below the ceiling.

Similar to the results for measurements at x = 1.2 m, when the initial gas temperature was elevated lower carbon monoxide levels were observed and repeatable results were observed for the same initial gas temperatures. Although, repeatable results could be obtained if the experiments were conducted with the same initial gas temperatures, conducting multiple experiments for each test condition to obtain a detailed mapping at each axial location was not feasible. Due to the large thermal mass of the hallway, returning the facility to ambient temperatures required long cool periods. [Vandsburger 2002] Also, a minimal of fifteen tests would be required at each axial location for each test condition.

5.2.3 Species Transport

Although a detailed analysis of the entire upper layer was not possible with the present test configuration, some analysis based on single point measurements of gases within the upper layer of the hallway, along the hallway centerline could be made. Data for measurements at x = 1.2 m (two tests) and x = 3.7 m for the same heat release rate and initial boundary temperatures of approximately 300 K are shown in Figure 5-6.

Comparison between the results indicates similar carbon monoxide mole fractions at both axial locations. This data implies that carbon monoxide levels are frozen. These results agree with those reported by Gottuk *et al.* [2000] who reported that all oxidation reactions had occurred by the flame tip, and all reactions were frozen beyond the flame tip. Visual observations during the tests indicated that the flame tip did not extend more then 0.5 m from the compartment; therefore, both sampling locations were beyond the flame tip. No data at the two locations for the same initial elevated boundary temperatures are available for comparison.

Measurements along the centerline of the ceiling at axial locations of x = 1.2 m and x = 3.7 m were performed for the same compartment/hallway arrangement and a heat release rate of 250 kW. Time traces of the carbon monoxide mole fractions at both locations are presented in Figure 5-7. The duration of the two tests was not identical and therefore comparison between the two tests is only possible for 120 seconds after ignition. Both tests were conducted with the same initial boundary temperatures of 310 K. The time at which external burning occurs and ceases is also noted in Figure 5-7.

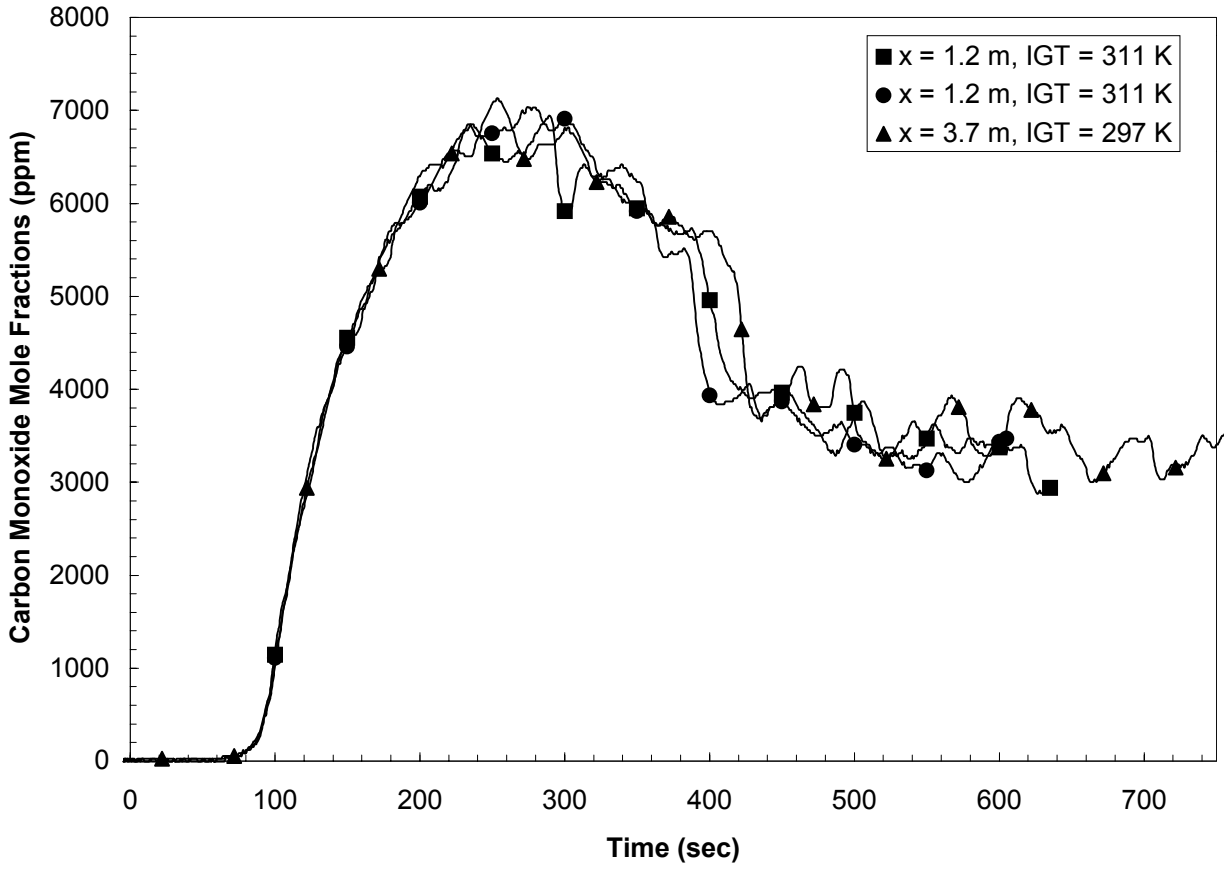

Figure 5-6: Comparison of carbon monoxide mole fractions measured at x = 1.2 m (results from two tests) and x = 3.7 m, along the hallway centerline, 0.1 m below the ceiling, for the same ambient conditions. The heat release rate was 95 kW for all three tests.

Several key observations should be noted from the data presented in Figure 5-7. The first is that the data at both locations follows the same trend, although the peak carbon monoxide mole fractions are not equal. The peak carbon monoxide mole fraction ($t \approx 40$ sec) at x = 1.2 m is approximately 4800 ppm, while the peak level at x = 3.7 m is approximately 4000 ppm. The difference between the two values is either a result of oxidation reactions occurring between the two sampling locations or due to dilution with newly entrained air along the hallway. Results published by Gottuk *et al.* [2000]

indicated that no reactions occur beyond the flame tip, since both measurements were taken beyond the flame tip, the difference between the peak values is attributed to dilution.

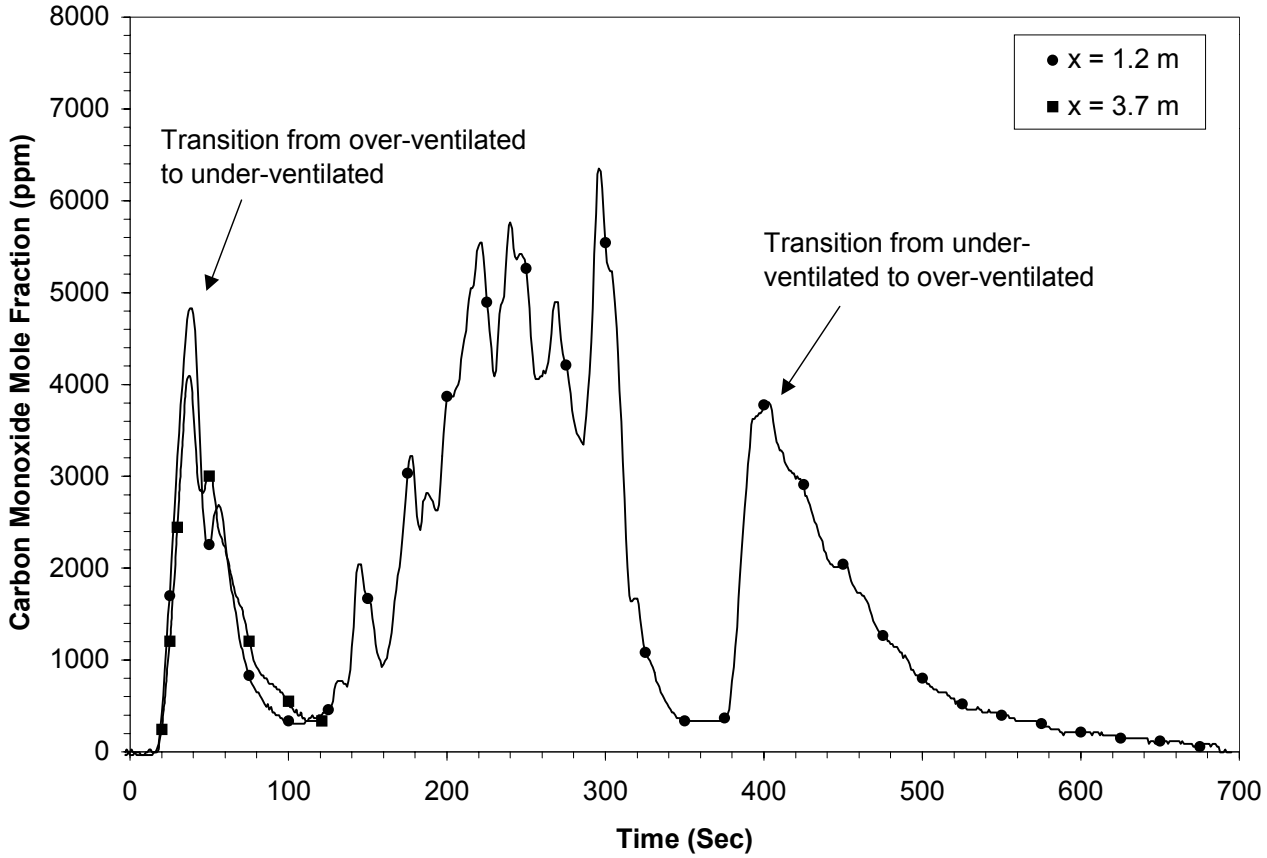

Figure 5-7: Comparison of carbon monoxide mole fractions measured at x = 1.2 m and x = 3.7 m, along the hallway centerline, 0.1 m below the ceiling, for the same ambient conditions. The heat release rate was 250 kW.

With the sliver doorway arrangement external burning was observed for all heat release rates. A typical fire history for this test series was a quickly developing fire within the compartment that transitioned from an over-ventilated fire to an under-ventilated fire, the degree of external burning was dependent on the heat release rate. Once the flow of propane was terminated the fire slowly decreased in size and retreated

back into the compartment. The data presented in Figure 5-7 for the x = 1.2 m sampling location were collected over the entire test duration, from ignition to flame extinction. For a heat release rate of 250 kW, visual observations indicated that flames emerging from the compartment extended approximately 1.22 m down the hallway. Therefore, a portion of the data reported for the 1.2 m sampling location were taken directly within the fire plume.

The data at the x = 1.2 m sampling location indicates that the carbon monoxide levels generated within the compartment and transported downstream are the highest at the time where the combustion within the compartment transitions from over-ventilated to under-ventilated burning. Once external burning begins, the carbon monoxide levels at x = 1.2 m and x = 3.7 m decrease by an order of magnitude. The carbon monoxide levels at x = 1.2 m increase again once the fire plume reaches the sampling probe and measurements are being taken within the flaming region. Once the flow of propane is terminated, at t = 285 seconds, the fire begins to subside and the flames retract into the compartment. Shortly afterward the carbon monoxide mole fractions increase to levels seen just prior to the onset of external burning, this peak occurs as the fire transitions from under-ventilated to over-ventilated burning within the compartment. This data provides an indication that the transition between burning conditions within the compartment may be critical to carbon monoxide formation.

5.3 HALLWAY STUDY WITH BASELINE COMPARTMENT DOORWAY

Tests conducted with the propane burner located within the compartment can be used to represent a variety of compartment fires scenarios. Experiments with the compartment/hallway configuration, however, are more complicated. In real scenarios additional flammable objects would typically be present in the adjacent space whose ignition and subsequent burning could no longer be properly represented by a single burner located within the compartment. With the sliver doorway at x = 0 m, external burning was observed for all heat release rates examined, therefore, it was decided to

conduct all further tests for the second phase of the study, with the baseline doorway at x = 0 m instead of the sliver doorway. Also, the heat release rates selected for these tests insured minimal or no external burning.

The decision to keep the fire plume confined within the compartment was based on the data presented in previous sections that indicated steady-state conditions could not be achieved for tests with external burning. This is attributed to the scale of the facility whose thermal capacity requires an extremely long period of time for steady-state conditions to be achieved.

The final test matrix for the transport study consisted of nine tests conditions which are listed in Table 5-1. The compartment ventilation was kept constant and the effects of the hallway ventilation and the heat release rate on the species levels generated and transported were examined. Measurements were performed at axial locations of x = 0 m and x = 6.1 m, i.e. the compartment doorway and hallway doorway. No measurements were taken along the hallway. A total of ten experiments were conducted, one for each test condition listed in Table 5-1, and one repeat of the baseline/baseline configuration and a heat release rate of 127 kW.

Table 5-1: Transport Study Test Matrix

Compartment Ventilation	Hallway Ventilation	Heat Release Rate (kW)
Baseline	Narrow	85, 127, 150
Baseline	Baseline	85, 127, 150
Baseline	Wide	85, 127, 150

The effect of the hallway and hallway ventilation on the air entrainment rates and species generation are examined first. The data are presented based on the methodology proposed in Chapter 4, and then presented as a function of the axial location to examine species transport.

5.3.1 Doorway Flow and Air Entrainment Rates

5.3.1.1 Compartment and Hallway Doorway Flow Rates

The species generated within the compartment are a function of the fire size and the air flow rate into the compartment. The calculated air flow rates into the compartment as a function of the ideal heat release rate and hallway ventilation are presented in Figure 5-8. Each set of data have been fitted with a linear trendline. Along with the compartment/hallway data, baseline doorway data for the standalone compartment are also included for comparison.

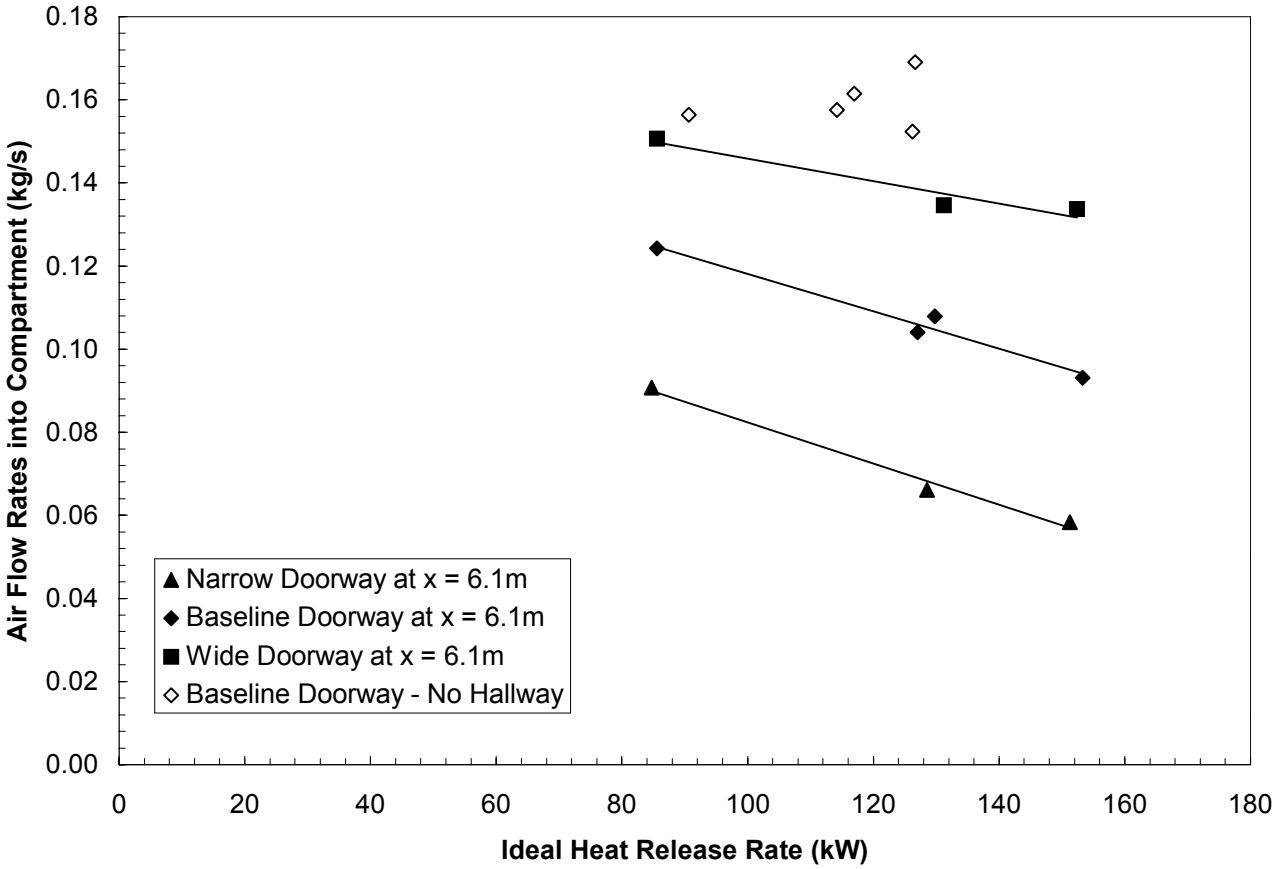

Figure 5-8: Air flow rates into the compartment as a function of the ideal heat release rate and hallway ventilation.

The data in Figure 5-8 indicate that the air flow rates into the compartment with the baseline doorway and the hallway connected are a function of both the ideal heat release rate and hallway ventilation. For all three hallway ventilation conditions air flow rates into the compartment were lower than for the standalone compartment. The data indicate that as the hallway ventilation decreases the air flow rates into the compartment also decrease. An inverse dependence is seen between the air flow rates into the compartment and the ideal heat release rate.

It has been previously reported by Kawagoe [1958] from experimental data and by Drysdale [2001] from a theoretical approach, that the air flow rate into the compartment is only a function of the geometrical parameters of the compartment ventilation, i.e. $\dot{m}_{air} \propto A\sqrt{H}$. Therefore, the flow rate of air into the compartment should be constant. Examining the theoretical analysis presented by Drysdale [2001], which is based on the application of the Bernoulli equation to determine flow rates in and out of the compartment, the impact of the hallway on the air flow rates into the compartment can be understood. From the analysis, Drysdale derived Equation 5-1 for determining the air flow rate into the compartment,

$$\dot{m}_{air} = \frac{2}{3} A_w \sqrt{H}\, C_d\, \rho_o \sqrt{2g} \left(\frac{((\rho_o - \rho_F)/\rho_o)}{\left(1 + (\rho_o/\rho_F)^{\frac{1}{3}}\right)^3} \right)^{\frac{1}{2}} \qquad (5\text{-}1)$$

If typical values are used for C_d, ρ_o, ρ_f, and g then Equation 5-1 reduces to that proposed by Kawagoe, i.e. $\dot{m}_{air} = 0.52\, A_w \sqrt{H}$.

Equation 5-1 was derived based on the assumptions that the gases inside and outside the compartment are 'well stirred' and at a uniform temperature. The density (and temperature) of the air in the hallway, however, varies spatially is not uniform. However, if the assumption that a well-stirred environment exists both within the

compartment and within the hallway is made, the air flow rates into the compartment as a function of the hallway gas temperature can be examined. The calculated air flow rates into the compartment for three different compartment gas temperatures, which cover the range of temperatures measured within the compartment, as a function of the hallway temperature are presented in Figure 5-9. The hallway gas temperatures are varied between ambient and the maximum temperature measured near the ceiling at x = 1.2 m.

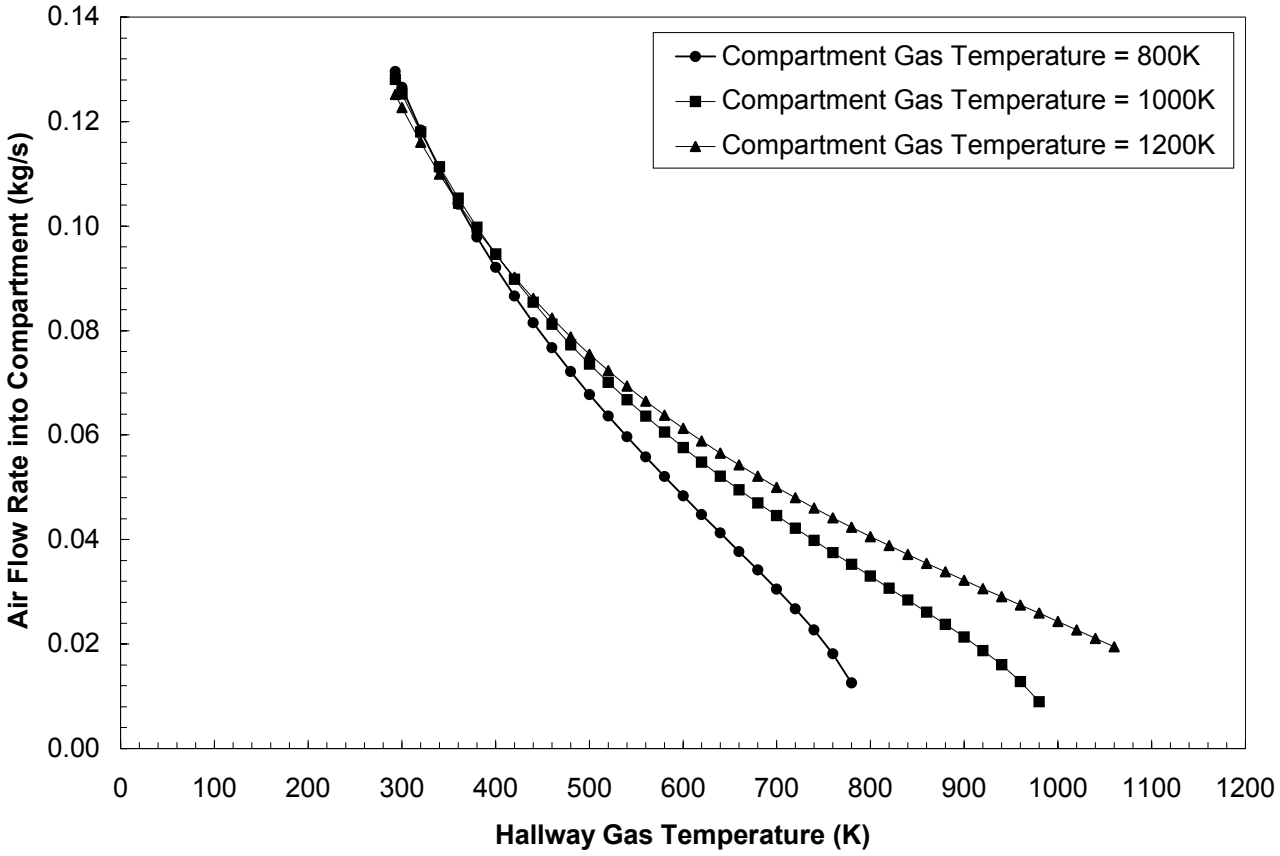

Figure 5-9: Calculated air flow rates into the compartment based on Equation 5-1 as function of the hallway gas temperature.

It is seen that the data in Figure 5-8 encompass the measured air flow rates presented in Figure 5-8. This range of temperatures is not unreasonable for gas

temperatures within the hallway. The analysis provides an explanation for the results presented in Figure 5-8.

The air flow rates into the hallway were examined too and the rates are presented in Figure 5-10 as a function of the ideal heat release rate and hallway ventilation.

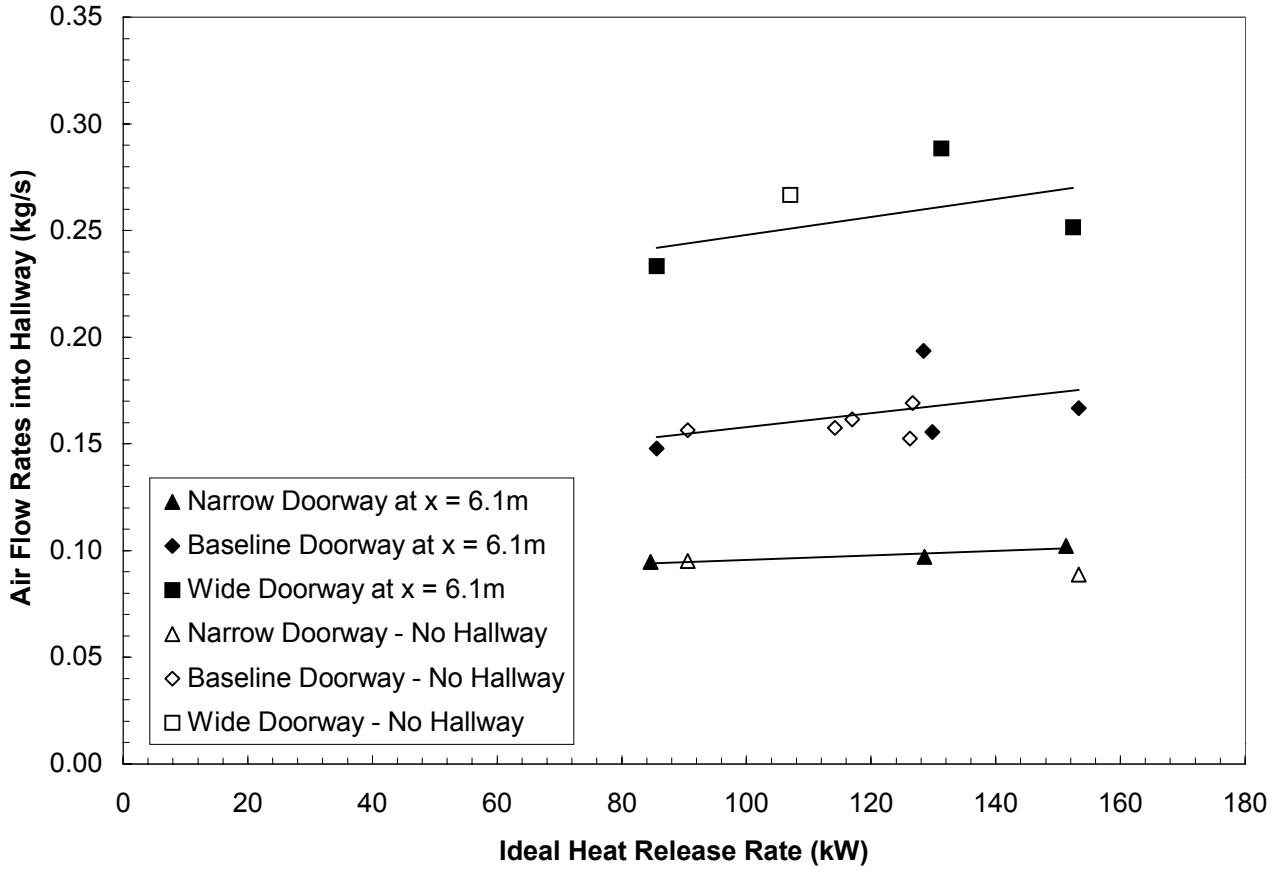

Figure 5-10: Air flow rates into hallway as a function of the ideal heat release rate and hallway ventilation.

A linear fit trendline is included for each data set. Included in Figure 5-10 are the data (open symbols) for the three ventilation conditions without the hallway. Three separate curves corresponding to each of the three hallway ventilation conditions are seen, this is expected based on the results from Kawagoe [1958] and Drysdale [2001]. Furthermore, the data indicate that the total flow rate of air into the system, where the

system consists of just the compartment or the compartment and hallway, is equal and is only a function of the ventilation size, and independent of the ideal heat release rate.

5.3.1.2 Ceiling Jet Air Entrainment Rates

A very limited amount of work has been done on air entrainment into ceiling jets along the hallway; notable discussions include work by Zukoski [1985] and Zukoski *et al.* [1985]. The focus of the work done by Zukoski and his colleagues was on the developing stages of the ceiling jet. The results from their research indicated that entrainment of fresh air from the lower layer into the ceiling jet along the hallway, typically occurred near the point where the smoke plume impinged on the ceiling and during the developing stages of the ceiling jet. During the steady-state period a uniform depth layer developed along the hallway, which propagated along the ceiling with a constant mass flux.

Detailed measurements along the hallway were not made during this study, therefore, the exact region along the hallway where the highest degree of air entrainment occurred is not known. If steady-state conditions are assumed with no losses due to leakage within the compartment or hallway, and a control volume consisting of the compartment and hallway is selected, the total air entrainment into the ceiling jet can be determined. Conservation of mass dictates that the difference between the hallway entrainment rate and compartment air entrainment rate must be the rate of air entrainment into the ceiling jet along the hallway.

The difference between the flow rate of air into the hallway and that into the compartment for each test are presented in Figure 5-11 as a function of the ideal heat release rate and hallway ventilation. A linear trendline is included with each data set. The data indicate that the air entrainment into the ceiling jet along the hallway increases with doorway width and the ideal heat release rate.

The results from this analysis have implications regarding the transport of species to remote locations. The entrained air into the ceiling jet can act as either a source of

oxygen for further oxidation reactions along the hallway or as a dilutent of any combustion products transported downstream of the compartment, this will be further discussed in Section 5.3.4.

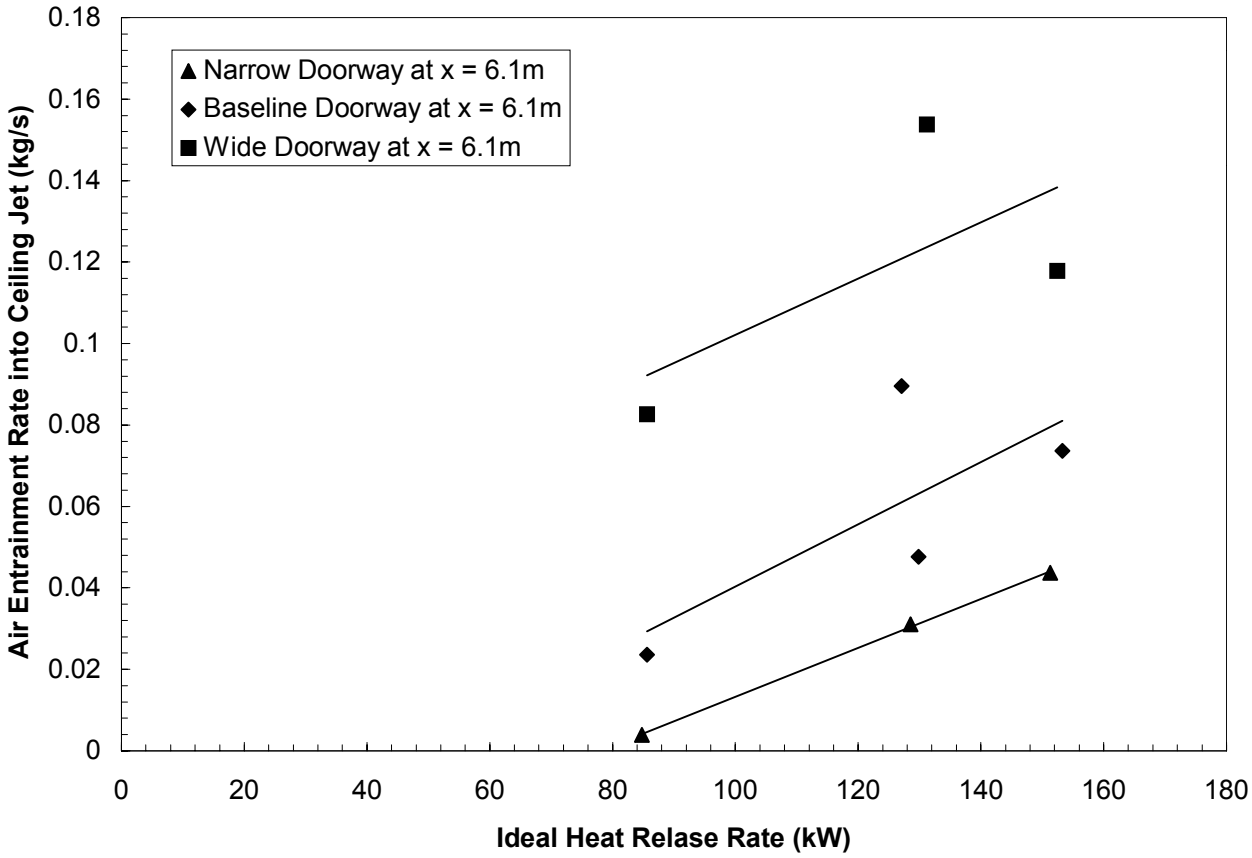

Figure 5-11: Air entrainment rates into upper layer of hallway as a function of the ideal heat release rate and hallway ventilation.

5.3.2 Species Generation as a Function of Hallway Ventilation

Applying the methodology proposed in Chapter 4 to the data obtained at the compartment exit plane (x = 0 m), the species yields based on combustion within the compartment as a function of the non-dimensional heat release rate, $\tilde{Q}$, are presented in Figure 5-12 through Figure 5-14.

Unburned hydrocarbons are not included since the measured values were within the noise of the analyzer. The data for the other three species agrees well with the previous data. This implies that for over-ventilated compartment fires, the hallway ventilation has little or no impact on the species generation within the compartment.

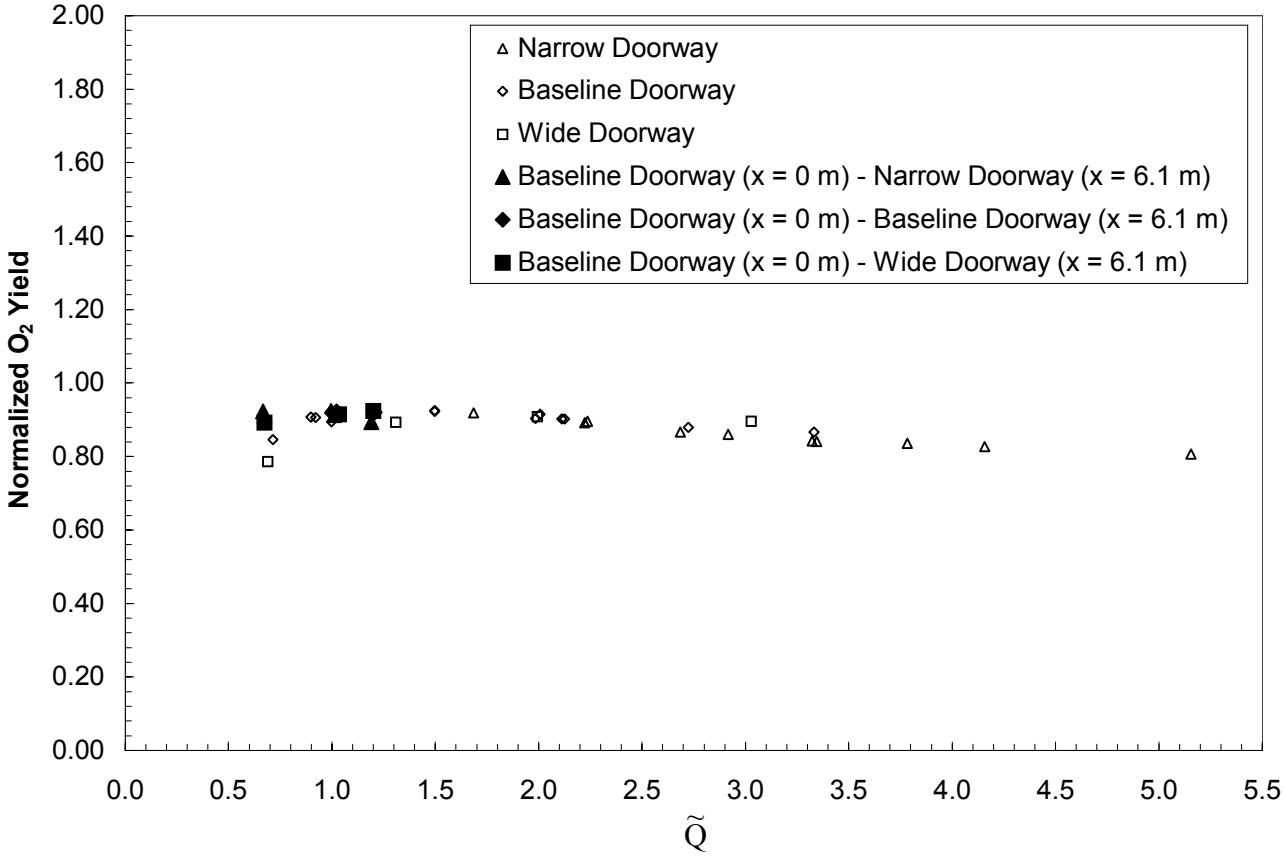

Figure 5-12: Oxygen yields at compartment exit plane based on combustion within the compartment as a function of $\tilde{Q}$. Open symbols are from the standalone compartment study, solid symbols are for the compartment/hallway study.

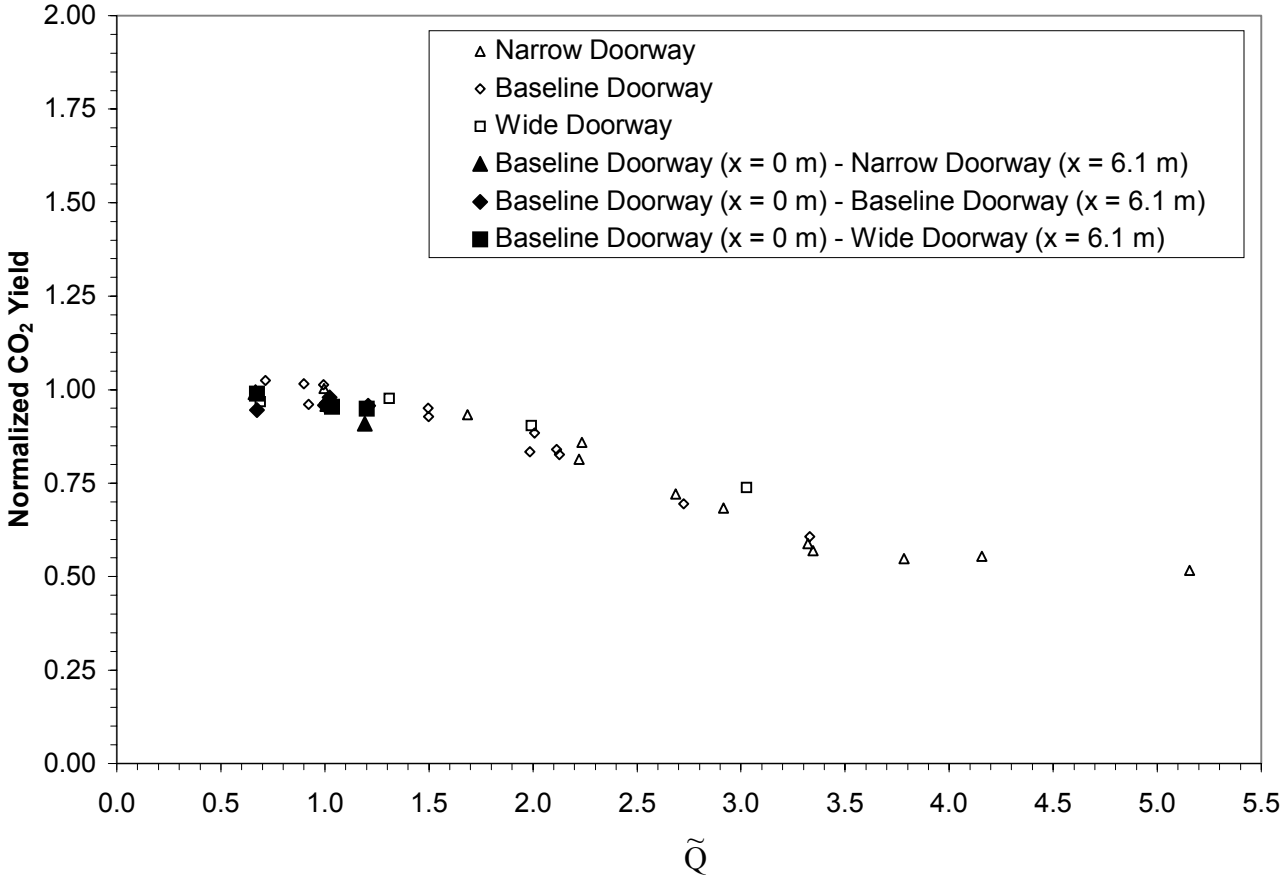

Figure 5-13: Carbon dioxide yields at compartment exit plane based on combustion within the compartment as a function of $\tilde{Q}$. Open symbols are from the standalone compartment study, solid symbols are for the compartment/hallway study.

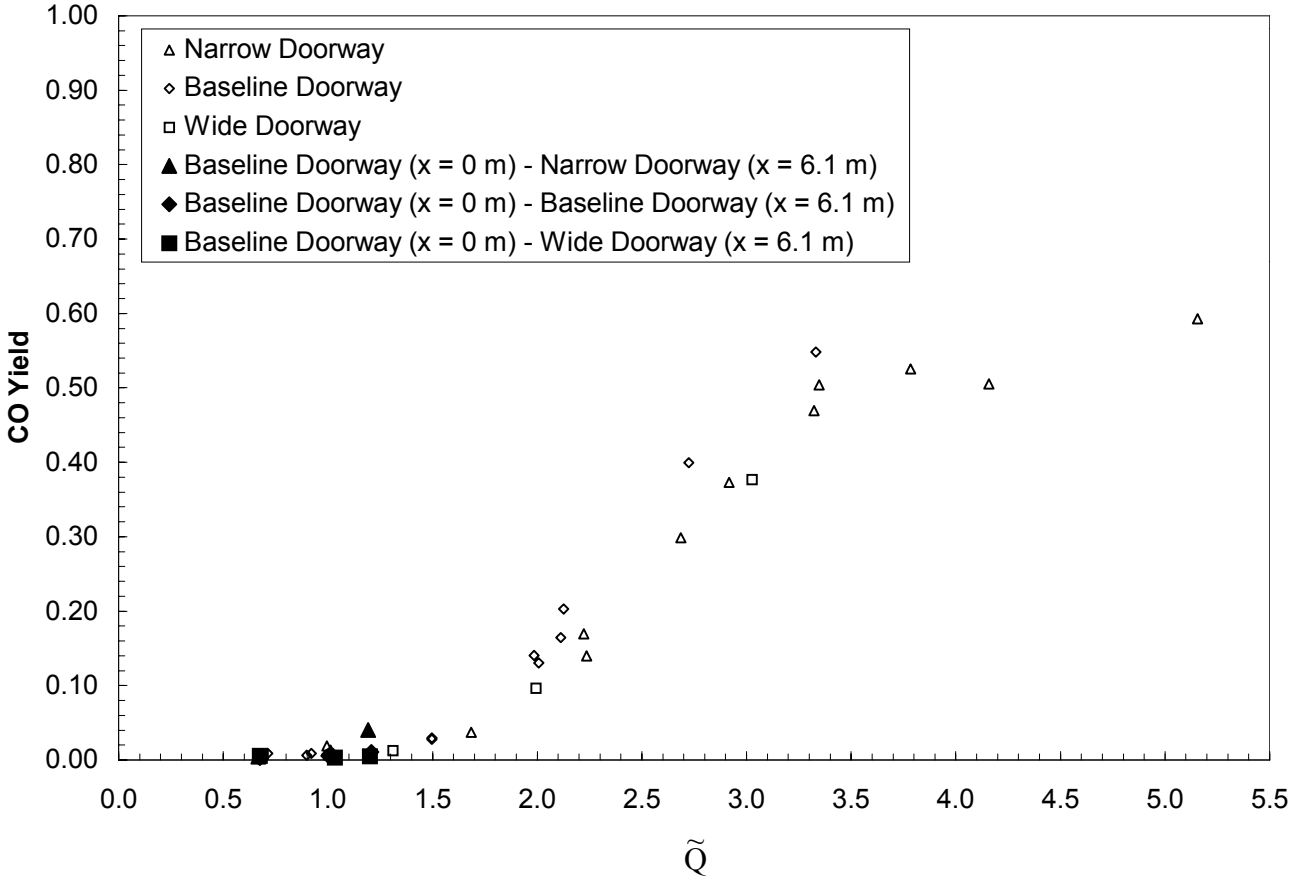

Figure 5-14: Carbon monoxide yields at compartment exit plane based on combustion within the compartment as a function of $\widetilde{Q}$. Open symbols are from the standalone compartment study, solid symbols are for the compartment/hallway study.

5.3.3 Species Transport

The area averaged mole fractions of oxygen, carbon dioxide, and carbon monoxide at axial locations of x = 0 m and x = 6.1 m are presented in Figure 5-15 through Figure 5-17. As mentioned previously, unburned hydrocarbons are not presented since the levels were within the noise level of the gas analyzer.

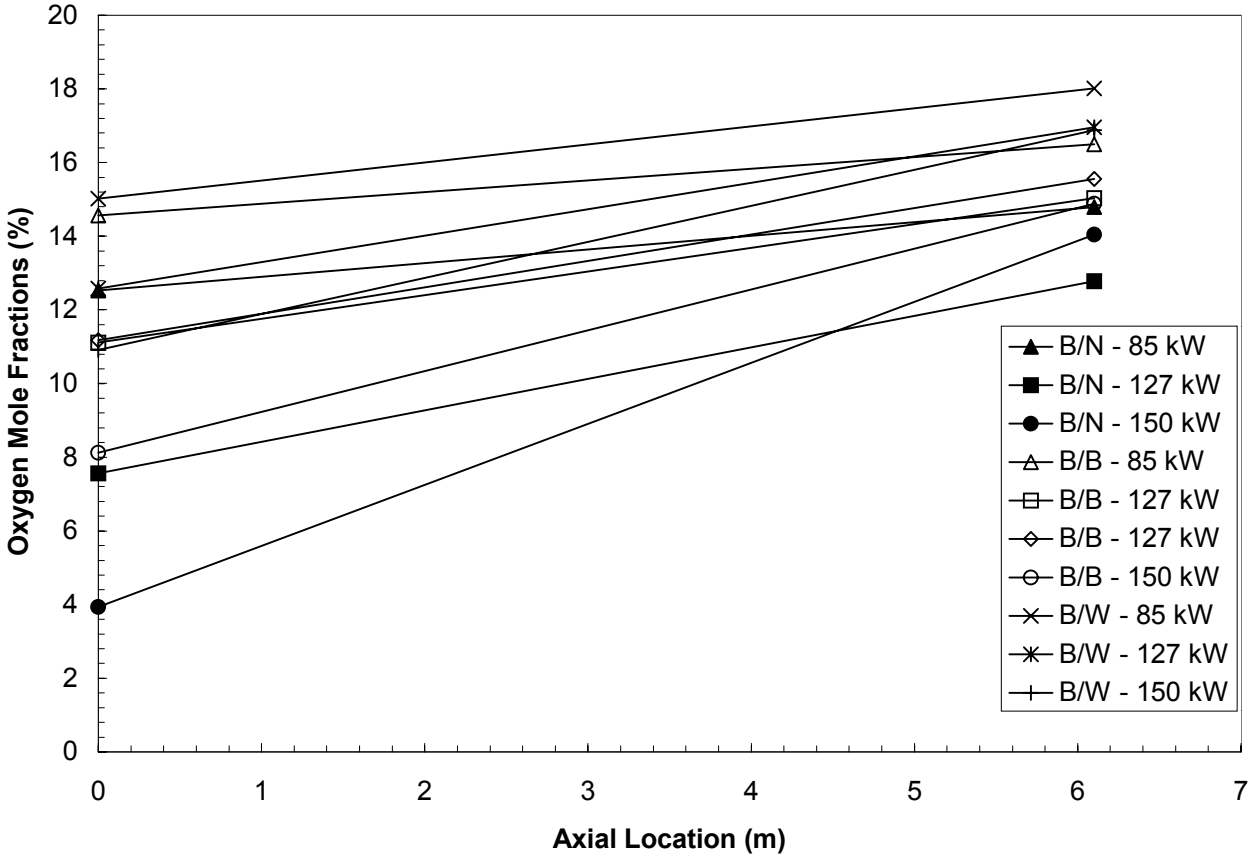

Figure 5-15: Area averaged oxygen mole fractions as a function of axial location. The chosen symbols correspond to the hallway ventilation condition. Solid symbols, e.g. ♦, are for the narrow doorway, open symbols, e.g. ◊, are for the baseline doorway, and the crossed symbols, e.g. +, ×, are for the wide doorway. The legend format consists of 'compartment ventilation/hallway ventilation – ideal heat release rate', where B, N, and W correspond to the baseline, narrow, and wide doorway.

Also, in each plot, the chosen symbols correspond to the ventilation condition at x = 6.1 m, solid symbols are for the narrow doorway, open symbols are for the baseline doorway, and the crossed symbols are for the wide doorway. Also, the data points are connected with a straight line to indicate data points corresponding to the same tests, this does not imply a linear fit between the data points. The legend format consists of

'compartment ventilation/hallway ventilation – ideal heat release rate', where B, N, and W correspond to the baseline, narrow, and wide doorways.

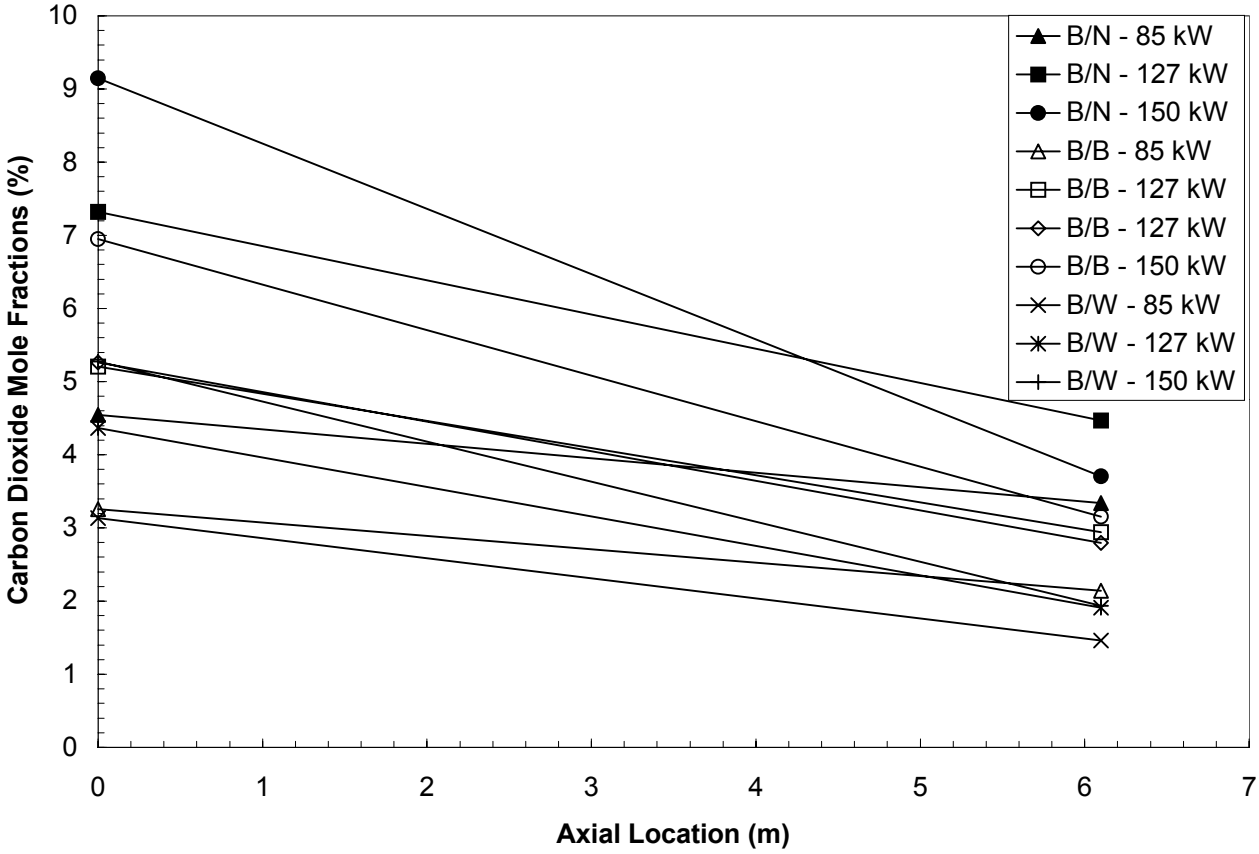

Figure 5-16: Area averaged carbon dioxide mole fractions as a function of axial location. The chosen symbols correspond to the hallway ventilation condition. Solid symbols, e.g. ♦, are for the narrow doorway, open symbols, e.g. ◊, are for the baseline doorway, and the crossed symbols, e.g. +, ×, are for the wide doorway. The legend format consists of 'compartment ventilation/hallway ventilation – ideal heat release rate', where B, N, and W correspond to the baseline, narrow, and wide doorway.

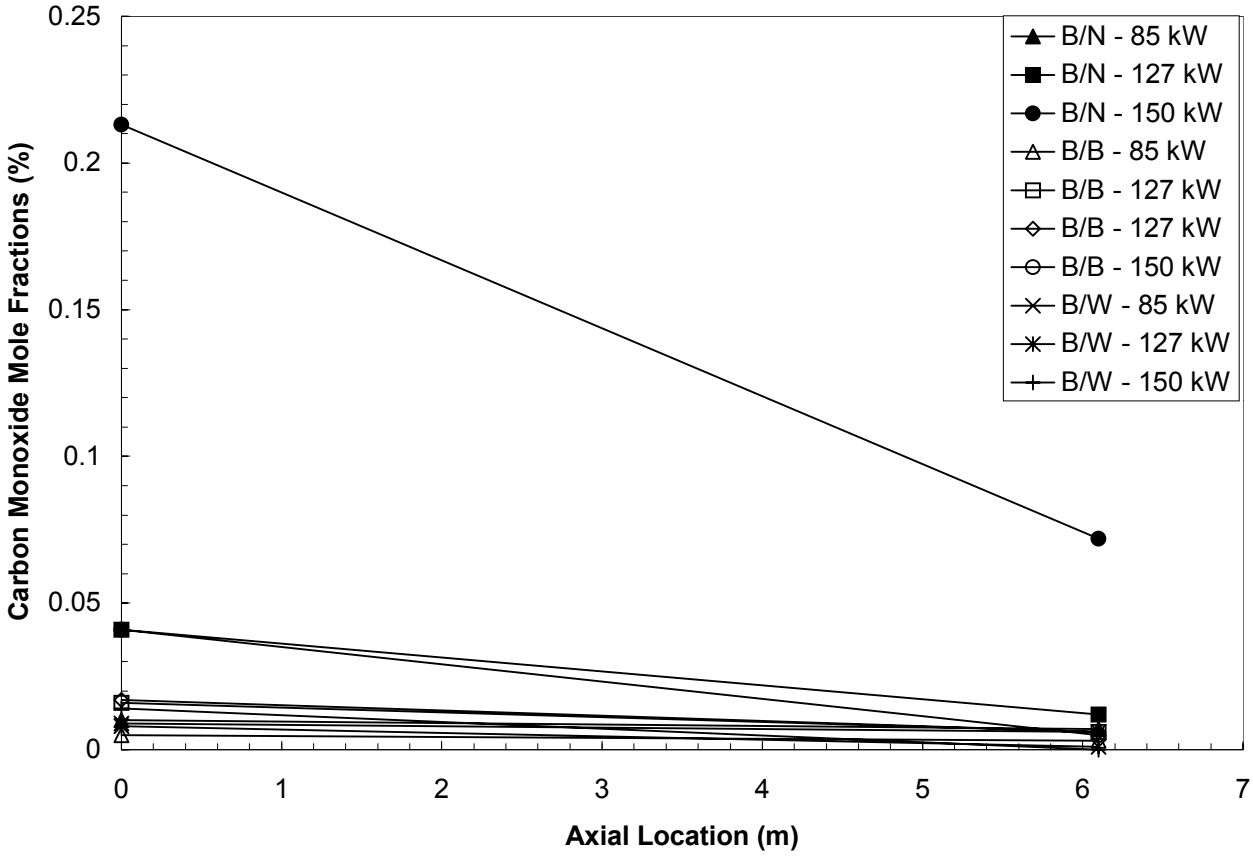

Figure 5-17: Area averaged carbon monoxide mole fractions as a function of axial location. The chosen symbols correspond to the hallway ventilation condition. Solid symbols, e.g. ♦, are for the narrow doorway, open symbols, e.g. ◊, are for the baseline doorway, and the crossed symbols, e.g. +, ×, are for the wide doorway. The legend format consists of 'compartment ventilation/hallway ventilation – ideal heat release rate', where B, N, and W correspond to the baseline, narrow, and wide doorway.

The oxygen mole fractions at the compartment exit plane (x = 0 m) and hallway exit plane (x = 6.1 m) are presented in Figure 5-15. Higher oxygen mole fractions were measured at the hallway exit plane compared to the compartment exit plane. Conversely, the mole fractions of carbon dioxide and carbon monoxide, Figure 5-16 and Figure 5-17

respectively, indicate lower levels of each species at the hallway exit plane compared to the compartment exit plane.

5.3.4 Discussion

The data presented in the previous sections provides the necessary information to evaluate the mechanisms effecting the species levels transported downstream of the compartment. The heat release rates, for the transport study, were selected such that the burning regimes consisted of minimal or no external burning. Based on the theoretical flame length calculations, see Appendix A, external burning may have occurred for heat release rates of 127 kW and 150 kW. Due to the depth of the smoke layer within the hallway, no visual observations of the flame structure at the compartment doorway could be made to validate the calculations. For situations with external burning, the species measured at the compartment exit plane are species measured in the fire plume, therefore, the species measured at the hallway exit plane, for these scenarios, will be a result of oxidation reactions and dilution with entrained air.

The length of the reaction zone, if any, along the hallway, can not be determined from species measurements at the entrance and exit plane of the hallway alone. The occurrence of additional reactions, however, can be determined by comparing the ratio of carbon monoxide and carbon dioxide between the two sampling points. The data presented in Section 5.3.1 indicated that air was entrained into the ceiling jet for all hallway ventilation conditions, therefore, dilution of the species along the hallway is expected. If no additional reactions occurred along the hallway, then both carbon dioxide and carbon monoxide should have been diluted in similar proportions. Conversely, if oxidation reactions did occur within the hallway, then two factors will effect both the carbon monoxide and carbon dioxide species levels. Oxidation reactions will decrease the carbon monoxide levels and increase the carbon dioxide levels, and dilution will decrease both species levels. Therefore, the ratio of carbon monoxide to carbon dioxide in the upper layer at the hallway exit will be lower then the ratio at the hallway inlet.

The carbon monoxide to carbon dioxide ratios at x = 0 m and x = 6.1 m are listed in Table 5-2. It can be seen from the data presented in Table 5-2 that for an ideal heat release rate of 85 kW the same ratio of carbon monoxide to carbon dioxide is seen at both x = 0 m and x = 6.1 m, for the narrow and baseline hallway ventilation. As the ideal heat release rate increases lower carbon monoxide to carbon dioxide ratios are seen at x = 6.1m compared to x = 0 m, for all three hallway ventilation conditions. Based on the previous discussion this indicates that additional reactions had occurred within the hallway for heat release rates of 127 kW and 150 kW.

Table 5-2: Carbon monoxide to carbon dioxide ratios at x = 0 m and x = 6.1 m.

Hallway Ventilation	Ideal Heat Release Rate (kW)	$\tilde{Q}$	CO/CO_2 x = 0 m	CO/CO_2 x = 6.1 m
Narrow	85	0.7	0.0022	0.0021
Narrow	127	1.0	0.0056	0.0027
Narrow	150	1.2	0.0233	0.0194
Baseline	85	0.7	0.0015	0.0014
Baseline	127	1.0	0.0031	0.0020
Baseline	127	1.0	0.0032	0.0021
Baseline	150	1.2	0.0059	0.0016
Wide	85	0.7	0.0029	0.0041
Wide	127	1.0	0.0018	0.0005
Wide	150	1.2	0.0027	0.0000

The reported noise level for the carbon monoxide analyzer was reported by the manufacturer to be 1% of the lowest possible measuring range, which is 10,000 ppm (1 %). For the case of the wide doorway at x = 6.1 m and a heat release rate of 85 kW, the highest carbon monoxide levels measured at the compartment exit plane were 120 ppm; lower levels were measured at the hallway exit plane, therefore, the ratios presented in Table 5-2 for that case should be viewed with caution.

CHAPTER 6

SUMMARY AND CONCLUSIONS

6.1 INTRODUCTION

The aim of the present research was to gain a better understanding of the species generation and transport from compartment fires. The primary parameters in this investigation were the heat release rate, compartment ventilation, and hallway ventilation. To meet the objectives of the research, the project was divided into two phases. The objective of the first phase was to gain an understanding of the species generation. The objective of the second phase was to gain an understanding of species transport to remote locations.

The species generation experiments were conducted with a half-scale ISO 9705 compartment with three different ventilation conditions and heat release rates ranging from 50 kW to 500 kW. The transport study was conducted by expanding the facility to include a 6.1 m long hallway, connected to the compartment in a head-on configuration. All measurements were performed at the compartment or hallway exit plane during the steady-state period of the fire. Measurements included species mole fractions, gas pressure (used to determine gas velocities), and gas temperatures.

6.2 GENERATION STUDY SUMMARY

Previous research has been conducted by numerous investigators using bench-scale (Beyler [1983], [1986a], [1986b], Morehart *et al.* [1990], Toner *et al*. [1984]), small-scale (Gottuk [1992], Pitts [1994]), and full-scale (Blomqvist [2001], Tewarson [1984]) test apparatus. The primary conclusion from these studies was that the species generation could be correlated to a meaningful fuel-to-air ratio. The methodology that has been most widely accepted by the fire protection engineering community is that

proposed by Beyler [1983] who correlated the species yields as a function of the plume (global) equivalence ratio. The methodology, termed the global equivalence ratio concept, has been extended to full-scale environments although the primary database and statistical correlations are based on bench-scale test data. In order to extend the methodology from bench-scale experiments to full-scale facilities, a key assumption needs to be made. The assumption is that the plume equivalence ratio is equal to the global equivalence ratio. For this assumption to be valid two conditions must be true. The first is that all the air drawn into the compartment is entrained into the fire plume. The second condition is that a well-mixed uniform upper layer must exist so that the species measurements are spatially independent. Neither of these conditions has been fully investigated for compartment fires with prototypical building features.

Detailed species mappings performed as part of this study, at the exit plane of the compartment indicated that spatial variations exist in the species mole fractions. Horizontal and vertical gradients in the species mole fractions were observed for all ventilation conditions and heat release rates. The gradients in the species became more pronounced as the width of the ventilation opening increased. In addition it was observed that oxygen was a component of the exiting gas stream, indicating that not all of the air entrained into the compartment was entrained into the fire plume.

The detailed measurements performed at the compartment exit plane allowed the global equivalence ratio concept to be applied and evaluated on a truly global scale. The compartment global equivalence ratio could be determined based on the calculated air entrainment rates and mass flow rates of fuel. Since the species mappings indicated that not all the air flowing into the compartment was entrained into the fire plume, the global equivalence ratio, in this study, was not equal to the plume equivalence ratio. Due to the spatial variations in the species at the exit plane, the dependent variable in the correlation, the species yields, were based on area averaged mole fractions over the exiting portion of the doorway.

The analysis of the data indicated that the global equivalence ratio concept was not appropriate parameter for this present scenario. Although, good correlation between the normalized oxygen yields and the global equivalence ratio was observed, carbon dioxide, carbon monoxide, and unburned hydrocarbons did not correlate well. The species indicated additional dependencies on the ventilation then that captured by the global equivalence ratio parameter. In addition, the carbon monoxide yields, in the present study were significantly higher then those reported by previous investigators.

A new methodology, more appropriate for compartment fires, was developed. The proposed methodology correlates the species yields based on the combustion within the compartment as a function of a non-dimensional heat release rate, $\widetilde{Q}$. The non-dimensional heat release rate is based on the fuel load and geometrical parameters of the compartment. $\widetilde{Q}$ is defined as the ideal heat release rate divided by the heat release rate required for the tip of the fire plume to reach the compartment doorway. Similar to the equivalence ratio, the value of $\widetilde{Q}$ provides an indication of the fire scenario within the compartment. For values below $\widetilde{Q}_{critical}$, which is dependent on the ventilation dimensions, the compartment is over-ventilated, above $\widetilde{Q}_{critical}$ the compartment is under-ventilated. In addition to indicating whether or not a compartment fire is over- or under-ventilated, values between 1.0 and $\widetilde{Q}_{critical}$ indicate external burning due to flame extensions.

Presenting the data in this manner indicates a good correlation for all four species. For the conditions examined, the data appear to be independent of the ventilation. Due to the nature of the previous studies, an appropriate value for $\widetilde{Q}$ could not be calculated and no comparison between the present study and previous studies could be made. Correlations based on regression analysis were developed for normalized carbon dioxide, carbon monoxide, and unburned hydrocarbon yields. The correlations were developed using the software program CurveExpert (version 1.34). Non-linear regression

techniques were applied to the carbon dioxide and carbon monoxide data. The data were best represented as a sigmoidal or "S-shaped" growth curve. A linear regression analysis was applied to the unburned hydrocarbon data.

The species at the exit plane of a compartment with prototypical building features can be readily determined from Equations 4-5, 4-6a, and 4-6b. The present methodology in applicable to situations where a well-mixed uniform layer is not present and the overall global conditions are of interest to the fire protection engineer. It should be kept in mind that the species calculated via the proposed methodology are not the final species transported downstream. These species levels are the inlet boundary conditions for the adjacent space. The species levels observed downstream will be a function of the transport processes, which may consist of further reactions of dilution with entrained air.

6.3 TRANSPORT STUDY SUMMARY

The transport of species downstream of the compartment was examined with a 6.1 m long hallway connected to the compartment in the head-on configuration. The primary objective of this phase of the study was to gain an understanding of the species transport to remote locations during the steady-state period of the fire.

The tests matrix for the transport study consisted of nine test conditions. Experiments were conducted with the baseline doorway at x = 0 m (the compartment/hallway interface) and three different ventilation conditions at x = 6.1 m (end of hallway). The three hallway ventilation conditions consisted of the narrow, baseline, and wide doorways. The heat release rates examined were selected to insure that the fire plume was contained to the compartment with minimal or no external burning.

The hallway ventilation and ideal heat release rate effect the air temperature in the hallway, which has a direct impact on the air flow rates into the compartment when the hallway is connected. However, the air flow rates into the system, where the system can

consist of the compartment or compartment and hallway, are independent of the ideal heat release rate and are only a function of the ventilation opening to the system.

Although, the addition of the hallway appeared to impact the air flow rate into the compartment, the results from the tests indicated that for over-ventilated compartment fires the hallway and hallway ventilation had no impact on the species generation within the compartment.

Differences in species mole fractions between x = 0 m and x = 6.1 m were shown to be a result of air entrainment into the ceiling jet within the hallway. The air entrainment resulted in the dilution of carbon dioxide and carbon monoxide mole fractions along the hallway, for $\widetilde{Q} < 1.0$. For $\widetilde{Q} \geq 1.0$ the reduction in carbon monoxide levels along the hallway was a result of additional oxidation reactions within the hallway and dilution with entrained air into the ceiling jet.

Although not the initial objective of the research, the data collected during the evaluation phase of the study indicated that steady-state conditions do not generate the most hazardous environments. Conversely, the hazardous conditions are generated early in the fire when the boundary temperatures are at ambient temperatures. Multiple tests examining the repeatability of the results indicated that the initial boundary temperatures had a significant impact on the carbon monoxide mole fractions measured along the hallway. An inverse relationship between the carbon monoxide mole fractions and the initial boundary temperatures was observed.

In addition, higher levels of carbon monoxide were observed during the transition between over-ventilated and under-ventilated conditions within the compartment. It is recommended that future research examine species levels generated during the transient period along with those generated during the steady-state periods.

CHAPTER 7

RECOMMENDATIONS FOR FUTURE WORK

The results from the current research study provide a new insight into understanding species generation and transport from compartment fires with prototypical building features. However, the study was by no means exhaustive and the present results have generated new questions that should be investigated in future research endeavors. Additional experiments examining both species generation and species transport need to be conducted. Variables that need to be examined include burner dimensions, burner location, and burner elevation. In addition, the present research was conducted with only a single gaseous fuel, previous research has indicated that species generation is a function of fuel composition and should be investigated within the boundaries of the present study. [Beyler 1983, Karlsson 2001]

Values for the denominator of the new correlating parameter, $\widetilde{Q}$, were based on experimental data. A methodology to determine the heat release rate for flame extensions to occur needs to be developed so the correlation can be extended to other scenarios. A general methodology has been proposed based on an empirical correlation from Pchelintsev *et al.* [1997] for estimating the horizontal flame length of a fire plume impinging on the ceiling. The correlation is based on experiments conducted with an unconfined fire plume. In the present study, a correction factor based on limited data was incorporated into the correlation to take into account the fire plume confinement. To date, no experiments have been conducted to determine the horizontal flame length of an impinging fire plume for confined fires. Experiments that examine the effects of variables which impact entrainment into the fire plume need to be conducted and the correlation refined. These variables include burner location within the enclosure, burner elevation, burner size, degree of confinement i.e. compartment size and ventilation size.

The initial experiments conducted with the hallway indicate that carbon monoxide levels generated during the developing stages of a fire, i.e. transitioning from over-ventilated to under-ventilated combustion were significantly higher then those generated during the steady-state period. Fires in real life scenarios will be continuously changing as one fuel source burns out and another ignites; therefore, experiments that examine the transient species levels are essential. With that said, it is understood that examining the transient levels is extremely difficult since multiple simultaneous measurements need to be performed to capture the spatial and temporal variations in the species. Therefore, prior to initiating a research study aimed at gaining an understanding of transient species levels, new experimental techniques for performing the species measurements need to be developed.

Experiments conducted with gaseous fuels are very conducive to research studies. However, phenomena such as smoldering and flame spread are not represented by gaseous experiments. These phenomena occur in real scenarios and may contribute to toxic species generation. Replacing the gaseous fuel source with solid or liquid fuels needs to be considered. Experiments with solid or liquid fuels will be finite in duration and may lack any substantial steady-state burning period, therefore, the measurements techniques discussed previously need to be developed prior to conducting these studies.

The final parameter that needs to be examined is scale. Although, small-scale experiments are less expensive to conduct, scaling fire experiments is not as straight forward as scaling other fluid phenomena; therefore, some full scale experiments are required to validate any correlations developed based on bench-scale or small-scale experiments.

REFERENCES

Babrauskas, V., "Flame Lengths Under Ceilings," *Fire and Materials,* Vol. 4, No. 3, (1980), 119-126.

Beckwith, T., and Marangoni, R., "Mechanical Measurements," 4th edition, Addison-Wesley Publishing Company, (1990) pg. 37-94.

Beyler, C., "Development and Burning of a Layer of Products of Incomplete Combustion Generated by a Buoyant Diffusion Flame," Ph.D. Thesis Harvard University, Cambridge, MA, (1983).

Beyler, C., "Major Species Production by Diffusion Flames in a Two-layer Compartment Fire Environment," *Fire Safety Journal*, 10, (1986a) 47-56.

Beyler, C.L., "Major Species Production by Solid Fuels in a Two Layer Compartment Fire Environment," in Fire Safety Science - Proceedings of the First International Symposium, Hemisphere, Washington, D.C., (1986b).

Blevins, L. and Pitts, W., "Modeling of Bare and Aspirated Thermocouples in Compartment Fires," *Fire Safety Journal,* 33, (1999) 239-259.

Bryner, N., Johnsson, R. J., Pitts, W. M., "Carbon Monoxide Production in Compartment Fires – Reduced-Scale Enclosure Test Facility", National Institute of Standards and Technology, NISTIR 5568, (1994).

Blomqvist, P. and Lönnermark, A., "Characterization of the Combustion Products in Large-scale Fire Tests: Comparison of Three Experimental Configurations," *Fire and Materials*, 25, pg. 71-81, (2001).

Conti, R., "Responders to Underground Mine Fires," Proceedings from The 32nd Annual Conference of the Institute on Mining Health, Safety and Research, Salt Lake City, Utah, August 5-7, (2001).

Drysdale, D., *Introduction to Fire Dynamics*, 2nd edition, John Wiley and Sons, (2001).

Egan, M., "Smoke, Carbon Monoxide, and Hydrogen Chloride Production from the Pyrolysis of Conveyor Belting and Brattice Cloth," Information Circular 9304, United States Department of the Interior, Bureau of Mines, (1991).

Emmons, H., "Vent Flows," *SFPE Handbook,* 2nd edition, P.J. DiNenno (Ed.), SFPE/NFPA, Quincy, MA, (1995).

Ewens, D., "The Transport and Remote Oxidation of Compartment fire Exhaust Gases," Master of Science Thesis, Virginia Polytechnic Institute, (1994).

Floyd, J., National Institute of Standards and Technology, Building Fire Research Laboratory, Private communications, (2001).

Floyd, J., Hughes Associates Inc., unpublished data, (2003).

Gann, R.J., Babrauskas, V., and Peacock, R.D., "Fire Conditions for Smoke Toxicity Measurements," Fire and Materials, 18 (3), 193-199 (1994).

Gottuk, D. and Lattimer, B., "Effect of Combustion Conditions on Species Production," *Society of Fire Protection Engineering Handbook,* 3rd edition, Section 2, Chapter 5, (2002).

Gottuk, D., "The Generation of Carbon Monoxide in Compartment Fires," Ph.D. Dissertation, Virginia Polytechnic Institute and State University, Department of Mechanical Engineering, Blacksburg, VA (1992).

Hall, J.R., "Burns, Toxic Gases, and Other Hazards Associated with Fires: Deaths and Injuries in Fire and Non-Fire Situations," National Fire Protection Association, November (1997).

Hartman, H., Mutmansky, J., Ramani, R., and Wang, Y., *Mine Ventilation and Air Conditioning*, 3rd edition, John Wiley and Sons, Inc., New York, (1997).

Hasemi, Y., Yokobayahi, S., Wakamatsu, T., Ptchelintsev, A., "Firesafety of Building Components Exposed to a Localized Fire-Scope and Experiments on Ceiling/Beam System Exposed to a Localized Fire," Proceedings of ASIAFlam 1995, 1st International Conference, 351-361 (1995).

Hinkley, P., Wraight, H., and Theobald, C., "The Contribution of Flames Under Ceilings to Fire Spread in Compartments," *Fire Safety Journal*, 7, (1984) 227-242.

Janssens, M. and Tran, H. C., "Data Reduction of room Tests for Zone Model Validation," *Journal of Fire Sciences*, 10, 528-555, (1992).

Karlsson, B., Quintiere, J., *Enclosure Fire Dynamics*, CRC Press, (2001).

Karter Jr., M.J., "Fire Loss in the United States During 1999," National Fire Protection Association, September (2000).

Kawagoe, K., "Fire Behavior in Rooms," Report No. 27, Building Research Institute, Tokyo, Japan, (1958).

Lattimer, B., "The Transport of High Concentrations of Carbon Monoxide to Locations Remote from the Burning Compartment," Ph.D. Dissertation, Virginia Polytechnic Institute and State University, Department of Mechanical Engineering, Blacksburg, VA (1996).

Launhardt, R., "Emergency Preparedness and Response," in *Mine Health and Safety Management,* Karmis, M. (editor), Society of Mining, Metallurgy, and Exploration, Inc., (2001).

Litton, C., "Relationships between Smoke and Carbon Monoxide and Their Implication Toward Improved Mine Fire Detection," International Conference of Safety in Mines Research Institutes, Proceedings of the 23rd International Conference of Safety in Mines Research Institutes, September 11-15, (1989) 77-82.

Lönnermark, A., Blomqvist, P., Mansson M., and Persson, H., "TOXFIRE – Fire Characteristics and Smoke Gas Analysis in Under-ventilated Large-scale Combustion Experiments: Tests in the ISO 9705 Room, SP Report 45. SP Swedish National Testing and Research Institute: Boras, (1997).

Loomis, I., Stevenson, J., Tisdale, J., Mitchell, D., and Marston, B., "Mine Fires and Explosions," in *Mine Health and Safety Management,* Karmis, M. (editor), Society of Mining, Metallurgy, and Exploration, Inc., (2001).

McCaffrey, B.J. and Heskestad, G., Brief Communications: A Robust Bidirectional Low Velocity Probe for Flame and Fire Application," *Combustion and Flame*, 26, (1976) 125-127.

McGrattan, K., et al., "Fire Dynamics Simulator – Technical Reference Guide," National Institute of Standards and Technology, NISTIR 6467, 2000a.

McGrattan, K., and Forney, G., "Fire Dynamics Simulator – User's Manual," National Institute of Standards and Technology, NISTIR 6469, 2000b.

McKay, C., "Carbon Monoxide Generation in a Compartment with a Doorway During a Fire," Master of Science Thesis, Virginia Polytechnic Institute and State University, Department of Mechanical Engineering, Blacksburg, VA (2002).

McPherson, M., *Subsurface Ventilation and Environmental Engineering,* Chapman & Hall Inc., London, (1993).

Morehart, J. H., E. E. Zukoski, and T. Kubota, "Species Produced in Fires Burning in Two-Layered and Homogeneous Vitiated Environments," National Institute of Standards and Technology, Center for Fire Research, Report NBS-GCR-90-585, (1990).

National Institute for Occupational Safety and Health, www.cdc.gov/niosh/mining/data/disall.html, (2001).

Nelson, H., "An Engineering Analysis of Fire Development in the Hospice of Southern Michigan, December 15, 1985," Fire Safety Science – Proceedings of the Second International Symposium, 927-938.

Nelson, H.E., "FPETOOL: Fire Protection Engineering Tools for Hazard Estimation," National Institute of Standards and Technology, Internal Report 4380, 93-100, (1990).

NFPA, Carbon Monoxide Risks at Home," Fact Sheet, National Fire Protection Association, (2000).

NFPA 101, *Lifesafety Code*, National Fire Protection Association, (1994)

NIOSH, "Behavioral and Organizational Dimensions of Underground Mine Fires," IC 9450, U.S. Department of Health and Human Services, May (2000).

Pchelintsev, A., Hasemi, Y., Wakamatsu, T., and Yokobayashi, Y., "Experimental and Numerical Study on the Behaviour of a Steel Beam under Ceiling Exposed to a Localized Fire," Fire Safety Science – Proceedings of the Fifth International Symposium, 1153-1164 (1997).

Pitts, W., "The Global Equivalence Ratio Concept and the Prediction of Carbon Monoxide Formation in Enclosure Fires," *NIST Monograph 179*, National Institute of Standards and Technology, (1994).

Pitts, W., Personal communication during a joint progress meeting held on December 20-21, 1999 at the Mechanical Engineering Department of Virginia Tech.

Pitts, W., Braun, E., Peacock, R., Miter, H., Johnsson, E., Reneke, P., Blevins, L., "Temperature uncertainties for bare-bead and aspirated thermocouple measurements in fire environments," 14th meeting of the United States-Japan Conference on Development of Natural Resources (UJNR) Panel on Fire Research and Safety, May 1998.

Pon, M., Gibert-Jones, I., "Other Industrial Hygiene Concerns," in *Mine Health and Safety Management,* Karmis, M. (editor), Society of Mining, Metallurgy, and Exploration, Inc., (2001).

Purser, D., "Toxic Product Yields and Hazard Assessment for Fully Enclosed Design Fires," *Polymer International*, 49, (2000) 1232-1255.

SFPE Handbook of Fire Protection Engineerin, 2nd edition, National Fire Protection Association, Quincy, MA, (1995), pgs. 1-64, A-34.

Tewarson, A., "Fully Developed Enclosure Fires of Wood Cribs", 20th Symposium (International) on Combustion, pp. 1555-1566, (1984).

Tewarson, A., "Generation of Heat and Chemical Compounds in Fires," *SFPE Handbook of Fire Protection Engineering*, 2nd ed., National Fire Protection Association, Quincy, MA, (1995).

Tewarson, A., "Generation of Heat and Chemical Compounds in Fires," *SFPE Handbook of Fire Protection Engineering*, 3rd ed., National Fire Protection Association, Quincy, MA, (2002).

Toner, S. J., E. E. Zukoski, and T. Kubota, "Entrainment, Chemistry, and Structure of Fire Plumes," National Institute of Standards and Technology, Center for Fire Research, Report NBS-GCR-87-528, (1987).

Vandsburger, U., **"**Evolution of Compartment Exhaust Gases, Providing Evaluation Criteria and Design Tools," Final Report, Grant Number 60NANB7D0066, National Institute of Standards and Technology, Gaithersburg, MD, 2001.

Vandsburger, U., **"**Evolution of Compartment Exhaust Gases in Buildings, Providing Evaluation Criteria and Design Tools," Annual Report, Grant Number 60NANB1D0086, National Institute of Standards and Technology, Gaithersburg, MD, 2002.

Zukoski, E., "Fluid Dynamic Aspects of Room Fires," Fire Safety Science – Proceedings of the First International Symposium, 1985.

Zukoski, E., Kubota, T., and Lim C., "Experimental Study of Environment and Heat Transfer in a Room Fire. Mixing in Doorway Flows and Entrainment in Fire Plumes," NBS Report NBS-GCR-85-493, National Bureau of Standards, Gaithersburg, MD., 1985.

APPENDIX A

FLAME EXTENSION CALCULATIONS

A.1 INTRODUCTION

As part of this research study the issue of external burning was explored. Fires occurring within a compartment may exhibit burning external to the compartment boundaries. It has been previously reported that external flaming occurs at or after the onset of flashover within the compartment. [Drysdale, 2001] Flashover is defined as "The transition from the fire growth period to the fully developed stage in the enclosure fire development." [Karlsson 2001] For an experimental setup, such as the one used in this study, where the only fuel source is a gas burner, flashover is defined as the transition point between over-ventilated and under-ventilated burning. The occurrence of flashover is quantified by a global equivalence ratio of 1.0. The global equivalence ratio is the actual compartment fuel to air ratio divided by the stoichiometric fuel to air ratio.

It was proposed that external burning may also occur as a result of flame extensions. Flame extensions occur when the fire plume impinges on the ceiling and the horizontal length of the impinging flames exceeds the distance from the plume centerline to the compartment opening. Flame extensions can occur in over-ventilated fires.

A.2 FLAME EXTENSION ANALYSIS

The methodology used to determine the potential for flame extensions requires the determination of the fire size necessary to obtain a flame length equal to the vertical distance between the fuel source and the ceiling plus the radial distance from the fire plume centerline to the opening. A correlation for determining the length of the flame flowing under a ceiling was determined by Pchelintsev *et al.* [1997] and Hasemi *et al*. [1995], and was given as:

$$L_f = H\left(2.04\left(\dot{Q}^*\right)^{0.33} - 1\right) \qquad \text{(A-1)}$$

where: H is the distance between the fuel source and the ceiling (m)

L_f is the length of the flame flowing under the ceiling (m)

Q^* is a non-dimensional heat release rate, defined as

$$\dot{Q}^* = \frac{\dot{Q}}{\rho_{amb}\, c_p\, T_{amb}\, \sqrt{g}\, D\, H^{1.5}} \qquad \text{(A-2)}$$

Where $\dot{Q}$ is the heat release rate of the fire (kW), and under STP conditions, ρ_{amb} = 1.2 kg/m^3, c_p = 1.0 kJ/(kg K), T_{amb} = 293 K, and g = 9.81 m/s^2, which results in

$$\dot{Q}^* = \frac{\dot{Q}}{1090\, D\, H^{1.5}} \qquad \text{(A-2a)}$$

Where D is the diameter of the fuel source (m).

Substitution of Equation A-2a into A-1 results in an expression which can be solved directly for $\dot{Q}$; which in this case would be the heat release rate required for the fire plume to reach the compartment opening,

$$\dot{Q} = 1090\, D\, H^{1.5}\left(\sqrt[0.33]{\frac{1}{2.04}\left(\frac{L_f}{H}+1\right)}\right) \qquad \text{(A-3)}$$

Solving Equation A-3 for the present experimental geometry, D = 0.305 m, H = 1.17 m, and L_f = 0.89 m. The heat release rate for flame extensions is determined to be 269.3 kW. This value is based on an axisymmetric fire plume without any confinement. In

the case of a compartment with one opening the fire plume is bound by the enclosure boundaries and air can only be entrained through the opening.

The minimum heat release rates for which flames were experimentally observed to begin to exit the compartment are listed in Table A-1 along with the corresponding global equivalence ratio. These values are a function of the compartment ventilation width. For the baseline doorway the fire size was gradually increased until the flames just began to exit the compartment. For the narrow doorway at a heat release rate of 91 kW "tiny wisps of flames" were observed to exit the compartment. For the wide doorway only four tests were performed. At the lowest heat release rate, 107 kW, no flames were observed coming from the compartment, while a continuous flame extending from the compartment was observed at a heat release rate of 203 kW.

Table A-1: Experimental $\dot{Q}_{\text{Flame Extensions}}$ and corresponding equivalence ratio

Doorway Geometry	$\dot{Q}_{\text{Flame Extensions}}$ **(kW)**	**Experimental Equivalence Ratio**
Narrow	91	0.32
Baseline	127	0.26
Wide	107 – 203	0.13 – 0.24

The values reported in Table A-1 are lower then the theoretical value calculated using Equation A-3, again this is attributed to the fact that the original correlation was developed based on an unconfined flame impinging on the ceiling. A correction factor is therefore necessary to account for the confinement of the flame within the compartment. Using the experimental data for the narrow and baseline doorway and plotting the ratio of $\dot{Q}_{\text{Experiment}} / \dot{Q}_{\text{Theory}}$ as a function of $A\sqrt{H_o}$ and applying a linear fit to the data the following equation for the confinement correction factor, κ, is obtained,

$$\kappa = 1.09\ A\sqrt{H_o} + 0.204 \qquad \text{(A-4)}$$

The heat release rate for flames to reach the compartment exit plane, for the current configuration, can be determined by multiplying the theoretical heat release rate determined via Equation A-3 by the confinement correction factor,

$$\dot{Q}_{\text{Flame Extensions, confind}} = \kappa\, \dot{Q}_{\text{Flame Extensions, unconfined}} = 1090\, \kappa\, D\, H^{1.5} \left(\sqrt{\frac{1}{2.04}\left(\frac{L_f}{H} + 1\right)} \right) \qquad \text{(A-5)}$$

Using Equation A-4, κ for the wide doorway is calculated to be 0.74, using this value and Equation A-5 the theoretical heat release rate for flame extensions is 199 kW. Comparing this value to those listed in Table A-1, it is seen that the theoretical value falls in between the two. The theoretical value is slightly higher than that used in the analysis presented in Chapter 4.

The theoretical global equivalence ratio at which external burning due to flame extensions will occur can be determined by calculating the mass burning rate required for flame extensions,

$$\dot{m}_{\text{fuel}} = \frac{\dot{Q}_{\text{Flame Extensions}}}{\Delta h_c} \qquad \text{(A-6)}$$

and the mass flow rate of air into the compartment, given by the ventilation limit as

$$\dot{m}_{\text{air}} = 0.52\ A\sqrt{H} \qquad \text{(A-7)}$$

then the global equivalence ratio can be calculated from Equation A-8,

$$\phi = \frac{\left(\frac{\dot{m}_{fuel}}{\dot{m}_{air}}\right)}{\left(\frac{\dot{m}_{fuel}}{\dot{m}_{air}}\right)_{stoic.}}. \qquad \text{(A-8)}$$

The methodology outlined above was used to estimate the minimum fire size and equivalence ratio necessary for flame extensions in the current study, results of these calculations are shown in Table A-2.

Table A-2: Minimum Fire Size and Equivalence Ratio for Flame Extension

Test Configuration	Fire Size (kW)	Burning Rate (kg/sec)	Air Entrainment (kg/sec)	Theoretical Equivalence Ratio [a]
Narrow Doorway	91	0.0019	0.061	0.49
Baseline Doorway	127	0.0027	0.123	0.34
Wide Doorway [b]	199	0.0042	0.245	0.27

[a] $(fuel/air)_{stoic,\ propane} = 0.064$

[b] Values based on calculated heat release rate for flame extensions using methodology outlined in Section A.2.

A.3 SUMMARY

It was determined from experimental observations that external burning occurs from either flame extensions or under-ventilated burning. Under-ventilated burning is a function of the ventilation opening and mass flow rate of fuel, while flame extensions are a function of the ventilation opening, mass flow rate of fuel, compartment dimensions, and fire location. By definition, under-ventilated burning conditions always occur at a global equivalence ratios greater then 1.0; however, flame extensions may occur at global equivalence ratios below 1.0, i.e. for over-ventilated compartment fires.

The correlation developed by Pchelintsev *et al.* [1997] and Hasemi *et al*. [1995] for flame extensions under a ceiling in an unconfined geometry, was modified based on the experimental data from the narrow and baseline doorway and a confinement

coefficient was defined. The modified methodology appears to agree with measured data for the present scenario and can be used to estimate the occurrence of flame extensions for different ventilation conditions and burner configurations. Further data from other experimental configurations is required to determine if this methodology can be applied universally.

APPENDIX B

RESULTS AND DISCUSSION: SLIVER DOORWAY

B.1 INTRODUCTION

The forth ventilation condition that was investigated during this study was termed as the sliver doorway. The doorway width was half the width of the narrow doorway, measuring 0.08 m and provided the lowest ventilation for the compartment, and therefore the highest global equivalence ratios. After testing with the sliver doorway was completed it was noticed that the area of the sliver doorway, 0.06 m^2, was smaller then the area of the gas burner, 0.07 m^2. The compartment became in effect the burner, no combustion was occurring inside the compartment. This scenario represented a jet diffusion flame as opposed to a typical compartment fire. Therefore, the results from the experiments were not comparable to the other doorway data. Since this scenario does not fall into the parameters of primary interest for this study, the data is presented and a basic overview of the results are presented, however, no analysis of the results was done.

B.2 MOLE FRACTIONS VERSUS IDEAL HEAT RELEASE RATE

The species mole fractions as a function of the ideal heat release rate are shown in Figure B-1 through Figure B-4 for the various door widths. Data from studies performed by Bryner *et al.*[1994] and Gottuk [1992] are also included for comparison.

The exit vent in Gottuk's compartment varied between 0.04 m^2 and 0.16 m^2 while the smallest opening in the present study is the sliver doorway, 0.062 m^2. Therefore, it can be anticipated that better agreement will be seen between the sliver doorway results and Gottuk's results than with the wide doorway results.

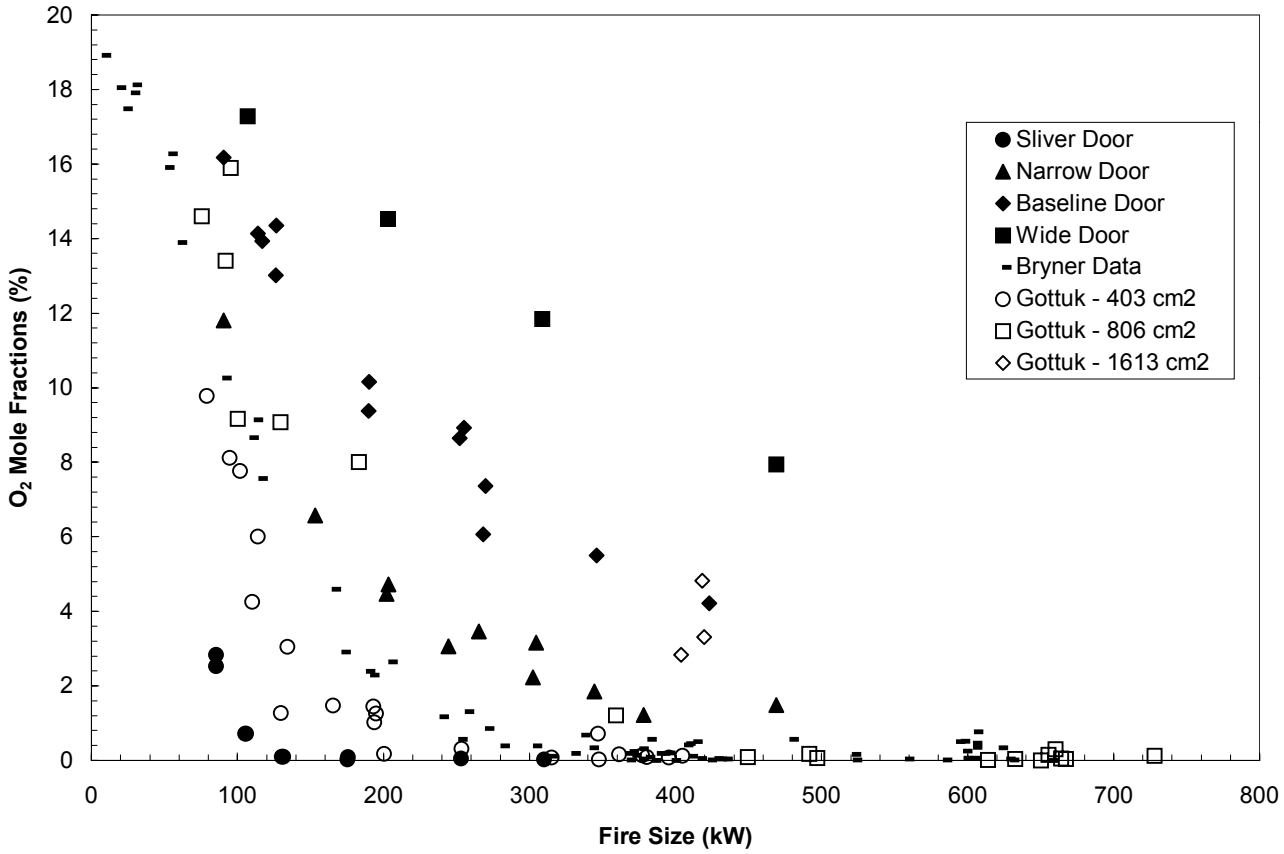

Figure B-1: Oxygen mole fractions as a function of ideal heat release rate and door width compared with data from Gottuk [1992] and Bryner *et al.* [1994].

For each of the species shown in Figure B-1 through Figure B-4 four clearly defined curves are seen, one for each ventilation condition. The lowest mole fractions of oxygen are seen for the sliver doorway, Figure B-1.

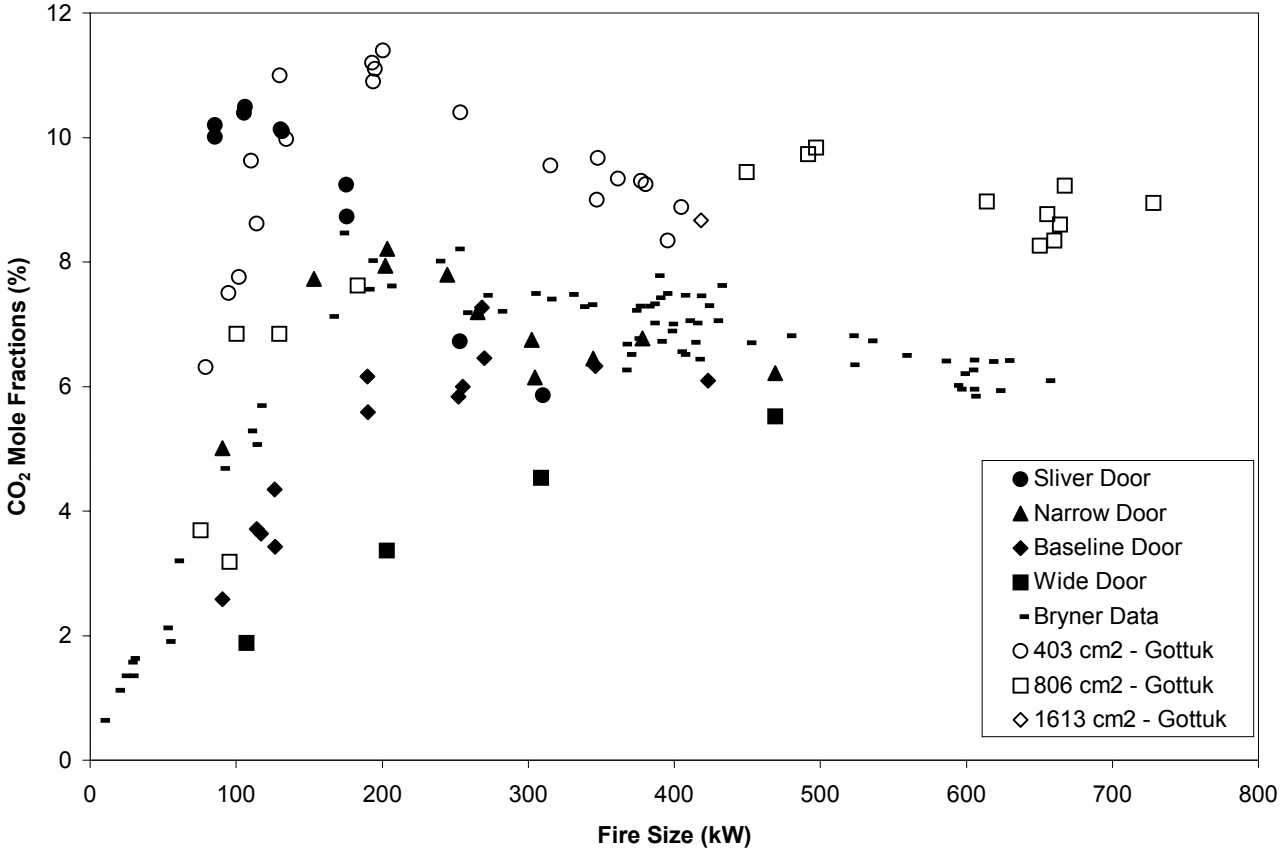

Figure B-2: Carbon dioxide mole fractions as a function of ideal heat release rate and door width compared with data from Gottuk [1992] and Bryner *et al.* [1994].

Examination of the carbon dioxide levels, Figure B-2, shows that the levels first increase, reach a maximum, and then taper off. This trend is seen with the present data and data from previous studies. Carbon dioxide levels measured with the sliver doorway peak at approximately 10.0 % and then decrease to less then 6.0 % for the largest heat release rates examined. The trend indicates that carbon dioxide levels will continue to decrease at higher heat release rates. The same trend is observed for all four ventilation conditions; however, the peak values decrease as the doorway width increases.

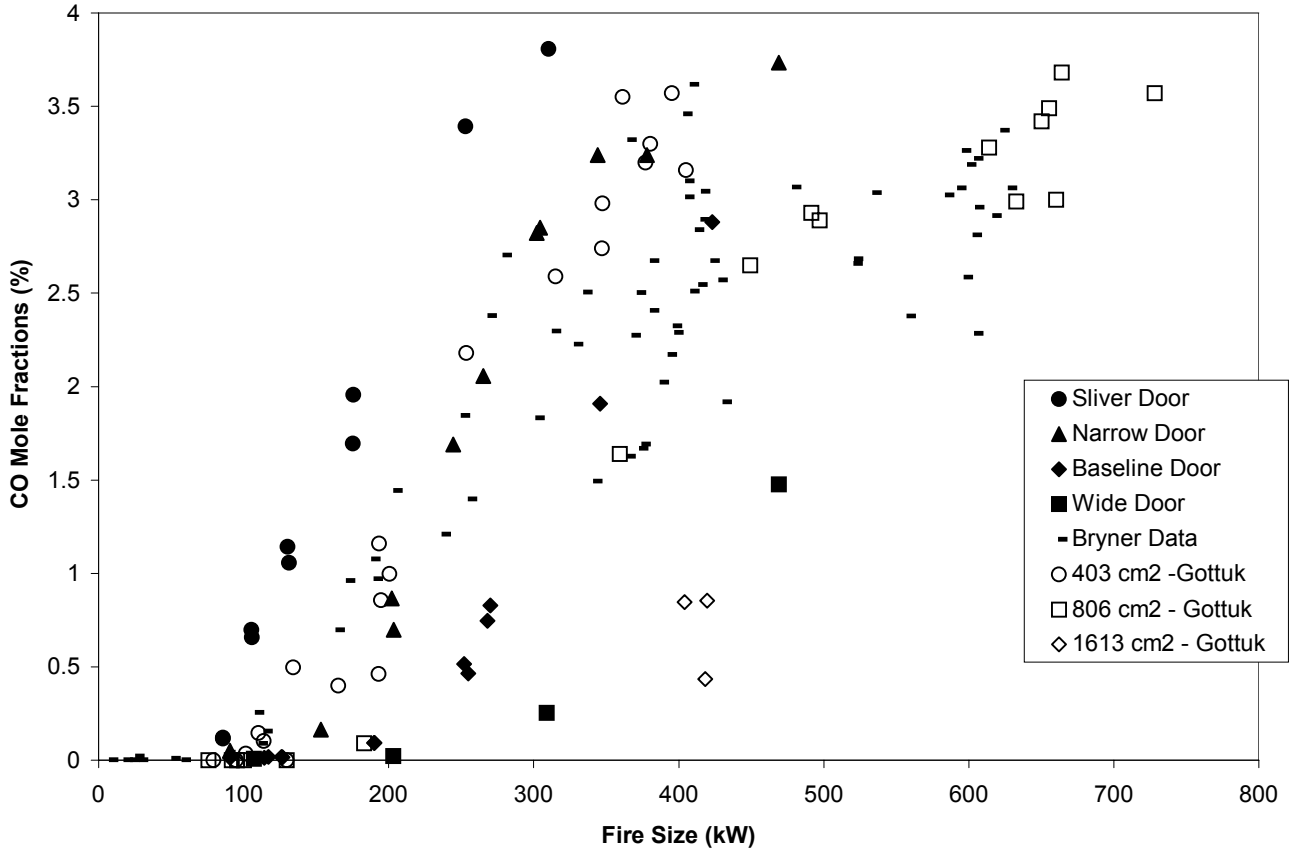

Figure B-3: Carbon monoxide mole fractions as a function of ideal heat release rate and door width compared with data from Gottuk [1992] and Bryner *et al.* [1994].

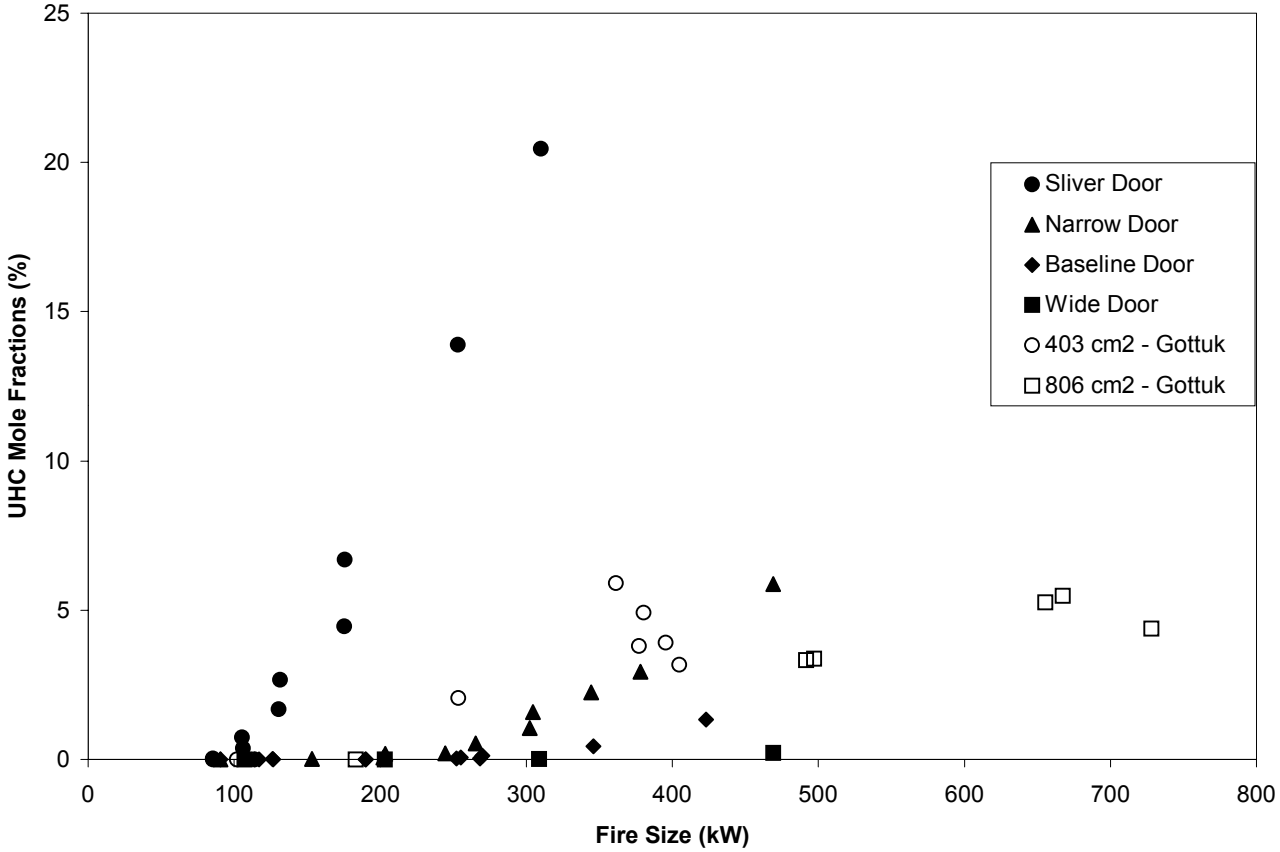

Figure B-4: Unburned hydrocarbon mole fractions as a function of ideal heat release rate and door width compared with data from Gottuk [1992] and Bryner *et al*. [1994].

The highest levels of carbon monoxide and unburned hydrocarbons are expected to occur under the lowest ventilation conditions since there is less oxygen available for the combustion process to go to completion. Indeed, the highest levels of carbon monoxide and unburned hydrocarbons, Figure B-3 and Figure B-4 respectively, are seen with the sliver doorway and the lowest levels with the wide doorway.

B.3 SPECIES YIELDS VERSUS THE GLOBAL EQUIVALENCE RATIO

The calculated species yields based on standard fire protection engineering practice, for oxygen, carbon dioxide, carbon monoxide, and unburned hydrocarbons are presented in Figure B-5 through Figure B-8. The oxygen and carbon dioxide data are presented as normalized yields, while the carbon monoxide and unburned hydrocarbon yields are presented as un-normalized yields. Reported data from previous studies of Gottuk [1992] and Belyer [1983,1986a] are also included for comparison.

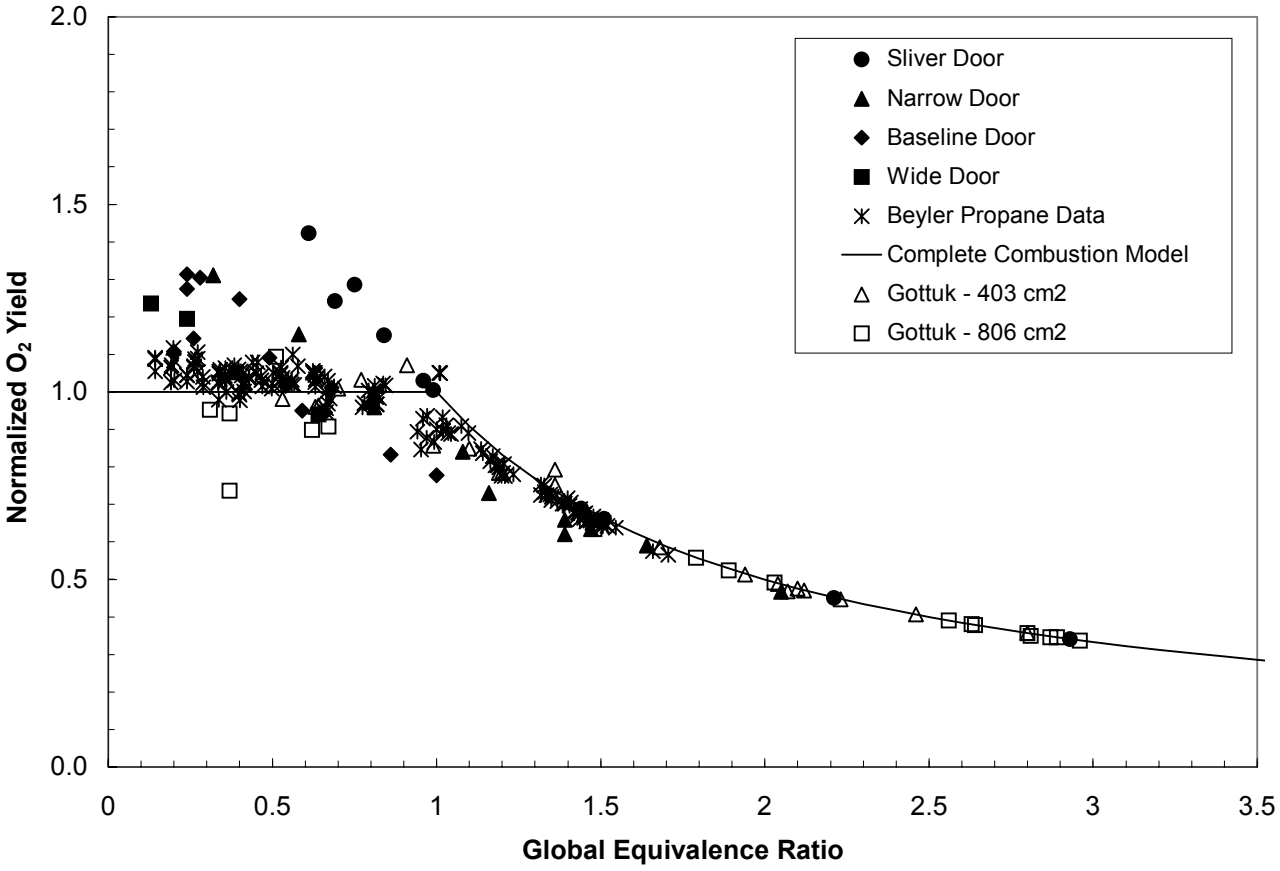

Figure B-5: Normalized O_2 yields as a function of the equivalence ratio and door width compared with data from Gottuk [1992] and Beyler [1983], in addition to the model for complete combustion.

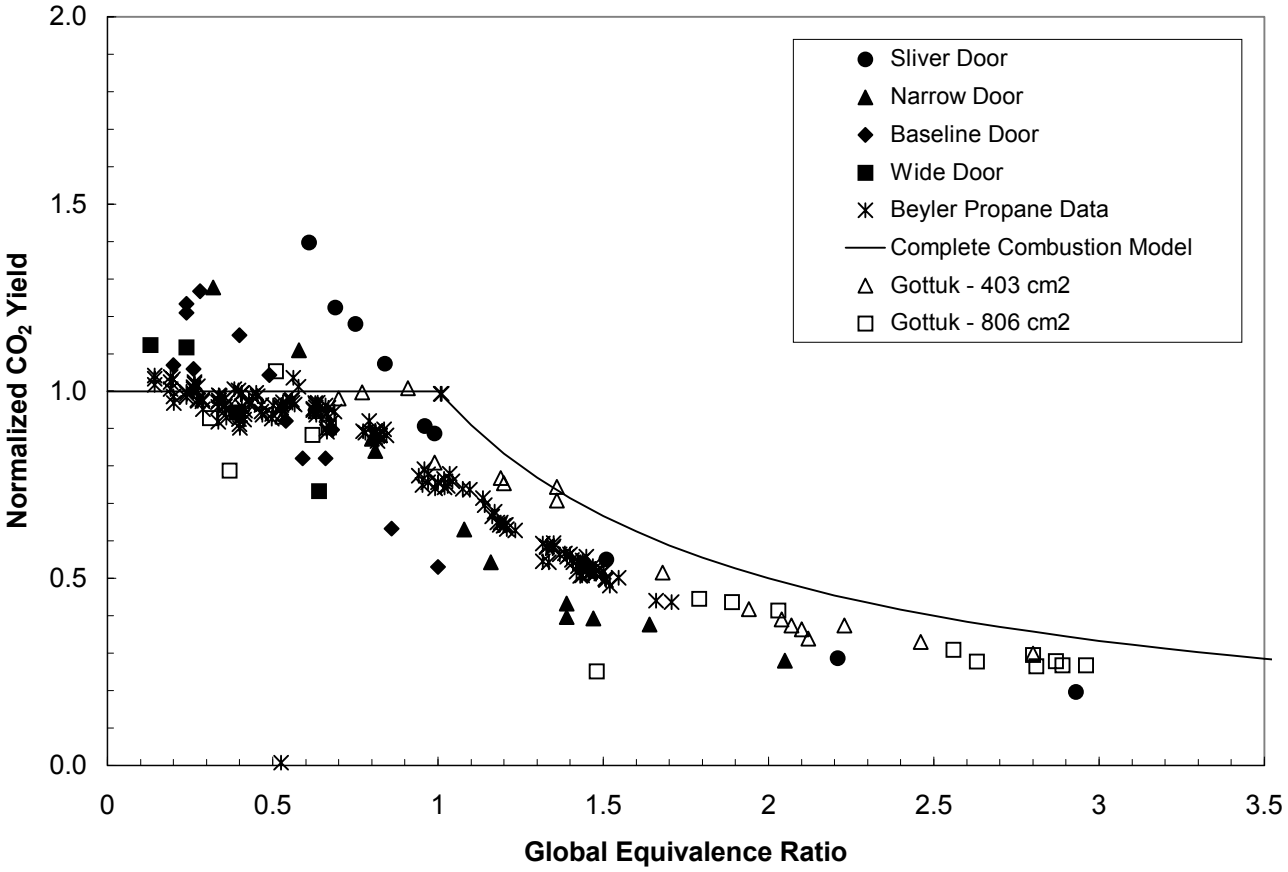

Figure B-6: Normalized CO_2 yields as a function of the equivalence ratio and door width compared with data from Gottuk [1992] and Beyler [1983], in addition to the model for complete combustion.

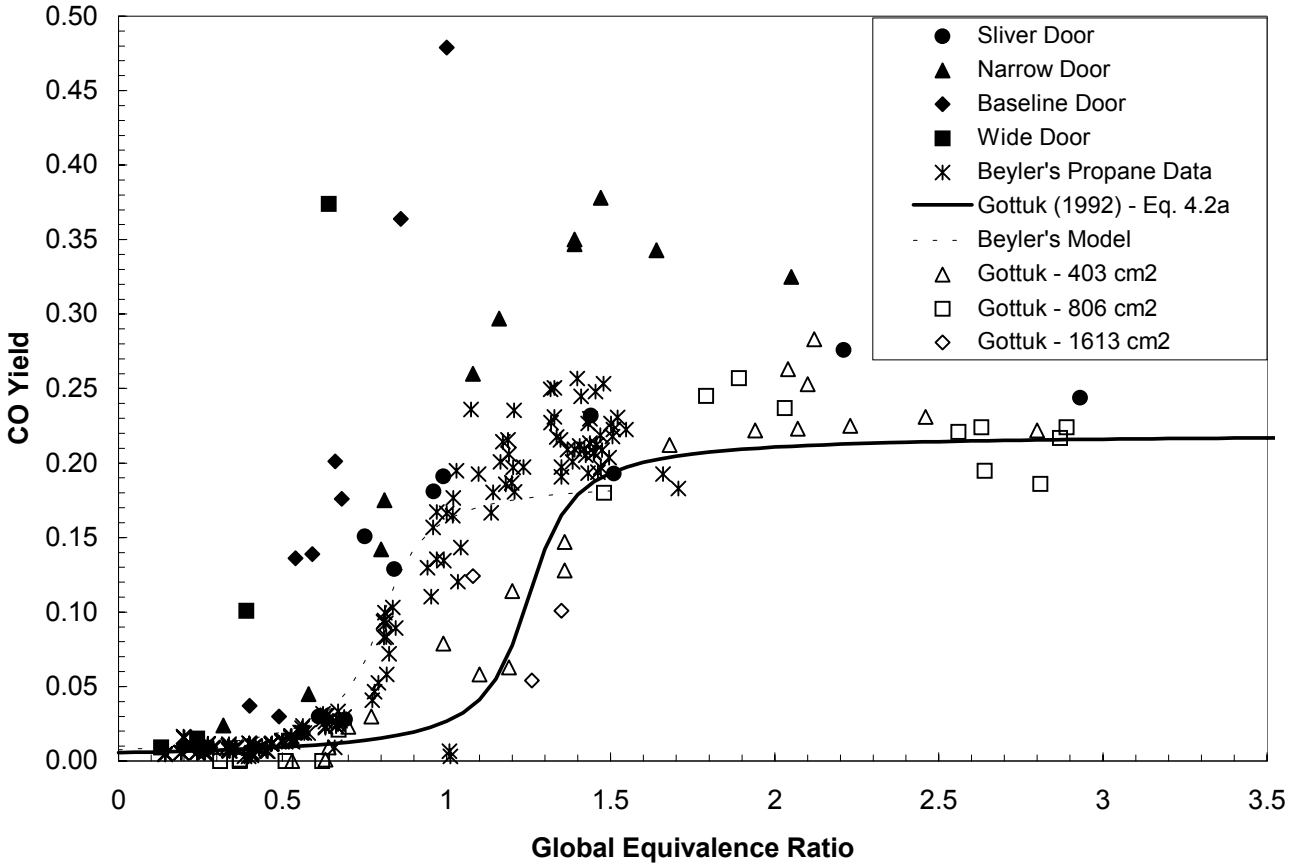

Figure B-7: Carbon monoxide yields as a function of the equivalence ratio and door width compared with data from Gottuk [1992] and Beyler [1983], in addition to models from Gottuk [1992] and Beyler [1983].

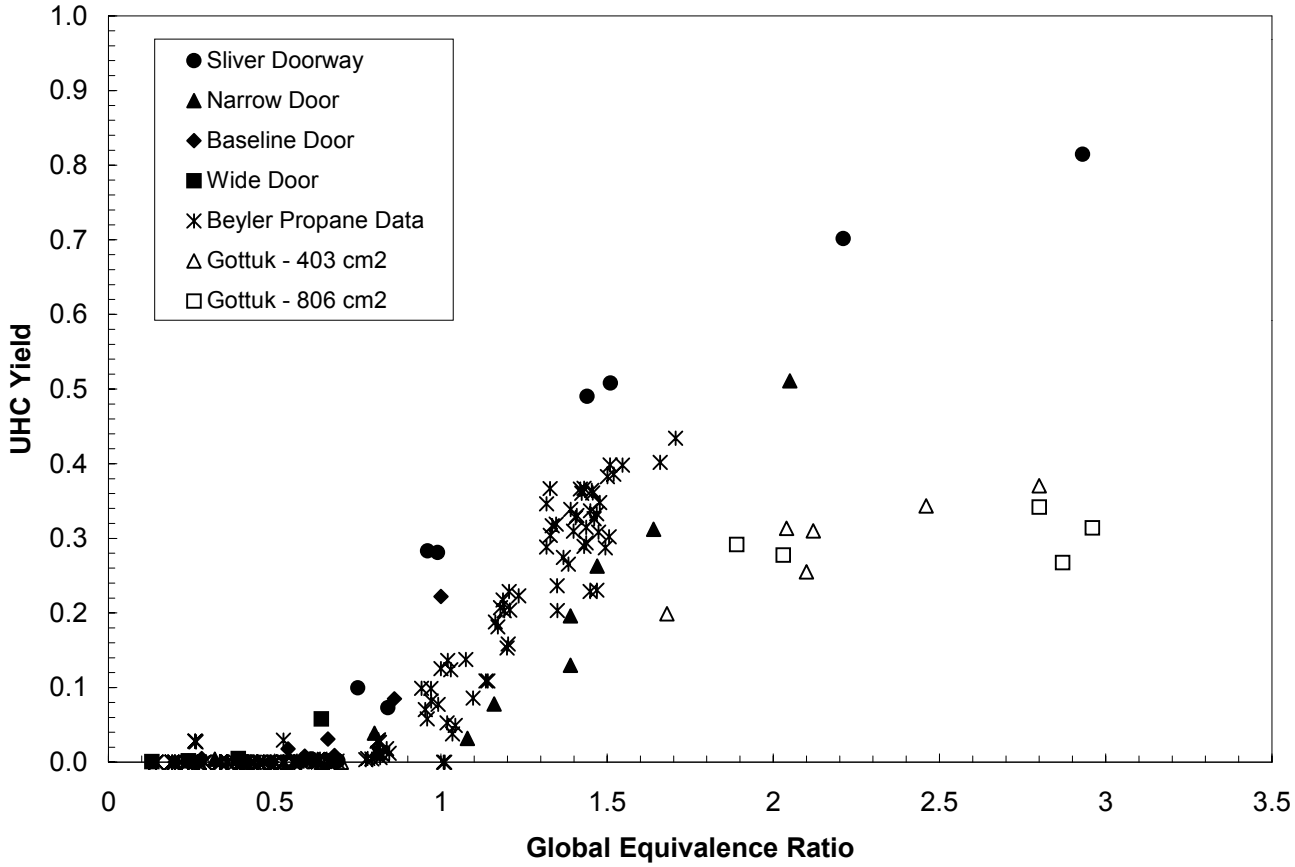

Figure B-8: Unburned hydrocarbon yields as a function of the equivalence ratio and door width compared with data from Gottuk [1992] and Beyler [1983].

The normalized oxygen data shown in Figure B-5 indicates good agreement with the studies of Beyler [1983] and Gottuk [1992]. Similar agreement is seen for the carbon dioxide yields in Figure B-6. Although there is some variation, the data for all four ventilation conditions appears to collapse to a single curve when presented in this fashion.

The CO yield as a function of the equivalence ratio, shown in Figure B-7, indicates a different curve for each of the four ventilation conditions. The sliver doorway data appears to follow the same trend as that of the data from Beyler [1983]. In light of the differences in the sampling points, i.e. Beyler's data taken in the upper layer beyond

the flame and the present data collected at the exit plane of the compartment and therefore in the flame for the sliver doorway, the agreement between the data should be considered fortuitous. Similar to Beyler, the data plateaus at a value of approximately 0.23 g_{co}/g_{fuel}.

An increase in the UHC levels, shown in Figure B-8, is seen for all four ventilation conditions and follows the same trend as the data from Beyler [1983]. As the door width increases larger mass flow rates of fuel are required to produce the same equivalence ratio. Therefore, higher levels of unburned hydrocarbons are expected for larger doorways at lower equivalence ratios. The wide, baseline, and narrow doorway data follow the expected trend; however, the sliver doorway data do not. This is attributed to the area of the sliver doorway, 0.06 m^2, relative to the area of the gas burner, 0.07 m^2, within the compartment. Since the area of the doorway is smaller than that of the burner, the compartment becomes, in effect, the burner. Therefore, any increase in the gas flow rate to the burner will be seen as a direct increase in the measured unburned hydrocarbons in the compartment opening.

APPENDIX C

EXPERIMENTAL UNCERTAINTY ANALYSIS

C.1 INTRODUCTION

An estimate of the uncertainty associated with the measured parameters and subsequent calculations using those parameters is present in the following sections.

C.2 CALCULATION OF UNCERTAINTY

Uncertainties in direct measurements of parameters are typically based on the assumption that all of the contributing factors are linearly dependent. The associated uncertainty for each measured parameter is based on Equation C-1,

$$\varepsilon^2 = \varepsilon_1^2 + \varepsilon_2^2 + \varepsilon_3^2 + \varepsilon_4^2 \ldots \qquad \text{(C-1)}$$

Uncertainties associated with calculations based on measured quantities are determined using the Pythagorean summation of discrete uncertainties [Beckwith and Marangoni 1990], Equation C-2,

$$u_f = \sqrt{\left(u_{x_1}\frac{\partial f}{\partial x_1}\right)^2 + \left(u_{x_2}\frac{\partial f}{\partial x_2}\right)^2 + \ldots + \left(u_{x_n}\frac{\partial f}{\partial x_n}\right)^2} \qquad \text{(C-2)}$$

where f is the parameter of interest, u is the uncertainty associated with a variable, and the x's are the variables in the equation.

C.3 UNCERTAINTY IN MEASURED PARAMETERS

C.3.1 Species Mole Fractions

The uncertainty associated with the measured species mole fractions was attributed to four potential sources:

1. Analyzer repeatability, ε_{AR} (manufacture specification)
2. Analyzer Linearization, ε_{AL} (manufacture specification)
3. Calibration gas, ε_{CG} (manufacture specification)
4. Experimental repeatability, ε_{ER} (based on experimental results)

The values for each source of uncertainty associated with each species are listed in Table C-1, along with the total estimated uncertainty for each species.

Table C-1: Estimated Uncertainty in Species Mole Fraction Measurements

Species	ε_{AR}	ε_{AL}	ε_{CG}	ε_{ER}	ε_{dry} (%)
Oxygen	0.01	0.00	0.015	0.05	5.3
Carbon Dioxide	0.01	0.02	0.015	0.05	5.7
Carbon Monoxide	0.01	0.02	0.015	0.05	5.7
Unburned Hydrocarbons*	0.02	0.00	0.015	0.05	15.2

* Unburned hydrocarbons are measured directly on a wet basis

C.3.2 Gas Temperature

The uncertainty in the gas temperature measurements is a combination of the uncertainty in the accuracy of the measurement technique and the repeatability between tests. Aspirated thermocouple measurements have a reported uncertainty between ±5% and ±20% depending on if the measurements are being conducted in the upper layer or lower layer of the compartment respectively. [Blevins and Pitts 1999] Due to soot clogging and experimental variations, the difference in temperature measurements between two tests is estimated to be no greater then 100°. In the upper layer where the typical gas temperatures are approximately 1000 K, the repeatability uncertainty is

±10%, in the lower layer based on an average gas temperature of 400 K, the repeatability uncertainty is ±25%.

The uncertainty in the total temperature measurements is therefore ±11.2% for measurements in the upper layer and ±32.0% for measurements in the lower layer. The calculations of interest in this study involve species in the upper layer, therefore, for all uncertainty analysis calculations involving the gas temperatures, the estimated uncertainty for temperatures in the upper layer will be used, i.e. ±11.2%.

C.3.3 Gas Pressure

The accuracy of the Setra Systems Inc. Model 264 bi-directional pressure transducer is reported by the manufacture to be ±1% of full-scale. The uncertainty associate with experimental repeatability is assumed to be about ±5%. The total uncertainty associated with the pressure measurement is therefore ±5.1%.

C.3.4 Fuel Mass Flow Rate

The reported manufactures uncertainty for the Sierra model 780S mass flow meter is ±2% for flow rates between 100 and 1000 slpm. However, conversations with technicians at Sierra Instruments Inc. determined that the meter was not linear below 250 slpm, the primary operating range for the present study, therefore, a correction factor needed to be developed. A correction curve was therefore developed for flow rates between 30 slpm and 280 slpm. The correction curve is shown in Figure C-1.

The correction curve was developed by calibrating the Sierra Instruments Inc. meter against a dry gas test meter. The procedure consisted of connecting the dry test flow meter in series with the Sierra Instruments Inc. meter and flowing propane through the system. The dry gas meter was analog in nature and indicated the total volume of flow. A time interval to achieve a fixed volume of flow was determined using a stopwatch. The volumetric flow rate could then be determined, and subsequently the fuel mass flow rate.

Potential uncertainties in the methodology include the accuracy of the dry gas meter, accuracy of the stopwatch, and reaction time activating the stopwatch. The individual contributions from these variables can not be quantified; therefore, an uncertainty of ±5% has been assumed for the combined uncertainties in the correction curve values.

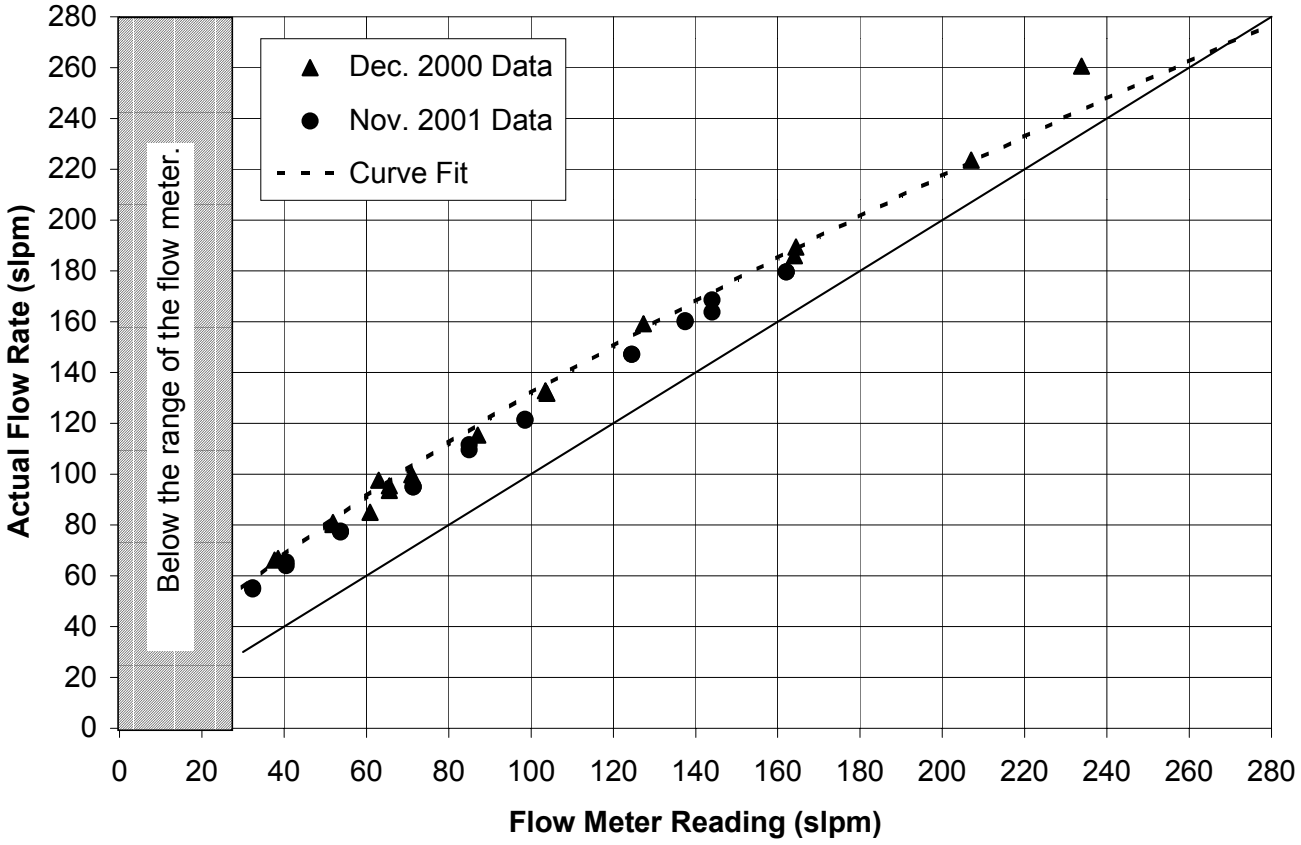

Figure C-1: Correction curve for Sierra Instruments Inc. flow meter. Data collected on two separate days.

Assuming an uncertainty in experimental repeatability of ±5%, the total uncertainty in the mass flow meter measurements is therefore ±7.4% for mass flow rates between 0 slpm and 250 slpm. For flow rates greater then 250 slpm, total uncertainty,

using the manufacture's value of ±2% FS plus the experimental repeatability error of ±5%, is ±5.4%. The majority of the experiments were conducted with the mass flow rate below 300 slpm.

C.4 UNCERTAINTY IN CALCULATED PARAMETERS

C.4.1 Uncertainty Associated with Calculations Involving Measured Parameters

C.4.1.1 Species Mole Fractions Not Measured Directly

Two species required for many of the calculations, which are not measured directly, are water and nitrogen.

The mole fraction of water in the sample is estimated based on the assumption that the molar ratio, c, of H_2O to CO_2 at any equivalence ratio is equal to the calculated molar ratio at stoichiometric conditions. [Gottuk 1992, Lattimer 1996, McKay 2002] Gottuk [1992] estimated that this calculation was valid to ±6%.

Assuming that the gas composition consisted of oxygen, carbon dioxide, carbon monoxide, unburned hydrocarbons, water, and nitrogen, the mole fraction of nitrogen is determined by,

$$X_{N_2} = 1.0 - \sum X_i \qquad \text{(C-3)}$$

The uncertainty associated with the nitrogen calculation is based on the uncertainties associated with each individual species mole fraction. The estimated uncertainty in the nitrogen calculation is ±16.4%.

C.4.1.2 Wet Species Mole Fractions

Measurements of oxygen, carbon dioxide, and carbon monoxide are made on a dry gas basis. To account for the water vapor removed from the sample, the previously stated assumption that the molar ratio, c, of H_2O to CO_2 at any equivalence ratio is equal to the calculated molar ratio at stoichiometric conditions is used. The wet species mole

fractions are then determined from the measured dry species mole fractions via Equation C-4,

$$X_{i,wet} = \frac{X_{i,dry}}{1 + c\left(X_{CO_{2\,dry}}\right)} \qquad \text{(C-4)}$$

Gottuk [1992] estimated that this methodology was valid to ±6%. Lattimer [1996] reported that Equation C-3 becomes less accurate for high global equivalence ratios, $\phi > 3.0$. Therefore, as a further improvement, Equation C-4 was modified to include the measured dry carbon monoxide mole fractions, Equation C-5,

$$X_{i,wet} = \frac{X_{i,dry}}{1 + c\left(X_{CO_{dry}} + X_{CO_{2\,dry}}\right)} \qquad \text{(C-5)}$$

At low equivalence ratios, where carbon monoxide levels are negligible, Equation C-5 reduces to Equation C-4.

Table C-2: Estimated Uncertainties in Wet Species Mole Fractions

Species	ε_{dry} (%)	ε_{wet} (%)
Oxygen	5.3	11.9
Carbon Dioxide	5.7	9.7
Carbon Monoxide	5.7	8.3
Unburned Hydrocarbons*	NA	15.2
Water	NA	6.0
Nitrogen	NA	16.4

* Unburned hydrocarbons are measured directly on a wet basis

It is estimated that taking into account the dry carbon monoxide mole fractions will improve wet species calculations to below the previously reported uncertainty of

±6%. Taking a value of ±6% as the estimated uncertainty in this calculation into account with the previous errors listed in Table C-1, the uncertainty associated with the wet species mole fractions are listed in Table C-2.

C.4.1.3 Molecular Weight of Mixture

The molecular weight of the mixture is determined via,

$$MW_{mixture} = \sum X_i MW_i \qquad \text{(C-6)}$$

The molecular weigh of each species is a well defined value and does not contribute to the uncertainty calculation. The uncertainty in the calculation of the mixture molecular weight is therefore only a function of the uncertainties associated with the measured mole fractions,

$$\varepsilon_{MW_{mixture}} = \sqrt{\sum \left(\varepsilon_{X_i}\right)^2} \qquad \text{(C-7)}$$

The calculated error is ±23%.

C.4.1.4 Mass Fraction of Species i

The mass fraction of species i is determined by,

$$Y_i = \frac{X_i MW_i}{MW_{mixture}} \qquad \text{(C-8)}$$

Assuming the species molecular weight does not contribute to uncertainty,

$$\varepsilon_{Y_i} = \sqrt{\left(\varepsilon_{X_i}\right)^2 + \left(\varepsilon_{MW_{mixture}}\right)^2} \qquad \text{(C-9)}$$

The calculated uncertainties for each species are listed in Table C-3.

Table C-3: Estimated Uncertainties in Species Mass Fractions

Species	ε_{Yi} (%)
Oxygen	24.5
Carbon Dioxide	24.6
Carbon Monoxide	24.6
Unburned Hydrocarbons	23.8
Water	23.9
Nitrogen	28.4

C.4.1.5 Heat Release Rate

The ideal heat release rate is,

$$\dot{Q}_{ideal} = \dot{m}_{fuel}\ \Delta H_c \qquad \text{(C-10)}$$

the heat of combustion is a constant, therefore, the uncertainty in the heat release rate calculation is the same as the uncertainty in the mass flow rate of fuel, $\varepsilon_{\dot{Q}_{ideal}} = \varepsilon_{\dot{m}_{fuel}} = \pm 7.4\%$.

C.4.1.6 Gas Density

The density of individual species is determined by,

$$\rho_i = \frac{X_i\ MW_i\ P_{amb}}{R\ T} \qquad \text{(C-11)}$$

The variables MW_i, P_{amb}, and R are assumed to be well defined values that do not contribute to the uncertainty calculation. The uncertainty in the species gas density is

therefore a function of the uncertainty in the measured mole fractions and the local gas temperature,

$$\varepsilon_{\rho_i} = \sqrt{\left(\varepsilon_{X_i}\right)^2 + \left(\varepsilon_T\right)^2} \qquad \text{(C-12)}$$

The estimated uncertainties for each species density are listed in Table C-4

Table C-4: Estimated Uncertainties in Species Density

Species	$\varepsilon_{\rho i}$ (%)
Oxygen	13.8
Carbon Dioxide	13.9
Carbon Monoxide	13.9
Unburned Hydrocarbons	12.5
Water	12.7
Nitrogen	19.8

The total gas density is the summation of each of the individual species densities, therefore, the uncertainty in the total gas density is

$$\varepsilon_{\rho,\text{total}} = \sqrt{\sum\left(\varepsilon_{\rho_i}\right)^2} \qquad \text{(C-13)}$$

and calculated to be ±35.9%

C.4.1.7 Gas Velocity

From a simple Bernoulli's analysis the local gas velocity is determined by,

$$V = \sqrt{\frac{2\,\Delta P}{\rho_{air}}} \qquad \text{(C-14)}$$

The local air density is a function of the local air temperature, therefore,

$$V = \sqrt{\frac{2\,\Delta P}{\rho_{air}}} = \sqrt{\frac{2\,\Delta P}{\left(\frac{353}{T}\right)}} = \sqrt{\frac{2\,\Delta P\,T}{353\left(\frac{kg\,K}{m^3}\right)}} \qquad \text{(C-15)}$$

The velocity is a combination of the pressure measurements and temperature measurements.

$$\varepsilon_V = \sqrt{\left(\frac{1}{2}\varepsilon_{\Delta P}\right)^2 + \left(\frac{1}{2}\varepsilon_T\right)^2} \qquad \text{(C-16)}$$

The calculated uncertainty in the velocity measurement is estimated to be ±6.1%.

C.4.1.8 Air Entrainment Rate

The air entrainment rate is determined from the conservation of mass.

$$\dot{m}_{air,in} = \dot{m}_{out} - \dot{m}_{fuel} \qquad \text{(C-17)}$$

Where $\dot{m}_{out}$ is determined from

$$\dot{m}_{out} = \sum \dot{m}_{out,i} = \iint \rho_i \; V \; dA \qquad \text{(C-18)}$$

The uncertainty in the air entrainment rate is a combination of two uncertainties. The first is the uncertainty in the measured variables and the second is the uncertainty in the grid resolution, discussed in detailed in Section C.4.2.1.

$$\varepsilon_{\dot{m}_{air,in}} = \sqrt{\sum \left(\varepsilon_{\rho_i}\right)^2 + \left(\varepsilon_{\dot{m}_{fuel}}\right)^2 + \left(\varepsilon_{GE}\right)^2} \qquad \text{(C-19)}$$

The uncertainty associated with the grid resolution, ε_{GE} is ±5%, see Section C.4.2.1. The uncertainties associated with the species densities and mass flow rate of fuel were reported previously, the resulting uncertainty in the air entrainment rate calculations is ±37.5%.

C.4.1.9 Global Equivalence Ratio

The uncertainty in the global equivalence ratio calculation is a combination of the uncertainty in the fuel mass flow rate and the air entrainment rate.

$$\varepsilon_{\phi} = \sqrt{\left(\varepsilon_{\dot{m}_{fuel}}\right)^2 + \left(\varepsilon_{\dot{m}_{air}}\right)^2} \qquad \text{(C-20)}$$

The calculated error is ±38.2%.

C.4.1.10 Species Yields

The species yields for products generated are determined from,

$$Y_i = \frac{\overline{X}_i MW_i (\dot{m}_{fuel} + \dot{m}_{air})}{\dot{m}_{fuel} MW_{UL}} \qquad \text{(C-21)}$$

And the depleted yield of oxygen is determined from,

$$Y_{O_2} = \frac{MW_{O_2} (X_{O_2,amb} \dot{m}_{air} - \overline{X}_{O_2} \dot{m}_{total})}{\dot{m}_{fuel} MW_{UL}} \qquad \text{(C-22)}$$

Similar to the air entrainment rate calculations, the uncertainty associated with the species yields will be a combination of the uncertainty in the individual measurements and uncertainty associated with the grid resolution, see section C.4.2.3.

$$\varepsilon_{Y_i} = \sqrt{\left(\varepsilon_{X_i}\right)^2 + \left(\varepsilon_{\dot{m}_{fuel}}\right)^2 + \left(\varepsilon_{\dot{m}_{air,inl}}\right)^2 + \left(\varepsilon_{MW_{UL}}\right)^2 + \left(\varepsilon_{GE}\right)^2} \qquad \text{(C-23)}$$

The resulting uncertainty for each species is listed in Table C-5.

Table C-5: Estimated Uncertainties in Species Yields

Species	ε_{Yi} (%)
Oxygen	51.8
Carbon Dioxide	51.8
Carbon Monoxide	51.8
Unburned Hydrocarbons	51.5

C.4.1.11 Compartment Combustion Rate

The mass flow rate of fuel consumed within the compartment is based on the methodology presented by Drysdale [2001],

$$\dot{m}_{fuel,\,compartment} = \frac{\dot{Q}_{compartment}}{\chi\,\Delta H_c} = \frac{\left(0.21 - X_{o_2}\right)\rho_{O_2}\,\Delta H_{c,ox}\,\dot{V}}{\Delta H_c} \qquad \text{(C-24)}$$

It is reported by Drysdale [2001] that the uncertainty associated with Equation C-24 is ±5%. Taking into account the uncertainty associated with the measured mole fraction of oxygen and the mass flow rate of gas exiting the compartment, along with the uncertainty associated in the methodology, the total uncertainty is estimated to be ±37.9%.

C.4.1.12 Non-Dimensional Heat Release Rate

The non-dimensional heat release rate is defined as,

$$\widetilde{Q} = \frac{\dot{Q}_{ideal}}{\dot{Q}_{Flame\ Extensions}} \qquad \text{(C-25)}$$

The uncertainty associated with Equation C-25 is a combination of the uncertainties associated with the ideal heat release rate and the heat release rate required for flame extensions. The uncertainty in the ideal heat release rate was calculated to be ±7.4%. No uncertainty can be assigned to the flame length calculations due to a lack of experimental data. Therefore, the uncertainty associated with the non-dimensional heat release rate is assumed to be equal to the uncertainty in the ideal heat release rate calculation, ±7.4%.

C.4.1.13 Species Yields based on Combustion within the Compartment

The uncertainty in the species yields based on combustion within the compartment will be based on the same values as those for the standard yields calculation with the exception of the value for $\dot{m}_{fuel}$ which instead will now be the uncertainty associated with $\dot{m}_{fuel,\ compartment}$. The uncertainty in the species yields based on combustion within the compartment is listed in Table C-6.

Table C-6: Estimated uncertainty in species yields based on combustion within the compartment

Species	ε_{Yi} (%)
Oxygen	63.8
Carbon Dioxide	63.8
Carbon Monoxide	63.8
Unburned Hydrocarbons	63.5

C.4.2 Impact of Grid Resolution

Uncertainties in the area-averaged parameters will be a combination of the uncertainties in the single point measurements of species mole fractions, gas

temperatures, and gas velocities, along with the resolution of the measurement sampling grid at the compartment doorway. The accuracy of the area-averaged values will be dependent on the resolution of the sampling grid used to capture the spatial variations. The three primary variables that may be impacted by the grid resolution are the air entrainment rate, area-averaged species mole fractions, and area-averaged species yields.

To capture the variations in the species composition, gas velocities, and gas temperatures, four vertical measurements were taken at three horizontal locations for the baseline and wide doorway experiments. This provided a 12-point sampling grid in the exiting flow of the compartment doorway. To evaluate the impact of the grid resolution on the calculated parameters, comparison was made between the values calculated based on the 12-point sampling grid and calculations performed using only a 4-point sampling grid (centerline data). Discussion of the calculations for three test conditions, two baseline tests and one wide doorway test are presented. Two baseline doorway tests are included to examine the results as function of the global equivalence ratio. Measurements with the narrow doorway and sliver doorway were only taken along the centerline, so no evaluation of the effect of the grid resolution could be made.

C.4.2.1 Air Entrainment Rate

The air entrainment into the compartment was determined by,

$$\dot{m}_{air,in} = \dot{m}_{out} - \dot{m}_{fuel} \qquad \text{(C-26)}$$

where, $\dot{m}_{out}$ is based on the summation of each of the individual mass flow rates of species exiting the compartment,

$$\dot{m}_{out} = \sum \dot{m}_{out,i} = \iint \rho_i \; V \; dA \qquad \text{(C-27)}$$

The calculated air entrainment rates based on 12-point and 4-point (centerline) data are listed in Table C-7 for three test conditions.

Table C-7: Air entrainment rates based on 12-point and 4-point (centerline) sampling data.

	12-Pt Resolution	Centerline	Difference (%)
Baseline (ϕ = 0.26)	0.163	0.157	3.7
Baseline (ϕ = 1.0)	0.141	0.130	7.7
Wide (ϕ = 0.64)	0.249	0.242	2.7

The differences between the calculated air entrainment rates for each test condition are below ±8.0%. For low global equivalence ratios the difference between the two values is below ±4.0%. The data implies that the resolution of the sampling grid has little impact in determining the air entrainment rates. Based on the results presented in Table C-7 it is assumed that the uncertainty associated with the resolution of the sampling grid is ±5.0%.

C.4.2.2 Area-Averaged Carbon Monoxide Mole Fractions

The area-averaged mole fractions of species i are determined by,

$$\overline{X}_i = \frac{\overline{y}_i \, MW_{mixture}}{MW_i} \tag{C-28}$$

where

$$\overline{y}_i = \frac{\int \rho \, y_i \, V \, dA}{\int \rho \, V \, dA} = \frac{\int \rho(x,y) y_i(x,y) V(x,y) \, db \, dH}{\int \rho(x,y) \, V(x,y) \, db \, dH} \tag{C-29}$$

The calculated area-averaged carbon monoxide mole fractions based on 12-point and 4-point (centerline) sampling grids are listed in Table C-8 for three test conditions.

The impact of the grid resolution is seen in the calculated mole fractions. The calculated values based on the centerline data are between ±7% and ±64% lower then the values based on the 12-point sampling grid. A large difference, ±64%, is seen between the 12-point and the 4-point sampling grid data for the wide doorway. This is expected since it was previously reported in Chapter 3 that as the width of the doorway increased the horizontal and vertical variations in the species mole fractions increased, therefore, measurements along the centerline are not sufficient to capture the spatial variations. Increasing the grid resolution beyond 12-points would further improve the calculated values, however, any increase in the grid-resolution has a direct impact in the time duration required to conduct an experiment. In this study, no experiments were conducted with more then twelve sampling points; therefore, no estimate in the improvement of the calculated values can be made. A potential uncertainty of ±25% is assigned to the grid resolution for the area-averaged species mole fractions. This value is somewhat arbitrary and a grid dependency analysis should be conducted in the future.

Table C-8: Area-averaged mole fractions based on 12-point and 4-point (centerline) sampling data.

	12-Pt Resolution	Centerline	Difference (%)
Baseline (ϕ = 0.26)	0.014	0.013	7.1
Baseline (ϕ = 1.0)	2.881	2.077	27.9
Wide (ϕ = 0.64)	1.476	0.535	63.8

C.4.2.3 Area-Averaged Carbon Monoxide Yields

The calculated air entrainment rates and area-averaged species mole fractions are used to determine the area-averaged species yields,

$$Y_i = \frac{\overline{X}_i \, MW_i \, (\dot{m}_{fuel} + \dot{m}_{air})}{\dot{m}_{fuel} \, MW_{UL}} \qquad \text{(C-30)}$$

therefore, the grid dependence observed in the area-averaged mole fraction calculations will also be seen in the area-averaged species yields calculations. The calculated area-averaged carbon monoxide yields for three test conditions and two sampling grid resolutions are listed in Table C-9.

As anticipated, a strong dependence on the grid resolution is observed. The results directly parallel those observed in the area-averaged mole fraction calculations. The same value for the grid resolution uncertainty of ±25% used for the area-averaged species mole fractions is assigned to the area-averaged species yields.

Table C-9: Area-averaged carbon monoxide yields based on 12-point and 4-point (centerline) sampling data.

	12-Pt Resolution	**Centerline**	**Difference (%)**
Baseline (ϕ = 0.26)	0.008	0.007	12.5
Baseline (ϕ = 1.0)	0.479	0.315	34.2
Wide (ϕ = 0.64)	0.374	0.131	65.0

C.5 CONCLUSIONS

The uncertainty analysis for this study was conducted in hindsight as opposed to during the experimental planning stages. Conducting an uncertainty analysis prior to conducting the experiments is recommended so that "one can readily determine which of the various parameters must be controlled with care and which are of less importance." [Beckwith and Marangoni 1990] From the uncertainty analysis it was determined that the critical parameter in a majority of the calculations was the gas temperature. For example, if the uncertainty associated with the measured gas temperature is changed from ±11.2% to that associated with measurements in the lower layer, ±32%, see Section

C.3.2, the uncertainty associated with the area-averaged carbon monoxide yields changes from ±51.8% to ±91.1%. An uncertainty of this magnitude would invalidate any conclusions stemming from the reported study; therefore, care should be taken to insure accurate temperature measurements during all tests.

In addition, the resolution of the sampling grid was shown to impact the calculated area-averaged species mole fractions and consequently the area-averaged species yields. For tests conditions consisting of the wide doorway and high global equivalence ratios, an analysis of the benefit between an increased accuracy in the calculated values compared to the additional experimental duration resulting from a larger sampling grid should be preformed. This analysis is also essential to any measurements conducted along the hallway, where the cross sectional area of the hallway is equal to the cross sectional area of the compartment.

VITA

The author was born in Holyoke, Massachusetts on the thirteenth day of May in 1972. He obtained his undergraduate degree in Mechanical Engineering at Western New England College in Springfield, Massachusetts, completing his Bachelor's of Science degree in Mechanical Engineering in May of 1994. After taking a year off, the author returned to school and began working toward a Master's degree in Fire Protection Engineering at Worcester Polytechnic Institute in the Fall of 1995. In the course of that time, he participated in a one year internship with Rolf Jensens and Associates, Inc. in the Houston, Texas office. After the internship, he returned to WPI and completed his Master's degree in October of 1998. In the final stages of working on his Masters degree the author was presented with an opportunity to continue his education at Virginia Polytechnic Institute and State University at the Building Fire Research Laboratory, where he worked on the carbon monoxide production and transport study. The author has accepted a position as a Senior Research Scientist in the protection division of FM Global in Norwood, Massachusetts, beginning in August of 2003.

Christopher John Wieczorek